

**Modeling and Simulation of Brownian Motion  
Attributable to Thermal Agitation  
for Predicting Dynamics of Nano-Robots**

**THESIS**

Submitted in partial fulfillment  
of the requirements for the degree of

**DOCTOR OF PHILOSOPHY**

By

**NITI NIPUN SHARMA**

Under the Supervision of

**Dr. R.K. MITTAL**

PROF & DEAN



**BIRLA INSTITUTE OF TECHNOLOGY AND SCIENCE  
PILANI (RAJASTHAN) INDIA**

2004

BIRLA INSTITUTE OF TECHNOLOGY AND SCIENCE  
PILANI (RAJASTHAN) INDIA

**CERTIFICATE**

This is to certify that the thesis entitled “**Modeling and Simulation of Brownian Motion Attributable to Thermal Agitation for Predicting Dynamics of Nano-Robots**” and submitted by Mr. Niti Nipun Sharma, ID. No. 1999PHXF006 for award of Ph.D. Degree of the Institute embodies original work done by him under my supervision.

  
**Signature of Supervisor**

**R. K. MITTAL**

Name in Capital  
Block Letters

**Prof. & Dean**  
Designation

Date: Dec. 6, 2004

## ACKNOWLEDGEMENTS

I wish to convey my sincere gratitude and thanks to my guide Prof. R.K. Mittal for allowing me to work in the emerging area of Nanotechnology, providing me all guidance, helping me understand the concepts, continuous encouragement and moral support. It is from him that I learned the traits of research and developed a desire to excel.

I am highly indebted to Prof. M. Ganesh, Mathematics Group and convey my deepest regards to him. He is one person without whom; the realization of facts in the thesis would not have been that easy. I can only say that words do not mean anything when someone has done so much for you.

I thank Dr. S. Venkateswaran, Vice Chancellor, BITS, Pilani for allowing me to pursue my thesis in the Institute.

I wish to express my gratitude to Prof. L.K. Maheshwari, Director, BITS, Pilani for his keen interest in the area of Nanotechnology and for his timely encouragements.

I would be failing in my duties if I do not mention the names of Prof. T. Fukuda, Chairman, IEEE Council of Nanotechnology, Dr. Chandrasekhar, Director, CEERI, Pilani and Prof. R. Mehrotra, Physics Group, BITS, Pilani for their encouraging remarks, which boosted my morals and prompted to pursue the problem with enriched confidence. I am also thankful to the constructive criticisms on the work by Prof. Rudra Pratap Singh, Mechanical Group, IISc, Bangalore, which helped me in organizing the work in a better way.

My sincere thanks are due to all who directly and indirectly contributed in the completion of this work.

TO MY WIFE

## TABLE OF CONTENTS

Abstract	(i)
List of Figures	(iii)
List of Tables	(ix)
Notations	(x)
<b><u>CHAPTER 1</u></b>	<b>1-7</b>
<b>DYNAMICS IN NANO-DOMAINS</b>	
1.1 INTRODUCTION	1
1.2 HOW SMALL IS SMALL?	2
1.3 IMPORTANCE OF BROWNIAN MOTION	4
1.4 PROBLEM DESCRIPTION	5
<b><u>CHAPTER 2</u></b>	<b>8-28</b>
<b>LITERATURE REVIEW</b>	
2.1 INTRODUCTION	8
2.2 THE BROWNIAN MOTION	8
2.3 DEVELOPMENTS IN BROWNIAN MOTION THEORY	9
2.3.1 Stage I - Discovery, Observations and Conflicts	10
2.3.2 Stage II - Theoretical Formulations	12
2.3.3 Stage III-Quantitative Confirmations, Modeling and Applications	13
2.3.4 Stage IV-Brownian Motion in Nano-domains	18
2.4 REVIEW OF DYNAMIC MODELING	24
2.5 ANALYTICAL APPROACHES TO BROWNIAN MOTION	26
2.6 EPILOGUE	28
<b><u>CHAPTER 3</u></b>	<b>29-56</b>
<b>IMPACT PROCESS MODELING OF BROWNIAN MOTION OF NANO-SIZED BODIES</b>	
3.1 INTRODUCTION	29
3.2 MODEL OF NANOPARTICLE	29
3.2.1 Non-Rigid Nanoparticle Model	29
3.2.2 Impact Transfer Process	30

3.3	RESISTANCE TO GLOBAL MOTION OF NANOPARTICLE	31
3.4	RESISTANCE TO LOCAL MOTION OF NANOPARTICLE	31
3.5	MODEL OF IMPACT TRANSFER IN RIGID NANOPARTICLE	32
3.6	SUB-SYSTEM MODEL OF NON-RIGID NANOPARTICLE	36
3.7	MODELS OF IMPACT TRANSFER IN NON-RIGID NANOPARTICLE	37
3.8	MATHEMATICAL MODELS FOR IMPACT TRANSFER MODELS	39
3.8.1	Mathematical Model for Model 2	39
3.8.2	Mathematical Model for Model 3	40
3.8.3	Mathematical Model for Model 4	41
3.8.4	Mathematical Model for Model 5	41
3.9	DEVELOPMENT OF VARIANCE MODELS FOR NON-RIGID NANOPARTICLE	42
3.10	VARIANCE FOR DIFFERENT IMPACT TRANSFER MODELS	43
3.10.1	Variance for Model 2	44
3.10.2	Variance for Model 3	47
3.10.3	Variance for Model 4	50
3.10.4	Variance for Model 5	52
3.11	EPILOGUE	55
<b><u>CHAPTER 4</u></b>		<b>57-89</b>
<b>IMPACT TRANSFER MODEL VALIDATION BY SIMULATION</b>		
4.1	INTRODUCTION	57
4.2	VALIDITY CRITERION FOR MODELS OF BROWNIAN MOTION OF NANOPARTICLE	57
4.2.1	Validity Criterion 1	58
4.2.2	Validity Criterion 2	59
4.3	VERIFICATION OF PARAMETRIC RELATION FOR SIMULATION	59
4.4	SIMULATION OF IMPACT TRANSFER MODELS	62
4.4.1	Simulation for Silicon Nanoparticle	63
4.4.2	Simulation for Polystyrene Nanoparticle	70
4.5	NEW IMPACT TRANSFER MODELS	75

4.6	VARIANCE FOR NEW IMPACT TRANSFER MODELS	76
4.6.1	Variance for Model 6	76
4.6.2	Variance for Model 7	81
4.7	SIMULATION OF NEW IMPACT TRANSFER MODELS	82
4.7.1	Simulation for Silicon Nanoparticle	83
4.7.2	Simulation for Polystyrene Nanoparticle	85
4.8	EPILOGUE	88
 <b><u>CHAPTER 5</u></b>		90-137
<b>BROWNIAN MOTION MODELS OF NANO-SIZED BODIES: SYSTEMS</b>		
<b>MODELING APPROACH</b>		
5.1	INTRODUCTION	90
5.2	SYSTEM MODEL FOR BROWNIAN MOTION OF RIGID NANOPARTICLE	90
5.3	SYSTEM MODEL FOR BROWNIAN MOTION OF NON-RIGID NANOPARTICLE	93
5.4	ALGORITHM FOR BUILDING ALL POSSIBLE FOUR-PARAMETERS MODELS OF NANOPARTICLE	94
5.5	SELECTION OF KINEMATICALLY VALID-SYSTEMS	103
5.5.1	Selection Criterion 1	103
5.5.2	Selection Criterion 2	106
5.5.3	Selection Criterion 3	108
5.6	SELECTED SYSTEM MODELS	118
5.7	FORMULATION OF VARIANCE EXPRESSION	121
5.8	SIMULATION OF THREE NON-RIGID MODELS	122
5.8.1	Time Dependent Functions Corresponding to Variance of Three Models	123
5.8.2	Simulation of Function $\psi$ for Silicon Nanoparticle	124
5.8.3	Simulation of Function $\psi$ for Polystyrene Nanoparticle	126
5.9	VERIFICATION OF MODELS WITH EXPERIMENTAL RESULTS	128
5.9.1	Brownian Motion of Silicon Nanoparticle	129
5.9.2	Brownian Motion of Polystyrene Nanoparticle	131
5.10	COMPARISON OF SYSTEM MODELS WITH IMPACT TRANSFER MODELS	135
5.11	EPILOGUE	136

**CHAPTER 6** 138-148

**APPLICATION OF NON-RIGID NANOPARTICLE TO MODEL DIRECTED  
DIFFUSION MODE**

6.1	INTRODUCTION	138
6.2	INPUT MODELING	138
6.3	VARIANCE FOR TRANSIENT THERMAL NOISE	139
6.3.1	Variance from Model 8 with Transient Thermal Noise Input	141
6.3.2	Variance from Model 9with Transient Thermal Noise Input	141
6.3.3	Variance from Model 10 withTransient Thermal Noise Input	142
6.4	SIMULATION OF VARIANCE FOR TRANSIENT THERMAL NOISE INPUT	143
6.5	EPILOGUE	148

**CHAPTER 7** 149-164

**BROWNIAN MOTION APPLICATION FOR NANO-ROBOT DYNAMICS**

7.1	INTRODUCTION	149
7.2	ROBOTIC MANIPULATOR MOVING DOWN THE SIZE	149
7.3	STATE OF ART IN NANOMANIPULATION	150
7.4	DYNAMIC MODELING OF BROWNIAN MOTION IN NANO-ROBOTS	153
7.4.1	Classical Dynamic Model of 1-DOF Manipulator	153
7.4.2	Langevin Equation for 1-DOF Manipulator	154
7.5	VARIANCE FOR 1-DOF NANO-ROBOT	155
7.5.1	Rigid Body Model of Nano-Robot	155
7.5.2	Non-Rigid Models of Nano-Robot	156
7.6	SIMULATION OF BROWNIAN MOTION OF NANO-ROBOT	159
7.6.1	Simulation for Rigid Body Model	160
7.6.2	Simulation of Non-Rigid Model	160
7.7	EPILOGUE	163

**CHAPTER 8** 165-172

**CONCLUSIONS**

8.1	INTRODUCTION	165
-----	--------------	-----



<b>8.2</b>	<b>INFERENCES</b>	<b>166</b>
8.2.1	Non-Rigidity of Nanoparticle Influences Brownian Motion	166
8.2.2	An Impact Transfer Model for Non-Rigid Nanoparticle	166
8.2.3	Relation between Rigid and Non-Rigid Parameters	167
8.2.4	Brownian Motion Model of Non-Rigid Nanoparticle using Systems Approach	168
8.2.5	Application to Model Directed Diffusion Mode of Brownian Motion	169
8.2.6	Prediction of Dynamics of 1-DOF Nano-Robot	169
<b>8.3</b>	<b>FUTURE PERSPECTIVES</b>	<b>170</b>
	<b>APPENDIX I</b>	<b>173-178</b>
	<b>APPENDIX II</b>	<b>179-194</b>
	<b>REFERENCE</b>	<b>195-209</b>
	<b>LIST OF PUBLICATIONS</b>	<b>210</b>
	<b>BIOGRAPHIES</b>	<b>211-212</b>

## ABSTRACT

The present thesis is an attempt to investigate the dynamics in nano-domains keeping in view the fast developments in nanotechnology. The recent advancements in nano-regimes have made possible the developments of nano-devices and researchers have observed that modeling dynamics of the nano-devices like nano-robots will be challenging. The various forces, which are negligible in macro-sized devices, are going to contribute significantly in nano-domains. The force attributable to thermal agitation from surrounding medium will decide the controls and manipulation of nano-devices like nano-robots. The corresponding motion to thermal agitation is termed as Brownian motion. The thesis investigates the Brownian motion by modeling and simulation and predicts the dynamics of nano-robots due to thermal agitation from surrounding medium.

In order to model the dynamics owing to thermal agitation, a thorough literature survey on Brownian motion theory is done. Based on the literature survey, it is observed that Brownian motion models in available literature are based on the assumption of rigid bodies. It is also noted from literature survey that nano-sized bodies (nanoparticles) have very low spring constants implying that rigid body assumption is not correct in nano-domains. Therefore, non-rigidity is a primary concern and Brownian motion models are developed for non-rigid nanoparticles.

The modeling Brownian motion of non-rigid nanoparticles has been attempted using Langevin model in two ways. The first method of impact transfer modeling is akin to correlation technique, since correlation technique is used to analyze the Langevin model. The second method of modeling used the concept of lumped-parameter systems-modeling approach. The exhaustive possible interaction system-models (in all 360) are developed, which are then subjected to testify various validity criterions. Based on simulation and validity criterion, it is found that three Brownian motion models of non-rigid nanoparticle are valid and among the three, one is better and applicable in a wider range of size in nano-domains. The verification with published results of the non-rigid nanoparticle model and failure of rigid body model to

match the published results confirmed the hypothesis of non-rigidity being a prime concern in nano-domains.

The developed non-rigid models are applied to model directed diffusion mode by altering the input as closely related to white noise. The models are further used to predict the Brownian motion of nano-robot. The thesis concludes with facts convincingly demonstrated by modeling and simulation in the present work with presentation of future prospects on the present work.

## LIST OF FIGURES

FIGURE NO.	Page No.
<b>Fig. 3.1</b> Model of Nanoparticler and its Lumped Parameters	
(i) Nanoparticle Consisting of Number of Spring-Mass-Dashpot Systems	30
(ii) Three Lumped Parameters of a Nanoparticle	30
<b>Fig. 3.2</b> Integration of White Noise	34
<b>Fig. 3.3</b> Modified White Noise	34
<b>Fig. 3.4</b> Impact Transfer Model for Rigid Nanoparticle	35
<b>Fig. 3.5</b> Non-Rigid Properties Sub-System for Non-Rigid Nanoparticle	36
<b>Fig. 3.6</b> Impact Transfer Model for Non-Rigid Sub-System	37
<b>Fig. 3.7</b> Impact Transfer Model 2 for Brownian motion of Non-Rigid Nanoparticle	38
<b>Fig. 3.8</b> Impact Transfer Model 3 of Brownian motion of Non-Rigid Nanoparticle	38
<b>Fig. 3.9</b> Impact Transfer Model 4 of Brownian motion of Non-Rigid Nanoparticle	38
<b>Fig. 3.10</b> Impact Transfer Model 5 of Brownian motion of Non-Rigid Nanoparticle	39
<b>Fig. 4.1</b> Variation of Spring Constant $k$ with Length of Silicon Carbide Nanorods and Carbon Nanotubes	
(i) Simulation for Silicon Carbide Nanorods	61
(ii) Simulation for Carbon Nanotubes	61
<b>Fig. 4.2</b> Simulation of Model 2 for Silicon Nanoparticle	
(i) $\varphi$ vs $t$ in Parameter Range: $1 \times 10^{-10} \leq c' \leq 1 \times 10^{-8}$ m in steps of $1 \times 10^{-9}$ m	64
(ii) $\varphi$ vs $t$ in Parameter Range: $1 \times 10^{-8} \leq c' \leq 1 \times 10^{-6}$ m in steps of $1 \times 10^{-7}$ m	65
(iii) $\varphi$ vs $t$ in Parameter Range: $1 \times 10^{-6} \leq c' \leq 1 \times 10^{-4}$ m in steps of $1 \times 10^{-5}$ m	65
<b>Fig. 4.3</b> Simulation of Model 3 for Silicon Nanoparticle	
(i) $\varphi$ vs $t$ in Parameter Range: $1 \times 10^{-10} \leq c' \leq 1 \times 10^{-8}$ m in steps of $1 \times 10^{-9}$ m	66
(ii) $\varphi$ vs $t$ in Parameter Range: $1 \times 10^{-8} \leq c' \leq 7 \times 10^{-8}$ m in the steps of $1 \times 10^{-8}$ m	67
<b>Fig. 4.4</b> Simulation of Model 4 for Silicon Nanoparticle for $1 \times 10^{-10} \leq c' \leq 1 \times 10^{-8}$ m in steps of $1 \times 10^{-9}$ m	68

<b>Fig. 4.5</b>	<b>Simulation of Model 5 for Silicon Nanoparticle</b>	
(i)	$\varphi$ vs $t$ in Parameter Range: $1 \times 10^{-10} \leq c' \leq 1 \times 10^{-8}$ m in Steps of $1 \times 10^{-9}$ m	69
(ii)	$\varphi$ vs $t$ in Parameter Range: $1 \times 10^{-8} \leq c' \leq 1 \times 10^{-6}$ m in Steps of $1 \times 10^{-7}$ m	69
(iii)	$\varphi$ vs $t$ in Parameter Range: $1 \times 10^{-6} \leq c' \leq 5.1 \times 10^{-5}$ m in Steps of $1 \times 10^{-5}$ m	70
<b>Fig. 4.6</b>	<b>Simulation of Model 2 for Polystyrene Nanoparticle for <math>1 \times 10^{-6} \leq c' \leq 9.1 \times 10^{-5}</math> m in Steps of <math>1 \times 10^{-5}</math> m</b>	72
<b>Fig. 4.7</b>	<b>Simulation of Model 3 for Polystyrene Nanoparticle for <math>1 \times 10^{-10} \leq c' \leq 1 \times 10^{-8}</math> m in Steps of <math>1 \times 10^{-9}</math> m</b>	73
<b>Fig. 4.8</b>	<b>Simulation of Model 4 for Polystyrene Nanoparticle for <math>1 \times 10^{-10} \leq c' \leq 1 \times 10^{-8}</math> m in Steps of <math>1 \times 10^{-9}</math> m</b>	73
<b>Fig. 4.9</b>	<b>Simulation of Model 5 for Polystyrene Nanoparticle for <math>1 \times 10^{-10} \leq c' \leq 1 \times 10^{-8}</math> m in Steps of <math>1 \times 10^{-9}</math> m</b>	74
<b>Fig. 4.10</b>	<b>Impact Transfer Model 6 of Brownian Motion of Non-Rigid Nanoparticle</b>	76
<b>Fig. 4.11</b>	<b>Impact Transfer Model 7 of Brownian Motion of Non-Rigid Nanoparticle</b>	76
<b>Fig. 4.12</b>	<b>Simulation of Model 6 for Silicon Nanoparticle</b>	
(i)	$\varphi$ vs $t$ in Parameter Range: $1 \times 10^{-10} \leq c' \leq 1 \times 10^{-8}$ m in Steps of $1 \times 10^{-9}$ m	84
(ii)	$\varphi$ vs $t$ in Parameter Range: $1 \times 10^{-8} \leq c' \leq 1 \times 10^{-6}$ m in Steps of $1 \times 10^{-7}$ m	84
<b>Fig. 4.13</b>	<b>Simulation of Model 7 for Silicon Nanoparticle for <math>1 \times 10^{-10} \leq c' \leq 100</math> m in Steps of <math>1 \times 10^{-9}</math> m</b>	85
<b>Fig. 4.14</b>	<b>Simulation of Model 6 for Polystyrene Nanoparticle in Parametric Range:</b>	
(i)	$\varphi$ vs $t$ in Parameter Range: $1 \times 10^{-10} \leq c' \leq 1 \times 10^{-8}$ m in Steps of $1 \times 10^{-9}$ m	86
(ii)	$\varphi$ vs $t$ in Parameter Range $1 \times 10^{-5} \leq c' \leq 1 \times 10^{-4}$ m in Steps of $1 \times 10^{-5}$ m	87
<b>Fig. 4.15</b>	<b>Simulation of Model 7 for Polystyrene Nanoparticle for <math>1 \times 10^{-10} \leq c' \leq 100</math> m in Steps of <math>1 \times 10^{-9}</math> m</b>	88

<b>Fig. 5.1</b>	Two-Parameter System Block Diagram for Rigid Nanoparticle Brownian motion	91
<b>Fig. 5.2</b>	Equivalent Electric Circuit for Two Parameter Brownian motion Model of Rigid Nanoparticle	92
<b>Fig. 5.3</b>	Proposed Four Parameter System Block Diagram	93
<b>Fig. 5.4</b>	Three Possible Two-Unit Models	94
<b>Fig. 5.5</b>	Two Distinct Two-Unit Models	95
<b>Fig. 5.6</b>	Six Possible Three-Unit Models	95
<b>Fig. 5.7</b>	Five Distinct Three-Unit Models	96
<b>Fig. 5.8</b>	Fifteen Possible Four-Unit Models Obtained from Three-Unit Models	96-97
<b>Fig. 5.9</b>	Thirteen Possible Four-Unit Models Obtained from Three-Unit Models	98
<b>Fig. 5.10</b>	Twelve Possible Four-Unit Models Obtained from Two-Unit Models	99
<b>Fig. 5.11</b>	Seven Distinct Four-Unit Models Obtained from Two-Unit Models	99
<b>Fig. 5.12</b>	Distinct Four-Unit Models	100
<b>Fig. 5.13</b>	Combination-1: Four-Parameter System Models Corresponding to Model in Fig. 5.12(i)	102
<b>Fig. 5.14</b>	Possible System Models Satisfying Selection Criterion-1 and 2	109
<b>Fig. 5.15</b>	Possible Model I	110
<b>Fig. 5.16</b>	Possible Model II	110
<b>Fig. 5.17</b>	Possible Model III	111
<b>Fig. 5.18</b>	Possible Model IV	112
<b>Fig. 5.19</b>	Possible Model V	112
<b>Fig. 5.20</b>	Possible Model VI	113
<b>Fig. 5.21</b>	Possible Model VII	114
<b>Fig. 5.22</b>	Possible Model VIII	115
<b>Fig. 5.23</b>	Possible Model IX	115
<b>Fig. 5.24</b>	Possible Model X	116
<b>Fig. 5.25</b>	Possible Model XI	117
<b>Fig. 5.26</b>	Possible Model XII	118
<b>Fig. 5.27</b>	Equivalent Electric Analog Circuits for Three Models (i) Model 8 (ii) Model 9 and (iii) Model 10	120
<b>Fig. 5.28</b>	Simulation of $\psi$ v/s Time for Silicon Nanoparticle using Model 8	125
<b>Fig. 5.29</b>	Simulation of $\psi$ v/s Time for Silicon Nanoparticle using Model 9	126

<b>Fig. 5.30</b>	Function $\psi$ v/s Time for Polystyrene Nanoparticle using Model 8	
	(i) Simulation in Parameter Range $1 \times 10^{-10} \leq c' \leq 1 \times 10^{-9}$ m in Steps of $1 \times 10^{-9}$ m	127
	(ii) Simulation in Parameter Range $1 \leq c' \leq 100$ m in Steps of 10 m	128
<b>Fig. 5.31</b>	Simulation of $\psi$ v/s Time for Polystyrene Nanoparticle using Model 9 and Model 10	128
<b>Fig. 5.32</b>	Comparison of Variance in Position of Silicon Nanoparticle for Experimental Observation, Rigid body Model and Three Models:	
	(i) Model 8 (ii) Model 9 and (iii) Model 10	130-131
<b>Fig. 5.33</b>	Variance in Position of Polystyrene Nanoparticle for Developed Models	
	(i) Model 8 (ii) Model 9 and (iii) Model 10.	133-134
<b>Fig. 5.34</b>	Comparison of Variance in Position of Polystyrene Nanoparticle for Experimental observation, Rigid Body Model and Model 10	135
<b>Fig. 5.35</b>	Equivalent Electric Analog Circuits for Impact Transfer Model 7	136
<b>Fig. 6.1</b>	Variance of Silicon Nanoparticle for Model 8 with Transient Thermal Noise in Parametric range:	
	(i) $1 \times 10^{-10} \leq c' \leq 1 \times 10^{-8}$ m in Steps of $1 \times 10^{-10}$ m	143
	(ii) $1 \times 10^{-8} \leq c' \leq 1 \times 10^{-6}$ m in Steps of $1 \times 10^{-8}$ m	144
	(iii) $1 \times 10^{-6} \leq c' \leq 1 \times 10^{-4}$ m in Steps of $1 \times 10^{-4}$ m	144
<b>Fig. 6.2</b>	Variance of Silicon Nanoparticle for Model 9 with Transient Thermal Noise in Parametric Range:	
	(i) $1 \times 10^{-10} \leq c' \leq 5 \times 10^{-9}$ m in steps of $1 \times 10^{-9}$ m	145
	(ii) $5 \times 10^{-9} \leq c' \leq 1 \times 10^{-7}$ m in steps of $1 \times 10^{-8}$ m	145
	(iii) $1 \leq c' \leq 100$ m in steps of 10m	145
<b>Fig. 6.3</b>	Variance of Silicon Nanoparticle for Model 10 with Transient Thermal Noise in Parametric Range:	
	(i) $1 \times 10^{-10} \leq c' \leq 5 \times 10^{-9}$ m in steps of $1 \times 10^{-9}$ m	146
	(ii) $5 \times 10^{-9} \leq c' \leq 1 \times 10^{-7}$ m in steps of $1 \times 10^{-8}$ m	147
	(iii) $1 \leq c' \leq 100$ m in steps of 10m	147
<b>Fig. 7.1</b>	Single Walled Carbon Nanotube	152
<b>Fig. 7.2</b>	Variance in Angular Position of 1-DOF Nano-Robot using Rigid Body Model	160

<b>Fig. 7.3</b>	Variance in Angular Position of 1-DOF Nano-Robot v/s Time using Model 8	
	(i) $1 \times 10^{-10} \leq c' \leq 1 \times 10^{-9}$ m in Steps of $1 \times 10^{-9}$ m	161
	(ii) $1 \times 10^{-6} \leq c' \leq 1 \times 10^{-4}$ m in steps of $1 \times 10^{-5}$ m	161
<b>Fig. 7.4</b>	Variance in Angular Position of 1-DOF Nano-Robot v/s Time using model 9	162
<b>Fig. 7.5</b>	Variance in Angular Position of 1-DOF Nano-Robot v/s Time using model 10	163
<b>Fig. I.1</b>	Expected Value of Response $E\{x(t)\}$ for a System with Impulse Response $h(\tau)$ and Input with expected value $E\{y(t)\}$	173
<b>Fig. I.2</b>	Autocorrelation of Response $R_{xx}(t_1, t_2)$ of System with Impulse Response $h(\tau)$ and Input with autocorrelation $R_{yy}(t_1, t_2)$ for $(t_1 > t_2)$	174
<b>Fig. I.3</b>	Autocorrelation of Response $R_{xx}(t_1, t_2)$ of System with Impulse Response $h(\tau)$ and Input with autocorrelation $R_{yy}(t_1, t_2)$ for $(t_1 < t_2)$	174
<b>Fig. II.1</b>	Combination 1: Twenty-Four 4-P Models Corresponding to Model given in Fig.5.12(i)	179
<b>Fig. II.2</b>	Combination 2: Twenty-Four 4-P Models Corresponding to Model given in Fig.5.12(ii)	180
<b>Fig. II.3</b>	Combination 3: Twenty-Four 4-P Models Corresponding to Model given in Fig.5.12(iii)	180
<b>Fig. II.4</b>	Combination 4: Twenty-Four 4-P Models Corresponding to Model given in Fig.5.12(iv)	181
<b>Fig. II.5</b>	Combination 5: Twenty-Four 4-P Models Corresponding to Model given in Fig.5.12(v)	182
<b>Fig. II.6</b>	Combination 6: Twenty-Four 4-P Models Corresponding to Model given in Fig.5.12(vi)	182
<b>Fig. II.7</b>	Combination 7: Twenty-Four 4-P Models Corresponding to Model given in Fig.5.12(vii)	183
<b>Fig. II.8</b>	Combination 8: Twenty-Four 4-P Models Corresponding to Model given in Fig.5.12(viii)	184
<b>Fig. II.9</b>	Combination 9: Twenty-Four 4-P Models Corresponding to Model given in Fig.5.12(ix)	185
<b>Fig. II.10</b>	Combination 10: Twenty-Four 4-P Models Corresponding to Model given in Fig.5.8 (x)	186
<b>Fig. II.11</b>	Combination 11: Twenty-Four 4-P Models Corresponding to Model given in Fig.5.12(xi)	187
<b>Fig. II.12</b>	Combination 12: Twenty-Four 4-P Models Corresponding to Model given in Fig.5.12(xii)	188
<b>Fig. II.13</b>	Combination 13: Twenty-Four 4-P Models Corresponding to Model given in Fig.5.12(xiii)	188



<b>Fig. II.14</b>	Combination 14: Twenty-Four 4-P Models Corresponding to Model given in Fig.5.12(xiv)	189
<b>Fig. II.15</b>	Combination 1: Twenty-Four 4-P Models Corresponding to Model given in Fig.5.12(xv)	190
<b>Fig. II.16</b>	Single 4-P Model Corresponding to Combination 1 Satisfying Selection Criterion 1	190
<b>Fig. II.17</b>	Four 4-P Model Corresponding to Combination 2 Satisfying Selection Criterion 1	190
<b>Fig. II.18</b>	Twelve 4-P Model Corresponding to Combination 3 Satisfying Selection Criterion 1	191
<b>Fig. II.19</b>	Twelve 4-P Model Corresponding to Combination 4 Satisfying Selection Criterion 1	191
<b>Fig. II.20</b>	Six 4-P Model Corresponding to Combination 5 Satisfying Selection Criterion 1	191
<b>Fig. II.21</b>	Six 4-P Model Corresponding to Combination 6 Satisfying Selection Criterion 1	191
<b>Fig. II.22</b>	Six 4-P Model Corresponding to Combination 7 Satisfying Selection Criterion 1	192
<b>Fig. II.23</b>	Twelve 4-P Model Corresponding to Combination 8 Satisfying Selection Criterion 1	192
<b>Fig. II.24</b>	Six 4-P Model Corresponding to Combination 9 Satisfying Selection Criterion 1	192
<b>Fig. II.25</b>	Twelve 4-P Model Corresponding to Combination 10 Satisfying Selection Criterion 1	192
<b>Fig. II.26</b>	Four 4-P Model Corresponding to Combination 11 Satisfying Selection Criterion 1	193
<b>Fig. II.27</b>	Four 4-P Model Corresponding to Combination 12 Satisfying Selection Criterion 1	193
<b>Fig. II.28</b>	Single 4-P Model Corresponding to Combination 13 Satisfying Selection Criterion 1	193
<b>Fig. II.29</b>	Three 4-P Model Corresponding to Combination 14 Satisfying Selection Criterion 1	193
<b>Fig. II.30</b>	Three 4-P Model Corresponding to Combination 15 Satisfying Selection Criterion 1	193

## LIST OF TABLES

Table Details	Page No.
<b>Table 3.1</b> Summary of Equations giving Autocorrelation and Variance in Position of Non-Rigid Nanoparticle	55
<b>Table 5.1</b> Four Analogous Parameters According to Force Voltage Analogy	93
<b>Table 5.2</b> Possible Models of Four Parameter Systems	119
<b>Table 5.3</b> Parametric Values for Silicon and Polystyrene Nanoparticle Given in Published Experimental Results	123
<b>Table 5.4</b> Parametric Values Deduced for Brownian Motion of Non-Rigid Nanoparticle	123

## NOTATIONS

Symbol	Unit/Value of Symbol	Description/Expression
$\theta, \dot{\theta}, \ddot{\theta}$	rad, rad/s, rad/s	Angular Position, Velocity and acceleration
$\lambda$	$\text{m}^2/\text{s}$	Diffusion Constant
$\delta(\tau)$	---	Unit impulse at time $\tau$
$\rho$	$\text{kg}/\text{m}^3$	Density of Nanoparticle
$\tau$	s	Variable for Time
$\psi$	---	Time Dependent Part of the Variance
$\kappa$	$1.3807 \times 10^{-27} \text{ J/K}$	Boltzman Constant
$\omega$	rad/s	Characteristic Frequency of Nanoparticle
$\eta$	$\text{N s}/\text{m}^2$	Viscosity of the Surrounding Medium
$\Delta$	J	Lagrangian or Kinetic potential
$g(\tau)$	---	Impulse Response of Integrator
$h(\tau), H(\tau)$	---	Impulse Response of Rigid Body and Non-Rigid sub-System
$\bar{c}$	Farads	Capacitance of Nanoparticle
$c'$	m	Parameter having the dimension of length
$D$	---	Manipulator Inertia Tensor
$d_i$	m	Inner Diameter of Nanotube
$d_o$	m	Outer Diameter of Nanotube
$E\{z'^2(t)\}$	$\text{m}^2$	Variance in Physical Variable $z'$
$E\{x^2(t)\}$	$\text{m}^2$	Variance in Position
$F(t)$	N	External Stochastic Force, Mechanical Analogue of Electrical Voltage
$F'$	$\text{N s}/\text{m}$	Equivalent Damping Coefficient of Nanolink
$F_e(t)$	N	External Deterministic Force
$f, f', f_{eq}$	$\text{N s}/\text{m}$	Damping Coefficient of Surrounding Fluid,

		Nanoparticle and Total Damping Coefficient due to Surrounding and Nanoparticle, Electrical Analogue of Resistance
$G(\theta)$	---	Gravity Force Vector
$h$	$6.623 \times 10^{-34}$ J s	Planck's Constant
$h_i$	---	Friction in Manipulator
$i(t)$	Ampere	Current in System-Models
KE	J	Kinetic Energy
$k$	N/m	Spring Constant, Electrical Analogue of Capacitance of Nanoparticle
L	Henry	Inductance of Nanoparticle
$l$	m	Length of Nanolink
$M$	kg	Characteristic Mass of Nanolink
$m$	kg	Mass of Nanoparticle, Electrical Analogue of Inductance of Nanoparticle
$m_{nl}$	kg	Mass of Nanolink
$n$	---	Degrees of Freedom of a System
$n(t)$	---	White Noise
PE	J	Potential Energy
$\Delta p$	kg m/s	Uncertainty in Momentum
$q(t)$	Coulomb	Charge Flowing in system Models
$q_i$	---	$i^{\text{th}}$ Generalized Coordinate
$r$	m	Radius of Nanoparticle
$R$	Ohm	Resistance from Surrounding Medium
$R'$	Ohm	Resistance from Nanoparticle
$R_{z,z'}(t_1, t_2)$	$\text{m}^2$	Cross Correlation between $z$ and $z'$
$R_{zz}(t_1, t_2)$	$\text{m}^2$	Autocorrelation of Physical Variable $z$
$S_{z,z'}(\omega)$	---	Spectrum of $z'$
$T$	K	Temperature
$t$	s	Time
$\tau_i$	N m	Generalized Force at $i^{\text{th}}$ Degree of Freedom

$U(\tau)$	---	Unit Step Function
$v$	m/s	Velocity
$v_0$	m/s	Velocity of Nanoparticle at $t = 0$
$V(\theta, \dot{\theta})$		Centrifugal and Coriolis Forces
$V(t)$	Volt	Voltage
$w(t)$	---	Integrated White Noise
$x(t)$	m	Position of the Nanoparticle, Mechanical Analogue of Electrical Charge
$\Delta x$	m	Uncertainty in Position
$x_0$	m	Position of Nanoparticle at $t = 0$
$\dot{x}(t)$	m/s	Velocity of Nanoparticle, Mechanical Analogue of Electrical Current
$y(t), z'(t), y'(t), Z(t)$ $u(t), Y(t), Y'(t)$		Variables in Impact Transfer Model
$\alpha$	$m^2/s^3$	$\frac{2\kappa T f \delta(\tau)}{m^2}$
$\alpha', \xi$	Hz	$\frac{k}{f'}$
$\alpha''$	$m^2/kg s^2$	$\frac{2\kappa T F' l^2}{M^2}$
$\beta$	Hz	$\frac{f}{m}$
$\varphi$	---	$\frac{c'}{r}$

The whole burden of philosophy seems to consist in this, from the phenomenon of motions to investigate the force of nature, and from these forces to demonstrate the other phenomenon

*Sir Isaac Newton*

## CHAPTER 1

# DYNAMICS IN NANO-DOMAINS

## 1.1 INTRODUCTION

In near future, biological, medical and environmental technologies will become dominating new frontiers of technology to maintain and improve human life. These technologies will require new engineering techniques like microfabrication and new materials. Newer or altogether different concepts of design and controls will be required for these upcoming areas. These techniques will be indispensable for developing adaptable man-machine interface, equipment and artificial organs for life support. The most difficult and challenging field will be developing micromechanisms and micromachines to perform and carry out various tasks.

Micromachines are defined as machines that are constructed from micrometer sized mechanisms. Recently, the pursuance in research is to develop machines below the microdomains and the technology development in the sub-micro or nanodomains is a nagging problem for theoreticians and experimentalists. The smaller the machine becomes, the more difficult is the control of movements and still more difficult is their dynamic modeling [Mizoguchi 1992]. From micrometer to nanometer, there are hardly any attempt to investigate the dynamics of mechanisms and machines. When we go below the micro size and try to analyze or model the dynamic behavior of mechanical systems at the nanometer level, we must account for the motion due to thermal molecular agitation from the surrounding medium, which are quite pronounced in sub-micrometer domains. This thesis attempts to study the influence of thermal agitation on the dynamics of nanomachines. The nanomachines [Drexler 1992] are defined on the lines of micromachines as machines constructed of nanometer-sized mechanisms.

One such mechanism of practical importance is a nano-robotic manipulator with multi-degrees of freedom. With the advancement in nanotechnology, the realization of nano-robots is becoming a reality. The nano-robot development and application will bring the control issue in forefront and, therefore, the exploration of dynamics of nano-robots is quintessential. Nanomachines such as nano-robots will work either in vacuum or in an embedded environment of a fluid as mobile machines. For nanomachines embedded in a fluid, the thermal agitation due to the medium influences the machine movement substantially. The nanomachine itself can be regarded as a free-floating nanoparticle in a fluid. This nanoparticle is thermally agitated by fluid particles in time continuum.

The motion of small-size particles has interested many researchers and has been analyzed with novel thoughts and abstract mathematics. The English botanist Robert Brown discovered the small sized particle motion in 1827 as a physical phenomenon and it was named after him as Brownian motion [Brown 1966]. Albert Einstein derived a mathematical description of the phenomenon from the laws of physics in 1905.

Further moving down the dimensions, the dynamic behaviour of the systems starts showing quantum behaviour. The nanomachines are contiguous in size with micromachines at one-end and quantum domains at the other end. The genuine question is "Which theory, whether classical or quantum, is to be used for the analysis of nanomachines? What is the critical size of nanomachines for either of the theory to be used?" or in other words, "If quantum dynamics is to be applied to small sized objects then how small is small?"

## 1.2 HOW SMALL IS SMALL?

We know that an electron has a maximum size (diameter) of about  $10^{-18}$  m, a mass of  $9.1 \times 10^{-31}$  kg and a negative charge of  $1.602 \times 10^{-19}$  C. The nucleus of an atom is composed of a variety of particles and has a positive charge equal in magnitude to the aggregate charge of the attached electrons. The size and mass of a given nucleus depend on the number of attached electrons. The largest nuclei, typified by the Uranium nuclei, have diameters not exceeding  $10^{-13}$  m and mass in the neighborhood of  $10^{-24}$  kg.

neutrons  
Protons

A criterion for small size, in the quantum sense, can be established by considering the unusual circumstance that quantum theory frames its statement on system's observable in probabilistic terms. This represents a radical departure from classical methodology because it concedes that our knowledge of a system's state is tempered by a degree of uncertainty. Traditional dynamics takes the view that numbers defining position, momentum and so on can be computed to any degree of accuracy, and can be measured to an accuracy limited only by the physical instruments employed. However, quantum mechanics retreats from such positivist pronouncements and prefers uncertain atmosphere. This concept has been formalized into so called principle of limited certainty. The principle of limited certainty states that if the two observable measured correspond to a pair of canonically conjugate coordinates, then there exists a qualitative limitation on the accuracy to which the observable can be measured, namely

$$\Delta x \Delta p \geq h \quad (1.1)$$

where  $\Delta x$  is uncertainty in position,  $\Delta p$  is uncertainty in momentum and  $h (= 6.623 \times 10^{-34} \text{ J s})$  is Planck's constant. According to equation (1.1), the implication is that if the momentum of a rectilinearly translating particle can be determined with the ultimate precision of a vanishing deviation i.e.  $\Delta p \rightarrow 0$ , then no information is obtainable about its position ( $\Delta x \rightarrow \infty$ ) and the converse is likewise true. The principle of limited certainty confines itself to canonically conjugate variables such as position-momentum, angular displacement-angular momentum, and energy-time. It makes no statement on other pairs of simultaneous measurement in the sense that no interaction is involved if the observables are not canonically conjugate, which implies the possibility of obtaining theoretically exact measurements. Equation (1.1) is usually adopted as a quantitative gage for distinguishing between large and small in the systematic sense. In fact, it is modified as Heisenberg's uncertainty principle, which is given as [Beiser 1987]

$$\Delta x \Delta p \geq \frac{h}{4\pi} \quad (1.2)$$

The judgment is made not based on spatial size alone but because of the product of two conjugate coordinates uncertainties, which is called as action [Groesberg 1968]. As a typical example, consider the one electron atom in its lowest energy state, the



electron's radial distance from the nucleus is roughly  $0.5 \times 10^{-10}$  m and the linear momentum is of the order of  $10^{-25}$  kg m/s. The product of two conjugate coordinates namely uncertainty in position and uncertainty in momentum given by equation (1.2) is  $1 \times 10^{-34}$  J s. In contrast, consider the situation typical of electronic devices such as vacuum tubes. Here the distances of separation between electrons are of the order of  $10^{-4}$  m and potential of the order of 200 V. The momentum roughly calculable as the energy divided by the speed of light is approximately  $10^{-27}$  J s/m. The product of uncertainty in position and uncertainty in momentum is therefore  $\sim 10^{-29}$  J s which is hundred thousand times the Planck's constant. According to Groesberg, such systems can be treated satisfactorily by means of the classical theories for particles. Thus, the same sized electron qualifies as small when action is of the order of Planck's constant and large when action is substantially larger than Planck's constant.

The nanomachines as nano-robots have size  $\sim 10^{-9}$  m, mass  $\sim 10^{-22}$  kg or more and the velocities induced because of thermal agitation  $\sim 10^1$  m/s. The product of uncertainties as calculated from equation (1.2) for these values mass, size and velocity *than/* is thousand times more (then) Plank's constant, which obviously brings all the bodily entities in this size domain out of the purview of Quantum analysis. The classical dynamics is, therefore, sufficient to model the motion of nano-robots but with the inclusion of the irregular motion termed as Brownian motion because it is quite appreciable in nanodomains. In a different perspective, if the same nano-robot is seen under a high-resolution microscope, then apart from Brownian motion of whole system as a nanoparticle, there can be possible Brownian motion of every link or each degree of freedom. Brownian motion, therefore, is a significant issue in nanomachines. The importance of Brownian motion is detailed in next section.

### 1.3 IMPORTANCE OF BROWNIAN MOTION

The Brownian motion is one of the most useful stochastic processes in applied probability theory. The Brownian motion analysis and modeling has a long history involving many a luminaries like Einstein, Perrin, Smoluchwski, Langevin and Chandrasekhar to name a few [Karlin 1966]. Since its discovery, the process has been used beneficially in diverse areas as statistical testing of goodness of fit, analyzing the

price levels in stock markets, and quantum mechanics. The variations of Brownian motion like geometric Brownian motion and integrated Brownian motion have been useful in modeling random situations where one is interested in percentage change or rate of change and not the absolute change of independently and identically distributed variables [Ross 1983].

The problems in science like colloidal statistics, theory of coagulation, sedimentation problem etc. have been successfully investigated using Brownian motion model. The Brownian motion applications span from stellar dynamics [Chandrasekhar 1943] at one end of dimension to motion of motor proteins in biophysics [Julicher 1995] at the other extreme. It is worth noting that the theory has been used in Medical imaging [Chen 1989]. Barraquand [Barraquand 1990] and Arakawa [Arakawa 1994] have applied the theory in robotics for modeling terrain. The estimation of extreme floods and droughts, stock markets [Grossman 1992, Smith 1994] and manufacturing systems where queuing networks and routing problems are involved [Wien 1990] have been investigated using Brownian motion models. The Decision making [Brekke 1994], aerosol particles motion problem [Gordon 1989], membrane dynamics, biomolecular motion [Saxton 1997] are some topics from physics and life science, which have been explained by Brownian motion theory.

The Brownian motion theory has come a long way since its humble beginning in the nineteenth century. This theory covers such a vast number of interesting aspects of life without one being aware of its role. The examples cited are a mere speck of the research that has been done to date. With random and unpredictable nature of events that take place in this world, it is no wonder that researchers are yet to find perfect solutions to unresolved problems. The literature contains mainly three approaches to model the Brownian motion, which are briefly described next and the objectives of this thesis are identified.

#### 1.4 PROBLEM DESCRIPTION

There are three common approaches to obtain the Brownian motion models: (i) Diffusion equation method, (ii) Langevin equation method, and (iii) Geometric

approach using fractals concept. In diffusion equation method, different diffusion equations relating variance in position with time are used to model different types of observed diffusion modes [Saxton 1997]. This approach models almost all types of Brownian motions, without considering the properties of the Brownian-particle. Similarly, use of fractals to model Brownian motion is a geometric approach, which is being used, in contemporary research. Strikingly, both the approaches do not consider the Brownian particle properties. In the Langevin equation approach [Chandrasekhar 1943], correlation technique is used to obtain variance of physical variable of interest. The Langevin equation is formulated considering the mass of the Brownian-particle and the damping from surrounding medium. In the entire available literature on Brownian motion, the particle is assumed as rigid. The rigid body assumption implies that the motion of the particle is not influenced by the deformations of the particles caused by the applied forces.

It has been observed that in nano-domains, the bodies have low value of spring constant [Wong 1997, Roukes 2000], which is closely related to Young's modulus and represents elasticity. This suggests that local deformations of a particle are of appreciable magnitude and may affect overall motion [Singh 2003]. It is therefore not correct to exclude the influence of local deformations on overall motion. Similarly, the matter of nanoparticle has some damping (dissipative) property. The two properties of matter, elasticity and dissipative nature, are assumed implicit or negligible in available literature. This does not allow for critical observation of mechanism of transfer of thermal impact from surrounding medium. The effects of inclusion of elasticity and dissipative properties of matter in nanodomains are explored here. In order to study these effects, a mathematical model of Brownian motion of non-rigid particle is based on Langevin equation considering elastic and dissipative properties of matter in addition to mass of the particle and resistance from surrounding fluid accounted by damping coefficient. The impact transfer mechanism is explored by alterations of rigid body model and mathematical models for Brownian motion of nanoparticle have been developed using system-modeling approach. Modeling of the input, closely related to variation of Gaussian noise, is done as another approach to explore the problem.

The consideration of additional properties in the rigid body Brownian motion model is relevant, as published experimental results do not match with results obtained using available models. The present work impregnates the problem of understanding the Brownian motion of non-rigid bodies in nano-domains from two different approaches:

- **Modeling Brownian motion using impact transfer mechanism,**
- **Modeling Brownian motion using systems modeling approach,**

The developed models are subjected to validation by simulation and verification with published experimental results. The modeling of Brownian motion starts with revisiting Einstein's rigid body model in Chapter 3. The new model considers the nanomachine links and elements as a nanosized body (nanoparticle) and the nanoparticle is considered as non-rigid. Different models are developed in Chapter 3 considering nanoparticle as non-rigid using the concept of impact transfer. The various models developed in Chapter 3 are validated by simulation in Chapter 4. A lumped parameter systems modeling approach to develop further Brownian motion model is done in chapter 5. The validation of models developed using systems modeling approach and verification of valid models with published experimental results has been done. It has been found that three models of Brownian motion of non-rigid nanoparticle are valid. The three models are simulated for transient thermal noise input to develop directed diffusion mode of Brownian motion in chapter 6. The application of models developed for Brownian motion to predict the dynamics of single degree of freedom robotic manipulator is done in Chapter 7. The last chapter gives the conclusions of present thesis and the scope of future work has been highlighted.

The subject of dynamics is quite old and it is apt to trace the salient developments and present status of the field in order to get an overall picture of dynamics to be applied to nano-robots or nanomachines. This is done along with the literature review on Brownian motion in the next chapter.

If at first, the idea is not absurd, then there is no hope for it

*Albert Einstein*

## CHAPTER 2

### LITERATURE REVIEW

#### 2.1 INTRODUCTION

The literature review in this chapter is organized in two parts; one is on Brownian motion and the second is a review of various analytical models available for Brownian motion. The first part presents review on Brownian motion theory from its humble beginning in nineteenth century to the renewed interests in the Brownian motion model in nano-domains due to recent advances in nanotechnology. The later part of the chapter includes historical notes and the various models available to explore dynamic behavior of systems including models that analyze contribution of Brownian motion to overall dynamic behaviour of the system.

The Brownian motion is described in the next section to get an overall picture of status of Brownian motion theory as applied to nano-robots or nanomachines.

#### 2.2 THE BROWNIAN MOTION

Many models and algorithms have been continuously formulated for the prediction of matters involving uncertainty. One of the uncertain situations is motion of small-sized particles due to thermal agitation from surrounding medium. Robert Brown (1773-1858), a Scottish botanist has made his name for a systematic observation of this motion in his works related to botany during expeditions to New South Wales. In 1827, he observed the zigzagging motions of pollen grains under the microscope and found that small particles suspended in a fluid were in continuous motion and from his experiments; he concluded that this motion was due to the activity of collisions with the molecules of surrounding fluid. The incessant random motion of small-sized particles was named after him as Brownian motion.

Robert Brown's discovery [Brown 1966] did not receive much attention for a long time, until before the turn of 20<sup>th</sup> century when A. Einstein gave a mathematical formulation for the Brownian motion and since then Einstein's model is the most established rigid body model of Brownian motion [Einstein 1905]. Smoluchowski in 1907 [Smoluchowski 1907] and Langevin in 1908 [Langevin 1908] developed independently quantitative theories for the description of Brownian motion. The experimental work of Jean Perrin in 1908 brought it to the attention of physics world that Brownian motion constituted a clear demonstration of the existence of molecules in continuous motion. An English translation of his work appeared in 1990 [Perrin 1990]. Ito extended the mathematical formulation such that peculiarities in Brownian motion find a simple explanation in terms of general framework of stochastic processes [Ito 1964].

According to quantitative theories, bodies of micro and sub-microscopic sizes suspended in a liquid will perform irregular movement due to thermal agitation. The review of the research work done on Brownian motion is presented in next section.

### 2.3 DEVELOPMENTS IN BROWNIAN MOTION THEORY

The historical development of science of Brownian motion can be classified in four stages characterized by (i) discovery, observations and conflicts (1827-1905), (ii) theoretical predictions (1905-1908), (iii) quantitative confirmations, modeling and applications (1908-1990) and (iv) renewed interests of researchers in nanosciences in recent times. The four stages represent important turning points in the development of Brownian motion theory. In the first stage (1827-1905), the development was quite slow and scientists were struggling hard to give an explanation of the Brownian motion based on the then known physical laws. The second stage (1905-1908), though of short duration, represents remarkable developments in the Brownian motion theory. The observed phenomenon was put on firm quantitative formulation and various mathematical models were presented in the span of three years. The period was a turning point since it gave a basis to explain the phenomenon, which till that time was an observation only. This stage was followed by fine-tuning the proposed models and

applying them to explain various problems in physics. The modeling of various aspects of Brownian motion continued till the last decade of 20<sup>th</sup> century and is pursued in contemporary research. Haw has presented brief qualitative description of development of Brownian motion theory upto the late 1980's [Haw 2002]. The last one-decade also witnessed tremendous advancements in nanotechnology [Fukuda 2003] and application of Brownian motion theory in the nano-domains. The compilation of work on nano-robots by Requicha explicitly mentions the role of Brownian motion in nanomachines [Requicha 2003]. The application of Brownian motion theory in nano-domains is considered as the fourth stage. Among other developments in this stage, one important achievement is construction of working Brownian motor. The Brownian motor works with the noise energy and in principles defies second law of thermodynamics. Remarkably, the experimentalists in the first stage always argued about the impossibility of realization of Brownian motor. The construction of working Brownian motor was possible because of developments in nanotechnology. Thus, the last decade is considered as an important period in the development of Brownian motion theory and has been presented as fourth stage. A detailed stage wise review of the work is presented in following sub-section.

### **2.3.1 Stage I - Discovery, Observations and Conflicts**

A lot many discoveries in microworld followed after the invention of microscope in 1696. Almost a century after the invention of microscope, in 1827, Robert Brown examined pollen grains of a plant specie *Clarkia Pulchella*, which had a diameter of 0.3-1  $\mu\text{m}$ . The observations of Robert Brown gave detailed account of the motion of pollens in a fluid. According to Haw, Adolph Bronqniart in France made similar observations in the same year 1827 [Haw 2002]. Both Brown and Bronqniart at first assumed a living origin for motion of pollens. Brown extended his observations to numerous species belonging to different families of plants with live and dead pollens and also observed motion of powdered coal and glass in a fluid. Brown concluded that motion of particles occurred in every thing he picked, provided it was reducible to a powder, sufficiently fine to suspend in water.

Subsequent to the discovery of the motion of small-sized bodies, which in meantime was named as Brownian motion, there was confusion among scientist as to the cause of motion. The researchers argued in favor of external forces, such as vibration, microscopic currents, thermal gradients, temperature variations and surface tension as possible causes of Brown motion. According to Nye, even after seventy years, it was claimed that motion was due to temperature difference [Nye 1973]. One vital development in the period was that Brownian motion was brought out of the realm of Biology and the quest to explain Brownian motion was pursued in physics.

Powles had given a brief account of developments on Brownian motion from its observation in 1827 till Einstein's mathematical formulation in 1905 [Powles1978]. According to Powles, the publication of Leon Guoy in late 1880 based on the series of experiments carried out by Guoy himself demonstrated convincingly that Brownian motion was not a result of external vibrations, temperature gradients or surface tension. Rather, it was found to be a fundamental physical property of fluid to initiate such motion. Guoy (1895) also tried to establish breakdown of second law of thermodynamics in sub-micro domains. Although Guoy's work was an important step in the development of Brownian motion theory, the scientists were not convinced by the propositions forwarded by Guoy. As mentioned by Powles, scientists like Ostwald (1895) opposed vehemently the hypothesis of any theory breaking down the second law of thermodynamics in sub-micro domains. The main argument of Ostwald to reject the hypothesis was that the concept couldn't be experimentally verified. The reason was good enough at that time and remarkably it took a little more than a complete century to develop Brownian motors to experimentally verify the proposition of Guoy.

At the beginning of 20<sup>th</sup> century, the confusion was so deep, that even when Albert Einstein gave first mathematical formulation of Brownian motion, he was quite coy about explicitly connecting his theoretical ideas with Brownian motion. The period of three years after the first publication of Einstein model was important because three theoretical models on Brownian motion were published in that period giving a quantitative basis to the phenomenon. This is considered as second stage of Brownian motion theory.



### 2.3.2 Stage II - Theoretical Formulations

Tremendous amount of scientific activities in 19<sup>th</sup> century led to a better understanding of physical world, which became the foundation for propositions of mathematical models of Brownian motion. In the year 1872, Ludwig Boltzman published the Boltzman equation for gaseous system giving a mathematical formulation of non-equilibrium aspect of statistical mechanics. The Boltzman equation based on molecular-kinetic theory gave the forces governing collisions between molecules in rarified gas medium.

Einstein at the beginning of 20<sup>th</sup> century took the cue from the Boltzman's work. He reasoned that as heat is attributed to irregular motion of atoms, the thermal motion of fluid molecule must be transmitted to a small-sized particle floating in the fluid. An intuitive thought of observation of such motion occurred to Einstein without the knowledge that Robert Brown had already observed the motion. Einstein obtained the expression for motion of the particle in terms of expected values [Einstein 1905]. He introduced a parameter diffusion coefficient and related the new parameter as time function of expected value of displacement of small-sized particles.

M. Von Smoluchowski obtained almost same expression as Einstein for the time dependence of displacement of Brownian particles, though with a different coefficient [Smoluchowski 1907]. As compared to Einstein's formulation, the model developed by Smoluchowski was quite complex and based on rigorous probabilistic theory. Smoluchowski introduced the term probability after-effects and transition probability. He gave one important argument against the molecular origins of irregular motion of particles, that is, any molecular impact could never give a strong enough push to generate the observed displacement.

This argument was proved to be erroneous by P. Langevin, who derived the time dependence of displacement of Brownian particle in a spectacularly simple and direct form [Langevin 1908]. The Langevin formulation modified the Newton's force balance equation, the first law of motion, by including a stochastic force term. The added stochastic force represented the random impacts of surrounding medium molecules on

Brownian particle. Langevin concluded the need for exploration of resistive force, which he assumed to follow Stokes law. The exploration of resistive force had been the main subject of research in third stage of Brownian motion, where various models for resistive force have been presented.

### 2.3.3 Stage III - Quantitative Confirmations, Modeling and Applications

According to Wiener, in Brownian motion, the random impacts from molecules of surrounding medium causes a stochastic driving force responsible for fluctuating motion of small-sized particle [Wiener 1923]. The resistance to Brownian motion also was caused by the random impacts resulting into dissipation of energy of impacts. Nyquist used the fluctuation and dissipation in Brownian motion to predict the characteristics of noise intrinsic to the system [Nyquist 1929]. Uhlenbeck also observed that fluctuation and dissipation are two aspects of Brownian motion and are related to each other [Uhlenbeck 1930]. The fluctuation-dissipation phenomenon was further used to derive the resistance from the medium [Onsager 1931].

From fluctuation-dissipation concept, Wiener proposed that surrounding medium is the source and sink of the motion [Wiener 1938]. Undoubtedly, therefore, the focus of modeling was on the forces coming from the surrounding medium. The friction force, for example, had been extensively investigated by a number of researchers since Langevin formulation of Brownian motion. The friction force from medium with Stokes approximation has been used at normal temperature and pressure condition and was found to be in good agreement with experimental observations [Uhlenbeck 1930]. There exists an instantaneous time correlation between force acting on the Brownian particle and its velocity in Stokes approximation and is used in contemporary research for viscous fluids. At low-pressure condition, Uhlenbeck proposed that the friction is given by Doppler equation. Chandrasekhar has used the Stokes approximation while applying Brownian motion theory to stellar dynamics, sedimentation problem and coagulation theory [Chandrasekhar 1943]. He had reviewed various aspects and applications of Brownian motion theory. His work was reprinted as a classic in 1959 [Wax 1959]. Wang described some unresolved problems in the theory of Brownian motion [Wang 1945].

The Brownian motion is categorized by different modes given by Diffusion equation for different parametric values. In diffusion mode termed as Wiener process [Wiener 1949], the parameter mean in position is zero and variance in position is constant. This is also known as Normal Diffusion mode and exactly resembles the Einstein's model. Wiener compared Brownian motion with a random walk event. He had shown that random walk in the limiting case of step size and step time tending to zero is like Brownian motion. The modeling of Brownian motion is based on the two basic assumptions: (i) The driving force is Gaussian and (ii) its correlation in time is instantaneous. Such processes, for which the correlation of physical variables is instantaneous, are called Markovian process. Chandrasekhar proposed that stellar dynamics is analogous to Brownian motion and applied the Brownian motion theory to explain many stellar phenomenons [Chandrasekhar 1949].

The concept of fluctuation-dissipation was further established in different works. Callen made a quantum formulation of fluctuation-dissipation theorem [Callen 1951]. Takahashi made a classical formulation of fluctuation-dissipation theory following the Gibb's formulation of entropy [Takahashi 1952]. Cox has treated Brownian motion from the point of view of statistical theory of irreversible processes [Cox 1952]. The treatment resembles the method of Callen in introducing statistical mechanics but differs from Callen's work, which adopts the general method of Gibb's entropy formulation.

Brownian motion by that time was studied mostly in quiescent fluids or under uniform velocity. Taylor for the first time investigated the coupling effect of flow of fluid and Brownian motion [Taylor 1953]. He had shown the enhancement of diffusion in the direction of flow. In another type of application, Gross had studied the effect of Brownian motion on radiation of the particles [Gross 1955]. Gross obtained a model of spectral line of radiating particles assuming that the position of the particle remains unchanged after impact. Sack had shown that generalized Liouville equation could be simplified by a Fourier transformation with regard to velocities and could be used effectively to model Brownian motion [Sack 1956].

Landau introduced the Boussineq-Basset correction to the Stokes assumption of friction force [Landau 1960]. The correction led to a non-instantaneous correlation between force and velocity. The velocities and, thus, position of the particle were shown to be correlated over large time. Kursnoglou, while doing research on plasma, formulated Brownian motion model of electrons and ions in plasma across magnetic field with the anisotropic friction assumption [Kursnoglou 1963]. He had shown that there was enhancement in diffusion due to the anisotropic assumption of friction force. Considerable parallel efforts were being made to obtain a Brownian motion model from Liouville equation. The first rigorous analysis to obtain Brownian motion from Liouville equation was by Lebowitz [Lebowitz 1963]. Subsequently, Resibois applied expansion series for including higher order correlations in Liouville equation approach and extended the work of Lebowitz [Resibois 1964]. Berne has assumed an exponential decaying time correlation of driving force and has demonstrated that it is possible to obtain higher diffusion coefficients in viscoelastic medium [Berne 1966]. Williamson had derived the Brownian motion of a particle less massive than the fluid particles [Williamson 1968]. He had used Ornstein-Uhlenbeck model and had shown that variance in position of a less massive particle could be obtained without any additional approximation to a good accuracy. Extending the work of Resibois, Fokker-Planck equation was derived by Cuckier for a heavy Brownian particle in a dense fluid from the Liouville equation [Cuckier 1969].

Fox had analyzed the Brownian motion with non-Gaussian and non-Markovian forces on arbitrary shaped Brownian particles [Fox 1970]. Stokes law for the friction was generalized to arbitrary frequency, compressibility and viscoelasticity of the fluid [Zwanzig 1970]. The persistence of correlation had been studied by Case giving a general form of friction term using relaxation concept [Case 1971]. In the theory of relaxation, it is assumed that a physical system subjected to weak external force resumes its equilibrium state exponentially. Montgomery had shown that approach of kinetic theory developed by Boltzman in 1872 in general can be applied to Brownian motion as other approaches do [Montgomery 1971].

Chow had shown that a more accurate diffusion coefficient value could be obtained in comparison to other approximations by including an inertial term in autocorrelation of stochastic force [Chow 1972]. Kato has studied the resistive forces in polymeric solutions [Kato 1972]. In the pursuit to study the effect of flow conditions on Brownian motion, the two-dimensional convection flow effects on Brownian motion had been explored by McCarty [McCarty1973]. The enhancement in diffusion coefficient due to oscillatory flows had been shown by Haugh [Haugh 1973]. Dufty has extended the study on friction force modeling by investigating the decay of non-instantaneous correlation in velocity and hence position [Dufty 1974]. The corrections in friction term given by Dufty led to conclusion that correlation decays slower than and not as fast as predicted by earlier work. Arnold gave models for various modes of diffusion and has defined Wiener process with drift, which has constant mean and variance in position [Arnold 1974]. Szu had obtained elastic displacement space-time correlation function for a Brownian particle using relaxation theory [Szu 1975]. Zwanzig has studied compressibility effects of the surrounding medium on Brownian motion [Zwanzig 1975]. Jasnow had solved the Langevin equation introducing stochastic resistance concept in place of deterministic Stokes approximation of resistance [Jasnow 1975]. The stochastic model of fluid resistance was an attempt to realize changing viscosity in binary or a mixture of fluids constituting the surrounding medium. Harris had obtained the diffusion coefficient for a Brownian particle utilizing non-equilibrium statistical mechanics concepts [Harris 1976]. Mehaffey obtained Stokes-Einstein law giving diffusion coefficient of Brownian particle from solution of Navier-Stokes equations with the boundary condition that fluid sticks to the sphere's surface [Mehaffey 1977]. Frisch had obtained Fokker-Planck equation from the solution of the dynamic inverse of Liouville equation [Frisch 1979].

Another point of investigation in Brownian motion was consideration of surrounding medium as inhomogeneous. Brownian particle travels through distinct diffusion areas of various sizes and geometrical arrangements in heterogeneous environment. Foister had worked effect of several types of flow on Brownian motion [Foister 1980]. The main effect of the flow found by Foister was to change the time

dependence of the variance of the position along the flow from linear to cubic. Foister also presented a brief qualitative discussion on presence of boundary walls. Broeck had investigated longitudinal diffusion in uniaxial flows [Broeck 1982]. Broeck considered elastic properties in addition to the viscosity in modeling the surrounding medium. The viscoelastic model represents Maxwellian fluids or Non-Newtonian fluids and are characterized by two parameters namely; relaxation time and viscosity. Marshall had discussed the relative merits of Boltzman entropy and Gibb's entropy for describing Brownian motion and concluded that Gibb's entropy is a superior concept [Marshall 1982]. Marshall had also presented a historical development of the Boltzman work on second law of thermodynamics. Fernandez de la Mora [Fernandez 1982] had generalized the Brownian motion Fokker-Planck model from the particle suspended in a rarified gas to the case of non-homogenous dense gas mixture. It was shown by Fernandez that diffusion attributed to non-homogeneity of the gas-velocity field were small in comparison to the shear force contribution to diffusion due to relative gas-particle velocity.

A new concept of fractals was presented by Mandelbrot to model uncertainty in nature [Mandelbrot 1982]. The contemporary research is also applying fractal concept as a major approach to model Brownian motion. The fractal model uses the fractal dimension to simulate the Brownian motion. In another development, Modak had derived the relation representing fluctuation-dissipation theorem for a free Brownian particle from first principles using a simple model for the collision of fluid molecules with Brownian particle [Modak 1984]. Sparling had shown that relative importance of fluid inertia, compressibility and viscoelasticity on Brownian motion depend on size of Brownian particle [Sparling 1984]. The effect on diffusion due to spatially periodic hydrodynamic flow has been studied by Sagues [Sagues 1986]. In the year 1986, a review on Brownian motion theory was published [Kubo 1986]. Shariman had carried out investigations in special types of flow like flow in Rayleigh-Benard convection cell [Shariman 1987]. Rodriguez had shown that diffusion is enhanced for Maxwellian fluids with Stokes approximation of friction [Rodriguez 1988]. He showed that the diffusion is less in Maxwellian fluids in comparison to Newtonian fluid with Bossineq-

Basset correction to friction term. Ryskin had shown that diffusion in a rotating fluid is anisotropic and smaller than in a fluid at rest [Ryskin 1988]. Applied to ultracentrifuge, it was shown that diffusion of biomolecules decreased by 50% in comparison to steady flow conditions. On the observation of Brownian motion, Kruglak has presented a simple laboratory experiment using video microscopy [Kruglak 1988]. Rull calculated diffusion coefficient of a Brownian particle immersed in a Lennard-Jones fluid [Rull 1989]. He had shown that diffusion coefficient is independent of the mass when the Brownian particle has the same volume, as the solvent particle and only a weak mass-dependence appears when the volume of Brownian particle is increased.

The Brownian particle inertia has been included in standard methods using Liouville equation [Sack 1956] and Langevin equation [Chandrasekhar 1943, Wang 1945]. Gross has discussed a number of possible types of collisions [Gross 1955]. He categorized collisions on the basis of mass and size of surrounding medium particles and the floating Brownian particle viz: (i) small collisions where surrounding medium particle are much smaller than floating particle (ii) large collision where surrounding medium particle are considerably larger than floating particle and (iii) very large collisions where the surrounding medium particle are disproportionately larger than floating particle.

The next important stage in Brownian motion is an overlap of conventional modeling on Brownian motion and application of Brownian motion theory in nano-domains. The review of work in this last stage is presented next.

#### **2.3.4 Stage IV-Brownian Motion in Nano-domains**

Atomic force microscopy (AFM) technique for surface characterization at atomic scales was developed in mid-eighties [Bining 1985], which has brought revolutionary advancement in nanotechnology and has opened new frontiers in science. In the AFM technique, an atomic tip is attached to a freely vibrating cantilever, which is used to scan the surface and is also used as nano-robotic arm [Ratner 2003]. The Brownian motion of freely vibrating cantilever near a clean solid surface under ultrahigh vacuum conditions has been investigated by Dorofeyev [Dorofeyev 1999]. He

used the concept of Brownian motion of a microparticle under the action of thermal fluctuating electromagnetic field. The Brownian motion represents the uncontrollable motion, which puts a limit on the spatial accuracy of manipulation. In the AFM technique, the nano-robotic manipulations are done using macro-sized auxiliary mechanisms. The realization of nanometer-sized nano-robots is hotly pursued in contemporary research.

Recently, the demonstration of working nanomotors to be used as nanoactuators in nanomachines has brought possibility of making nano-robots a step closer to its realization. The nanomotors are based on Brownian motion theory and are also called as Brownian motors. They work on the concept that it is possible to produce work from unbiased microscopic fluctuations. The first explanation principle of Brownian motors, now known as nanomotors, is credited to Smoluchowski [Smoluchowski 1907]. The principle was revisited and further clarified by Feynman [Feynman 1963]. Magnasco showed that Brownian particles subject to an external force having time correlation could exhibit a non-zero drift speed [Magnasco 1993]. The work of Magnasco became the foundation stone for realization of Brownian motors. Rousselet experimentally showed a biased motion of Brownian particle [Rousselet 1994]. Austumian developed a model on biased motion of Brownian particle [Austumian 1994]. The biased motion also called as rectified or direction motion of Brownian particle was further studied in the presence of periodic potential by Chauwin [Chauwin 1995]. Chen had shown that directional motion depends not only on the length of asymmetric potential in a cycle but also on the shape of potential function [Chen 1999].

Directional Brownian motion was used to analyze the motor protein motion by Fox [Fox 2001]. Motor proteins are enzymes responsible for transport of biological material in living organisms. Lyshevski discussed various key problems in modeling, analysis, simulation and controls of nanobiomotors [Lyshevski 2001] and then in next year developed various models on nanobiomotors [Lyshevski 2002]. Lee developed an analytically solvable Brownian motor model [Lee 2003] while Wang discussed mathematical theory and properties of nanomotors and presented a mathematical framework for extracting motor potential profile from measured time series of motor



position [Wang 2003]. Fennimore had reported fabrication and successful operation of a fully synthetic nanometer scale electromechanical actuator [Fennimore 2003]. Girish has presented a review on Brownian actuator models and related problems [Girish 2004].

The research on the conventional side of Brownian motion modeling also continued simultaneously in Stage IV, where a lot of work started on modeling of Brownian motion with fractal concept. Several methods were developed and presented to estimate fractal dimension of Brownian motion [Zhang 1990]. Fractal dimension provides a way to measure roughness of fractal curves representing Brownian motion [Bransley 1993]. The fractals is a geometric model and is deficient in giving physical interpretation to Brownian motion, but has been helpful in analyzing wider class of stochastic problems in comparison to other approaches.

Birdsall had reviewed early attempts to incorporate Lorentz force in Brownian motion model in environment inside magnetic fusion devices; semiconductors processing chambers and planetary magnetosphere that show Brownian motion coupling with magnetic fields [Birdsall 1991]. In the various models reviewed by Birdsall, the coupling has been modeled by adding Lorentz force in the Brownian motion model given by Uhlenbeck. Meanwhile, Verga investigated the Brownian motion in a fixed area using method of functional integration [Verga 1991]. Before Trefan, there were two distinct but related formalisms of Brownian motion: (i) Langevin equation, which is stochastic and (ii) Fokker-Planck equation, which is equation of evolution for the probability distribution that leads to deterministic partial differential equation [Trefan 1992]. Both the formalisms are based on the assumption of randomness at initial stages of development. Trefan had derived the traditional description of Brownian motion relating chaos at the microscopic level to the statistical behavior at the macroscopic level and that too without resorting to randomness assumption. The input modeling had been done by Koyama considering generalized Lorentzian spectrum in place of instantaneous Gaussian noise spectrum [Koyama 1992]. Koyama concluded that a randomly activated system in the steady state could be modeled by spectrum termed as  $1/f$  noise spectrum, where  $f$  is frequency in Hz.

The contemporary research of Knobloch in the direction to explore coupling between Brownian motion and flow condition had shown that diffusion enhances in oscillatory flows and confirmed the results of Haugh published long back in 1973 [Knobloch 1992]. Clercx investigated Brownian motion in shear flow with a harmonic potential present as an external force [Clercx 1992]. He had shown that variance in position is strongly influenced by backflow effects in the fluid resulting in non-instantaneous correlation in velocity of the particle. Wang had shown the existence of a non-instantaneous correlation of driving force for anomalous diffusion [Wang 1992]. Xiang investigated Brownian motion of charged particle in a stochastic magnetic field [Xiang 1993]. Gillespie had given a continuous time random walk model, which was called as Jump-Markov process and the predictions from his model have been found to precisely duplicate the Langevin equation model [Gillespie 1993]. A simple model of one-dimensional Brownian motion of single particle in a singular potential field had been proposed by Ouyang [Ouyang 1994]. The model explores  $1/f$  noise in place of white noise as cause of Brownian motion.

Gillespie had given a numerical simulation algorithm that yields exact solution of Brownian motion model [Gillespie 1996(i)]. In another work same year, Gillespie gave a simple explanation of continuous Markov process clarifying the mathematical connection between the two very different approaches to Brownian motion taken by Einstein and Langevin [Gillespie 1996 (ii)]. Hernandez-Contreras modeled the translational and rotational Brownian motion of a non-spherical particle with surrounding medium composed of spherical particles [Hernandez 1996]. Raikher had studied a two-dimensional rotational Brownian motion in Maxwellian fluid [Raikher 1996] and Katayama solved the stochastic equation to study Brownian motion under a steady homogenous flow and presented the analysis of the effect of shear on Brownian motion of free particle in more explicit and pedagogical way in comparison to earlier works [Katayama 1996].

Chow had shown anomalous diffusion of microstructures on quenched surfaces because of correlated non-Gaussian noise [Chow 1997]. The modeling of diffusion coefficient has enabled analysis of some special modes of Brownian motion observed in

bio-species [Saxton 1997]. The anomalous diffusion [Bouchard 1990, Fedder 1996] and Corralled motion [Saxton 1990, Kusumi 1996] are such special modes, which have been investigated extensively. Srokowski solved the Langevin equation with the stochastic force having a correlation inversely proportion to time [Srokowski 1998]. Leggas observed the Brownian motion of red blood cell (RBC) in flowing blood and found that motion is anomalous mode of diffusion [Leggas 1999] while Lemons obtained an exact solution to coupled Brownian motion model of a charged particle in a steady uniform magnetic field [Lemons1999].

The Ornstein-Uhlenbeck model of Brownian motion [Uhlenbeck 1930] has been modified considering mean in position to be proportional to displacement and the variance in position to be constant by Grimmett [2000]. In another research, a viscoelastic model of surrounding medium is presented by Nemoto [Nemoto 2000] to investigate bio-species motion using passive mechanical elements viz spring and dashpot. The approach is quite simple and promising but needs further exploration as concluded by the investigations of Nemoto. A three-dimensional non-Markovian rotational Brownian motion model had been reported for axisymmetric particles moving in Maxwell fluids by Volkov [Volkov 2001]. Mori had developed a projection operator method for the statistical formulation of chaotic or turbulent transport and has transformed the deterministic non-linear equation to a stochastic equation modeling Brownian motion [Mori 2001]. Czopnik extended the work on Brownian motion in magnetic field describing the stochastic process completely [Czopnik2001] while Srokowski extended his earlier work using various types of colored noise expressed as Kangaroo-process to explore generalized Langevin equation [Srokowski 2001]. Cao has confirmed the earlier observations on Brownian motion in heterogeneous surrounding medium comprising of many ingredients [Cao 2001] and Piasceski has extended the study to investigate inhomogeneous medium with unequal temperature and density [Piasceski 2002]. These studies have shown that Brownian motion is non-markovian in an inhomogeneous environment. Lim studied some Gaussian-models for anomalous diffusion [Lim 2002]. The study indicated that single parameter description commonly used in earlier works on anomalous diffusion is insufficient to characterize the

underlying mechanism. The recent work of Benesch improves on the theory of Brownian motion in confinement [Benesch 2003].

The investigation of the motion of Brownian particles, which have the ability to take up energy from the environment, to store it at an internal depot, and convert internal energy into kinetic energy, had been done by Schweitzer [Schweitzer 1998]. The developed model adds an extra acceleration term in Langevin equation. Schweitzer has discussed the model in context to biospecies where external supply of energy is crucial to maintain metabolism. Deng has introduced the concept of active Brownian particles, which refers to the particles that can store energy [Deng 2004]; the stored energy can be used for active motion of the particle and has potential application to motion of biological and social swarms. He had used stochastic averaging for quasi-integrable Hamiltonian system representing stationary distribution for the motion of active Brownian particles.

The work of Schweitzer and Deng suggests the storage of energy by Brownian particle. Schweitzer model is simple to understand and is based on energy balance equation. Deng had given a complicated mathematical model of active Brownian particle motion. Neither of the work talks of storage of thermal energy. A review on Brownian motors in the present chapter in Section 2.3.4 suggests that thermal energy can be utilized effectively. A storage device can store thermal impact energy and can utilize that in the motion.

Moreover, in nano-size regime, the surrounding particles become considerably similar and comparable, in size to floating nanoparticle. It is possible to attain extremely high fundamental frequencies while simultaneously preserving very small spring constants in nano-domains [Roukes 2000]. It has been observed also that the nanoparticles have low values of spring constant  $k$  [Wong 1997] and not infinite as in case of rigid body model of nanoparticle, which suggests that in nano-domains, local deformations are of appreciable magnitude and must affect overall motion. Therefore, the additional property like elasticity represented by spring constant should be included in nanoparticle motion modeling. The analysis of motion assumes particle to be rigid in

the entire literature available on Brownian motion. The rigid body assumption implies that the motion of the body is not influenced by the deformations of the particles caused by the applied forces, which is contrary to suggestions emerging in nano-domains. In order to develop non-rigid models, impact transfer models have been developed [Sharma 2004(i)] and general approach of systems-modeling has been used to develop models for non-rigid nanoparticle Brownian motion [Sharma 2004 (ii)]. A modeling of input in non-rigid models has been attempted [Sharma 2003 (ii)]. All these developments are discussed in detail in this thesis. In order to attempt to model for dynamics of nano-robotic manipulator attributable to thermal agitation, the major approaches to dynamics are detailed next.

## 2.4 REVIEW OF DYNAMIC MODELING

The science of dynamics has its objective of study of motion of material bodies, and its aim is to describe the facts concerning the motion [Kittel 1981]. The modeling of dynamics has a long history of development dating back to the era of Greek and Roman civilizations, which proposed theoretical hypotheses concerning the relationship between force and motion.

The postulates in dynamics have been evolved through seventeenth to twentieth century to take present days shape. Initial developments were in two distinct parts, one was for describing terrestrial bodies such as projectile or a pendulum, and the other was for dealing with celestial bodies, in particular the planets. Sir Issac Newton brought these two apparently distinct approaches together, whose book *Principia Philosophiae* (1686) is rightly acknowledged as the first complete formulation of classical theory of dynamics. The theory today stands well developed to be applied to a very wide range of physical situations. Some concepts have been clarified and others have been added with the passage of time.

A new scientific thinking of relativity emerged in the first part of twentieth century, which tried to discard Newton's theory. The concepts of space-time relationship were introduced. A new theory of gravitation put forward the involved concepts of curved space. These were a shock to generation that had been schooled on

the Euclidean space concept. Quantum theory was an additional blow to Newton's formulation. But, these new theories of relativity and quantum mechanics were found to be supplementing Newton's classical dynamic theory [Blinder 1974, Taylor 1976].

Newton's formulation builds up with the definition of force. Force being a vector quantity, the Newton's approach to dynamics becomes cumbersome and difficult to be applied to multi-degree of freedom dynamic systems. The other formulations like Lagrange-Euler (1759) and Newton-Euler (1744) were developed which ensured the analysis of complex dynamic system in an easier way. The Lagrange-Euler formulation is a scalar approach to dynamics and builds upon two concepts namely, work and equilibrium. Since dealing with scalar quantities is easier, the approach is well suited for multi-degree of freedom systems where vector approach can be difficult. Bernoulli (1749) proposed a principle that described the equilibrium of static system in terms of work components, and D'Alembert (1750) extended the principle to include dynamic systems. Lagrange used these postulates as foundation to complete the energy based formulation of dynamics [Goldstein 2002], which for an  $n$  degree of freedom system is

$$\frac{d}{dt} \left( \frac{\partial \Delta}{\partial \dot{q}_i} \right) - \left( \frac{\partial \Delta}{\partial q_i} \right) = \tau_i \quad (2.1)$$

where  $i = 1, 2, \dots$ , and  $\Delta = KE - PE$  is known as Lagrangian or Kinetic potential of the system; KE is the kinetic energy and PE is the potential energy of the system;  $q_i$  is the  $i^{\text{th}}$  generalized coordinate and  $\tau_i$  is the generalized force at  $i^{\text{th}}$  degree of freedom. Another useful model found in literature is Hamiltonian formulation and is presented in Housner [Housner 1961]. The Hamiltonian approach considers some property of the dynamic system over its entire motion to be maximum or minimum. This concept is a further step over scalar dynamics of Lagrange-Euler. According to Groesberg, it is possible to analyze dynamic systems using Hamiltonian approach where very little information is available about the system and other approaches fail [Groesberg 1968].

The nano-dynamics is governed by classical model with substantial contribution from stochastic forcing due to thermal agitation from surrounding medium [Fujimasa 1996]. The major approaches to model Brownian motion are briefed in next part.

## 2.5 ANALYTICAL APPROACHES TO MODEL BROWNIAN MOTION

In a dilute solution; there is a process of diffusion<sup>1</sup> of solute, which is caused by the Brownian motion of the suspended molecules. Another process proceeding in the opposite direction of the diffusion also occurs and is known as Osmosis<sup>2</sup>.

A mathematical modeling of this phenomenon, based on the kinetic molecular theory of heat, gives an expression for the diffusion coefficient. This coefficient was found to be independent of the nature of the solution except for the viscosity of the solvent and for the size of the solute molecules.

The unpredictable and irregular features of Brownian motion come under the purview of broader area of stochastic processes [Karlin 1966]. There are three major approaches to the problem emerging from literature review done in the present chapter namely: (i) Langevin Equation (ii) Diffusion Equation and (iii) Geometric approach using fractal concept.

In Langevin equation approach, the attention is focused on the actual random variation in time of the displacement, or voltage or whichever variable of the system, one is interested in. According to Wang, the method has been applied systematically to a whole series of problems and is also known as Fourier series method [Wang 1945]. In modeling of Brownian motion, the spectrum can be found from Langevin equation. For free particle, which is defined as, not bound by any external force, the Langevin equation is given as [Papoulis 1991]

$$m \frac{dv}{dt} = -fv + F(t) + F_e(t) \quad (2.2)$$

where  $m$  is the mass of particle,  $f$  is the damping coefficient of the surrounding fluid and  $v$  is the velocity of the particle,  $F(t)$  and  $F_e(t)$  are external forces of stochastic and deterministic nature, respectively.

---

<sup>1</sup> Diffusion: A process of interpenetration between two substances without chemical combination, by the natural movement of the particles.

<sup>2</sup> Osmosis: It is the passage of solvent from a less concentrated into a more concentrated solution through a semi-permeable membrane i.e. permeable to the solvent but not to the solution.

According to Ochi, a time domain solution of equation (2.2) using convolution integrals is termed as correlation technique of solving stochastic differential equations [Ochi 1990]. The correlation technique and the application of the technique to free particle are detailed in Appendix I. The response to stochastic force can be obtained in terms of variance in position, denoted by  $E\{x^2(t)\}$ , using correlation technique, where  $x(t)$  represents the position of the particle at time  $t$ .

In correlation technique, the first step is to obtain the autocorrelation of the driving force by taking Fourier transform of the spectrum of the driving force. The autocorrelation is the expected value of the product of a physical variable at two instances of time. The expected value of the product at same time is known as variance of the variable. Once the autocorrelation is obtained, the next step is to get cross-correlation between the driving force and the position of the particle, which is obtained by evaluating convolution integral between autocorrelation of driving force and the impulse response of the dynamic system. Further convolution of cross-correlation with impulse response of the system yields the autocorrelation of the position of the particle. The variance in position can be obtained considering two instances of time in autocorrelation of the position to be same time. For a free particle, the variance is given as (Refer Appendix I for details)

$$E\{x^2(t)\} = \frac{\alpha}{2\beta^3} (1 - e^{-\beta t}) (2\beta t - 1 + e^{-\beta t}) \quad (2.3) \leftarrow$$

where 
$$\alpha = \frac{2\kappa T f}{m^2} \quad (2.4)$$

with  $\kappa = 1.3807 \times 10^{-23} \text{ J/K}$  as the Boltzman's constant,  $\beta = f/m$  and  $T$  as absolute temperature. The model given by equation (2.3) is called as Ornstein-Uhlenbeck model and is the Brownian motion model of a rigid small-sized particle. Substituting  $t \gg 1/\beta$  in the equation. (2.3) renders the exponential terms as negligible and the model reduce to Einstein's model [Einstein 1905], that is:

$$E\{x^2(t)\} = \frac{\alpha t}{\beta^2} \quad (2.5) \leftarrow$$



The Einstein's model, equation (2.5), is a linear variation of variance in position of Brownian particle with respect to time. The Ornstein-Uhlenbeck model is the most established rigid body model of Brownian motion and will be used for comparison with non-rigid Brownian motion models developed in this work.

## 2.6 EPILOGUE

The present chapter reviewed the development of Brownian motion theory since the observation of Brownian motion in 1827 with a view to identify the need for investigation on Brownian motion in nano-domains. The recent advancement in nanotechnology has revived interest in Brownian motion in nano-domains. The review further contained citation of developments on nanodevices using Brownian motion. A note on dynamics attributable to Brownian motion approached from classical dynamics was elaborated.

The later part of the chapter contained a review of major approaches to model Brownian motion and identification of non-rigidity as a matter of concern in nano-domains. The properties like, elasticity and dissipation of surrounding medium have been modeled and explored extensively by many researchers but the floating Brownian particle is assumed rigid in available literature. Since the surrounding medium molecule and nanoparticle are similar in nano-domains, it suggests that elasticity and dissipative properties of nanoparticle should also be considered in motion analysis. As the Langevin equation approach considers properties of particle and medium, it is used to develop the new models of Brownian motion in nano-domains.

As the first approach to develop Brownian motion models of non-rigid nanoparticle, an impact transfer model is obtained for Ornstein-Uhlenbeck Brownian motion model in next chapter. A few alterations of the Ornstein-Uhlenbeck's rigid body model with inclusion of non-rigidity and dissipative properties are attempted to develop the Brownian motion model of non-rigid nanoparticle in next chapter.

Ignorance more frequently begets confidence than does knowledge:  
it is those who know little, and not those who know much,  
who so positively assert that this or that problem will never be solved by science

*Charles Darwin*

## CHAPTER 3

# **IMPACT PROCESS MODELING OF BROWNIAN MOTION OF NANO-SIZED BODIES**

## **3.1 INTRODUCTION**

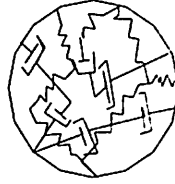
In the previous chapter, it was pointed out that non-rigidity of nanoparticle is a matter of concern in nano-domains. The effect of inclusion of non-rigidity of nanoparticle on Brownian motion needs to be explored. As the first approach to include the non-rigidity of nanoparticle, the Brownian motion model is investigated from the viewpoint of impact process. The models for impact process in rigid and non-rigid body are developed in this chapter. The impact transfer in rigid body model is developed first. The non-rigid model is developed by exploring possible variations of the impact process in rigid body model required for including elastic and dissipative properties of nanoparticle. The next section presents the non-rigid model of nanoparticle.

## **3.2 MODEL OF NANOPARTICLE**

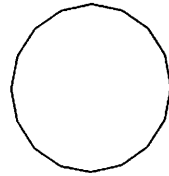
The Brownian motion of small-sized particle in a fluid is because of continuous random impacts from the surrounding medium. It is assumed that impacts occur from all directions and are impulsive in nature. The small-sized particle is non-rigid in nano-domains. The model of nanoparticle is given in next section.

### **3.2.1 Non-Rigid Nanoparticle Model**

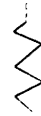
In rigid body models, the nanoparticle is modeled as a sphere of radius  $r$  and proof mass  $m$  and it is assumed to have no elasticity and dissipative properties. In reality, the nanoparticle consisting of large number of atoms can be modeled as a combination of number of spring-mass-dashpot systems oriented or attached randomly in the spherical space as shown in Fig. 3.1(i).



(i) Nanoparticle Consisting of Number of Spring-Mass-Dashpot Systems



Mass ( $m$ )



Spring ( $k$ )



Damper ( $f'$ )

(ii) Three Lumped Parameters of a Nanoparticle

**Fig. 3.1** Model of Nanoparticle and its Lumped Parameters

In a lumped parameter model, the proof mass of nanoparticle  $m$  is the lumped mass of all mass elements (matter). Similarly, equivalent structural/hysteretic damping is represented by the lumped coefficient  $f'$  and lumped spring constant is  $k$  as shown in Fig. 3.1(ii). The damping coefficient of nanoparticle is represented by  $f'$  because  $f$  is widely used in literature to represent damping characteristics of surrounding medium. The rigid body model of nanoparticle has only mass corresponding to a matter having perfect rigidity ( $k = \infty$ ) and non-dissipative nature ( $f' = 0$ ). The simplified rigid body model of nanoparticle has been analyzed widely in the available literature. In the present work, the non-rigid model of nanoparticle that includes passive elements  $k$  and  $f'$  accounting for elastic and dissipative behavior of matter, is considered.

### 3.2.2 Impact Transfer Process

Consider a non-rigid nanoparticle and assume it receives only one impact from some random direction. The nanoparticle being non-rigid will be deformed i.e. the nanoparticle will get compressed at the impact site. This is considered as local motion of the nanoparticle. The nanoparticle will also move (get displaced) from its location. This is considered as global motion of the nanoparticle. In the rigid body model, there is no local motion. The non-rigid nanoparticle will experience resistance to both global and local motions. The resistance to global motion is offered by the damping

characteristics of the surrounding medium, while the resistance to local motion is due to dissipative properties of nanoparticle. It is logical to assume that there is a coupling of the resistance offered by the medium and nanoparticle to global and local motions of nanoparticle. The resistance to global motion from surrounding medium has been explored extensively and is briefly described in next section.

### 3.3 RESISTANCE TO GLOBAL MOTION OF NANOPARTICLE

The resistance force from the medium is the resisting force to global motion and has been modeled for rigid Brownian particles in available literature. The Stokes approximation of resistance force from the medium is the most established model under normal temperature and pressure conditions. In Stokes approximation, the resisting force is proportional to the velocity  $\dot{x}$  of the particle and the proportionality constant, called as damping coefficient  $f$ , is equal to  $6\pi r\eta$ , where  $\eta$  is the viscosity of the surrounding medium [Uhlenbeck 1930]. The formulation of  $f$  gets modified to  $4\pi r\eta$  for the assumption that there is no adhesion of surrounding medium molecules with nanoparticle [Zwanzig 1970]. The consideration of time-dependent velocity correlations also modifies Stokes model of resistance force to global motion. The time dependent Stokes approximation is also known as Bossineq-Basset correction [Landau 1960]. The resistance to global motion also depends on flow conditions, frequency of excitation, and viscoelastic consideration of surrounding medium [Chow 1972].

The present thesis explores the non-rigidity of nanoparticle assuming the surrounding medium being characterized by a viscous steady flow condition. The resistance to local motion is presented next.

### 3.4 RESISTANCE TO LOCAL MOTION OF NANOPARTICLE

In the physical sense, the nanoparticle absorbs a part from the total energy of impact given to nanoparticle, another part is dissipated and the remaining energy is utilized in causing a motion of the nanoparticle. The dissipation of energy characterizes the resistance from nanoparticle to impact from surrounding medium. Whereas the resistance to global motion comes from the surrounding medium, the resistance to local

motion comes from the nanoparticle itself. A cue from resistance to global motion has been taken to model resistance to local motion. Therefore, as  $f$  characterizes resistance to global motion, the parameter  $f'$  is assumed to characterize the resistance from nanoparticle to local motion.

The total resistance to motion is assumed to be characterized by a combination of  $f$  and  $f'$ . The total resistance is represented by  $f_{eq}$ , which opposes the impacts. The impacts are stochastic in nature and are defined by autocorrelation. The autocorrelation of impact  $R_{FF}(t_1, t_2)$  has been obtained in case of rigid body model as [Nyquist 1929]

$$R_{FF}(t_1, t_2) = 2\kappa T f \delta(\tau) \quad (3.1)$$

where  $\delta(\tau)$  is unit impulse at time  $\tau$ . In non-rigid nanoparticle since total resistance is  $f_{eq}$ , this suggests a modification of autocorrelation of impacts obtained by replacing  $f$  with  $f_{eq}$  in equation (3.1) as

$$R_{FF}(t_1, t_2) = 2\kappa T f_{eq} \delta(\tau) \quad (3.2)$$

The modified impacts can get transmitted to inertial element  $m$  of nanoparticle in number of ways resulting in different models of impact transfer. The impact transfer models for rigid and non-rigid nanoparticle are developed next.

### 3.5 MODEL OF IMPACT TRANSFER FOR RIGID NANOPARTICLE

A nanoparticle embedded in a viscous fluid is subjected to random impacts. Due to these impacts, the nanoparticle performs global and local motion. The resulting motion  $x(t)$  of the nanoparticle can be obtained using correlation technique. The motion being stochastic in nature is expressed in terms of mean and variance of  $x(t)$ . The Langevin equation, equation (2.2), represents the model of a rigid nanoparticle performing Brownian motion in a viscous fluid. Assuming deterministic forces  $F_e(t) = 0$ , the equation (2.2) is

$$m \frac{dv}{dt} = -fv + F(t) \quad (3.3)$$

The substitution of velocity  $v = dx/dt$  in equation (3.3) and rearranging gives

$$\frac{d^2x}{dt^2} + \frac{f}{m} \frac{dx}{dt} = \frac{F(t)}{m} \quad (3.4)$$

or

$$\frac{d^2x}{dt^2} + \beta \frac{dx}{dt} = n(t) \quad (3.5)$$

where  $\beta = f/m$  and  $n(t) = F(t)/m$  is a stochastic process called white noise. The white noise is the actual input from the surrounding medium to the nanoparticle. The autocorrelation of  $F(t)$  for rigid nanoparticle is given by equation (3.1). The autocorrelation of  $n(t)$  is obtained by dividing the autocorrelation of  $F(t)$  by the square of constant quantity  $m$  [Papoulis 1991]. Therefore the autocorrelation of  $n(t)$  for rigid nanoparticle is given as

$$R_{nn}(t_1, t_2) = \frac{2\kappa T f}{m^2} \delta(\tau) \quad (3.6)$$

or

$$R_{nn}(t_1, t_2) = \alpha \delta(\tau) \quad (3.7)$$

where  $\alpha = 2\kappa T f / m^2$ . The autocorrelation and variance of the output  $x(t)$  for the rigid nanoparticle model given by equation (3.5) in the time interval  $t_1$  and  $t_2$  can be obtained as (equations I.25 and I.26)

$$R_{xx}(t_1, t_2) = \frac{\alpha}{2\beta^3} (2\beta t_1 - 1 + e^{-\beta t_1}) (1 - e^{-\beta t_2}) \quad (3.8)$$

and

$$E\{x^2(t)\} = \frac{\alpha}{2\beta^3} (2\beta t - 1 + e^{-\beta t}) (1 - e^{-\beta t}) \quad (3.9)$$

The detailed derivation of equations (3.8) and (3.9) are given in Appendix I. The first step to obtain the variance equation (3.9) using correlation technique is to integrate the equation (3.5). The integration of equation (3.5) gives

$$\frac{dx}{dt} - \frac{dx_0}{dt} + \beta(x - x_0) = \int n(t) dt \quad (3.10)$$

where  $x_0$  is the position of particle at  $t_1 = 0$ ,  $dx_0/dt$  is velocity of nanoparticle at  $t_1 = 0$ . In order to develop an impact transfer model of rigid nanoparticle Brownian motion given by equation (3.10) following assumptions are made. The integral on right hand side is denoted as

$$w(t) = \int n(t) dt \quad (3.11)$$

where  $w(t)$  is the integrated white noise. The  $w(t)$  is the modification of  $n(t)$  by the integrator and can be obtained by performing the convolution integration of  $n(t)$  with the impulse response of integrator. The impulse response of the integrator is unit step given as

$$g(\tau) = U(\tau) \quad (3.12)$$

The convolution of  $n(t)$  with  $g(\tau)$  to obtain  $w(t)$  is conventionally represented as

$$w(t) = n(t) * g(\tau) \quad (3.13)$$

In order to represent convolution given by equation (3.13) in the impact transfer, a block diagram is used as shown in Fig. 3.2.

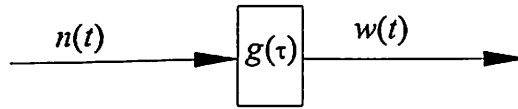


Fig 3.2 Integration of White Noise

Assuming  $x_0 = 0$  and velocity as stationary that is  $dx_0/dt = v_0$ , equation (3.10) gets modified as

$$\frac{dx}{dt} - v_0 + \beta x = w(t) \quad (14) \quad (3.14)$$

Next, the rearrangement of equation (3.12) gives a first order differential equation in terms of position of nanoparticle as

$$\frac{dx}{dt} + \beta x = w(t) + v_0 \quad (3.15)$$

The right hand side of rearranged equation (3.15) is like augmenting  $w(t)$  with  $v_0$ . The augmented signal  $w(t) + v_0$  is called as modified white noise and is denoted by  $y(t)$ . The modified white noise is shown by adding  $v_0$  to  $w(t)$  in Fig. 3.3.

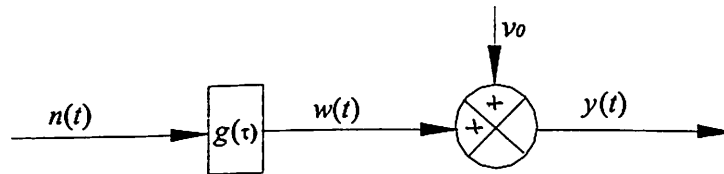


Fig 3.3 Modified White Noise

Equation (3.14) can be written as

$$\frac{dx}{dt} + \beta x = y(t) \quad (3.16)$$

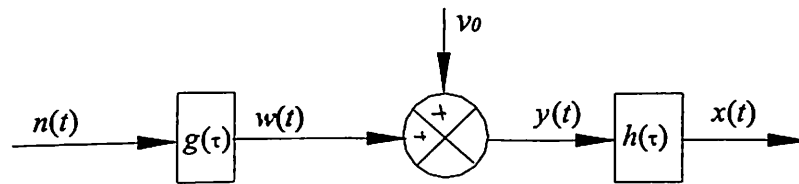
It can be interpreted from equation (3.16) that the modified white noise  $y(t)$  is forcing function to the system modeled by left-hand side of equation (3.16). The  $x(t)$  is the modification of the input signal  $y(t)$  by the system and can be obtained by doing convolution integration of autocorrelation of input  $y(t)$  with impulse response of the system. The convolution integration step gives the Ornstein-Uhlenbeck model given in equation (3.9). The impulse response  $h(\tau)$  of the system represented by equation (3.16) is given as [Nagrath 1993]

$$h(\tau) = e^{-\beta\tau} \quad (3.17)$$

The convolution of  $y(t)$  with  $h(\tau)$  to obtain  $x(t)$  is conventionally represented as

$$x(t) = y(t) * h(\tau) \quad (3.18)$$

In order to represent convolution given by equation (3.18) in the impact transfer, the convolution is shown by a block with impulse response  $h(\tau)$  and is attached to Fig. 3.3 completing the impact transfer model in rigid body as shown in Fig. 3.4.



**Fig. 3.4** Impact Transfer Model for Rigid Nanoparticle

The impact transfer model in Fig. 3.4 is referred as **Model 1** and represents the Brownian motion of rigid nanoparticles. In order to develop impact transfer models of Brownian motion of non-rigid nanoparticle, non-rigid sub-system is included in the rigid body impact transfer models. The non-rigid sub-system model of nanoparticle is given in next section.



### 3.6 SUB-SYSTEM MODEL OF NON-RIGID NANOPARTICLE

It is assumed that the properties of nanoparticle are characterized by lumped parameters. The mass, elasticity and dissipation properties of non-rigid nanoparticle are characterized by parameters  $m$ ,  $k$  and  $f'$  respectively. In order to develop a model of non-rigid nanoparticle, the non-rigidity properties  $k$  and  $f'$  are assumed as a sub-system of the elements  $k$  and  $f'$  with an impulse response  $H(\tau)$ .

The choice of the sub-system is arbitrary since a priori knowledge on the interaction among the parameters is not available. The concept required to be explored for the first time and it was assumed to start with a fixed arrangement of elements. Assuming that dissipation of energy from incoming signal to sub-system occurs first through a resistor and remaining energy is stored in a capacitor, the sub-system is shown in Fig. 3.5 with electrical analogous quantities resistance ( $f'$ ) and capacitance ( $1/k$ ) using force-voltage analogy.

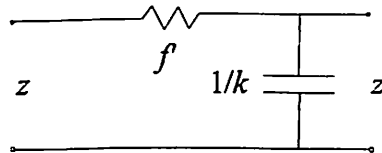


Fig. 3.5 Non-Rigid Properties Sub-System for Non-Rigid Nanoparticle

This is the conventional resistance-capacitance circuit with input  $z$ , output  $z'$ . The mathematical model for the sub-system in Fig. 3.5 is given as

$$\frac{1}{k} \frac{dz'}{dt} + \frac{z'}{f'} = z \quad (3.19)$$

The impulse response  $H(\tau)$  for the system given by equation (3.19) is [Nagrath 1993]

$$H(\tau) = \alpha' e^{-\alpha' \tau} \quad (3.20)$$

where  $\alpha' = k/f'$ . The output  $z'$  is obtained by performing the convolution integral of input with the impulse response  $H(\tau)$  conventionally given as

$$z'(t) = z(t) * H(\tau) \quad (3.21)$$

The convolution in equation (3.21) is shown with the block diagram in Fig.3.6 as impact transfer in non-rigid sub-system.

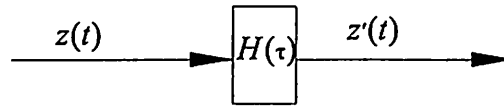


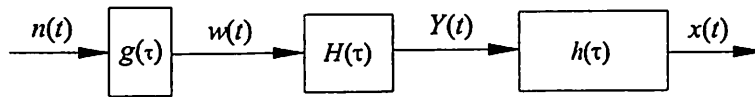
Fig. 3.6 Impact Transfer Model for Non-Rigid Sub-System

The conjuncture is that this sub-system is included in the impact transfer model of rigid body developed in section 3.5 to get a new Brownian motion model to describe Brownian motion of the non-rigid nanoparticle. The exercise of its inclusion in the impact transfer has been explored by considering various possibilities is next step. Thus, a two-step modeling approach has been used for development of Brownian motion models of non-rigid nanoparticle considering first the modeling of nanoparticle and then that of impact transfer itself. The impact transfer models of non-rigid nanoparticle are obtained in next section.

### 3.7 MODELS OF IMPACT TRANSFER FOR NON-RIGID NANOPARTICLE

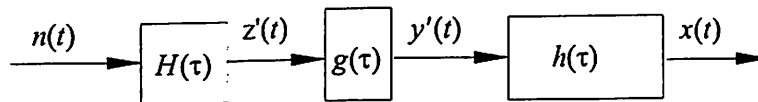
In the non-rigid model of nanoparticle, integrated white noise acts on the proof mass through the sub-system shown in Fig. 3.5 containing transmitting elements  $f'$  and  $k$ . The impact transfer model developed for rigid nanoparticle, earlier in this chapter, is modified to include the non-rigid properties sub-system in four different possible ways.

To start with, it is contemplated that immediately after the integration of the impact; a part of the impact energy gets dissipated because of presence of damping property of nanoparticle. The remaining energy is absorbed as strain energy of spring representing elastic property of nanoparticle. The energy stored in contemplated spring element gets released at a frequency  $\omega$ . The released energy is in the form of another force signal  $Y(t)$  to be applied to further sub-system in impact process. The next sub-system to which the force signal is applied is the rigid body model with impulse response given by equation (3.17). The impact transfer model is shown in Fig. 3.7 and is referred as **Model 2**.



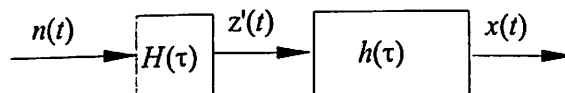
**Fig. 3.7** Impact Transfer Model 2 for Brownian motion of Non-Rigid Nanoparticle

Alternate models for impact process are obtained by considering possible variations. A possible alteration is that individual impacts first get modified by the non-rigid sub-system and then gets integrated. It is like individual impact, first looses energy <sup>lose</sup> and then remaining part of energy gets absorbed in the nanoparticle. The synchronized release of remaining energy in the form of a forcing signal  $z'(t)$  gets integrated next. The integrated signal representing a force is applied to rigid model sub-system. This is like integration is done after the hypothesized non-rigid sub-system with impulse response  $H(\tau)$ . This is shown in Fig. 3.8 and is called as **Model 3**.



**Fig. 3.8** Impact Transfer Model 3 for Brownian motion of Non-Rigid Nanoparticle

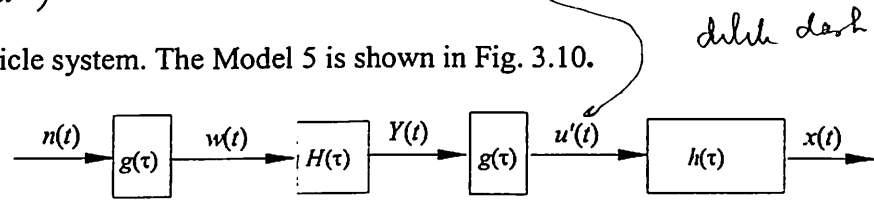
The Model 2 and Model 3 presents possibilities of the placement of sub-system on either side of integrator, but may be no integrator is present in the impact transfer in Brownian motion. The non-existence of integration in impact transfer physically implies that signal does not change its form from input to output and both represent either force (noise) or position. At least, there seems to be a need to explore the motion because of impact transfer without integration. The impact process without integration is shown in Fig. 3.9 and is referred as **Model 4**.



**Fig. 3.9** Impact Transfer Model 4 for Brownian motion of Non-Rigid Nanoparticle

*2nd order integration*

The last and fifth model of impact transfer in non-rigid nanoparticle, **Model 5**, is obtained by considering presence of integration on both sides of non-rigid sub-system. The double integration hypothesizes another model of impact process in non-rigid nanoparticle. If the output signal is to be position of the particle, then as we move backwards to the input signal (white noise) through elastic sub-systems, the double integration model should physically mean that input signal is a higher order jerk  $\left(\approx \frac{d^3x}{dt^3}\right)$ . The integration of  $Y(t)$  gives  $u(t)$ , which is input to the rigid nanoparticle system. The Model 5 is shown in Fig. 3.10.



**Fig. 3.10** Impact Transfer Model 5 for Brownian motion of Non-Rigid Nanoparticle

In order to compute the variance in position for impact transfer models, the mathematical models of every sub-system in each model is developed. The mathematical models relate the input and output of the sub-system with impulse response and are represented as a differential equation. The mathematical models are given in next section.

### 3.8 MATHEMATICAL MODELS FOR IMPACT TRANSFER MODELS

The rigid nanoparticle impact transfer model is obtained from mathematical equations (3.10) through (3.18) where each equation correspond to a sub-system or process depicted as blocks or variable. For reference and completeness sake, the mathematical equations for each block representing a sub-system in impact transfer models, Model 2 through to Model 5 are presented.

#### 3.8.1 Mathematical Model for Model 2

From Fig. 3.7, it is observed that integrated white noise  $w(t)$  is input to non-rigid sub-system. With  $w(t)$  as input and  $Y(t)$  as output in non-rigid sub-system, equation (3.19) becomes

$$\frac{1}{k} \frac{dY(t)}{dt} + \frac{Y(t)}{f'} = w(t) \quad (3.22)$$

The signal  $Y(t)$  is input to the rigid nanoparticle system with impulse response  $h(\tau)$ . For the rigid nanoparticle block shown with impulse response  $h(\tau)$  in Fig. 3.7 with input  $Y(t)$  and output  $x(t)$ , the differential equation is obtained by replacing  $w(t) + v_0$  by  $Y(t)$  in equation (3.15) as

$$\frac{dx}{dt} + \beta x = Y(t) \quad (3.23)$$

Equations (3.22) and (3.23) are used to obtain variance in position for Model 2.

### 3.8.2 Mathematical Model for Model 3

From Fig. 3.8, it is observed that an individual impact of white noise is input to non-rigid sub-system. The output from the non-rigid sub-system is  $z'(t)$ . The mathematical model for the non-rigid sub-system is obtained by replacing  $z(t)$  by  $n(t)$  in equation (3.19), which gives

$$\frac{1}{k} \frac{dz'(t)}{dt} + \frac{z'(t)}{f'} = n(t) \quad (3.24)$$

The signal  $z'(t)$  is first integrated and then is input to the rigid nanoparticle system. With  $z'(t)$  as input and  $y'(t)$  as output of the integrator, equation (3.11) becomes

$$y'(t) = \int z'(t) dt \quad (3.25)$$

The  $y'(t)$  is input to rigid nanoparticle system with  $x(t)$  as output. The mathematical model for rigid nanoparticle system is obtained by replacing  $w(t) + v_0$  with  $y'(t)$  in equation (3.15). The mathematical model obtained is given as

$$\frac{dx}{dt} + \beta x = y'(t) \quad (3.26)$$

Equation (3.24) to equation (3.26) are used to obtain the variance for Model 3.

Fig. 3.9

### 3.8.3 Mathematical Model for Model 4

From Fig. 3.7 and Fig. 3.8, it is observed that in Model 4, there is no integration of  $z'(t)$ . In Model 4,  $z'(t)$  is a direct input to the rigid nanoparticle sub-system, which otherwise is similar to Model 3. Therefore the mathematical model for Model 4 is obtained from that given for Model 3 by omitting equation (3.25) and replacing  $y'(t)$  by  $z'(t)$  in equation (3.26). The two equations giving mathematical model for impact transfer model, Model 4, are

$$\frac{1}{k} \frac{dz'(t)}{dt} + \frac{z'(t)}{f'} = n(t) \quad (3.27)$$

$$\frac{dx}{dt} + \beta x = z'(t) \quad (3.28)$$

Equation (3.27) and (3.28) are used to obtain the variance for Model 4.

### 3.8.4 Mathematical Model for Model 5

From Fig. 3.7 and Fig. 3.10, it is observed that in Model 5, there is an additional integration of  $Y(t)$ . The mathematical model for first integrator sub-system is same as equation (3.22) as

$$\frac{1}{k} \frac{dY(t)}{dt} + \frac{Y(t)}{f'} = w(t) \quad (3.29)$$

The integrated  $Y(t)$  represented by  $u'(t)$  is input to the rigid nanoparticle sub-system. The mathematical model for additional integrator sub-system is obtained by replacing  $n(t)$  and  $w(t)$  with  $Y(t)$  and  $u'(t)$  equation (3.11) as

$$u'(t) = \int Y(t) dt \quad (3.30)$$

With  $u'(t)$  as input to rigid body sub-system, equation (3.15) becomes

$$\frac{dx}{dt} + \beta x = u'(t) \quad (3.31)$$

Equation (3.29) to equation (3.31) are used to obtain the variance for Model 5. In order to obtain the variance models, the algorithm to develop variance models for non-rigid nanoparticle is given in next section.

### 3.8.3 Mathematical Model for Model 4

Fig. 3.9

From Fig. 3.7 and Fig. 3.8, it is observed that in Model 4, there is no integration of  $z'(t)$ . In Model 4,  $z'(t)$  is a direct input to the rigid nanoparticle sub-system, which otherwise is similar to Model 3. Therefore the mathematical model for Model 4 is obtained from that given for Model 3 by omitting equation (3.25) and replacing  $y'(t)$  by  $z'(t)$  in equation (3.26). The two equations giving mathematical model for impact transfer model, Model 4, are

$$\frac{1}{k} \frac{dz'(t)}{dt} + \frac{z'(t)}{f'} = n(t) \quad (3.27)$$

$$\frac{dx}{dt} + \beta x = z'(t) \quad (3.28)$$

Equation (3.27) and (3.28) are used to obtain the variance for Model 4.

### 3.8.4 Mathematical Model for Model 5

From Fig. 3.7 and Fig. 3.10, it is observed that in Model 5, there is an additional integration of  $Y(t)$ . The mathematical model for first integrator sub-system is same as equation (3.22) as

$$\frac{1}{k} \frac{dY(t)}{dt} + \frac{Y(t)}{f'} = w(t) \quad (3.29)$$

The integrated  $Y(t)$  represented by  $u'(t)$  is input to the rigid nanoparticle sub-system. The mathematical model for additional integrator sub-system is obtained by replacing  $n(t)$  and  $w(t)$  with  $Y(t)$  and  $u'(t)$  equation (3.11) as

$$u'(t) = \int Y(t) dt \quad (3.30)$$

With  $u'(t)$  as input to rigid body sub-system, equation (3.15) becomes

$$\frac{dx}{dt} + \beta x = u'(t) \quad (3.31)$$

Equation (3.29) to equation (3.31) are used to obtain the variance for Model 5. In order to obtain the variance models, the algorithm to develop variance models for non-rigid nanoparticle is given in next section.

### 3.9 DEVELOPMENT OF VARINCE MODELS FOR NON-RIGID NANOPARTICLE

The mathematical models for variance of four impact transfer models developed in the last section, is carried out in a systematic manner. The systematic procedure is given in the form of an algorithm below. The variances of the models are obtained using this algorithm.

#### Algorithm 1: Algorithm for Computing Variance

Let the autocorrelation of a physical variable  $z$  is denoted by  $R_{zz}(t_1, t_2)$ , where  $t_1$  and  $t_2$  are two instances of time ( $t_1 < t_2$ ). If input to a sub-system in the impact transfer models is  $z$  and output is  $z'$ , then autocorrelation of  $z'$  ( $R_{z'z'}(t_1, t_2)$ ) is obtained using following steps:

**Step I** Get autocorrelation of input signal  $R_{zz}(t_1, t_2)$  as follows

IF input is white noise AND nanoparticle is modeled as non-rigid, THEN autocorrelation  $R_{zz}(t_1, t_2)$  obtained replacing  $f$  by  $f_{eq}$  in equation (3.6)

$$R_{zz}(t_1, t_2) = \frac{2\kappa T f_{eq} \delta(\tau)}{m^2} \quad (3.32)$$

ELSE the autocorrelation  $R_{zz}(t_1, t_2)$  is the autocorrelation of output from previous sub-system.

**Step II** Obtain impulse response  $h(\tau)$  of the sub-system as follows

GET the mathematical model of the sub-system.

TAKE the Laplace transform of the mathematical model.

OBTAIN the transfer function from Laplace transform.

OBTAIN the impulse response of the sub-system by taking Fourier transform of transfer function.

$\hat{h}(\tau)$

**Step III** Compute cross-correlation between input and output as follows



The cross correlation is obtained from equation (I.7), which for input  $z$  and output  $z'(t)$  becomes

$$R_{z'z}(t_1, t_2) = \int_{-\infty}^{\infty} R_{zz}(t_1 - \tau, t_2) h(\tau) d\tau \quad (3.33)$$

**Step IV** Compute autocorrelation of output of sub-system as follows

The autocorrelation is obtained from equation (I.9), which for output  $z'(t)$  becomes

$$R_{z'z'}(t_1, t_2) = \int_{-\infty}^{\infty} R_{z'z}(t_1, t_2 - \tau) h(\tau) d\tau \quad (3.34)$$

**Step V** IF the sub-system is last one in the model, go to Step VI

ELSE go to Step I and repeat the steps for next sub-system.

**Step VI** Compute variance of output of model as follows

The variance of the output of the model  $E\{x^2(t)\}$  is obtained using equation (I.10), which for output  $x(t)$  is

$$E\{x^2(t)\} = R_{xx}(t, t) \quad (3.35)$$

The above algorithm is applied for computation of variance in position of nanoparticle to each Models 2 through 5. The detailed computations are given in next section.

### 3.10 VARIANCE FOR DIFFERENT IMPACT TRANSFER MODELS

According to Step I, the autocorrelation of the input to first sub-system of all impact transfer models of non-rigid nanoparticle is white noise with autocorrelation given by equation (3.22). Moreover, according to Step II, we will require impulse response of the three sub-systems in the models namely, non-rigid sub-system, rigid body sub-system and the integrator sub-system. The impulse responses for the three sub-systems are given by equation (3.20), equation (3.17) and equation (3.12) respectively. These three impulse responses are used repeatedly in developing variance models. The detailed derivation for every model is done next.

### 3.10.1 Variance for Model 2

For Model 2 (refer Fig. 3.7), the first sub-system is the integrator with input  $n(t)$  and output  $w(t)$ . Using Step 1 to Step 4 of the Algorithm 1, the autocorrelation of  $w(t)$  for rigid nanoparticle has been computed by Papoulis [1991] for  $t_1 < t_2$  as

$$R_{ww}(t_1, t_2) = \frac{2\kappa T f t_1}{m^2} \quad (3.36)$$

According to Step 1, for non-rigid nanoparticle,  $f_{eq}$  replaces  $f$  in equation (3.36), The replacement of  $f$  with  $f_{eq}$  in equation (3.36) modifies the autocorrelation of integrated white noise. The autocorrelation of output denoted as  $R_{ww}(t_1, t_2)$  from first sub-system of Model 2, therefore, is given by

$$R_{ww}(t_1, t_2) = \frac{2\kappa T f_{eq} t_1}{m^2} \quad (3.37)$$

From Fig. 3.7, it can be observed that the output from first sub-system with autocorrelation  $R_{ww}(t_1, t_2)$  is input to the second sub-system of the Model 2 with impulse response  $H(\tau)$ . For the second sub-system of Model 2, the mathematical model for Step II, relating input and output is given by equation (3.22). From the Step III of the Algorithm 1, the cross-correlation between the output  $Y(t)$  from second sub-system and the modified input  $W(t)$  is obtained as

$$R_{wY}(t_1, t_2) = \int_{-\infty}^{\infty} R_{ww}(t_1 - \tau, t_2) H(\tau) d\tau \quad (3.38)$$

Substituting for  $H(\tau)$  from equation (3.20),  $R_{ww}(t_1, t_2)$  from equation (3.37) and replacing  $t_1$  with  $t_1 - \tau$  in equation (3.38) gives

$$R_{wY}(t_1, t_2) = \frac{2\kappa T f_{eq}}{m^2} \int_0^{t_1} (t_1 - \tau) \alpha' e^{-\alpha' \tau} d\tau \quad (3.39)$$

or

$$R_{wY}(t_1, t_2) = \frac{2\kappa T f_{eq} \alpha'}{m^2} \int_0^{t_1} (t_1 e^{-\alpha' t} - \tau e^{-\alpha' t}) d\tau \quad (3.40)$$

The instance  $t_1$  or  $t_2$  are considered as fixed parameters in evaluating the integration and  $\tau$  is considered as variable time. The integration of equation (3.40) by parts gives

$$R_{wY}(t_1, t_2) = \frac{2\kappa T f_{eq} \alpha'}{m^2} \left[ t_1 \int_0^{t_1} e^{-\alpha' \tau} d\tau - \left\{ \tau \int_0^{t_1} e^{-\alpha' \tau} d\tau - \int_0^{t_1} \frac{d(\tau)}{d\tau} \int e^{-\alpha' \tau} d\tau \right\} \right] \quad (3.41)$$

or

$$R_{wY}(t_1, t_2) = \frac{2\kappa T f_{eq} \alpha'}{m^2} \left[ t_1 \left( \frac{1 - e^{-\alpha' t_1}}{\alpha'} \right) - \left\{ \frac{\tau e^{-\alpha' \tau}}{-\alpha'} \Big|_0^{t_1} - \int_0^{t_1} \frac{e^{-\alpha' \tau}}{-\alpha'} d\tau \right\} \right] \quad (3.42)$$

Further solving the integral in equation (3.42), the cross correlation  $R_{wY}(t_1, t_2)$  is obtained as

$$R_{wY}(t_1, t_2) = \frac{2\kappa T f_{eq} \alpha'}{m^2} \left[ \frac{t_1}{\alpha'} - \frac{t_1 e^{-\alpha' t_1}}{\alpha'} - \left\{ -\frac{t_1 e^{-\alpha' t_1}}{\alpha'} + \frac{1}{\alpha'} \left( \frac{1 - e^{-\alpha' t_1}}{\alpha'} \right) \right\} \right] \quad (3.43)$$

or

$$R_{wY}(t_1, t_2) = 2\kappa T f_{eq} \left( t_1 - \frac{1}{\alpha'} + \frac{e^{-\alpha' t_1}}{\alpha'} \right) \quad (3.44)$$

Now according to Step IV of the Algorithm 1, the autocorrelation of the output  $Y(t)$  from the second sub-system of Model 2 can be obtained by performing convolution integral between cross-correlation  $R_{wY}(t_1, t_2)$  and impulse response  $H(\tau)$ . The autocorrelation of  $Y(t)$  denoted by  $R_{YY}(t_1, t_2)$  according to equation (3.34) is given as

$$R_{YY}(t_1, t_2) = \int_{-\infty}^{\infty} R_{wY}(t_1, t_2 - \tau) H(\tau) d\tau \quad (3.45)$$

Substituting for  $R_{wY}(t_1, t_2)$  from equation (3.44), impulse response  $H(\tau)$  from equation (3.20) in equation (3.45) gives

$$R_{YY}(t_1, t_2) = \frac{2\kappa T f_{eq}}{m^2} \int_0^{t_2} \left( t_1 - \frac{1}{\alpha'} + \frac{e^{-\alpha' t_1}}{\alpha'} \right) \alpha' e^{-\alpha' \tau} d\tau \quad (3.46)$$

or

$$R_{YY}(t_1, t_2) = \frac{2\kappa T f_{eq}}{m^2} (\alpha' t_1 - 1 + e^{-\alpha' t_1}) \int_0^{t_2} e^{-\alpha' \tau} d\tau \quad (3.47)$$

which on integration gives

$$R_{YY}(t_1, t_2) = \frac{2\kappa T f_{eq}}{m^2 \alpha'} (\alpha' t_1 - 1 + e^{-\alpha' t_1}) (1 - e^{-\alpha' t_2}) \quad (3.48)$$

According to Step V, since the sub-system is not the last one in the model (refer Fig. 3.7), the process is to be repeated starting from Step I. According to Step I, the

signal  $Y(t)$  with autocorrelation given by equation (3.48) is input to the third sub-system. The mathematical model for the third sub-system is given by equation (3.23). The impulse response  $h(\tau)$  for the model given by equation (3.23) according to Step II is given by equation (3.17). Therefore, according to Step III of the Algorithm 1, the cross correlation between output signal  $x(t)$  and input signal  $Y(t)$  of the third sub-system is given by equation (3.33) as

$$R_{xy}(t_1, t_2) = \int_{-\infty}^{\infty} R_{YY}(t_1 - \tau, t_2) h(\tau) d\tau, t_1 < t_2 \quad (3.49)$$

Substituting the expression for  $R_{YY}(t_1, t_2)$  from equation (3.48) and impulse response from equation (3.17), in equation (3.49) gives

$$R_{xy}(t_1, t_2) = \int_0^{t_1} \frac{2\kappa T f_{eq}}{m^2 \alpha'} (\alpha'(t_1 - \tau) - 1 + e^{-\alpha'(t_1 - \tau)}) (1 - e^{-\alpha t_2}) e^{-\beta \tau} d\tau \quad (3.50)$$

or

$$R_{xy}(t_1, t_2) = \frac{2\kappa T f_{eq}}{m^2 \alpha'} (1 - e^{-\alpha t_2}) \int_0^{t_1} (\alpha'(t_1 - \tau) - 1 + e^{-\alpha'(t_1 - \tau)}) e^{-\beta \tau} d\tau \quad (3.51)$$

which on integration gives

$$R_{xy}(t_1, t_2) = \frac{2\kappa T f_{eq}}{m^2 \alpha'} (1 - e^{-\alpha t_2}) \left[ \alpha' t_1 - (1 - e^{-\beta t_1}) \left( \frac{\alpha'}{\beta} + 1 \right) + \frac{\beta e^{-\alpha t_1}}{\alpha' - \beta} (e^{(\alpha' - \beta)t_1} - 1) \right] \quad (3.52)$$

According to step IV of the Algorithm 1, the autocorrelation of the output  $x(t)$  denoting the position of the particle can be obtained by substituting the expression of cross correlation from equation (3.52) and the impulse response from equation (3.17) in equation (3.34) as

$$R_{xx}(t_1, t_2) = \int_{-\infty}^{\infty} R_{xy}(t_1, t_2 - \tau) h(\tau) d\tau \quad (3.53)$$

or

$$R_{xx}(t_1, t_2) = \frac{2\kappa T f_{eq}}{m^2 \alpha'} \left[ \alpha' t_1 - (1 - e^{-\beta t_1}) \left( \frac{\alpha'}{\beta} + 1 \right) + \frac{\beta e^{-\alpha t_1}}{\alpha' - \beta} (e^{(\alpha' - \beta)t_1} - 1) \right] \int_0^{t_2} (1 - e^{-\alpha'(t_2 - \tau)}) e^{-\beta \tau} d\tau \quad (3.54)$$

which on integration gives

$$R_{xx}(t_1, t_2) = \frac{2\kappa T f_{eq}}{m^2 \alpha'} \left[ \alpha' t_1 - (1 - e^{-\beta t_1}) \left( \frac{\alpha'}{\beta} + 1 \right) + \frac{\beta e^{-\alpha' t_1}}{\alpha' - \beta} (e^{(\alpha' - \beta)t_1} - 1) \right] \left[ \left( \frac{1 - e^{-\beta t_2}}{\beta} \right) - \frac{e^{-\alpha' t_2}}{\alpha' - \beta} (e^{(\alpha' - \beta)t_2} - 1) \right] \quad (3.55)$$

From Step V of the Algorithm 1, since the third sub-system is the last sub-system of the Model 2, the process is forwarded to Step VI of the algorithm. According to Step VI, the variance in position of nanoparticle for Model 2 is obtained from the autocorrelation in position given by equation (3.55) by substituting  $t_1 = t_2 = t$  as

$$E\{x^2(t)\} = \frac{2\kappa T f_{eq}}{m^2 \alpha' \beta} \left[ \alpha' t - (1 - e^{-\beta t}) \left( \frac{\alpha'}{\beta} + 1 \right) + \frac{\beta e^{-\alpha' t}}{\alpha' - \beta} (e^{(\alpha' - \beta)t} - 1) \right] \left[ (1 - e^{-\beta t}) - \frac{\beta e^{-\alpha' t}}{\alpha' - \beta} (e^{(\alpha' - \beta)t} - 1) \right] \quad (3.56)$$

### 3.10.2 Variance for Model 3

For Model 3 (refer Fig. 3.8), the first sub-system is the non-rigid sub-system with input  $n(t)$  and output  $z'(t)$ . Using Step 1 to Step 4 of the Algorithm 1, the autocorrelation  $R_{n_e n_e}(t_1, t_2)$  of output  $n_e(t)$  with input  $F(t)$  for rigid nanoparticle has been computed by Papoulis [1991] as

$$R_{n_e n_e}(t_1, t_2) = \kappa T f_{eq} \alpha' e^{-\alpha'(t_1 - t_2)} (1 - e^{-2\alpha' t_2}) \quad (3.57)$$

For Model 3, the input to the non-rigid sub-system is  $n(t)$  instead of  $F(t)$  having autocorrelation given by equation (3.32) according to Step I of the Algorithm 1. Comparing the autocorrelation of input  $F(t)$  in equation (3.1) and  $n(t)$  in case of Model 3, it is observed that the autocorrelation of  $n(t)$  is obtained from that of  $F(t)$  replacing  $f$  by  $f_{eq}$  and dividing by  $m^2$ . Therefore, the autocorrelation  $R_{z' z'}(t_1, t_2)$  of output  $z'(t)$  from non-rigid sub-system in case of Model 3 is obtained from equation (3.57) replacing  $f$  by  $f_{eq}$  and dividing by  $m^2$  and is obtained as

$$R_{z' z'}(t_1, t_2) = \frac{\kappa T f_{eq} \alpha' e^{-\alpha'(t_1 - t_2)}}{m^2} (1 - e^{-2\alpha' t_2}) \quad (3.58)$$

According to Step V, since the first sub-system is not the last sub-system, the algorithm is repeated from Step I for the next sub-system, which is an integrator. According to Step I, the autocorrelation of input to integrator sub-system is the autocorrelation of output from previous sub-system given by equation (3.58). The impulse response for integrator, according to Step II is obtained from the mathematical model of the integrator (refer equation (3.25)) and is given by equation (3.12). From Step III, the cross correlation between output  $y'(t)$  from integrator and input  $z'$  can be obtained from equation (3.33) as

$$R_{y'z'}(t_1, t_2) = \int_{-\infty}^{\infty} R_{z'z'}(t_1 - \tau, t_2) h(\tau) d\tau \quad (3.59)$$

Substituting autocorrelation of  $z'$  from equation (3.58), replacing  $t_1$  with  $t_1 - \tau$  and using impulse response  $g(\tau)$  of the integrator from equation (3.12), equation (3.59) gives

$$R_{y'z'}(t_1, t_2) = \frac{\kappa T f_{eq} \alpha'}{m^2} \int_{-\infty}^{\infty} (1 - e^{-2\alpha' t_2}) e^{-\alpha'(t_1 - \tau - t_2)} U(\tau) d\tau \quad (3.60)$$

which on integration gives

$$R_{y'z'}(t_1, t_2) = \frac{\kappa T f_{eq} \alpha'}{m^2} (1 - e^{-2\alpha' t_2}) e^{-\alpha'(t_1 - t_2)} \left( \frac{1 - e^{-\alpha' t_1}}{\alpha'} \right) \quad (3.61)$$

The autocorrelation of the signal  $y'(t)$  can then be obtained using Step IV of the Algorithm 1 as

$$R_{y'y'}(t_1, t_2) = \int_0^{t_2} R_{y'z'}(t_1, t_2 - \tau) h(\tau) d\tau \quad (3.62)$$

Substituting the impulse response of the integrator and cross correlation  $R_{y'z'}$  from equation (3.61) in equation (3.62) gives

$$R_{y'y'}(t_1, t_2) = \frac{\kappa T f_{eq}}{m^2} (1 - e^{-\alpha' t_1}) \int_0^{t_2} (1 - e^{-2\alpha'(t_2 - \tau)}) (e^{-\alpha'(t_1 - (t_2 - \tau))}) U(\tau) d\tau \quad (3.63)$$

which can be arranged as

$$R_{y'y'}(t_1, t_2) = \frac{\kappa T f_{eq}}{m^2} (1 - e^{-\alpha' t_1}) \int_0^{t_2} (e^{-\alpha'(t_1 - t_2)} e^{-\alpha' \tau} - e^{-\alpha'(t_1 + t_2)} e^{-\alpha' \tau}) U(\tau) d\tau \quad (3.64)$$

Equation (3.64) on integration gives

$$R_{y'y'}(t_1, t_2) = \frac{\kappa T f_{eq}}{m^2 \alpha'} (1 - e^{-\alpha' t_1}) (e^{-\alpha'(t_2 - t_1)} - e^{-\alpha'(t_1 + t_2)} + 2e^{-\alpha' t_1}) \quad (3.65)$$

Since the integrator is not the last sub-system in Model 3, the procedure is repeated for the next sub-system. From Fig. 3.8, it can be observed that the signal  $y'(t)$  is input to the third sub-system having impulse response given by equation (3.16). The output from the system is  $x(t)$  which denotes the position of the particle. According to Step I, the autocorrelation of input to third sub-system is given by equation (3.65). From Step II, the impulse response corresponding to the mathematical model of the third sub-system (refer equation (3.26)) is given by equation (3.17). According to Algorithm 1, Step III, the cross correlation between  $y'(t)$  and  $x(t)$  is obtained using equation (3.34) as

$$R_{xy'}(t_1, t_2) = \int_{-\infty}^{\infty} R_{y'y'}(t_1 - \tau, t_2) h(\tau) d\tau \quad (3.66)$$

Substituting the expression for autocorrelation of  $y'(t)$  from equation (3.65), replacing parameter  $t_1$  with  $t_1 - \tau$  and the impulse response from equation (3.17), equation (3.66) can be written as

$$R_{xy'}(t_1, t_2) = \frac{\kappa T f_{eq}}{m^2 \alpha'} \int_0^{t_1} (1 - e^{-\alpha'(t_1 - \tau)}) (e^{-\alpha'(t_2 - \tau - t_1)} - e^{-\alpha'(t_1 - \tau + t_2)} + 2e^{-\alpha'(t_1 - \tau)}) e^{-\beta \tau} d\tau \quad (3.67)$$

Equation (3.67) on integration gives

$$R_{xy'}(t_1, t_2) = \frac{\kappa T f_{eq}}{m^2 \alpha'} \left[ \frac{(e^{(\alpha' - \beta)t_1} - 1)}{\alpha' - \beta} (e^{-\alpha'(t_1 - t_2)} - e^{-\alpha'(t_1 + t_2)} + 2e^{-\alpha' t_1}) - \frac{(e^{(2\alpha' - \beta)t_1} - 1)}{2\alpha' - \beta} (e^{-2\alpha' t_1 - \alpha' t_2} - e^{-2\alpha' t_1 + \alpha' t_2} + 2e^{-2\alpha' t_1}) \right] \quad (3.68)$$

The autocorrelation of  $x(t)$  can be obtained using Step IV, equation (3.34) of the Algorithm 1 as

$$R_{xx}(t_1, t_2) = \int_{-\infty}^{\infty} R_{xy'}(t_1, t_2 - \tau) h(\tau) d\tau \quad (3.69)$$

Substitution of expressions for cross correlation from equation (3.68), impulse response  $h(\tau)$  from equation (3.17) and replacing parameter  $t_2$  with  $t_2 - \tau$  in equation (3.69) gives

$$R_{xx}(t_1, t_2) = \int_0^{t_2} \frac{\kappa T f_{eq}}{m^2 \alpha'} \left[ \frac{(e^{(\alpha'-\beta)t_1} - 1)}{\alpha' - \beta} (e^{-\alpha'(t_1-(t_2-\tau))} - e^{-\alpha'(t_1+(t_2-\tau))} + 2e^{-\alpha't_1}) - \frac{(e^{(2\alpha'-\beta)t_1} - 1)}{2\alpha' - \beta} (e^{-2\alpha't_1 - \alpha'(t_2-\tau)} - e^{-2\alpha't_1 + \alpha'(t_2-\tau)} + 2e^{-2\alpha't_1}) \right] e^{-\beta\tau} d\tau \quad (3.70)$$

which on integration gives

$$R_{xx}(t_1, t_2) = \frac{\kappa T f_{eq}}{m^2 \alpha'} \left[ \frac{(e^{(\alpha'-\beta)t_1} - 1)}{\alpha' - \beta} \left\{ (e^{-\alpha'(t_1-t_2)}) \frac{e^{(\alpha'-\beta)t_2} - 1}{\alpha' - \beta} - e^{-\alpha'(t_1+t_2)} \frac{e^{(\alpha'-\beta)t_2} - 1}{\alpha' - \beta} + 2e^{-\alpha't_1} \frac{1 - e^{-\beta t_2}}{\beta} \right\} - \frac{(e^{(2\alpha'-\beta)t_1} - 1)}{2\alpha' - \beta} \left\{ (e^{-2\alpha't_1 - \alpha't_2}) \frac{e^{(\alpha'-\beta)t_2} - 1}{\alpha' - \beta} - e^{-2\alpha't_1 - \alpha't_2} \frac{1 - e^{-(\alpha'+\beta)t_2}}{(\alpha' + \beta)} + 2e^{-2\alpha't_1} \frac{1 - e^{-\beta t_2}}{\beta} \right\} \right] \quad (3.71)$$

Since the third sub-system is last sub-system in Model 3, therefore, according to Step V, the process is forwarded to next step. In the next Step VI, the variance in position, therefore, by substituting  $t_1 = t_2 = t$  in equation (3.71) is

$$E\{x^2(t)\} = \frac{\kappa T f_{eq}}{m^2 \alpha'} \left[ \frac{(e^{(\alpha'-\beta)t} - 1)}{\alpha' - \beta} \left\{ \frac{e^{(\alpha'-\beta)t} - 1}{\alpha' - \beta} (1 - e^{-2\alpha't}) + 2e^{-\alpha't} \frac{1 - e^{-\beta t}}{\beta} \right\} - \frac{(e^{(2\alpha'-\beta)t} - 1)}{2\alpha' - \beta} \left\{ e^{-3\alpha't} \frac{e^{(\alpha'-\beta)t} - 1}{\alpha' - \beta} - e^{-\alpha't} \frac{1 - e^{-(\alpha'+\beta)t}}{(\alpha' + \beta)} + 2e^{-2\alpha't} \frac{1 - e^{-\beta t}}{\beta} \right\} \right] \quad (3.72)$$

### 3.10.3 Variance for Model 4

The signal  $z'$  in Model 4 (refer Fig. 3.9) with autocorrelation given by equation (3.54) is fed to second sub-system with impulse response  $h(\tau)$ . The second sub-system have output  $x(t)$  and input  $z'$ . For the second sub-system, according to Step I, the autocorrelation of input is given by equation (3.58). According to Step II and mathematical model given by equation (3.28), the impulse response of the second sub-system in Model 4 is given by equation (3.17). Applying Step III of the Algorithm 1, the cross-correlation between output  $x(t)$  and input  $z'$  is

$$R_{xz'}(t_1, t_2) = \int_{-\infty}^{\infty} R_{z'z'}(t_1 - \tau, t_2) h(\tau) d\tau \quad (3.73)$$



Equation (3.73), on substitution of autocorrelation  $R_{z_2}(t_1, t_2)$  from equation (3.58), impulse response  $h(\tau)$  from equation (3.17) and replacing parameter  $t_1$  with  $t_1 - \tau$  gives

$$R_{x'} = \frac{\kappa T f_{eq}}{m^2} e^{\alpha' t_2} (1 - e^{-2\alpha' t_2}) \int_0^{t_1} e^{-\alpha'(t_1-\tau)} e^{-\beta\tau} d\tau \quad (3.74)$$

which can be rearranged as

$$R_{x'} = \frac{\kappa T f_{eq}}{m^2} e^{\alpha' t_2} (1 - e^{-2\alpha' t_2}) \int_0^{t_1} e^{-\alpha' t_1} e^{(\alpha' - \beta)\tau} d\tau \quad (3.75)$$

Equation (3.75) on integration gives

$$R_{x'} = \frac{\kappa T f_{eq}}{m^2} e^{\alpha' t_2} (1 - e^{-2\alpha' t_2}) \left( \frac{e^{-\beta t_1} - e^{-\alpha' t_1}}{\alpha' - \beta} \right) \quad (3.76)$$

The autocorrelation of  $x(t)$  from the Step IV of the Algorithm 1 can be obtained as

$$R_{xx}(t_1, t_2) = \int_{-\infty}^{\infty} R_{x'}(t_1, t_2 - \tau) h(\tau) d\tau \quad (3.77)$$

Substituting the expression for the cross correlation from equation (3.76), the expression for impulse response and replacing  $t_2$  with  $t_2 - \tau$  in equation (3.77) gives

$$R_{xx}(t_1, t_2) = \frac{\kappa T f_{eq}}{m^2} \left( \frac{e^{-\beta t_1} - e^{-\alpha' t_1}}{\alpha' - \beta} \right) \int_0^{t_2} e^{\alpha'(t_2-\tau)} (1 - e^{-2\alpha'(t_2-\tau)}) e^{-\beta\tau} d\tau \quad (3.78)$$

Equation (3.78) can be rearranged as

$$R_{xx}(t_1, t_2) = \frac{\kappa T f_{eq}}{m^2} \left( \frac{e^{-\beta t_1} - e^{-\alpha' t_1}}{\alpha' - \beta} \right) \int_0^{t_2} (e^{\alpha' t_2} e^{-(\alpha' + \beta)\tau} - e^{-\alpha' t_2} e^{(\alpha' - \beta)\tau}) d\tau \quad (3.79)$$

which on integration gives

$$R_{xx}(t_1, t_2) = \frac{\kappa T f_{eq}}{m^2} \left( \frac{e^{-\beta t_1} - e^{-\alpha' t_1}}{\alpha' - \beta} \right) \left( \frac{e^{\alpha' t_2} - e^{-\beta t_2}}{\alpha' + \beta} - \frac{e^{-\beta t_2} - e^{\alpha' t_2}}{\alpha' - \beta} \right) \quad (3.80)$$

The variance in position can be obtained using Step V of the Algorithm 1 as:

$$E\{x^2(t)\} = \frac{\kappa T f_{eq}}{m^2 (\alpha' - \beta)^2} (e^{-\beta t} - e^{-\alpha' t}) \left( (e^{\alpha' t} - e^{-\beta t}) \frac{\alpha' - \beta}{\alpha' + \beta} - (e^{-\beta t} - e^{\alpha' t}) \right) \quad (3.81)$$

### 3.10.4 Variance for Model 5

A comparison of Model 2 and Model 5 shown in Fig. 3.7 and Fig. 3.10 respectively shows that in Model 5, an additional integration is performed on the signal  $Y(t)$ . The mathematical model to be used in Step II for the additional integration is given by equation (3.30). According to Step III, the cross correlation between  $Y(t)$  and output signal  $u'(t)$  is obtained using equation (3.33) as:

$$R_{u'Y} = \int_{-\infty}^{\infty} R_{YY}(t_1 - \tau, t_2) U(\tau) d\tau \quad (3.82)$$

Substituting autocorrelation of signal  $Y(t)$  from equation (3.48), the impulse response of the integrator from equation (3.12) and replacing parameter  $t_1$  with  $t_1 - \tau$  in equation (3.82) gives

$$R_{u'Y} = \int_0^{t_2} \frac{2\kappa T f_{eq}}{m^2 \alpha'} (\alpha'(t_1 - \tau) - 1 + e^{-\alpha'(t_1 - \tau)}) (1 - e^{-\alpha' \tau}) U(\tau) d\tau \quad (3.83)$$

which can be rearranged as

$$R_{u'Y} = \frac{2\kappa T f_{eq}}{m^2 \alpha'} (1 - e^{-\alpha' t_2}) \int_0^{t_1} (\alpha'(t_1 - \tau) - 1 + e^{-\alpha'(t_1 - \tau)}) U(\tau) d\tau \quad (3.84)$$

or

$$R_{u'Y} = \frac{2\kappa T f_{eq}}{m^2 \alpha'} (1 - e^{-\alpha' t_2}) \int_0^{t_1} (\alpha' t_1 - \alpha' \tau - 1 + e^{-\alpha' t_1} e^{\alpha' \tau}) U(\tau) d\tau \quad (3.85)$$

Equation (3.85) is integrated to obtain

$$R_{u'Y} = \frac{2\kappa T f_{eq}}{m^2 \alpha'} (1 - e^{-\alpha' t_2}) \left( \frac{\alpha' t_1^2}{2} - t_1 - \frac{e^{-\alpha' t_1} - 1}{\alpha'} \right) \quad (3.86)$$

The autocorrelation of the signal  $u'(t)$  can then be obtained using Step IV of the Algorithm 1 as

$$R_{u'u'}(t_1, t_2) = \int_0^{t_2} R_{u'Y}(t_1, t_2 - \tau) U(\tau) d\tau \quad (3.87)$$

where  $U(\tau)$  is the impulse response of the integrator. Substituting cross correlation  $R_{u'Y}$  from equation (3.86) and replacing parameter  $t_2$  with  $t_2 - \tau$  in equation (3.87) gives

$$R_{u'u'} = \frac{2\kappa T f_{eq}}{m^2 \alpha'} \left( \frac{\alpha' t_1^2}{2} - t_1 - \frac{e^{-\alpha' t_1}}{\alpha'} + \frac{1}{\alpha'} \right) \int_0^{t_2} (1 - e^{-\alpha'(t_2 - \tau)}) U(\tau) d\tau \quad (3.88)$$

which can be arranged as

$$R_{u'u'} = \frac{2\kappa T f_{eq}}{m^2 \alpha'} \left( \frac{\alpha' t_1^2}{2} - t_1 - \frac{e^{-\alpha' t_1}}{\alpha'} + \frac{1}{\alpha'} \right) \int_0^{t_2} (1 - e^{-\alpha' \tau} e^{\alpha' \tau}) U(\tau) d\tau \quad (3.89)$$

Equation (3.89) on integration gives

$$R_{u'u'} = \frac{\kappa T f_{eq}}{m^2 \alpha'^3} (\alpha'^2 t_1^2 - 2\alpha' t_1 - 2e^{-\alpha' t_1} + 2) (\alpha' t_2 - 1 + e^{-\alpha' t_2}) \quad (3.90)$$

Since there is one more sub-system in the Model 5, according to Step IV of the algorithm, the process is repeated from Step I for the next sub-system. According to Step I, the autocorrelation of input  $u'(t)$  to the last sub-system is given by equation (3.90). The mathematical model for the last sub-system is given by equation (3.31) and according to Step II, the impulse response of the sub-system is given by equation (3.17). The output from the sub-system is  $x(t)$ , which denotes the position of the particle. According to Step III of Algorithm 1, cross correlation between  $u'(t)$  and  $x(t)$  is obtained from equation (3.34) as

$$R_{xu'}(t_1, t_2) = \int_{-\infty}^{\infty} R_{u'u'}(t_1 - \tau, t_2) h(\tau) d\tau \quad (3.91)$$

Substituting the expression for autocorrelation of  $u'(t)$  from equation (3.90), impulse response  $h(\tau)$  from equation (3.17) and replacing parameter  $t_1$  with  $t_1 - \tau$ , equation (3.91) gives

$$R_{xu'} = \int_{-\infty}^{\infty} \frac{\kappa T f_{eq}}{m^2 \alpha'^3} (\alpha'^2 (t_1 - \tau)^2 - 2\alpha' (t_1 - \tau) - 2e^{-\alpha' (t_1 - \tau)} + 2) (\alpha' t_2 - 1 + e^{-\alpha' t_2}) e^{-\beta \tau} d\tau \quad (3.92)$$

which can be rearranged as

$$R_{xu'} = \frac{\kappa T f_{eq}}{\alpha'^3} (\alpha' t_2 - 1 + e^{-\alpha' t_2}) \int_0^{t_1} (\alpha'^2 (t_1 - \tau)^2 - 2\alpha' (t_1 - \tau) - 2e^{-\alpha' (t_1 - \tau)} + 2) e^{-\beta \tau} d\tau \quad (3.93)$$

which on integration gives

$$\begin{aligned} R_{xu'} = \frac{\kappa T f_{eq}}{\alpha'^3} (\alpha' t_2 - 1 + e^{-\alpha' t_2}) & \left[ \alpha'^2 t_1^2 \frac{1 - e^{-\beta t_1}}{\beta} - \alpha'^2 t_1^2 \frac{e^{-\beta t_1}}{\beta} - 2\alpha'^2 t_1 \frac{e^{-\beta t_1}}{\beta^2} \right. \\ & + 2\alpha'^2 \frac{1 - e^{-\beta t_1}}{\beta^3} + 2\alpha'^2 t_1^2 \frac{e^{-\beta t_1}}{\beta} - 2t_1 \frac{\alpha'^2}{\beta^2} (1 - e^{-\beta t_1}) - 2\alpha' t_1 \frac{1 - e^{-\beta t_1}}{\beta} \\ & \left. - 2\alpha' t_1 \frac{e^{-\beta t_1}}{\beta} + \frac{2\alpha'}{\beta^2} (1 - e^{-\beta t_1}) - 2e^{-\alpha' t_1} \frac{e^{(\alpha' - \beta) t_1}}{\alpha' - \beta} + 2 \frac{1 - e^{-\beta t_1}}{\beta} \right] \quad (3.94) \end{aligned}$$

Now the autocorrelation in position can be obtained using Step IV of the Algorithm 1 from equation (3.34) as

$$R_{xx}(t_1, t_2) = \int_0^{t_2} R_{xu'}(t_1, t_2 - \tau) h(\tau) d\tau \quad (3.95)$$

Substitution of expressions for cross correlation  $R_{xu'}(t_1, t_2)$  from equation (3.94), using impulse response  $h(\tau)$  and replacing parameter  $t_2$  with  $t_2 - \tau$  in equation (3.95) gives

$$\begin{aligned} R_{xx}(t_1, t_2) = & \frac{\kappa T f_{eq}}{\alpha'^3} \left[ \alpha'^2 t_1^2 \frac{1 - e^{-\beta_1}}{\beta} - \alpha'^2 t_1^2 \frac{e^{-\beta_1}}{\beta} - 2\alpha'^2 t_1 \frac{e^{-\beta_1}}{\beta^2} + 2\alpha'^2 \frac{1 - e^{-\beta_1}}{\beta^3} \right. \\ & + 2\alpha'^2 t_1^2 \frac{e^{-\beta_1}}{\beta} - 2t_1 \frac{\alpha'^2}{\beta^2} (1 - e^{-\beta_1}) - 2\alpha' t_1 \frac{1 - e^{-\beta_1}}{\beta} - 2\alpha' t_1 \frac{e^{-\beta_1}}{\beta} + \frac{2\alpha'}{\beta^2} (1 - e^{-\beta_1}) \\ & \left. - 2e^{-\alpha' t_1} \frac{e^{(\alpha' - \beta)t_1}}{\alpha' - \beta} + 2 \frac{1 - e^{-\beta_1}}{\beta} \right] \int_0^{t_2} (\alpha'(t_2 - \tau) - 1 + e^{-\alpha'(t_2 - \tau)}) e^{-\beta\tau} d\tau \end{aligned} \quad (3.96)$$

which can be rearranged and simplified as:

$$\begin{aligned} R_{xx}(t_1, t_2) = & \frac{\kappa T f_{eq}}{\alpha'^3} \left[ \alpha'^2 t_1^2 \frac{1 - e^{-\beta_1}}{\beta} - \alpha'^2 t_1^2 \frac{e^{-\beta_1}}{\beta} - 2\alpha'^2 t_1 \frac{e^{-\beta_1}}{\beta^2} + 2\alpha'^2 \frac{1 - e^{-\beta_1}}{\beta^3} \right. \\ & + 2\alpha'^2 t_1^2 \frac{e^{-\beta_1}}{\beta} - 2t_1 \frac{\alpha'^2}{\beta^2} (1 - e^{-\beta_1}) - 2\alpha' t_1 \frac{1 - e^{-\beta_1}}{\beta} - 2\alpha' t_1 \frac{e^{-\beta_1}}{\beta} + \frac{2\alpha'}{\beta^2} (1 - e^{-\beta_1}) \\ & \left. - 2e^{-\alpha' t_1} \frac{e^{(\alpha' - \beta)t_1}}{\alpha' - \beta} + 2 \frac{1 - e^{-\beta_1}}{\beta} \right] \int_0^{t_2} (\alpha' t_2 e^{-\beta\tau} - \alpha\tau e^{-\beta\tau} - e^{-\beta\tau} + e^{-\alpha' t_2} e^{(\alpha' - \beta)\tau}) d\tau \end{aligned} \quad (3.97)$$

which on integration gives

$$\begin{aligned} R_{xx}(t_1, t_2) = & \frac{\kappa T f_{eq}}{\alpha'^3} \left[ \alpha'^2 t_1^2 \frac{1 - e^{-\beta_1}}{\beta} - \alpha'^2 t_1^2 \frac{e^{-\beta_1}}{\beta} - 2\alpha'^2 t_1 \frac{e^{-\beta_1}}{\beta^2} + 2\alpha'^2 \frac{1 - e^{-\beta_1}}{\beta^3} \right. \\ & + 2\alpha'^2 t_1^2 \frac{e^{-\beta_1}}{\beta} - 2t_1 \frac{\alpha'^2}{\beta^2} (1 - e^{-\beta_1}) - 2\alpha' t_1 \frac{1 - e^{-\beta_1}}{\beta} \\ & \left. - 2\alpha' t_1 \frac{e^{-\beta_1}}{\beta} + \frac{2\alpha'}{\beta^2} (1 - e^{-\beta_1}) - 2e^{-\alpha' t_1} \frac{e^{(\alpha' - \beta)t_1}}{\alpha' - \beta} + 2 \frac{1 - e^{-\beta_1}}{\beta} \right] \\ & \left[ \alpha' t_2 \frac{1 - e^{-\beta_2}}{\beta} - \alpha' t_2 \frac{e^{-\beta_2}}{\beta} + \frac{\alpha'}{\beta^2} (1 - e^{-\beta_2}) - \frac{1 - e^{-\beta_2}}{\beta} + e^{-\alpha' t_2} \frac{e^{(\alpha' - \beta)t_2} - 1}{\alpha' - \beta} \right] \end{aligned} \quad (3.98)$$

According to Step V, the process is forwarded to Step VI. The variance in position is obtained according to Step VI of the Algorithm 1 by substituting  $t_1 = t_2 = t$  in equation (3.98) as

$$\begin{aligned}
 E\{x^2(t)\} = \frac{\kappa T f_{eq}}{\alpha'^3} & \left[ \alpha'^2 t^2 \frac{1-e^{-\beta t}}{\beta} - \alpha'^2 t^2 \frac{e^{-\beta t}}{\beta} - 2\alpha'^2 t \frac{e^{-\beta t}}{\beta^2} + 2\alpha'^2 \frac{1-e^{-\beta t}}{\beta^3} \right. \\
 & + 2\alpha'^2 t^2 \frac{e^{-\beta t}}{\beta} - 2t \frac{\alpha'^2}{\beta^2} (1-e^{-\beta t}) - 2\alpha' t \frac{1-e^{-\beta t}}{\beta} \\
 & \left. - 2\alpha' t \frac{e^{-\beta t}}{\beta} + \frac{2\alpha'}{\beta^2} (1-e^{-\beta t}) - 2e^{-\alpha' t} \frac{e^{(\alpha'-\beta)t}}{\alpha'-\beta} + 2 \frac{1-e^{-\beta t}}{\beta} \right] \\
 & \left[ \alpha' t \frac{1-e^{-\beta t}}{\beta} - \alpha' t \frac{e^{-\beta t}}{\beta} + \frac{\alpha'}{\beta^2} (1-e^{-\beta t}) - \frac{1-e^{-\beta t}}{\beta} + e^{-\alpha' t} \frac{e^{(\alpha'-\beta)t} - 1}{\alpha' - \beta} \right]
 \end{aligned}
 \tag{3.99}$$

In all, four new models for Brownian motion have been developed in the present chapter. A tabular summary of the equations giving autocorrelation and variance models of Model 1 through to Model 5 is given in Table 3.1.

**Table 3.1** Summary of Equations giving Autocorrelation and Variance in Position of Non-Rigid Nanoparticle

Model	Autocorrelation of Output $x(t)$	Variance of $x(t)$
Model 1	Equation (3.8)	Equation (3.9)
Model 2	Equation (3.55)	Equation (3.56)
Model 3	Equation (3.71)	Equation (3.72)
Model 4	Equation (3.80)	Equation (3.81)
Model 5	Equation (3.98)	Equation (3.99)

*Rigid* (handwritten label with a bracket pointing to Model 1)

*Non-Rigid Nanoparticle* (handwritten label with an arrow pointing to the table)

### 3.11 EPILOGUE

In the first attempt to develop Brownian motion models of non-rigid nanoparticle, the impact transfer in Brownian motion was explored and a few possibilities were modeled. The impact transfer modeling is akin to the correlation technique and since we are using correlation technique to develop variance models of Brownian motion, we gave first consideration to impact transfer modeling. In order to

develop impact transfer models of Brownian motion of non-rigid nanoparticle, the nanoparticle was considered with elastic and dissipative properties in the first step. For this, a concept of equivalent damping coefficient representing resistance to global and local motion of non-rigid nanoparticle was introduced. In the next step, the Ornstein-Uhlenbeck model of Brownian motion of rigid nanoparticle was developed in the form of impact transfer model and an interaction of elastic and dissipative properties of nanoparticle was chosen as sub-system. The inclusion of sub-system in the Ornstein-Uhlenbeck model represented as impact transfer model presented various possibilities, which was done leading to four new impacts transfer models.

Lastly, the model of variance in position of non-rigid nanoparticle was obtained using an algorithm based on correlation technique. The method of modeling in the present chapter is based on a realistic consideration that nanoparticle is elastic rather than rigid. The developed models are testified for validity criterion by simulation in next chapter.

## CHAPTER 4

# IMPACT TRANSFER MODEL VALIDATION BY SIMULATION

### 4.1 INTRODUCTION

The four models of Brownian motion of non-rigid nanoparticles developed in the last chapter are subjected to a validity checks in the first part of this chapter. First, two validity criterions are defined and two nanoparticles are chosen having sizes corresponding to extremities in nano-domains. Next, the four models are simulated for the two chosen nanoparticles over a wide range of parametric variation. The simulation results are tested against the defined validity criterion. In the second part of the chapter, based on the lessons learned from the simulation of four models, two more models of impact transfer of Brownian motion of non-rigid nanoparticle are developed. These two new models are simulated and tested against validity criterion as is done in first part of the chapter.

### 4.2 VALIDITY CRITERION FOR MODELS OF BROWNIAN MOTION OF NANOPARTICLE

Based on Ornstein-Uhlenbeck model for Brownian motion of rigid nanoparticle, referred in this work as Model 1, four new models of non-rigid Brownian motion have been developed in previous chapter. The variances in position for five models are given by equations (3.9), (3.56), (3.72), (3.81) and (3.99) (Refer Table 3.1) respectively and are reproduced here for convenience. The variances for five models are given as

#### Model 1

$$E\{x^2(t)\} = \frac{\alpha}{2\beta^3} (1 - e^{-\beta t}) (2\beta t - 1 + e^{-\beta t}) \quad (4.1)$$

**Model 2**

$$E\{x^2(t)\} = \frac{2\kappa T f_{eq}}{m^2 \alpha' \beta} \left[ \alpha' t - (1 - e^{-\beta t}) \left( \frac{\alpha'}{\beta} + 1 \right) + \frac{\beta e^{-\alpha' t}}{\alpha' - \beta} (e^{(\alpha' - \beta)t} - 1) \right] \quad (4.2)$$

$$\left[ (1 - e^{-\beta t}) - \frac{\beta e^{-\alpha' t}}{\alpha' - \beta} (e^{(\alpha' - \beta)t} - 1) \right]$$

**Model 3**

$$E\{x^2(t)\} = \frac{\kappa T f_{eq}}{m^2 \alpha'} \left[ \frac{(e^{(\alpha' - \beta)t} - 1)}{\alpha' - \beta} \left\{ \frac{e^{(\alpha' - \beta)t} - 1}{\alpha' - \beta} (1 - e^{-2\alpha' t}) + 2e^{-\alpha' t} \frac{1 - e^{-\beta t}}{\beta} \right\} \right. \\ \left. - \frac{(e^{(2\alpha' - \beta)t} - 1)}{2\alpha' - \beta} \left\{ e^{-3\alpha' t} \frac{e^{(\alpha' - \beta)t} - 1}{\alpha' - \beta} - e^{-\alpha' t} \frac{1 - e^{-(\alpha' + \beta)t}}{(\alpha' + \beta)} + 2e^{-2\alpha' t} \frac{1 - e^{-\beta t}}{\beta} \right\} \right] \quad (4.3)$$

**Model 4**

$$E\{x^2(t)\} = \frac{\kappa T f_{eq}}{m^2 (\alpha' - \beta)^2} (e^{-\beta t} - e^{-\alpha' t}) \left( (e^{\alpha' t} - e^{-\beta t}) \frac{\alpha' - \beta}{\alpha' + \beta} - (e^{-\beta t} - e^{\alpha' t}) \right) \quad (4.4)$$

**Model 5**

$$E\{x^2(t)\} = \frac{\kappa T f_{eq}}{\alpha'^3} \left[ \alpha'^2 t^2 \frac{1 - e^{-\beta t}}{\beta} - \alpha'^2 t^2 \frac{e^{-\beta t}}{\beta} - 2\alpha'^2 t \frac{e^{-\beta t}}{\beta^2} + 2\alpha'^2 \frac{1 - e^{-\beta t}}{\beta^3} \right. \\ \left. + 2\alpha'^2 t^2 \frac{e^{-\beta t}}{\beta} - 2t \frac{\alpha'^2}{\beta^2} (1 - e^{-\beta t}) - 2\alpha' t \frac{1 - e^{-\beta t}}{\beta} \right. \\ \left. - 2\alpha' t \frac{e^{-\beta t}}{\beta} + \frac{2\alpha'}{\beta^2} (1 - e^{-\beta t}) - 2e^{-\alpha' t} \frac{e^{(\alpha' - \beta)t}}{\alpha' - \beta} + 2 \frac{1 - e^{-\beta t}}{\beta} \right] \\ \left[ \alpha' t \frac{1 - e^{-\beta t}}{\beta} - \alpha' t \frac{e^{-\beta t}}{\beta} + \frac{\alpha'}{\beta^2} (1 - e^{-\beta t}) - \frac{1 - e^{-\beta t}}{\beta} + e^{-\alpha' t} \frac{e^{(\alpha' - \beta)t} - 1}{\alpha' - \beta} \right] \quad (4.5)$$

Model 1 is an established valid model of Brownian motion for rigid particles. In order to explore the validity of the four non-rigid models, Model 2 to Model 5, two validity criteria are defined in following sub-sections.

**4.2.1 Validity Criterion 1**

The Brownian motion is a real physical process and, therefore, there should not be any imaginary value of any variable associated with the process. One physical variable of primary concern in Brownian motion is variance and this cannot be negative for all parametric values. A negative variance implies an imaginary deviation in



position, which is not [possible for a real physical process. Mathematically this criterion is expressed as

$$E\{x^2(t)\} > 0 \text{ for all parametric values} \quad (4.6)$$

#### 4.2.2 Validity Criterion 2

Another important physical constraint is that the variance values should be finite for finite parametric values in any real physical system. Thus boundedness of variance is another validity criterion for Brownian motion of nanoparticle, rigid or non-rigid. Mathematically, this is expressed as

$$E\{x^2(t)\} \neq \infty \text{ for finite parametric values} \quad (4.7)$$

Keeping in view, the validity criterion given by equation (4.7), it is observed from the equations (4.2) to (4.5) representing four non-rigid models, that denominator in the equations at some places contains a difference of  $2\alpha'$  and  $\beta$ . In that case if  $2\alpha'$  is equal to  $\beta$ , then denominator is zero and the variance becomes infinite. Since, the infinite variance for a real physical process is incorrect, it implies that  $2\alpha'$  can never be equal to  $\beta$ . Therefore, an assumption is made given as

$$2\alpha' = \varphi\beta \quad (4.8)$$

where  $\varphi$  is a dimensionless quantity, which cannot be unity. Further, it is assumed that  $\varphi = c'/r$  with  $c'$  as a constant having the dimension of length. The assumption of relating  $2\alpha'$  and  $\beta$  is helpful in simulation as this converts all  $\alpha'$  terms into  $\beta$  reducing one variable. Moreover,  $\alpha'$  and  $\beta$  have the same dimension. This assumption gives a parametric relation on substitution of expression for  $\alpha'$  and  $\beta$  in equation (4.8) as

$$f' = (2) m k / \varphi f \quad (4.9)$$

The equation (4.8) clubs the parameters used in the development of non-rigid Brownian motion model in nano-domains and needs to be verified. This assumption is verified in the next section.

### 4.3 VERIFICATION OF PARAMETRIC RELATION FOR SIMULATION

The various parameters in equation (4.9) characterize properties of nanoparticle ( $m, k, f'$ ) and surrounding medium ( $f$ ). The properties in sub-micron size domains are of considerable interest in design of systems. There is little direct knowledge of the key

structural properties. The published results of one such property of importance namely spring constant ( $k$ ) are available [Wong 1997] for two materials namely, Silicon Carbide (SiC) and Carbon. The spring constant  $k$ , which is directly related to Young's modulus, has been obtained as a function of characteristic dimension length  $l$  of Silicon carbide rods and carbon tubes. The  $k$  values obtained by measuring bending force in relation to displacement along the unpinned length of nanorods and are available in Fig. 2(b) and 3(b) of Wong. The relations between characteristic dimensions of various shapes are given in Welty [1984] according to which a spherical shape characterized by radius, as in case of spherical nanoparticle, can be related to length of nanorods and nanotubes as  $r = \frac{3}{4}l$ . Using this an equivalent spherical nanoparticle is hypothesized corresponding to a nanorods and nanotubes of length  $l$ . The relation of parameters given by equation (4.8) can be used to obtain the values of  $k$  analytically for the equivalent spherical nanoparticle. In order to compare the experimental observations of Wong with the results from equation (4.9), simulation over wide a range of parametric value is carried out. The spring constant is obtained by rearranging equation (4.9) giving

$$k = \frac{\varphi \ddot{f}'}{2m} \quad (4.10)$$

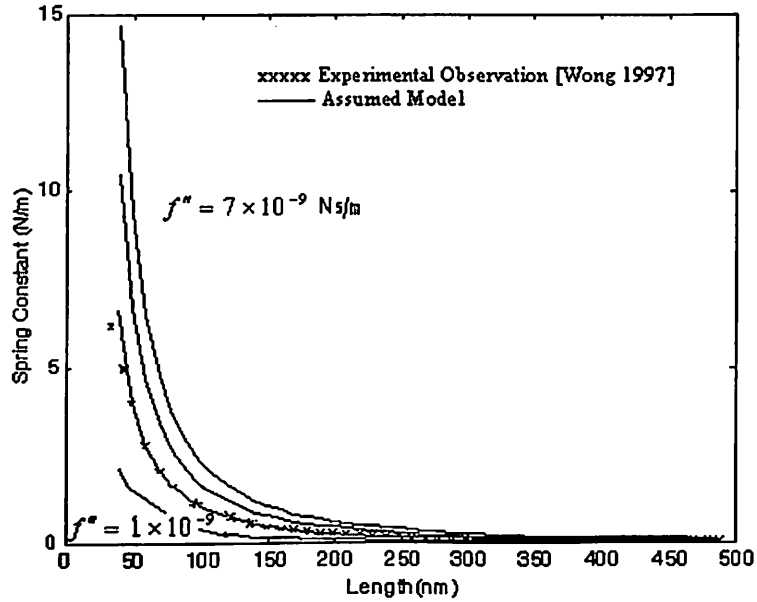
Assuming  $f'' = \varphi f'/2$ , equation (4.10) gives

$$k = \frac{\ddot{f}''}{m} \quad (4.11)$$

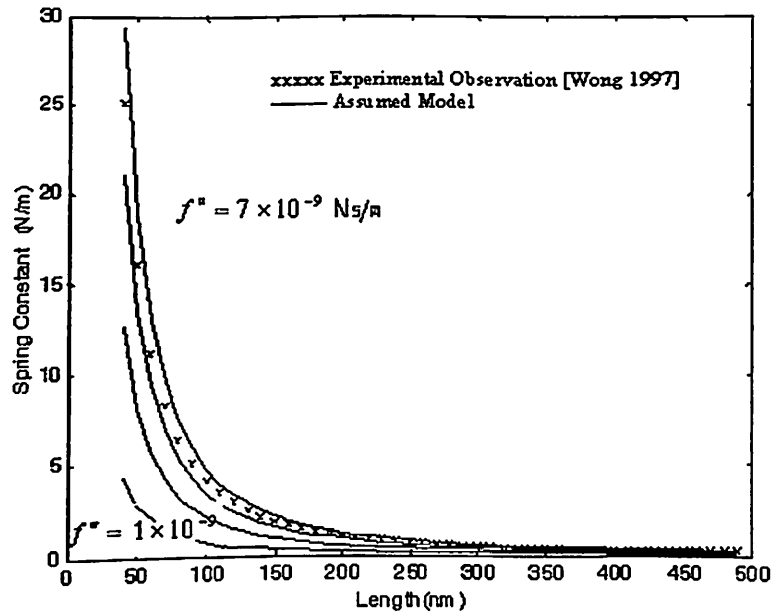
For the simulation of equation (4.11), following parameters are used for Silicon Carbide.

The density of Silicon Carbide is  $\rho = 3200 \text{ kg/m}^3$  and viscosity of surrounding water at room temperature is  $\eta = 1.003 \times 10^{-3} \text{ N s/m}^2$ . From these parameters, mass ( $m = 4\pi r^3 \rho/3$ ) and damping coefficient ( $f = 6\pi r \eta$ ) are computed as function of  $l$ . The values of  $m$  and  $f$  are substituted in equation (4.11) and  $f''$  are varied between  $1 \times 10^{-9}$  to  $7 \times 10^{-9} \text{ N s/m}$  in the step of  $2 \times 10^{-9} \text{ N s/m}$  to obtain  $k$  as a function of  $l$ . The results of simulations giving  $k$  are shown in Fig. 4.1(i). The experimental observations of Wong are also superimposed. It has been found that for  $f'' = 2.98 \times 10^{-9} \text{ N s/m}$ , the variation in  $k$  with size matches with the experimental observations. Similarly, for the second material carbon, using density of Carbon as  $1600 \text{ kg/m}^3$  the simulation results

are shown in Fig. 4.1(ii). For a parametric value  $f'' = 5.97 \times 10^{-9}$  N s/m, the  $k$  variation with  $l$  again matches with the reported experimental results, which are superimposed in Fig. 4.1(ii).



(i) Simulation for Silicon Carbide Nanorods



(ii) Simulation for Carbon Nanotubes

**Fig. 4.1** Variation of Spring Constant  $k$  with Length of Silicon Carbide Nanorods and Carbon Nanotubes

It is observed from the above simulation that the requirement of finite and bounded variance leading to the assumption  $2\alpha' = \varphi\beta$  (equation (4.8)) suggests a relation between four property parameters of concern in Brownian motion of non-rigid nanoparticle given by equation (4.9). The verification of relation between parameters  $k$  and  $f'$  with parameters of rigid body model  $f$  and  $m$  strongly justifies the exploration of non-rigid models in nano-domains. This work has been published [Sharma 2003(i)] and is used in simulation of the four-variance models of non-rigid nanoparticle.

The variance values of four non-rigid models devoid of positive scale multiplier are simulated using respective mathematical equations of variance for the four models in the next section.

#### 4.4 SIMULATION OF IMPACT TRANSFER MODELS

From equations (4.2) to (4.5), it is noted that the various constants and parameters required for simulation of four models are:  $\kappa$ ,  $T$ ,  $f$ ,  $r$ ,  $\eta$ ,  $m$ ,  $\beta$ ,  $\omega$ ,  $\alpha'$ ,  $f'$ ,  $k$ ,  $f_{eq}$  and  $t$ . The parameter  $f$  is a function of  $r$  and  $\eta$ ; and  $m$  is a function of  $r$  and  $\rho$ . The parameter  $f'$  is given by equation (4.9) and  $\beta$  is related to  $f$  and  $m$  as  $\beta = f/m$ . For simulation, time is incremented in steps of  $1/\beta$  so that  $\beta t$  term assumes integer values. The simulation of variance for four Brownian motion models of non-rigid nanoparticle is done considering two nanoparticles. The two nanoparticle are chosen for which the published experimental results are available. The first nanoparticle; namely Silicon has the size near the lower end of nano-domains. By the lower end, it is meant that further below the size quantum effects starts becoming appreciable. The second nanoparticle is of Polystyrene and has size equivalent to size at the upper boundary of nano-domains. At the upper boundary, the particle becomes micrometer size and nano-effects like non-rigidity is not a matter of concern. In order to find the valid models among the four non-rigid models, the simulation of variance in position with respect to time is done for silicon nanoparticle first and polystyrene nanoparticle next.

#### 4.4.1 Simulation for Silicon Nanoparticle

Sasaki [2000] has published the observed variances for Brownian motion of Silicon nanoparticle. The parameters required for simulation of models are taken as published in work of Sasaki and are given as follows

$$\text{Density } (\rho) = 2300 \text{ kg/m}^3,$$

$$\text{Temperature of surrounding } (T) = 273 \text{ K},$$

$$\text{Radius of nanoparticle } (r) = 40 \text{ nm},$$

$$\text{Viscosity of surrounding medium water } (\eta) = 1.8 \times 10^{-3} \text{ N s/m}^2,$$

These parameters give the values of mass  $m$  and  $f'$  of nanoparticle, damping coefficient of medium  $f$ , and  $\alpha'$  and  $\beta$  as

$$m = \frac{4}{3} \pi r^3 \eta \rho = 6.16 \times 10^{-19} \text{ kg}$$

$$f = 6\pi r \eta = 1.356 \times 10^{-9} \text{ N s/m}$$

$$f' = \frac{2mk}{\phi f} = \frac{2mkr}{c'f} = 6.51 \times 10^{-17} \frac{k}{c'} \text{ N s/m}$$

$$\beta = \frac{f}{m} = 2.26 \times 10^9 \text{ Hz}$$

$$\alpha' = \frac{2\kappa T f_{eq}}{m^2} = \frac{2\kappa T (f + f')}{m^2} = 1.98 \times 10^{16} \left( 1.356 \times 10^{-9} + 6.51 \times 10^{-17} \frac{k}{c'} \right) \text{ m}^2/\text{s}^3$$

where Boltzman's constant is  $\kappa = 1.3807 \times 10^{-23} \text{ J/K}$ . The value of  $k$  is small in nano-domains and is of the order of  $\sim 10^1$  as given by Roukes [2000]. It is assumed that  $k = 2.3 \text{ N/m}$ , time is varied from  $1/\beta$  to  $10/\beta$  and  $c'$  is varied from  $1 \times 10^{-10}$  to  $100 \text{ m}$ .

The variance value devoid of positive scale multiplier is time dependent part of the expression of variance in each model and is called as function  $\psi$ . The simulation of  $\psi$  is carried out in next section with  $c'$  and  $t$  as parameters. The simulation results of function  $\psi$  are plotted on y-axis with time on x-axis.

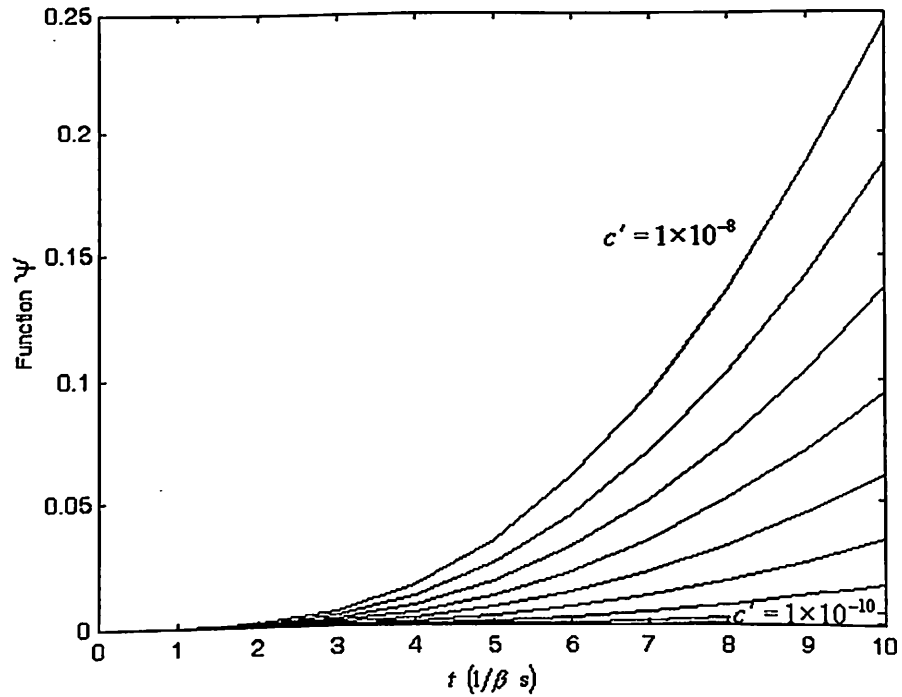
**(a) Simulation of Model 2**

For Model 2, the function  $\psi$  is obtained from equation (4.2) as the time dependent part devoid of positive scale multiplier given as

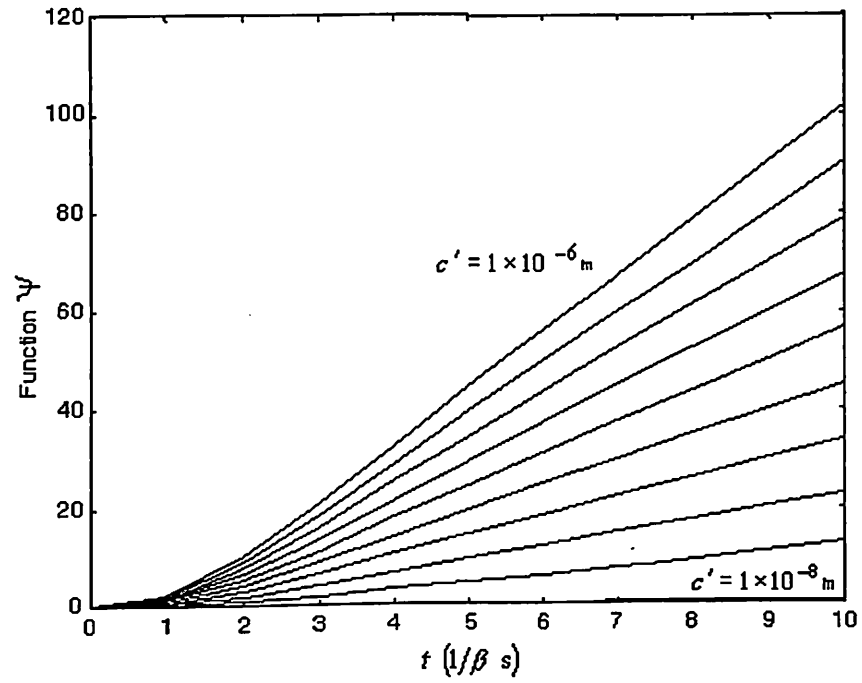
$$\psi = \left[ \alpha' t - (1 - e^{-\beta t}) \left( \frac{\alpha'}{\beta} + 1 \right) + \frac{\beta e^{-\alpha' t}}{\alpha' - \beta} (e^{(\alpha' - \beta)t} - 1) \right] \left[ (1 - e^{-\beta t}) - \frac{\beta e^{-\alpha' t}}{\alpha' - \beta} (e^{(\alpha' - \beta)t} - 1) \right] \quad (4.12)$$

The values of  $\psi$  are obtained using equation (4.12) for range of  $c'$  stated above and are shown in Fig. 4.2. It is observed that the function value is infinite for  $c' > 1 \times 10^{-6}$  m in finite time  $t$ . The infinite values depicting singularity are shown as the truncated plots in Fig. 4.2(iii).

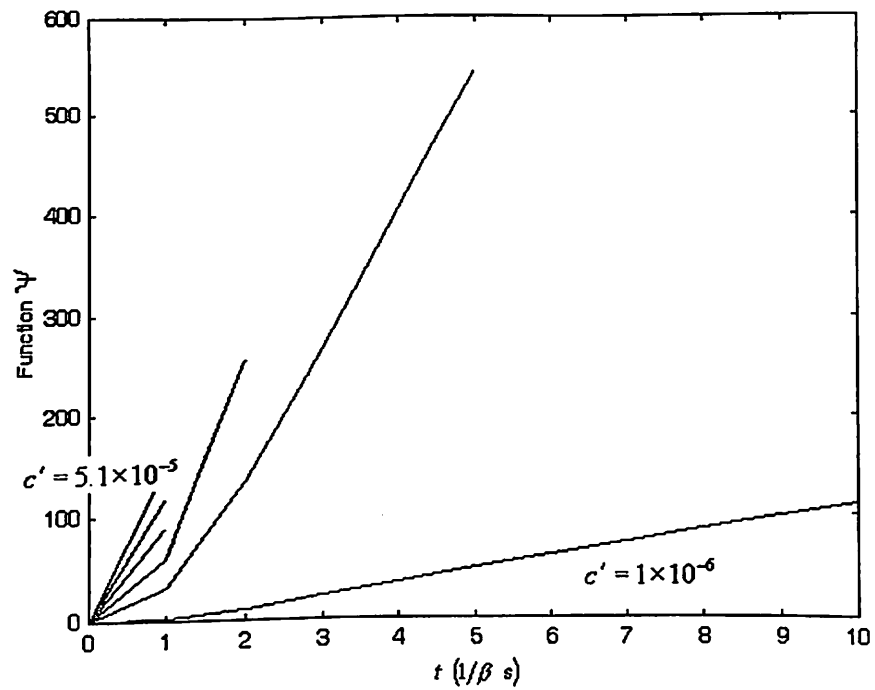
The singularity and infinite variance for finite parametric values are implausible for a valid model and therefore the Model 2 fails to satisfy validity criterion 2. For further confirmation of rejection of Model 2 another simulation is done with another set of parameters for polystyrene nanoparticle in next section.



(i)  $\psi$  vs  $t$  in Parameter Range:  $1 \times 10^{-10} \leq c' \leq 1 \times 10^{-8}$  m in steps of  $1 \times 10^{-9}$  m



(ii)  $\varphi$  vs  $t$  in Parameter Range:  $1 \times 10^{-8} \leq c' \leq 1 \times 10^{-6}$  m in steps of  $1 \times 10^{-7}$  m



(iii)  $\varphi$  vs  $t$  in Parameter Range:  $1 \times 10^{-6} \leq c' \leq 1 \times 10^{-4}$  m in steps of  $1 \times 10^{-5}$  m

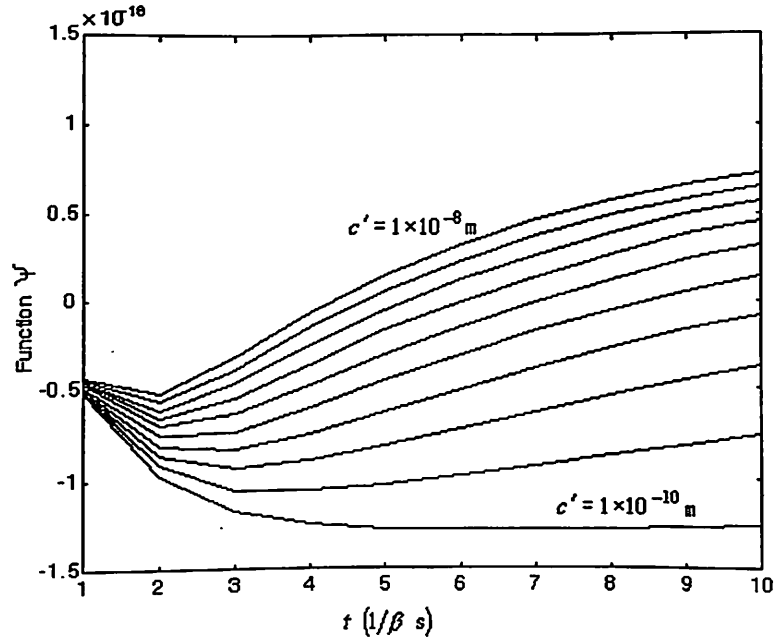
Fig. 4.2 Simulation of Model 2 for Silicon Nanoparticle

**(b) Simulation of Model 3**

For Model 3, the function  $\psi$  is obtained from equation (4.3) as the time dependent part devoid of positive scale multiplier and is given as

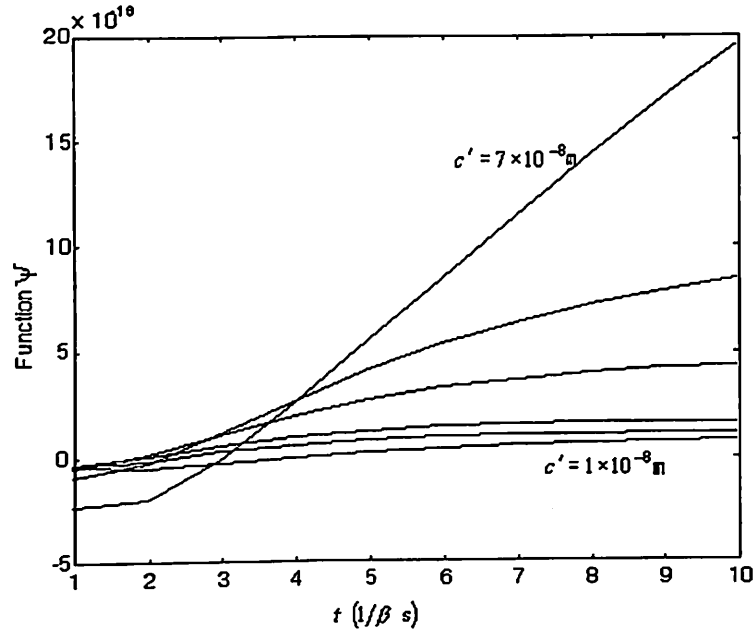
$$\psi = \left( \frac{e^{(\alpha'-\beta)t} - 1}{\alpha' - \beta} \left\{ \frac{e^{(\alpha'-\beta)t} - 1}{\alpha' - \beta} (1 - e^{-2\alpha't}) + 2e^{-\alpha't} \frac{1 - e^{-\beta t}}{\beta} \right\} - \frac{e^{(2\alpha'-\beta)t} - 1}{2\alpha' - \beta} \right. \\ \left. \left\{ e^{-3\alpha't} \frac{e^{(\alpha'-\beta)t} - 1}{\alpha' - \beta} - e^{-\alpha't} \frac{1 - e^{-(\alpha'+\beta)t}}{(\alpha' + \beta)} + 2e^{-2\alpha't} \frac{1 - e^{-\beta t}}{\beta} \right\} \right) \quad (4.13)$$

The values of  $\psi$  are simulated using equation (4.13) for range of  $c'$  stated above and are shown in Fig. 4.3. It is observed from simulation results that Model 3 predicts negative variance for parametric variation  $1 \times 10^{-10} \leq c' \leq 7 \times 10^{-8}$  m. The plots of function  $\psi$  in this parametric range are shown in Fig. 4.3(i) and Fig. 4.3(ii). It is also observed from simulation results that the function value is infinite for  $c' > 3.2 \times 10^{-6}$  m. The model prediction therefore neither test out the criterion of non-negativity of variance and nor does the model predicts finite value of variance for finite parametric values. Therefore, the Model 3 is a case for rejection according to both validity criterions. For further confirmation of rejection of model another simulation is done for polystyrene nanoparticle in next section.



(i)  $\psi$  vs  $t$  in Parameter Range:  $1 \times 10^{-10} \leq c' \leq 1 \times 10^{-8}$  m in steps of  $1 \times 10^{-9}$  m





(ii)  $\varphi$  vs  $t$  in Parameter Range:  $1 \times 10^{-8} \leq c' \leq 7 \times 10^{-8}$  m in the steps of  $1 \times 10^{-8}$  m

**Fig. 4.3** Simulation of Model 3 for Silicon Nanoparticle

#### (c) Simulation of Model 4

For Model 4, the function  $\psi$  is obtained from equation (4.4) as the time dependent part devoid of positive scale multiplier and is given as

$$\psi = (e^{-\beta t} - e^{-\alpha' t}) \left( (e^{\alpha' t} - e^{-\beta t}) \frac{\alpha' - \beta}{\alpha' + \beta} - (e^{-\beta t} - e^{\alpha' t}) \right) \quad (4.14)$$

The values of  $\psi$  are obtained using equation (4.12) for range of  $c'$  stated above and are shown in Fig. 4.4. It is observed from simulation results that Model 4 predicts negative variance for all time in complete parametric range  $1 \times 10^{-10} \leq c' \leq 100$  m. Since the trend is same in complete parametric range, only the plots of function  $\psi$  in parametric range  $1 \times 10^{-10} \leq c' \leq 1 \times 10^{-8}$  m are shown in Fig. 4.4. The negative function value invalidates the Model 3 according to validity criterion 1 and therefore the Model 3 is a case for rejection. For further confirmation of rejection of model another simulation is done for polystyrene nanoparticle in next section.

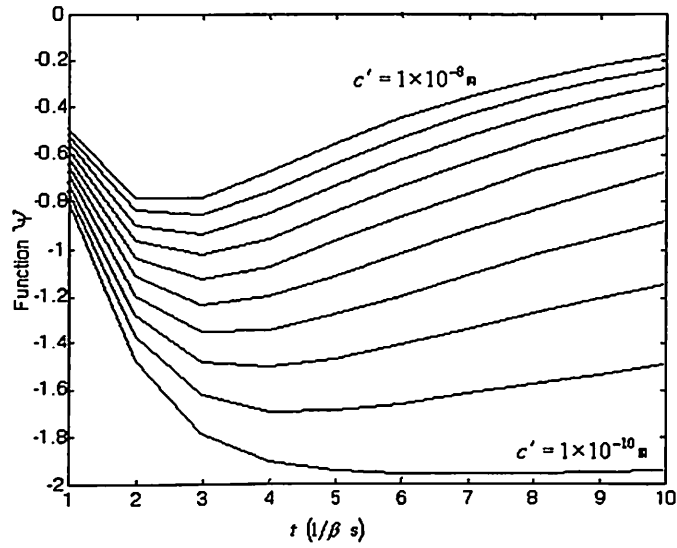


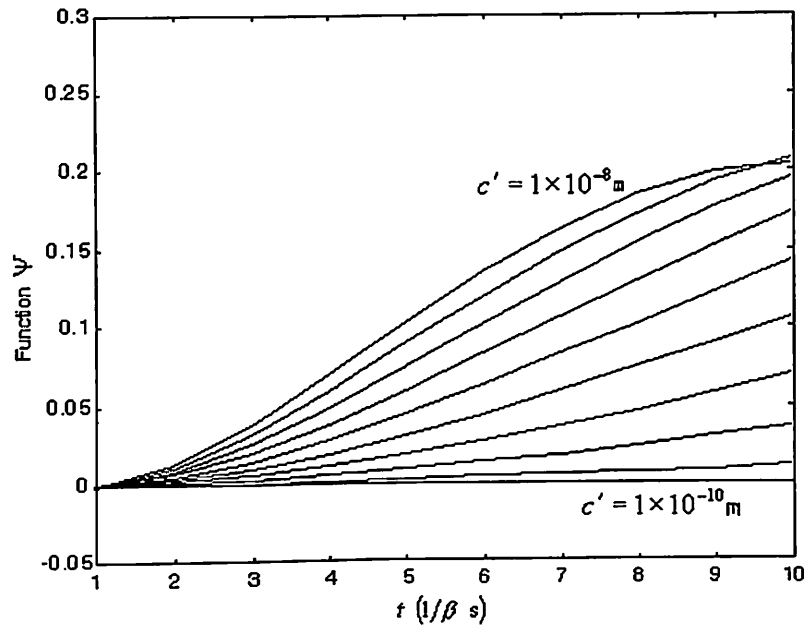
Fig. 4.4 Simulation of Model 4 for Silicon Nanoparticle for  $1 \times 10^{-10} \leq c' \leq 1 \times 10^{-8}$  m in steps of  $1 \times 10^{-9}$  m

#### (d) Simulation of Model 5

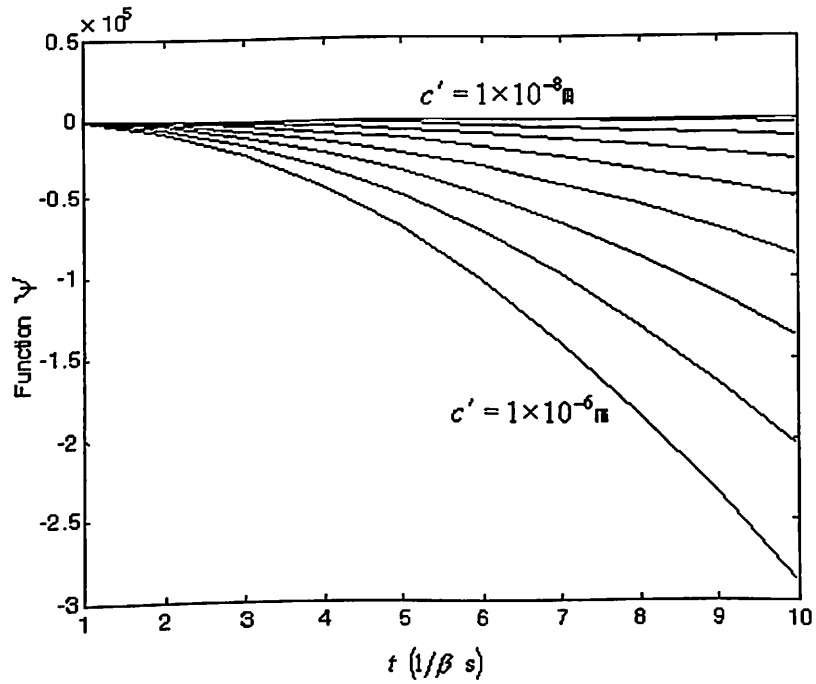
For Model 5, the function  $\psi$  is obtained from equation (4.5) as the time dependent part devoid of positive scale multiplier and is given as

$$\psi = \left( \alpha'^2 t^2 \frac{1}{\beta} + 2\alpha'^2 \frac{1-e^{-\beta t}}{\beta^3} - 2t \frac{\alpha'^2}{\beta^2} - 2\alpha' t \frac{1}{\beta} + \frac{2\alpha'}{\beta^2} (1-e^{-\beta t}) - 2e^{-\alpha t} \frac{e^{(\alpha'-\beta)t}}{\alpha'-\beta} \right. \\ \left. + 2 \frac{1-e^{-\beta t}}{\beta} \left( \alpha' t \frac{1-2e^{-\beta t}}{\beta} + \frac{\alpha'}{\beta^2} (1-e^{-\beta t}) - \frac{1-e^{-\beta t}}{\beta} + e^{-\alpha t} \frac{e^{(\alpha'-\beta)t} - 1}{\alpha'-\beta} \right) \right) \quad (4.15)$$

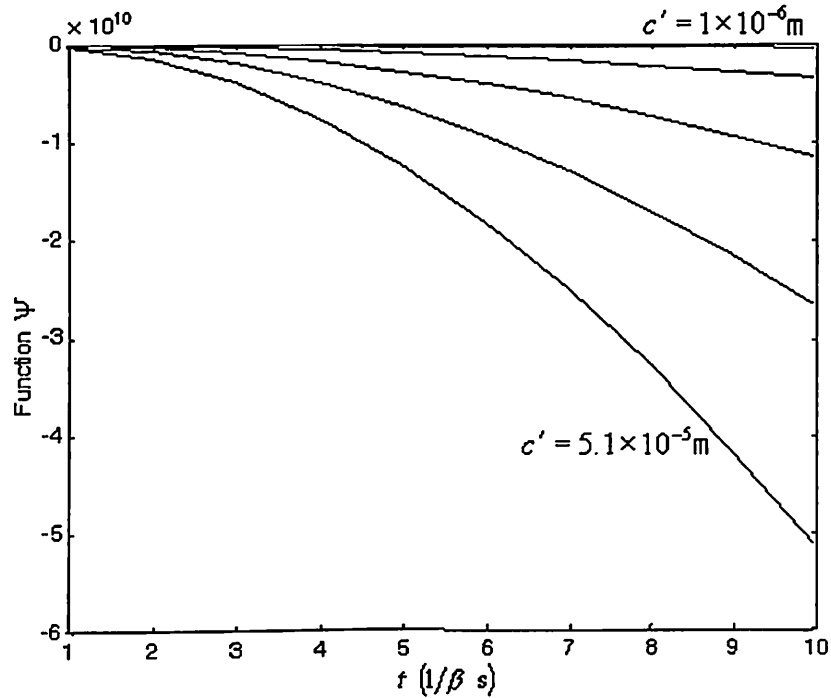
The values of  $\psi$  are obtained using equation (4.13) for specified range of  $c'$  and are shown in Fig. 4.5. It is observed from simulation results that the function values are negative for  $1 \times 10^{-7} \leq c' \leq 5.1 \times 10^{-5}$  m beyond which it becomes infinite. The plots showing negative function value are shown in Fig. 4.5(ii) and 4.5(iii). The model prediction therefore neither tests out the criterion of non-negativity of variance nor does the model predict finite value of variance for finite parametric values. Therefore, the model is a case for rejection according to both validity criteria. For further confirmation of rejection of model another simulation is done for polystyrene nanoparticle in next section.



(i)  $\varphi$  vs  $t$  in Parameter Range:  $1 \times 10^{-10} \leq c' \leq 1 \times 10^{-8} \text{ m}$  in Steps of  $1 \times 10^{-9} \text{ m}$



(ii)  $\varphi$  vs  $t$  in Parameter Range:  $1 \times 10^{-8} \leq c' \leq 1 \times 10^{-6} \text{ m}$  in Steps of  $1 \times 10^{-7} \text{ m}$



(iii)  $\varphi$  vs  $t$  in Parameter Range:  $1 \times 10^{-6} \leq c' \leq 5.1 \times 10^{-5}$  m in Steps of  $1 \times 10^{-5}$  m

**Fig. 4.5** Simulation of Model 5 for Silicon Nanoparticle

From the simulation of the four Brownian motion models of non-rigid nanoparticle, it is found that models predict either negative or infinite variance. It is critical to observe at this stage that the four developed impact transfer models are unable to capture the Brownian motion of non-rigid silicon nanoparticle and a vital link seems to be missing in the impact transfer models. For confirmation of the negative results, the impact transfer models are again simulated for another nanoparticle in next sub-section.

#### 4.4.2 Simulation for Polystyrene Nanoparticle

The proposed four Brownian motion models of non-rigid nanoparticle are simulated for a polystyrene nanoparticle in this section. The Brownian motion of Polystyrene nanoparticle is available as published result [Nakroshis 2003] as variance plots. The values of various parameters are taken from the work Nakroshis are

$$\text{Density } (\rho) = 1060 \text{ kg/m}^3$$

$$\text{Temperature of surrounding } (T) = 296.01 \pm 0.3 \text{ K}$$

$$\text{Radius of nano-particle } (r) = 0.51 \pm 0.01 \mu \text{ m}$$

$$\text{Viscosity of surrounding medium } (\eta) = (936 \pm 15) \times 10^{-6} \text{ N s/m}^2$$

These parameters give the values of mass  $m$  and  $f'$  of nanoparticle, damping coefficient of medium  $f$ , and  $\alpha'$  and  $\beta$  as

$$m = \frac{4}{3} \pi r^3 \eta \rho = (5.88 \pm 0.35) \times 10^{-16} \text{ kg}$$

$$f = 6\pi r \eta = (9.00 \pm 0.32) \times 10^{-9} \text{ N s/m}$$

$$f' = \frac{2mk}{\varphi f} = \frac{2mkr}{c'f} = (6.65 \pm 0.75) \times 10^{-14} \frac{k}{c'} \text{ N s/m}$$

$$\beta = \frac{f}{m} = (1.53 \pm 0.15) \times 10^7 \text{ Hz}$$

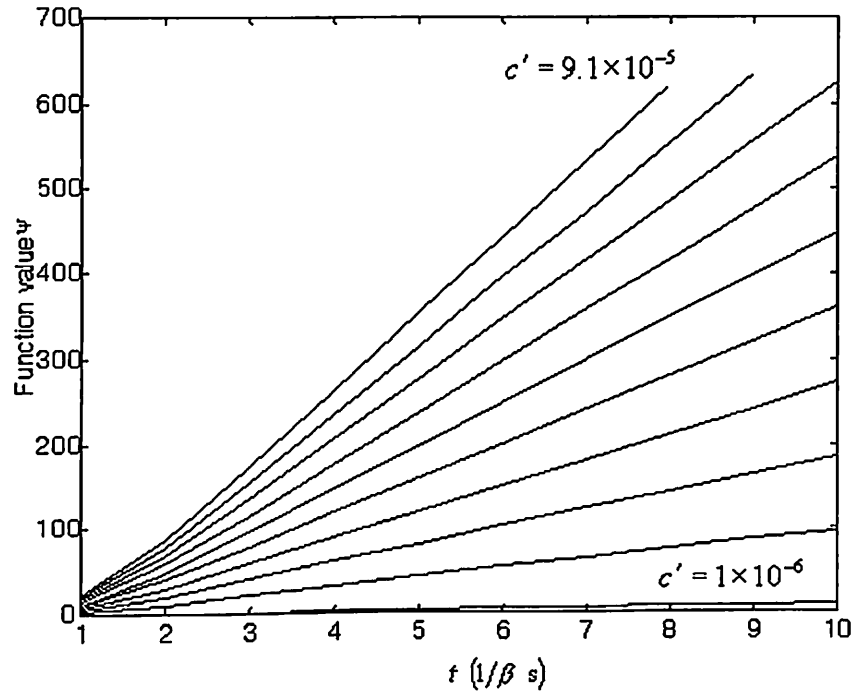
$$\alpha' = \frac{2\kappa T(f + f')}{m^2} = 2.36 \times 10^{10} \left( (9.0 \pm 0.32) \times 10^{-9} + (6.65 \pm 0.75) \times 10^{-14} \frac{k}{c'} \right) \text{ m}^2/\text{s}^3$$

For the simulation of function  $\psi$ , the tolerance values on the parameters are neglected and the value of  $k$  is assumed as  $k = 2.3 \text{ N/m}$ , time is varied from  $1/\beta$  to  $10/\beta$  and  $c'$  is varied from  $1 \times 10^{-10}$  to  $100 \text{ m}$ , similar to as in case of silicon nanoparticle. The simulation results for each model are given next.

#### (a) Simulation of Model 2

For Model 2, the function  $\psi$  is given by equation (4.12). The values of  $\psi$  are simulated using equation (4.12) for the chosen range of  $c'$ . It is observed from simulation results that Model 2 predicts function value to be infinite for  $c' > 8.1 \times 10^{-5} \text{ m}$  in finite time  $t$  and this is shown as the truncated plots in Fig. 4.6.

The truncation depicts the singularity in function. The singularity and infinite variance for finite parametric values are implausible. These results corroborate the observations made for silicon nanoparticle in section 4.4.1(a) and hence the model is rejected.



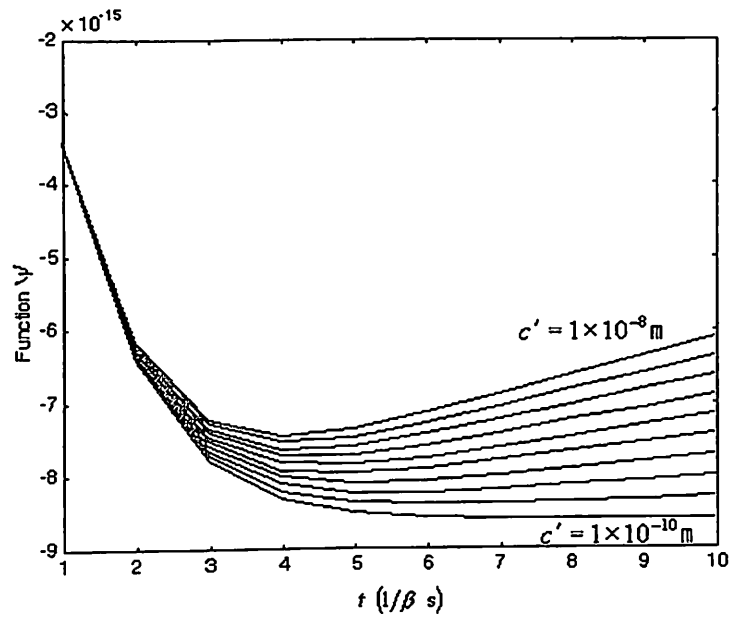
**Fig. 4.6** Simulation of Model 2 for Polystyrene Nanoparticle for  $1 \times 10^{-6} \leq c' \leq 9.1 \times 10^{-5}$  m in Steps of  $1 \times 10^{-5}$  m

**(b) Simulation of Model 3**

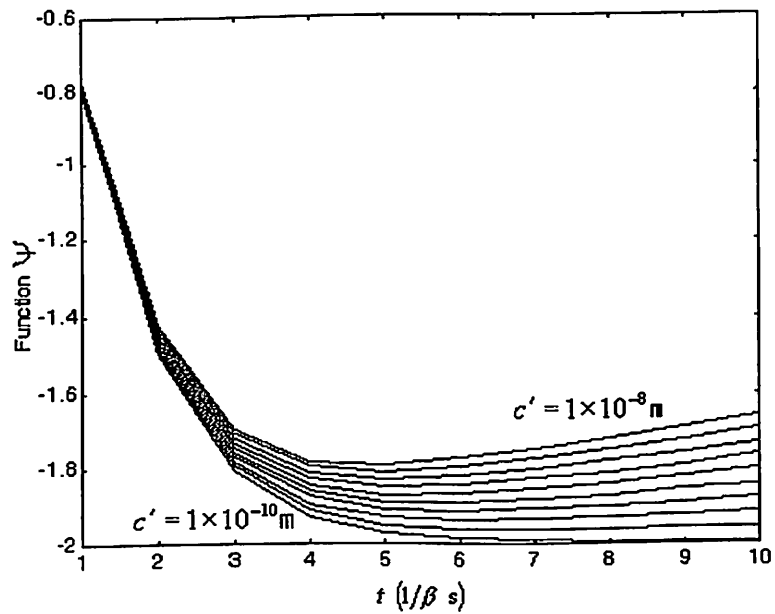
For Model 3, the function  $\psi$  is given by equation (4.13) and the values of  $\psi$  are simulated for chosen range of  $c'$ . It is observed from simulation results that Model 3 predicts negative function value for  $1 \times 10^{-10} \leq c' \leq 1 \times 10^{-6}$  m. Since the trend is same, the simulated results are shown only for  $1 \times 10^{-10} \leq c' \leq 1 \times 10^{-8}$  m in Fig. 4.7. The function values are infinite for  $c' > 1 \times 10^{-6}$ . The negative variance is not allowed according to Criterion 1 and infinite values violate Criterion 2. The results match the simulation results for silicon nanoparticle and hence the model is rejected.

**(c) Simulation of Model 4**

For Model 4, the function  $\psi$  is given by equation (4.14) and is simulated for the chosen range of  $c'$ .



**Fig. 4.7** Simulation of Model 3 for Polystyrene Nanoparticle for  $1 \times 10^{-10} \leq c' \leq 1 \times 10^{-8} \text{ m}$  in Steps of  $1 \times 10^{-9} \text{ m}$



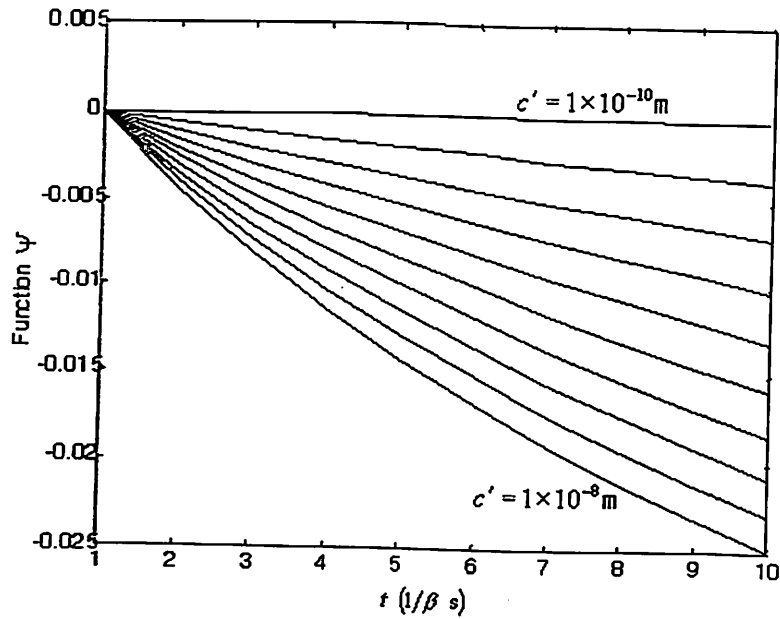
**Fig. 4.8** Simulation of Model 4 for Polystyrene Nanoparticle for  $1 \times 10^{-10} \leq c' \leq 1 \times 10^{-8} \text{ m}$  in Steps of  $1 \times 10^{-9} \text{ m}$

It is observed from simulation results that Model 4 predicts negative function value for complete parametric range  $1 \times 10^{-10} \leq c' \leq 100 \text{ m}$ . Since the trend is same,

only the plots of simulation results for  $1 \times 10^{-10} \leq c' \leq 1 \times 10^{-8}$  m are given in Fig. 4.8. The negative variance is not allowed according to Criterion 1. The results match the simulation results for silicon nanoparticle and hence the model is rejected.

**(d) Simulation of Model 5**

For Model 5, the function  $\psi$  is given by equation (4.15) and is simulated for chosen range of  $c'$ . It is observed from simulation results that Model 5 predicts negative function value for parametric range  $1 \times 10^{-10} \leq c' \leq 1 \times 10^{-4}$  m and becomes unbound for higher values of  $c'$ . Since the trend is same upto  $c' \leq 1 \times 10^{-4}$  m, the plots of simulation results are given in Fig. 4.9 for  $1 \times 10^{-10} \leq c' \leq 1 \times 10^{-8}$  m. The negative variance is not allowed according to Criterion 1 and infinite values according to Criterion 2. The results match the simulation results for silicon nanoparticle and hence the model is rejected.



**Fig. 4.9** Simulation of Model 5 for Polystyrene Nanoparticle for  $1 \times 10^{-10} \leq c' \leq 1 \times 10^{-8}$  m in Steps of  $1 \times 10^{-9}$  m

The four Brownian motion models of non-rigid nanoparticle are simulated over a wide range of parametric variation and for two test results available as published experimental results in this section. It was observed that all four models are rejected based on the simulation results not satisfying the validity criterion of positive and finite



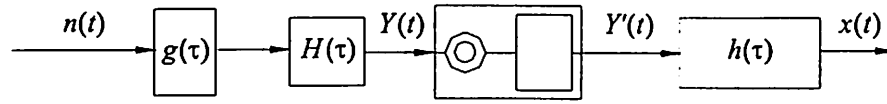
variance. Keeping in view that the models were developed with altered rigid nanoparticle impact transfer model by inclusion of non-rigid sub-system, the rejection suggests that there remains some physical aspect unmodeled in the impact transfer. The attempt to capture the unmodeled aspect of Brownian motion of non-rigid nanoparticle is done in next section.

#### 4.5 NEW IMPACT TRANSFER MODELS

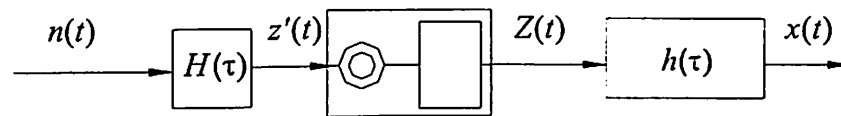
The rejection of all four Brownian motion models of non-rigid nanoparticle was discouraging but fortunately, the verification of parametric relation in Section 4.3 strongly suggests the validity of non-rigid nanoparticle model. A keen exploration yielded that the choice of non-rigid sub-system shown in Fig. 3.6, Section 3.6, is only one possibility among many other possible interactions. For example, the resistance and capacitance in the non-rigid sub-system can be in parallel arrangement instead of series. The modeling was the first attempt towards exploration of non-rigid nanoparticle and so the choice was made arbitrarily. The initial confirmation that choice of non-rigidity in nano-domains verifies observations (Refer Section 4.3), not explained otherwise, prompts for exploration of other interactions among properties in a more general way.

In order to explore the interaction among properties using impact transfer model, another sub-system is included in the impact transfer model. The new sub-system in place of actually integrating the output signal of  $f'$  and  $k$  subsystem in Model 2, does the one-dimensional Fourier transform of the autocorrelation of this signal. This is analogous to spectrum [Papoulis 1991]. If this analogous spectrum is substituted directly in equation (3.37) replacing  $2kTf_{eq}/m^2$ , it keeps the integrated white noise autocorrelation structure. This way of obtaining the autocorrelation is an assumption made to generate a different model of input to rigid nanoparticle sub-system with another sub-system introduced in series whose internal structure is unknown but behavior is known. This sub-system is represented with a symbol  $\textcircled{\square}$ . The two different possible models using this approach are explored are given next.

- (i) Impact process also includes integration in usual sense apart from  $\text{⊗-□}$ . This is shown in Fig. 4.10 and is referred as **Model 6**.
- (ii) Impact process may have no integration in and has only  $\text{⊗-□}$ . This is shown in Fig. 4.11 and is referred as **Model 7**.



**Fig. 4.10** Impact Transfer Model 6 of Brownian motion of Non-Rigid Nanoparticle.



**Fig. 4.11** Impact Transfer Model 7 of Brownian motion of Non-Rigid Body

For the two new impact transfer models, Model 6 and Model 7, the variance models are obtained using the Algorithm 1 given in Chapter 3, Section 3.9. The development of variance models is done in next section.

## 4.6 VARIANCE FOR NEW IMPACT TRANSFER MODELS

The autocorrelation of the input to impact transfer model of non-rigid nanoparticle will be  $2\kappa T f_{eq} / m^2$  for Model 6 and Model 7 according to Step I of the Algorithm 1 given in Section 3.9, Chapter 3. Moreover, according to Step II of the algorithm, we will require impulse response of the non-rigid sub-system (Refer equation (3.20)), impulse response of rigid nanoparticle sub-system (Refer equation (3.17)) and impulse response of integrator (Refer equation (3.12)). The detailed derivation of variance equation for the two new models is done next.

### 4.6.1 Variance for Model 6

A comparison of Model 2 and Model 6 (Refer Fig. 3.7 and Fig. 4.10) shows that in Model 6, an additional integration is performed on the signal output from non-rigid sub-system. The autocorrelation of  $Y(t)$  in Model 6 is same as that in Model 2 and is given by equation (3.48). The input to new sub-system introduced to obtain Model 6

requires the spectrum of the signal  $Y(t)$ , which is obtained by inverting, taking one dimensional Fourier transform, of the autocorrelation given by equation (3.48) as [Papoulis 1991]

$$S_{YY}(\omega) = \int_{-\infty}^{\infty} R_{YY}(t_1, t_2) e^{-j\omega\tau} d\tau \quad (4.14)$$

Substituting expression for autocorrelation of  $Y(t)$  from equation (3.48) in equation (4.14) gives

$$S_{YY}(\omega) = \frac{2\kappa T f_{eq}}{m^2 \alpha'} \int_{-\infty}^{\infty} (1 - e^{-\alpha't_2}) (\alpha't_1 - 1 - e^{-\alpha't_1}) e^{-j\omega\tau} d\tau \quad (4.15)$$

Assuming the impact transfer models are casual, the negative time becomes irrelevant and the limits of integration are changed to 0 to  $\infty$ . For  $t_1 = t_2 - \tau$ , rearrangement and simplification of equation (4.15) gives

$$S_{YY}(\omega) = \frac{2\kappa T f_{eq}}{m^2 \alpha'} \int_0^{\infty} (\alpha't_1 e^{-j\omega\tau} - \alpha't_1 e^{-\alpha't_1} e^{-(\alpha'+j\omega)\tau} - e^{-j\omega\tau} + e^{-\alpha't_1} e^{-(\alpha'+j\omega)\tau} - e^{-(\alpha'+j\omega)\tau} - e^{-2\alpha't_1} e^{-(\alpha'+j\omega)\tau}) d\tau \quad (4.16)$$

Integrating equation (4.16) and taking only the real part from the integrated results (since the process is a real physical phenomenon), the spectrum of  $Y(t)$  is obtained as

$$S_{YY}(\omega) = \frac{2\kappa T f_{eq}}{m^2 (\alpha'^2 + \omega^2)} (-\alpha't_1 e^{-\alpha't_1} + e^{-\alpha't_1} - 1 - e^{-2\alpha't_1}) \quad (4.17)$$

The autocorrelation of signal  $Y'(t)$  according to the modeled sub-system  $\boxed{\ominus-\square}$  is obtained by substituting expression from equation (4.17) as analogous spectrum  $(2\kappa T f_{eq}/m^2)$  in equation (3.37), autocorrelation of  $Y'(t)$  for  $t_1 < t_2$  is given as

$$R_{Y'Y'}(t_1, t_2) = \frac{2\kappa T f_{eq}}{m^2 (\alpha'^2 + \omega^2)} (-\alpha't_1 e^{-\alpha't_1} + e^{-\alpha't_1} - 1 - e^{-2\alpha't_1}) t_1 \quad (4.18)$$

and the cross correlation between output signal  $x(t)$  from rigid nanoparticle sub-system and  $Y'(t)$  can be obtained from Step III of the Algorithm 1 as

$$R_{xy'}(t_1, t_2) = \int_{-\infty}^{\infty} R_{yy'}(t_1 - \tau, t_2) h(\tau) d\tau \quad (4.19)$$

Substituting for  $R_{yy'}(t_1 - \tau, t_2)$  from equation (4.18) and impulse response from equation (3.17) and replacing  $t_1$  with  $t_1 - \tau$  in equation (4.19) gives

$$R_{xy'}(t_1, t_2) = \int_0^{t_1} \frac{2\kappa T f_{eq}}{m^2(\alpha'^2 + \omega^2)} \left( -\alpha'(t_1 - \tau) e^{-\alpha'(t_1 - \tau)} + e^{-\alpha'(t_1 - \tau)} - 1 - e^{-2\alpha'(t_1 - \tau)} \right) (t_1 - \tau) e^{-\beta\tau} d\tau \quad (4.20)$$

The simplification of terms in equation (4.20) gives

$$R_{xy'}(t_1, t_2) = \frac{2\kappa T f_{eq}}{m^2(\alpha'^2 + \omega^2)} \int_0^{t_1} \left( \begin{aligned} & -\alpha' t_1^2 e^{-\alpha' t_1} e^{(\alpha' - \beta)\tau} + \alpha' t_1 e^{-\alpha' t_1} \tau e^{(\alpha' - \beta)\tau} + t_1 e^{-\alpha' t_1} e^{(\alpha' - \beta)\tau} \\ & - t_1 e^{-\beta\tau} - t_1 e^{-2\alpha' t_1} e^{(2\alpha' - \beta)\tau} + \alpha' t_1 e^{-\alpha' t_1} \tau e^{(\alpha' - \beta)\tau} \\ & - \alpha' e^{-\alpha' t_1} \tau^2 e^{(\alpha' - \beta)\tau} - e^{-\alpha' t_1} \tau e^{(\alpha' - \beta)\tau} + \tau e^{-\beta\tau} + e^{-2\alpha' t_1} \tau e^{(2\alpha' - \beta)\tau} \end{aligned} \right) d\tau \quad (4.21)$$

The integration of each term in equation (4.21) is obtained respectively as

Term 1

$$\int_0^{t_1} -\alpha' t_1^2 e^{-\alpha' t_1} e^{(\alpha' - \beta)\tau} d\tau = -\alpha' t_1^2 e^{-\alpha' t_1} \frac{e^{(\alpha' - \beta)t_1} - 1}{\alpha' - \beta} \quad (4.22)$$

Term 2

$$\int_0^{t_1} \alpha' t_1 e^{-\alpha' t_1} \tau e^{(\alpha' - \beta)\tau} d\tau = \alpha' t_1 e^{-\alpha' t_1} \left[ \frac{t_1 e^{(\alpha' - \beta)t_1}}{\alpha' - \beta} - \frac{e^{(\alpha' - \beta)t_1} - 1}{(\alpha' - \beta)^2} \right] \quad (4.23)$$

Term 3

$$\int_0^{t_1} t_1 e^{-\alpha' t_1} e^{(\alpha' - \beta)\tau} d\tau = t_1 e^{-\alpha' t_1} \frac{e^{(\alpha' - \beta)t_1} - 1}{\alpha' - \beta} \quad (4.24)$$

Term 4

$$\int_0^{t_1} -t_1 e^{-\beta\tau} d\tau = -t_1 \frac{1 - e^{-\beta t_1}}{\beta} \quad (4.25)$$

Term 5

$$\int_0^{t_1} -t_1 e^{-2\alpha' t_1} e^{(2\alpha' - \beta)\tau} d\tau = -t_1 e^{-2\alpha' t_1} \frac{e^{(2\alpha' - \beta)t_1} - 1}{2\alpha' - \beta} \quad (4.26)$$

Term 6

$$\int_0^{t_1} \alpha' t_1 e^{-\alpha' t_1} \tau e^{(\alpha'-\beta)\tau} d\tau = \alpha' t_1 e^{-\alpha' t_1} \left[ \frac{t_1 e^{(\alpha'-\beta)t_1}}{\alpha' - \beta} - \frac{e^{(\alpha'-\beta)t_1} - 1}{(\alpha' - \beta)^2} \right] \quad (4.27)$$

Term 7

$$\begin{aligned} \int_0^{t_1} -\alpha' e^{-\alpha' t_1} \tau^2 e^{(\alpha'-\beta)\tau} d\tau &= -\alpha' e^{-\alpha' t_1} \left[ \frac{t_1^2 e^{(\alpha'-\beta)t_1}}{\alpha' - \beta} - \frac{2}{\alpha' - \beta} \left( \frac{t_1 e^{(\alpha'-\beta)t_1}}{\alpha' - \beta} - \frac{e^{(\alpha'-\beta)t_1} - 1}{(\alpha' - \beta)^2} \right) \right] \\ &= -\alpha' e^{-\alpha' t_1} \left[ \frac{t_1^2 e^{(\alpha'-\beta)t_1}}{\alpha' - \beta} - \frac{2t_1 e^{(\alpha'-\beta)t_1}}{(\alpha' - \beta)^2} + \frac{2e^{(\alpha'-\beta)t_1} - 2}{(\alpha' - \beta)^3} \right] \end{aligned} \quad (4.28)$$

Term 8

$$\int_0^{t_1} -e^{-\alpha' t_1} \tau e^{(\alpha'-\beta)\tau} d\tau = -e^{-\alpha' t_1} \left[ \frac{t_1 e^{(\alpha'-\beta)t_1}}{\alpha' - \beta} - \frac{e^{(\alpha'-\beta)t_1} - 1}{(\alpha' - \beta)^2} \right] \quad (4.29)$$

Term 9

$$\int_0^{t_1} \tau e^{-\beta\tau} d\tau = -\frac{t_1 e^{-\beta t_1}}{\beta} + \frac{1 - e^{-\beta t_1}}{\beta^2} \quad (4.30)$$

Term 10

$$\int_0^{t_1} e^{-2\alpha' t_1} \tau e^{(2\alpha'-\beta)\tau} d\tau = e^{-2\alpha' t_1} \left[ \frac{t_1 e^{(2\alpha'-\beta)t_1}}{2\alpha' - \beta} - \frac{e^{(2\alpha'-\beta)t_1} - 1}{(2\alpha' - \beta)^2} \right] \quad (4.31)$$

Where from equation (4.21) and equations (4.22) through to (4.31), the cross correlation between  $x(t)$  and  $Y'(t)$  is obtained as

$$\begin{aligned} R_{xY'}(t_1, t_2) &= \frac{2\kappa I f_{\omega}}{m^2(\alpha'^2 + \omega^2)} \left[ -\alpha' t_1^2 e^{-\alpha' t_1} \frac{e^{(\alpha'-\beta)t_1} - 1}{\alpha' - \beta} + \alpha' t_1 e^{-\alpha' t_1} \left[ \frac{t_1 e^{(\alpha'-\beta)t_1}}{\alpha' - \beta} \right. \right. \\ &\quad \left. \left. - \frac{e^{(\alpha'-\beta)t_1} - 1}{(\alpha' - \beta)^2} \right] + t_1 e^{-\alpha' t_1} \frac{e^{(\alpha'-\beta)t_1} - 1}{\alpha' - \beta} - t_1 \frac{1 - e^{-\beta t_1}}{\beta} - t_1 e^{-2\alpha' t_1} \frac{e^{(2\alpha'-\beta)t_1} - 1}{2\alpha' - \beta} \right. \\ &\quad \left. + \alpha' t_1 e^{-\alpha' t_1} \left[ \frac{t_1 e^{(\alpha'-\beta)t_1}}{\alpha' - \beta} - \frac{e^{(\alpha'-\beta)t_1} - 1}{(\alpha' - \beta)^2} \right] - \alpha' e^{-\alpha' t_1} \left[ \frac{t_1^2 e^{(\alpha'-\beta)t_1}}{\alpha' - \beta} - \frac{2t_1 e^{(\alpha'-\beta)t_1}}{(\alpha' - \beta)^2} \right. \right. \\ &\quad \left. \left. + \frac{2e^{(\alpha'-\beta)t_1} - 2}{(\alpha' - \beta)^3} \right] - e^{-\alpha' t_1} \left[ \frac{t_1 e^{(\alpha'-\beta)t_1}}{\alpha' - \beta} - \frac{e^{(\alpha'-\beta)t_1} - 1}{(\alpha' - \beta)^2} \right] - \frac{t_1 e^{-\beta t_1}}{\beta} \right. \\ &\quad \left. + \frac{1 - e^{-\beta t_1}}{\beta^2} + e^{-2\alpha' t_1} \left[ \frac{t_1 e^{(2\alpha'-\beta)t_1}}{2\alpha' - \beta} - \frac{e^{(2\alpha'-\beta)t_1} - 1}{(2\alpha' - \beta)^2} \right] \right] \end{aligned} \quad (4.32)$$

The autocorrelation in position  $x(t)$  from Step IV of Algorithm 1 is obtained as

$$R_{xx}(t_1, t_2) = \int_{-\infty}^{\infty} R_{xy'}(t_1, t_2 - \tau) h(\tau) d\tau \quad (4.33)$$

Substituting the cross correlation from equation (4.32) and impulse response from equation (3.17) in equation (4.33) gives

$$\begin{aligned} R_{xx}(t_1, t_2) = & \int_{-\infty}^{\infty} \frac{2\kappa T f_{ca}}{m^2(\alpha'^2 + \omega^2)} \left[ -\alpha' t_1^2 e^{-\alpha' t_1} \frac{e^{(\alpha'-\beta)t_1} - 1}{\alpha' - \beta} + \alpha' t_1 e^{-\alpha' t_1} \left[ \frac{t_1 e^{(\alpha'-\beta)t_1}}{\alpha' - \beta} \right. \right. \\ & \left. \left. - \frac{e^{(\alpha'-\beta)t_1} - 1}{(\alpha' - \beta)^2} \right] + t_1 e^{-\alpha' t_1} \frac{e^{(\alpha'-\beta)t_1} - 1}{\alpha' - \beta} - t_1 \frac{1 - e^{-\beta t_1}}{\beta} - t_1 e^{-2\alpha' t_1} \frac{e^{(2\alpha'-\beta)t_1} - 1}{2\alpha' - \beta} \right. \\ & \left. + \alpha' t_1 e^{-\alpha' t_1} \left[ \frac{t_1 e^{(\alpha'-\beta)t_1}}{\alpha' - \beta} - \frac{e^{(\alpha'-\beta)t_1} - 1}{(\alpha' - \beta)^2} \right] - \alpha' e^{-\alpha' t_1} \left[ \frac{t_1^2 e^{(\alpha'-\beta)t_1}}{\alpha' - \beta} - \frac{2t_1 e^{(\alpha'-\beta)t_1}}{(\alpha' - \beta)^2} \right. \right. \\ & \left. \left. + \frac{2e^{(\alpha'-\beta)t_1} - 2}{(\alpha' - \beta)^3} \right] - e^{-\alpha' t_1} \left[ \frac{t_1 e^{(\alpha'-\beta)t_1}}{\alpha' - \beta} - \frac{e^{(\alpha'-\beta)t_1} - 1}{(\alpha' - \beta)^2} \right] - \frac{t_1 e^{-\beta t_1}}{\beta} \right. \\ & \left. + \frac{1 - e^{-\beta t_1}}{\beta^2} + e^{-2\alpha' t_1} \left[ \frac{t_1 e^{(2\alpha'-\beta)t_1}}{2\alpha' - \beta} - \frac{e^{(2\alpha'-\beta)t_1} - 1}{(2\alpha' - \beta)^2} \right] \right] h(\tau) d\tau \end{aligned} \quad (4.34)$$

Equation (4.34) on integration gives

$$\begin{aligned} R_{xx}(t_1, t_2) = & \frac{2\kappa T f_{ca}}{m^2(\alpha'^2 + \omega^2)} \left[ -\alpha' t_1^2 e^{-\alpha' t_1} \frac{e^{(\alpha'-\beta)t_1} - 1}{\alpha' - \beta} + \alpha' t_1 e^{-\alpha' t_1} \left[ \frac{t_1 e^{(\alpha'-\beta)t_1}}{\alpha' - \beta} - \frac{e^{(\alpha'-\beta)t_1} - 1}{(\alpha' - \beta)^2} \right] \right. \\ & \left. + t_1 e^{-\alpha' t_1} \frac{e^{(\alpha'-\beta)t_1} - 1}{\alpha' - \beta} - t_1 \frac{1 - e^{-\beta t_1}}{\beta} - t_1 e^{-2\alpha' t_1} \frac{e^{(2\alpha'-\beta)t_1} - 1}{2\alpha' - \beta} + \alpha' t_1 e^{-\alpha' t_1} \left[ \frac{t_1 e^{(\alpha'-\beta)t_1}}{\alpha' - \beta} \right. \right. \\ & \left. \left. - \frac{e^{(\alpha'-\beta)t_1} - 1}{(\alpha' - \beta)^2} \right] - \alpha' e^{-\alpha' t_1} \left[ \frac{t_1^2 e^{(\alpha'-\beta)t_1}}{\alpha' - \beta} - \frac{2t_1 e^{(\alpha'-\beta)t_1}}{(\alpha' - \beta)^2} + \frac{2e^{(\alpha'-\beta)t_1} - 2}{(\alpha' - \beta)^3} \right] \right. \\ & \left. - e^{-\alpha' t_1} \left[ \frac{t_1 e^{(\alpha'-\beta)t_1}}{\alpha' - \beta} - \frac{e^{(\alpha'-\beta)t_1} - 1}{(\alpha' - \beta)^2} \right] - \frac{t_1 e^{-\beta t_1}}{\beta} + \frac{1 - e^{-\beta t_1}}{\beta^2} \right. \\ & \left. + e^{-2\alpha' t_1} \left[ \frac{t_1 e^{(2\alpha'-\beta)t_1}}{2\alpha' - \beta} - \frac{e^{(2\alpha'-\beta)t_1} - 1}{(2\alpha' - \beta)^2} \right] \right] \left[ \frac{1 - e^{-\beta t_2}}{\beta} \right] \end{aligned} \quad (4.35)$$

According to Step V, go to Step VI, since the sub-system is last sub-system of the Model 6. The variance in position for Model 6 is obtained from Step VI of the Algorithm 1 as

$$\begin{aligned}
E\{x^2(t)\} = & \frac{2\kappa T f_{eq}}{m^2(\alpha'^2 + \omega^2)} \left[ -\alpha' t^2 e^{-\alpha' t} \frac{e^{(\alpha'-\beta)t} - 1}{\alpha' - \beta} + \alpha' t e^{-\alpha' t} \left[ \frac{t e^{(\alpha'-\beta)t}}{\alpha' - \beta} - \frac{e^{(\alpha'-\beta)t} - 1}{(\alpha' - \beta)^2} \right] \right. \\
& + t e^{-\alpha' t} \frac{e^{(\alpha'-\beta)t} - 1}{\alpha' - \beta} - t \frac{1 - e^{-\beta t}}{\beta} - t e^{-2\alpha' t} \frac{e^{(2\alpha'-\beta)t} - 1}{2\alpha' - \beta} + \alpha' t e^{-\alpha' t} \left[ \frac{t e^{(\alpha'-\beta)t}}{\alpha' - \beta} \right. \\
& \left. \left. - \frac{e^{(\alpha'-\beta)t} - 1}{(\alpha' - \beta)^2} \right] - \alpha' e^{-\alpha' t} \left[ \frac{t^2 e^{(\alpha'-\beta)t}}{\alpha' - \beta} - \frac{2t e^{(\alpha'-\beta)t}}{(\alpha' - \beta)^2} + \frac{2e^{(\alpha'-\beta)t} - 2}{(\alpha' - \beta)^3} \right] \right. \\
& \left. - e^{-\alpha' t} \left[ \frac{t e^{(\alpha'-\beta)t}}{\alpha' - \beta} - \frac{e^{(\alpha'-\beta)t} - 1}{(\alpha' - \beta)^2} \right] - \frac{t e^{-\beta t}}{\beta} + \frac{1 - e^{-\beta t}}{\beta^2} \right. \\
& \left. + e^{-2\alpha' t} \left[ \frac{t e^{(2\alpha'-\beta)t}}{2\alpha' - \beta} - \frac{e^{(2\alpha'-\beta)t} - 1}{(2\alpha' - \beta)^2} \right] \right] \left[ \frac{1 - e^{-\beta t}}{\beta} \right] \quad (4.36)
\end{aligned}$$

#### 4.6.2 Variance for Model 7

On comparing Model 7 with Model 3 (Ref. Fig. 4.11 and Fig. 3.8), it is observed that the autocorrelation of  $z'(t)$  in Model 7 is same as that in Model 3 and is given by equation (3.58). The spectrum  $S_{z'z'}(\omega)$  of  $z'$  is computed using one-dimensional Fourier transform of autocorrelation as [Papoulis 1991]

$$S_{z'z'}(\omega) = \int_{-\infty}^{\infty} R_{z'z'}(t_1, t_2) e^{-j\omega\tau} d\tau \quad (4.37)$$

Substituting the autocorrelation from equation (3.72) in equation (4.37) gives

$$S_{z'z'}(t_1, t_2) = \frac{\kappa T f_{eq} \alpha'}{m^2} \int_{-\infty}^{\infty} e^{-\alpha'(t_1-t_2)} (1 - e^{-2\alpha' t_2}) e^{-j\omega\tau} d\tau \quad (4.38)$$

Assuming the impact transfer models are casual, the negative time becomes irrelevant and the limits of integration are changed to 0 to  $\infty$ . For  $t_1 = t_2 - \tau$ , integration of equation (4.38) gives

$$S_{z'z'}(\omega) = \frac{\kappa T f_{eq} (1 - e^{-2\alpha' t_2})}{m^2 (1 + (\omega f' / k)^2)} \quad (4.39)$$

Substituting  $\alpha' = k/f'$  in equation (4.39) and simplifying gives

$$S_{z'z'}(\omega) = \frac{\kappa T f_{eq}}{m^2} \left( \frac{\alpha'^2}{\alpha'^2 + \omega^2} \right) (1 - e^{-2\alpha' t_2}) = \alpha_{cov} \quad (\text{say}) \quad (4.40)$$

The autocorrelation of signal  $Z(t)$  according to the modeled sub-system  $\text{Ⓢ}$  in Model 7 is obtained by substituting expression from equation (4.17) as analogous spectrum  $(2\kappa T f_{eq}/m^2)$  in equation (3.37), autocorrelation of  $Z(t)$  for  $t_1 < t_2$  is given as

$$R_{ZZ}(t_1, t_2) = \alpha_{c\omega} t_1 \quad (4.41)$$

Then cross correlation between output  $x(t)$  and  $Z(t)$  is related by impulse response  $e^{-\beta r}$  and is obtained using Step III of the Algorithm 1 as

$$R_{xZ}(t_1, t_2) = \int_{-\infty}^{\infty} \frac{\kappa T f_{eq}}{m^2} \left( \frac{\alpha'^2}{\alpha'^2 + \omega^2} \right) (1 - e^{-2\alpha' t_2}) (t_1 - \tau) e^{-\beta r} d\tau \quad (4.42)$$

or

$$R_{xZ}(t_1, t_2) = \frac{\kappa T f_{eq}}{m^2 \beta^2} \left( \frac{\alpha'^2}{\alpha'^2 + \omega^2} \right) (1 - e^{-2\alpha' t_2}) (\beta t_1 - 1 + e^{-\beta t_1}) \quad (4.43)$$

Then according to Step IV of the Algorithm 1, the autocorrelation of the output  $x(t)$  is

$$\begin{aligned} R_{xx}(t_1, t_2) &= \int_{-\infty}^{\infty} R_{xZ}(t_1, t_2 - \tau) e^{-\beta r} d\tau \\ &= \frac{\kappa T f_{eq}}{m^2 \beta^2} \left( \frac{\alpha'^2}{\alpha'^2 + \omega^2} \right) (\beta t_1 - 1 + e^{-\beta t_1}) \int_{-\infty}^{\infty} (1 - e^{-2\alpha'(t_2 - \tau)}) e^{-\beta r} d\tau \end{aligned} \quad (4.44)$$

or

$$R_{xx}(t_1, t_2) = \frac{2\kappa T f_{eq} \alpha'^3}{m^2 \beta^3 (\alpha'^2 + \omega^2) (2\alpha' - \beta)} (\beta t_1 - 1 + e^{-\beta t_1}) (1 - e^{-\beta t_2}) \quad (4.45)$$

According to Step V, go to Step VI, since the sub-system is last sub-system of the Model 7. The variance in position can be obtained according to Step VI of the Algorithm 1 by substituting  $t_1 = t_2 = t$  in equation (4.45) as

$$E\{x^2(t)\} = \frac{2\kappa T f_{eq} \alpha'^3}{m^2 \beta^3 (\alpha'^2 + \omega^2) (2\alpha' - \beta)} (\beta t - 1 + e^{-\beta t}) (1 - e^{-\beta t}) \quad (4.46)$$

Equation (4.46) gives variance in position for Model 7 shown in Fig. 4.11. Next, in order to test the validity of the Model 6 given by equation (4.36) and Model 7 given by equation (4.46), the two models are simulated for the Silicon and Polystyrene nanoparticle over the entire range of  $c'$  and  $t$  as was done earlier for other four models.



The autocorrelation of signal  $Z(t)$  according to the modeled sub-system  $\textcircled{\square}$  in Model 7 is obtained by substituting expression from equation (4.17) as analogous spectrum  $(2\kappa T f_{eq}/m^2)$  in equation (3.37), autocorrelation of  $Z(t)$  for  $t_1 < t_2$  is given as

$$R_{ZZ}(t_1, t_2) = \alpha_{c\omega} t_1 \quad (4.41)$$

Then cross correlation between output  $x(t)$  and  $Z(t)$  is related by impulse response  $e^{-\beta r}$  and is obtained using Step III of the Algorithm 1 as

$$R_{xZ}(t_1, t_2) = \int_{-\infty}^{\infty} \frac{\kappa T f_{eq}}{m^2} \left( \frac{\alpha'^2}{\alpha'^2 + \omega^2} \right) (1 - e^{-2\alpha' t_2}) (t_1 - \tau) e^{-\beta r} d\tau \quad (4.42)$$

or

$$R_{xZ}(t_1, t_2) = \frac{\kappa T f_{eq}}{m^2 \beta^2} \left( \frac{\alpha'^2}{\alpha'^2 + \omega^2} \right) (1 - e^{-2\alpha' t_2}) (\beta t_1 - 1 + e^{-\beta t_1}) \quad (4.43)$$

Then according to Step IV of the Algorithm 1, the autocorrelation of the output  $x(t)$  is

$$\begin{aligned} R_{xx}(t_1, t_2) &= \int_{-\infty}^{\infty} R_{xZ}(t_1, t_2 - \tau) e^{-\beta r} d\tau \\ &= \frac{\kappa T f_{eq}}{m^2 \beta^2} \left( \frac{\alpha'^2}{\alpha'^2 + \omega^2} \right) (\beta t_1 - 1 + e^{-\beta t_1}) \int_{-\infty}^{\infty} (1 - e^{-2\alpha'(t_2 - \tau)}) e^{-\beta r} d\tau \end{aligned} \quad (4.44)$$

or

$$R_{xx}(t_1, t_2) = \frac{2\kappa T f_{eq} \alpha'^3}{m^2 \beta^3 (\alpha'^2 + \omega^2) (2\alpha' - \beta)} (\beta t_1 - 1 + e^{-\beta t_1}) (1 - e^{-\beta t_2}) \quad (4.45)$$

According to Step V, go to Step VI, since the sub-system is last sub-system of the Model 7. The variance in position can be obtained according to Step VI of the Algorithm 1 by substituting  $t_1 = t_2 = t$  in equation (4.45) as

$$E\{x^2(t)\} = \frac{2\kappa T f_{eq} \alpha'^3}{m^2 \beta^3 (\alpha'^2 + \omega^2) (2\alpha' - \beta)} (\beta t - 1 + e^{-\beta t}) (1 - e^{-\beta t}) \quad (4.46)$$

Equation (4.46) gives variance in position for Model 7 shown in Fig. 4.11. Next, in order to test the validity of the Model 6 given by equation (4.36) and Model 7 given by equation (4.46), the two models are simulated for the Silicon and Polystyrene nanoparticle over the entire range of  $c'$  and  $t$  as was done earlier for other four models.

## 4.7 SIMULATION OF NEW IMPACT TRANSFER MODELS

The simulation of the new models, Model 6 and Model 7, is done in same way as in Section 4.4 i.e. the various constants and parameters required for simulation of two new models are:  $\kappa$ ,  $T$ ,  $f$ ,  $r$ ,  $\eta$ ,  $m$ ,  $\beta$ ,  $\omega$ ,  $\alpha'$ ,  $f'$ ,  $k$ ,  $f_{eq}$  and  $t$ . For simulation, time is incremented in steps of  $1/\beta$  so that  $\beta t$  term assumes integer values. The simulation of variance for two new Brownian motion models of non-rigid nanoparticle is done considering same two nanoparticles, namely silicon and polystyrene, as in section 4.4. The simulation of variance in position with respect to time is done for silicon nanoparticle first and polystyrene nanoparticle.

### 4.7.1 Simulation for Silicon Nanoparticle

The silicon nanoparticle is characterized by parametric values given in subsection 4.4.1. The function values of two altered models namely Model 6 and Model 7 are simulated for the silicon nanoparticle in the following sub-sections.

#### (a) Simulation of Model 6

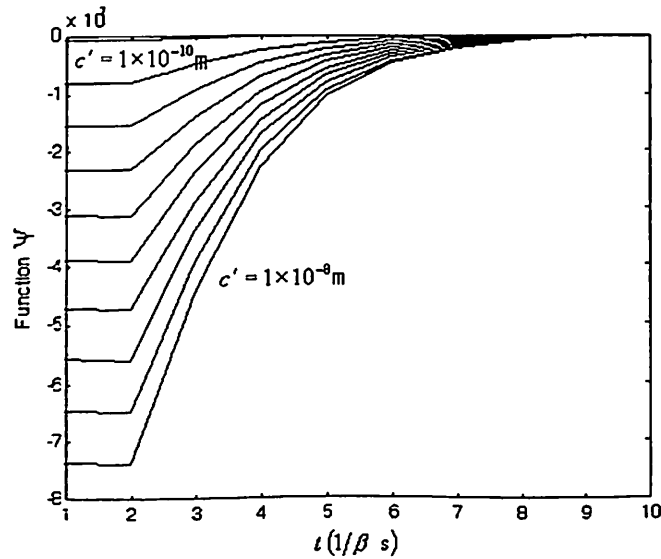
For Model 6, the function  $\psi$  is obtained from equation (4.36) as the time dependent part devoid of positive scale multiplier and is given as

$$\begin{aligned} \psi = & \left[ -\alpha' t^2 e^{-\alpha' t} \frac{e^{(\alpha'-\beta)t} - 1}{\alpha' - \beta} + \alpha' t e^{-\alpha' t} \left[ \frac{t e^{(\alpha'-\beta)t}}{\alpha' - \beta} - \frac{e^{(\alpha'-\beta)t} - 1}{(\alpha' - \beta)^2} \right] \right. \\ & + t e^{-\alpha' t} \frac{e^{(\alpha'-\beta)t} - 1}{\alpha' - \beta} - t \frac{1 - e^{-\beta t}}{\beta} - t e^{-2\alpha' t} \frac{e^{(2\alpha'-\beta)t} - 1}{2\alpha' - \beta} + \alpha' t e^{-\alpha' t} \left[ \frac{t e^{(\alpha'-\beta)t}}{\alpha' - \beta} \right. \\ & \left. - \frac{e^{(\alpha'-\beta)t} - 1}{(\alpha' - \beta)^2} \right] - \alpha' e^{-\alpha' t} \left[ \frac{t^2 e^{(\alpha'-\beta)t}}{\alpha' - \beta} - \frac{2t e^{(\alpha'-\beta)t}}{(\alpha' - \beta)^2} + \frac{2e^{(\alpha'-\beta)t} - 2}{(\alpha' - \beta)^3} \right] \\ & - e^{-\alpha' t} \left[ \frac{t e^{(\alpha'-\beta)t}}{\alpha' - \beta} - \frac{e^{(\alpha'-\beta)t} - 1}{(\alpha' - \beta)^2} \right] - \frac{t e^{-\beta t}}{\beta} + \frac{1 - e^{-\beta t}}{\beta^2} \\ & \left. + e^{-2\alpha' t} \left[ \frac{t e^{(2\alpha'-\beta)t}}{2\alpha' - \beta} - \frac{e^{(2\alpha'-\beta)t} - 1}{(2\alpha' - \beta)^2} \right] \right] \left[ \frac{1 - e^{-\beta t}}{\beta} \right] \end{aligned} \quad (4.47)$$

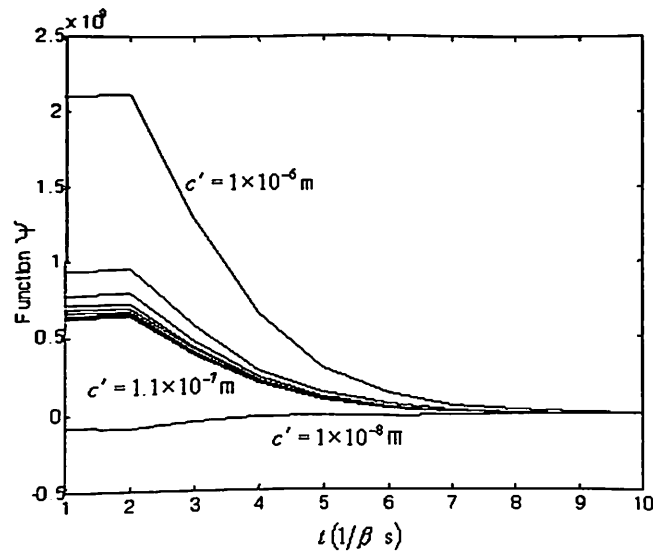
The values of  $\psi$  are obtained using equation (4.47) for specified range of  $c'$ . It is observed from simulation results that Model 6 predicts negative function value for parametric variation  $1 \times 10^{-10} \leq c' < 1 \times 10^{-7}$  m. The plots of function  $\psi$  in the

parametric range  $1 \times 10^{-10} \leq c' < 1 \times 10^{-6}$  m are shown in Fig. 4.12(i) and Fig. 4.12(ii). The simulation results predict infinite function values for  $c' > 1 \times 10^{-6}$  m.

The model prediction, therefore, neither test out the validity criterion of non-negativity of variance and nor does the model predicts finite value of variance for finite parametric values. Therefore the model is rejected according to both validity criterions. For further confirmation of rejection of model another simulation is done with another set of parameters given for polystyrene nanoparticle in next section.



(i)  $\varphi$  vs  $t$  in Parameter Range:  $1 \times 10^{-10} \leq c' \leq 1 \times 10^{-8}$  m in Steps of  $1 \times 10^{-9}$  m



(ii)  $\varphi$  vs  $t$  in Parameter Range:  $1 \times 10^{-8} \leq c' \leq 1 \times 10^{-6}$  m in Steps of  $1 \times 10^{-7}$  m

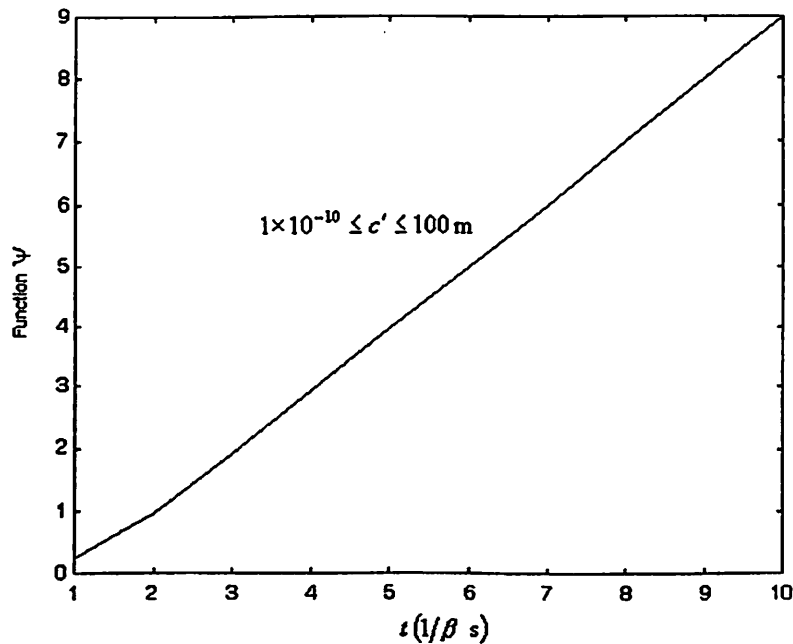
**Fig. 4.12** Simulation of Model 6 for Silicon Nanoparticle

**(b) Simulation of Model 7**

For Model 7, the function  $\psi$  is obtained from equation (4.46) as the time dependent part devoid of positive scale multiplier and is given as

$$\varphi = (\beta t - 1 + e^{-\beta t})(1 - e^{-\beta t}) \quad (4.48)$$

The values of  $\psi$  are obtained using equation (4.48) for specified range of  $c'$  and are shown in Fig. 4.13. It is observed from simulation results that Model 7 predicts positive and finite function value for complete parametric range  $1 \times 10^{-10} \leq c' < 100 \text{ m}$ . The model predictions test out the validity criterion of non-negativity of variance and finite value of variance. The model is a case for selection and considered for further exploration for polystyrene nanoparticle in next section.



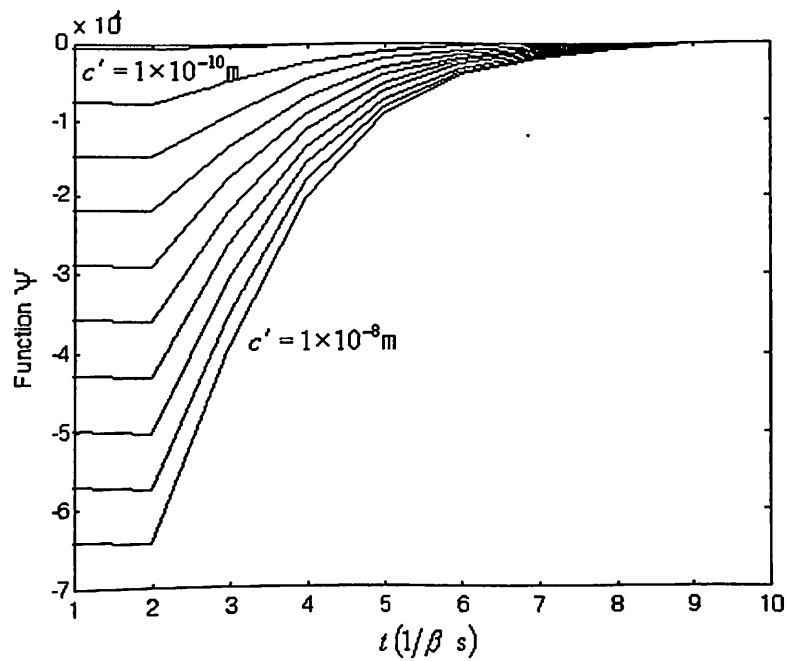
**Fig. 4.13** Simulation of Model 7 for Silicon Nanoparticle for  $1 \times 10^{-10} \leq c' \leq 100 \text{ m}$  in Steps of  $1 \times 10^{-9} \text{ m}$

**4.7.2 Simulation for Polystyrene Nanoparticle**

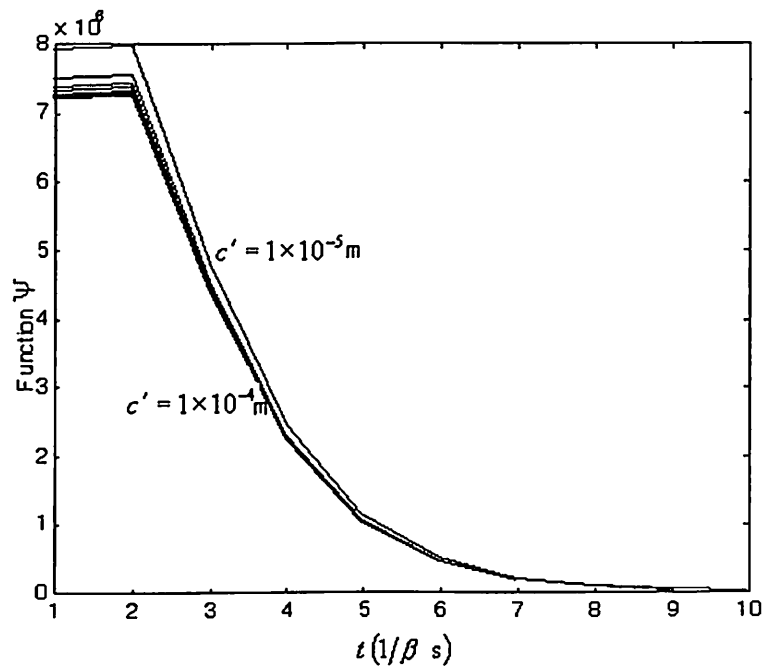
The polystyrene nanoparticle is characterized by parametric values given in subsection 4.4.2. The function values of two altered models namely Model 6 and Model 7 are simulated for the silicon nanoparticle in the following sub-sections.

**(a) Simulation of Model 6**

Further simulation for Model 6 is done assuming polystyrene nanoparticle in order to confirm the conclusions drawn in the previous sub-section. For Model 6, the function  $\psi$  is obtained from equation (4.47) for parametric values given for polystyrene nanoparticle. The values of  $\psi$  are obtained for specified range of  $c'$ . It is observed from simulation results that Model 6 predicts negative function value for parametric range  $1 \times 10^{-10} \leq c' \leq 1 \times 10^{-6}$  m. The plots of function value with respect to time in this parametric range are shown in Fig. 4.14(i) and Fig. 4.14(ii). The function value becomes unbound for higher values of  $c'$ . The negative variance is not allowed according to Criterion 1 and infinite values according to Criterion 2. This confirms the assessment in the case of silicon nanoparticle and hence the model is rejected.



(i)  $\psi$  vs  $t$  in Parameter Range:  $1 \times 10^{-10} \leq c' \leq 1 \times 10^{-8}$  m in Steps of  $1 \times 10^{-9}$  m



(ii)  $\psi$  vs  $t$  in Parameter Range:  $1 \times 10^{-5} \leq c' \leq 1 \times 10^{-4}$  m in Steps of  $1 \times 10^{-5}$  m

**Fig. 4.14** Simulation of Model 6 for Polystyrene Nanoparticle

**(b) Simulation of Model 7**

The simulation for Model 7 is done for polystyrene nanoparticle in order to confirm the conclusions drawn in the previous sub-section. For Model 7, the function  $\psi$  is obtained from equation (4.48) for parametric values given for polystyrene nanoparticle. The values of  $\psi$  are obtained for specified range of  $c'$ . It is observed from simulation results that Model 7 predicts once again positive and finite function value for entire parametric range  $1 \times 10^{-10} \leq c' \leq 100$  m. The plots of function value with respect to time are shown in Fig. 4.15. The positive and finite variance is in accordance to Criterion 1 and Criterion 2. This confirms the assessment of validity for Model 7 as in the case of silicon nanoparticle. The model represents first published [Sharma 2004 (i)] valid impact transfer model of Brownian motion of non-rigid nanoparticle

The simulation results of Model 6 did not tested with the validity criterion and hence Model 6 was rejected. The simulation exercise in this section yielded that the Model 7 is valid and test with the two validity criteria for two published observed

results. This suggests that there, in fact, was unmodeled aspect in the four Brownian motion models of non-rigid nanoparticle and the same can be captured in modeling by introduction of sub-system as in Model 7.

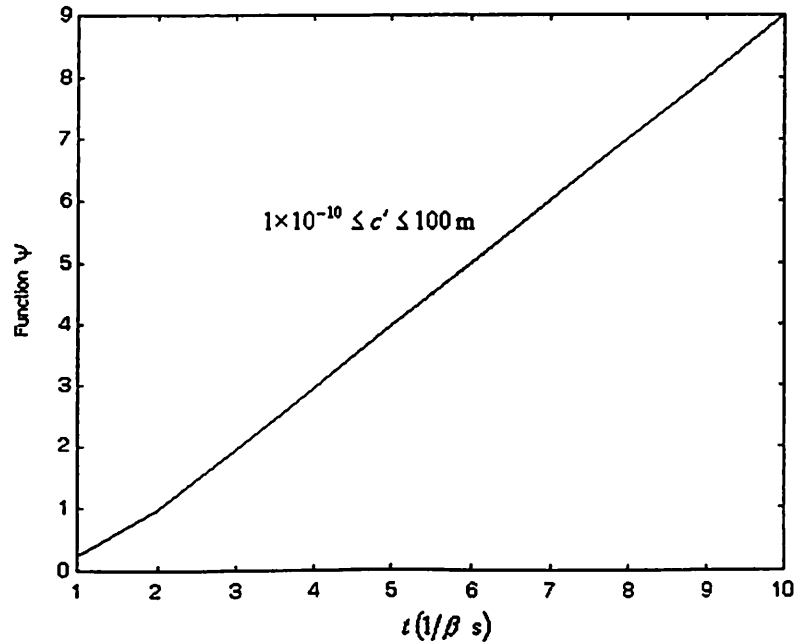


Fig. 4.15 Simulation of Model 7 for Silicon Nanoparticle for  $1 \times 10^{-10} \leq c' \leq 100$  m in Steps of  $1 \times 10^{-9}$  m

In order to explore the possibility of similar sub-systems featuring the property interaction in the Brownian motion model, the modeling is pursued further in next chapter.

#### 4.8 EPILOGUE

In the present chapter, an extensive simulation was carried out for different possible valid models (four models developed in previous chapter and two new models developed in present chapter) and function value plots were obtained. The simulation was done over a large range of parametric values. The simulation results are shown in Fig. 4.2 to Fig. 4.15. The proposed six models considered elasticity and dissipative properties of the nanoparticle explicitly to explore Brownian motion in nano-domains.

Model 2 and Model 3 failed to test out validity criterion 2 and Criterion 1 respectively and suggests that the arrangement of elements representing additional

properties, proposed in these models, is not correct. The failure of Model 5 and Model 6 against validity criterion 1, rules out double integration of forcing signal in impact transfer in any manner. If the output signal is to be position of the particle, then as we move backwards to the input signal (white noise) through elastic sub-systems, the double integration model should physically mean that input signal is a higher order jerk  $\approx d^3x/dt^3$ . The rejection of double integration models, Model 5 and Model 6, affirm that thermal noise cannot produce a jerk. The rejection of Model 4 indicates that single integration of forcing signal must take place. No integration in transfer mechanism (Model 4) physically implies that signal does not change its form i.e. input and output signals both represent position. The negation hypothesizes that the signal transformation does take place and survival of single integration models, Model 7 confirms the notion that thermal noise can produce a force at thermal equilibrium. The Model 7 is obtained by hypothesizing a physical process, which limits the physical explanation of the model. Another limitation of all six models presented is that a fixed interaction of additional elements ( $f'$  and  $k$ ) has been explored. This leaves a number of other possible and contending interactions for probable models of impact process.

Another attempt to obtain valid Brownian motion models of non-rigid nanoparticle is done in next chapter removing the above limitations. Since the non-rigid nanoparticle involves two additional parameters ( $f'$  and  $k$ ) in addition to  $m$  and  $f$ , a systems-modeling approach with four parameters ( $m$ ,  $f$ ,  $f'$  and  $k$ ) will be more appropriate. The exhaustive search for valid Brownian motion models of non-rigid nanoparticle is done using systems modeling approach as a second method and is presented in next chapter.



## CHAPTER 5

# **BROWNIAN MOTION MODELS OF NANOPARTICLE: SYSTEMS MODELING APPROACH**

### 5.1 INTRODUCTION

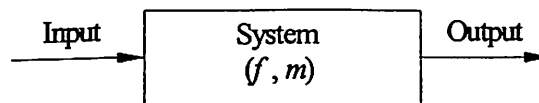
The assumed relation between various properties of nanoparticle was verified by simulation in the previous chapter. This suggests that inclusion of elastic and dissipative properties of nanoparticle in the Brownian motion model is a valid proposition. The Brownian motion Model 7 was limited because one of the sub-systems in the model was assumed to be having a fixed arrangement of elements representing the elastic and dissipative properties of nanoparticle and the other sub-system was assumed to be of unknown configuration. There can be many other possible arrangements, which can be possible models of Brownian motion of non-rigid nanoparticle. The present chapter attempts to characterize these fixed and unknown physical processes and a Brownian motion model has been developed removing the above two assumptions. In order to include elastic and dissipative properties of the nanoparticle, all-possible models of lumped passive elements corresponding to inertia, elasticity and dissipative properties are considered using system-modeling approach. The models developed are subjected to various validity constraints. The models testifying the constraints are simulated and verified with available results in next chapter to get a model of Brownian motion of non-rigid nanoparticle. The approach used for developing all possible system models is explained in next section.

### 5.2 SYSTEMS MODEL FOR BROWNIAN MOTION OF RIGID NANOPARTICLE

A system is a collection of components wherein individual components are combined by connecting inter-relationships and that the system as a whole fulfils some specific functions in response to varying inputs [Nagrath 1982]. The methodology of describing systems and their behavior is called as systems approach. Systems approach offers a strategy for solving complex engineering and social

problems. In order to describe large scale, complex, interactive system, the systems approach makes use of models that determines features and their possible interactions, which describes the system. In certain situations where system exact models are not available, we resort to certain idealizing assumptions and obtain mathematical model from the idealized system models.

In Brownian motion, the system comprises of the Brownian particle and the surrounding medium interaction. The phenomenon is quite complex and is analyzed in available literature under a number of idealizations like the surrounding medium is assumed to be viscous and Brownian particle is assumed as a rigid spherical particle of radius  $r$  and mass  $m$ . The damping from medium is assumed to follow Stokes law and the resistance force to Brownian motion from the surrounding medium due to damping is assumed to be proportional to velocity of the Brownian particle. The damping force is characterized by a proportionality constant called damping coefficient, which is given by  $f = 6\pi\eta$ . The input energy for the Brownian motion comes from the random impacts of surrounding medium molecules and is assumed as white noise. The output from the system is the information on position of the particle and is represented in terms of expected values, as the system input is stochastic in nature. The most established Brownian motion model, Ornstein-Uhlenbeck model, is obtained using correlation technique under the above mentioned assumptions. The idealized model is characterized with parameters  $f$  and  $m$ ; white noise as input and  $x(t)$  as output. Thus, system is a single input-single output system with two-parameter  $f$  and  $m$  and can be represented by a block-diagram and is shown Fig. 5.1.



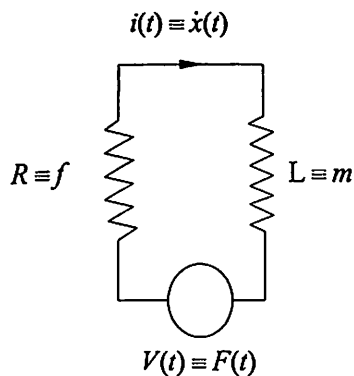
**Fig. 5.1** Two-Parameter System Block Diagram for Rigid Nanoparticle Brownian Motion

The Ornstein-Uhlenbeck model was obtained using Langevin equation (2.10). The Langevin equation is linear and it is assumed that the parameters of the system do not change with time making system time invariant. The assumption of white noise as input renders the system instantaneous and casual. The model further assumes parameters  $f$  and  $m$  being lumped at one point in space.

The lumped parameter assumption is valid in small sized domains even at high frequencies because the wavelength of high frequency signals is considerably larger than the size of the particle. Moreover, system is continuous time system because the frequency of collision is quite high ( $\sim 10^{21}$  collisions/s).

A mechanical system can be represented by an electrical analogous system using either Force-Voltage or Force-Current analogy. The driving energy in Brownian motion being a force, the force-voltage analogy is considered appropriate. The equivalent electrical analogous quantities, using Force-Voltage analogy for the Brownian motion system parameters are: resistance  $R$  is analogous to  $f$  ( $R \equiv f$ ), inductance  $L$  is analogous to  $m$  ( $L \equiv m$ ), current  $i(t)$  is analogous to velocity  $\dot{x}$  ( $i(t) \equiv \dot{x}(t)$ ), charge  $q(t) \equiv x(t)$ , and voltage is analogous to force ( $V(t) \equiv F(t)$ ). Since the Brownian motion is mechanical in nature, the use of mechanical analogous quantities is done in place of electrical parameters in rest of the thesis. For example, an inductance of  $m$  and a resistance of  $f$  or  $f'$  is used in development of systems-model for Brownian motion.

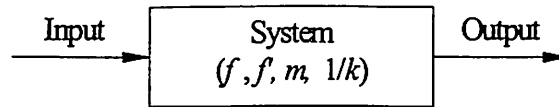
To develop a system model, we must know the relationship between different parameters of the system. The series inductance-resistance circuit shown in Fig. 5.2 is modeled by a second order linear differential equation, which can be obtained applying Kirchoff's law. The Brownian motion model represented by Langevin equation (3.4) is also a second order linear differential equation same as the circuit equation of inductance ( $m$ ) and resistance ( $f$ ) in series connected across a stochastic voltage source  $F(t)$ . The equivalent circuit, therefore, can be used to represents a Brownian motion model. In the of rigid nanoparticle model of Brownian motion, only significant parameters are  $m$  and  $f$  and hence circuit shown in Fig 5.2 represents the systems model of rigid body Brownian motion.



**Fig. 5.2** Equivalent Electric Circuit for Two Parameter Brownian motion Model of Rigid Nanoparticle

### 5.3 SYSTEMS MODEL FOR BROWNIAN MOTION OF NON-RIGID NANOPARTICLE

Non-rigidity is the prime point chosen to be explored in nano-domains. In order to develop Brownian motion model of a non-rigid nanoparticle, two more properties of nanoparticle need to be included in the model. The two properties are: elasticity of nanoparticle characterized by a lumped parameter  $k$  and dissipation by nanoparticle characterized by a lumped damping coefficient  $f'$ . The parameter  $k$  represents the energy storing property of the matter where as the  $f'$  represents the loss of energy due to nanoparticle. The two corresponding electrical elements are capacitor for storage and resistor for loss of energy. Using Force-Voltage analogy, these two-parameter in equivalent electrical quantities can be represented as a resistance  $R'$  as  $R' \equiv f'$  and a capacitance  $\bar{c}$  as  $\bar{c} \equiv 1/k$ . In all, therefore, there are four parameters in non-rigid model of system namely:  $m, f, f', 1/k$ . The block-diagram of the four parameter systems is shown in Fig. 5.3 and the four parameters based on Force-Voltage analogy are tabulated in Table 5.1.



**Fig. 5.3** Proposed Four Parameter System Block Diagram

**Table 5.1** Four Analogous Parameters According to Force-Voltage Analogy

S.No.	Nanoparticle System Parameter	Electrical System Parameter
1.	Mass of Nanoparticle, $m$	Inductance, $L$
2.	Reciprocal of Spring Constant of Nanoparticle, $1/k$	Capacitance, $\bar{c}$
3.	Damping from Nanoparticle, $f'$	Resistance, $R'$
4.	Damping from Surrounding, $f$	Resistance, $R$

As no information is available how these four elements interact with each other to describe Brownian motion of non-rigid nanoparticle, we are left with no choice other than to examine all possible interactions of the four parameters and posteriori verify the obtained models against physical constraints, validity criterion and available published results. The formulation of valid systems model

representing interactions among various parameters is done in the present chapter and follows next.

#### 5.4 ALGORITHM FOR BUILDING ALL POSSIBLE FOUR-PARAMETER MODELS OF NANOPARTICLE

In the model of the non-rigid nanoparticle Brownian motion, the four lumped system parameters  $m, f, f', 1/k$  interaction with each other is not clearly known or defined. The different ways in which the four elements can interact gives rise to different possible equivalent models of the nanoparticle system. Some of these models may violate the physical constraints. First, all possible four parameter models are developed and then these are filtered to get possible feasible models. An algorithm is developed to generate all possible four-parameter models. The steps of the algorithm to develop all possible four-parameter models are presented as an algorithm next.

##### Algorithm 2: Algorithm to Develop Four-Parameter Models

To develop all four parameter models, force-voltage electrical analogy discussed in section 5.2 is used. The four-parameters in systems model will correspondingly have four electrical elements and are represented by analogous mechanical quantities. In the first step, in order to develop all possible models, a box is assumed to represent any of the four elements and distinct all four block models are determined step-by step as follows.

##### Step I: Getting All Possible Two-Unit Models

First step is to develop all possible models with two blocks. To do this, one box as a unit is considered first, and one box is added to it. The second unit can be added in series in front of first unit or at the rear of first unit or in parallel to first unit resulting in three distinct two-unit models. These three possible two-unit models are shown in Fig. 5.4. This step is recursively applied to generate larger models.

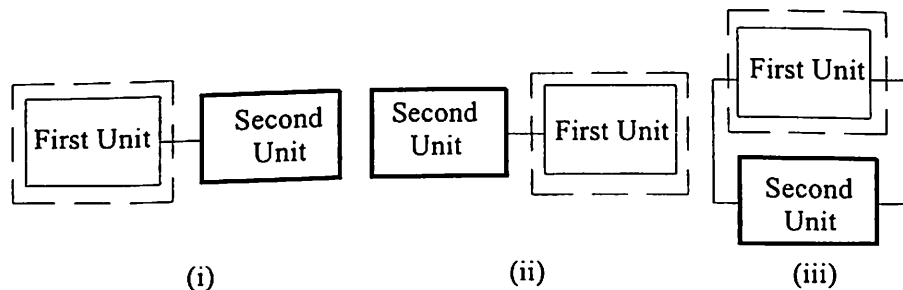


Fig. 5.4 Three Possible Two-Unit Models

In the system under consideration, there is no reason of preferential placement of elements  $(m, f, f', 1/k)$  in any particular box. Thus, all boxes represented by different units are equivalent and labeling of the boxes as first and second is removed. The label removal renders Fig. 5.4(i) and (ii) to be identical. Thus, distinct possible two-unit models are only two as shown in Fig. 5.5. This step is also used recursively to obtain distinct possible larger models.

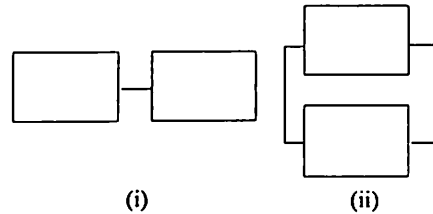


Fig. 5.5 Two Distinct Two-Unit Models

### Step II: Getting All Possible Three-Unit Models

The two-unit models in Fig. 5.5 are expanded by including one more unit. One more unit can be added in series or in parallel to two-unit models giving three unit models. For example, taking two-unit model in Fig. 5.5 (i) as a unit, third unit can be added in series to it in front or in rear or in parallel, as was done in Step I. The resulting three three-unit models are shown in Fig. 5.6(i), (ii) and (iii), respectively. Continuing the process similarly, for two unit models in Fig. 5.4(ii), three more three-unit models are obtained and are shown in Fig. 5.6(iv) through (vi). Hence, in all six three-unit models are obtained.

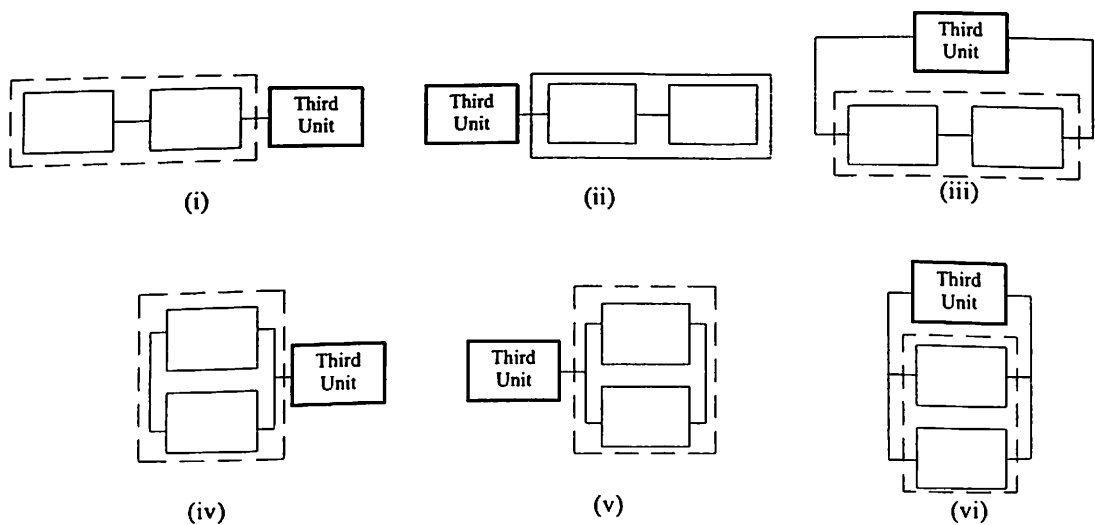
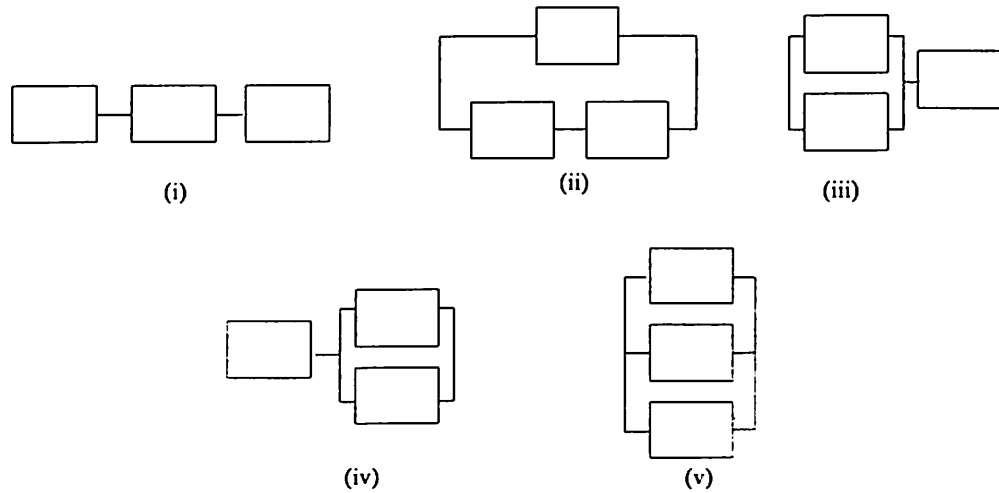


Fig. 5.6 Six Possible Three-Unit Models

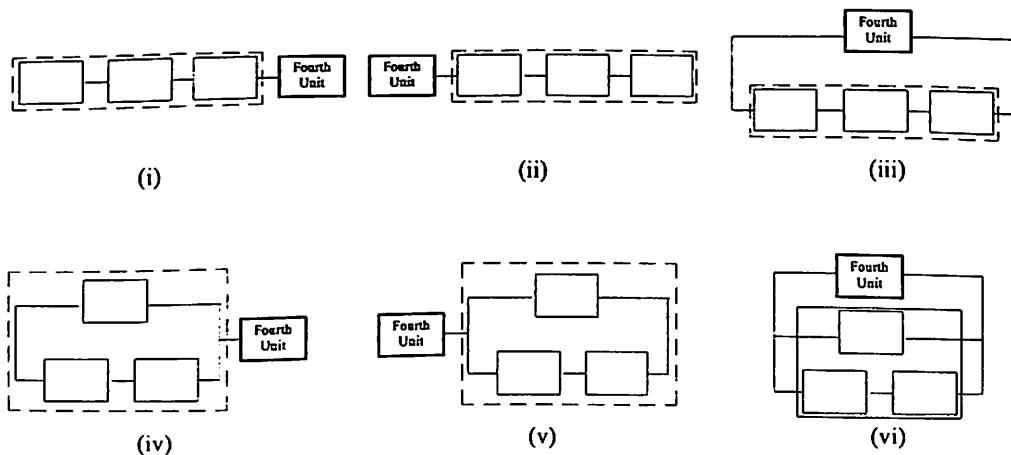
As in Step I, all boxes are equivalent and labeling of the boxes as third unit is removed. From the label removal, Fig. 5.6(i) and (ii) becomes identical. Thus, distinct possible three-unit models are only five as shown in Fig. 5.7.



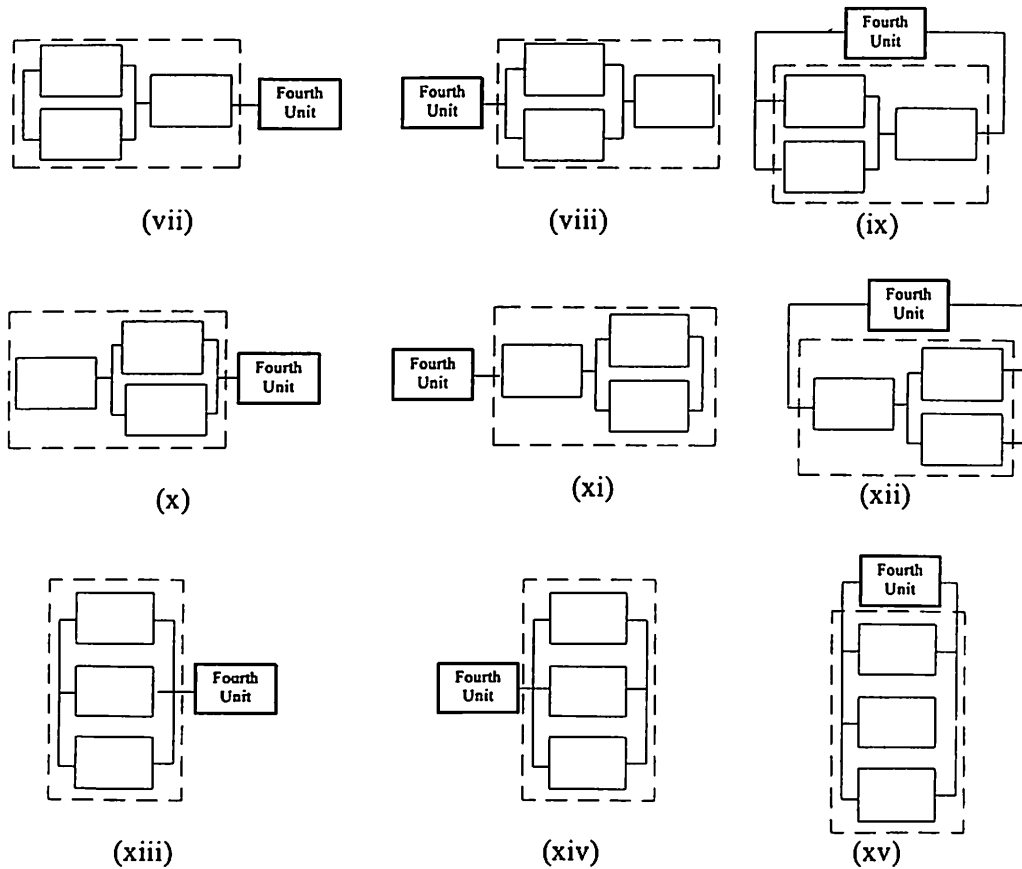
**Fig. 5.7 Five Distinct Three-Unit Models**

**Step III: Getting All Possible Four-Unit Models from Three-Unit Models**

Four-unit models are possible by adding one more unit to three-unit models in Fig. 5.7 and by adding two unit models to two-unit models in Fig. 5.5. In this step, first, adding one more unit to five three-unit models in Fig. 5.7 develops four-unit models. The addition of the unit is done systematically, as per Step I, to get all possible four-unit models. For example, considering the three-unit model in Fig. 5.7(i) as one entity, one more unit can be added in front and rear in series, and in parallel. This gives three models of four-units. The four-unit models, thus obtained, are shown in Fig. 5.8(i), (ii) and (iii).



**Fig. 5.8 (Contd.)**



**Fig. 5.8** Fifteen Possible Four-Unit Models Obtained from Three-Unit Models

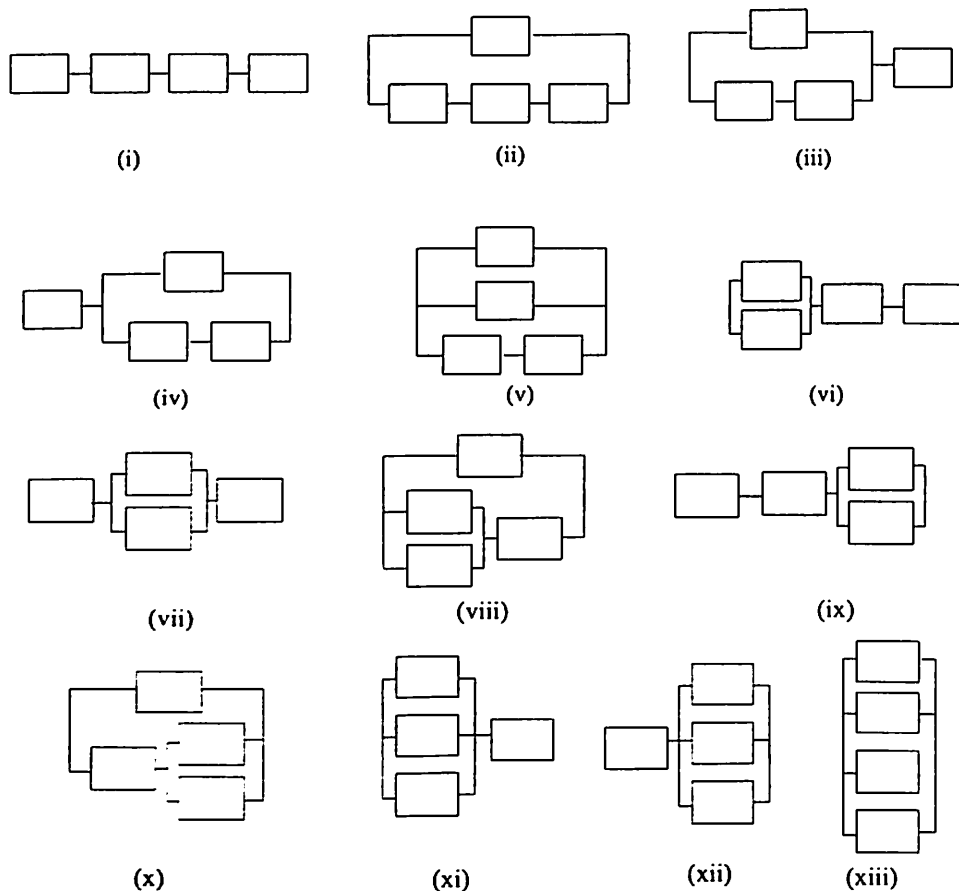
Repeating the procedure with remaining four three-unit models in Fig. 5.7 (ii) through (v), twelve more four-unit models are obtained, which are shown in Fig. 5.8 (iv) through (xv). In all, fifteen possible four-unit models are obtained from five distinct three-unit models.

As in Step I, all boxes are equivalent and labeling of the box as fourth unit is removed. From the label removal, Fig. 5.8(i) and (ii), Fig. 5.8(viii) and (x) becomes correspondingly identical. Thus, distinct possible four-unit models are only thirteen as shown in Fig. 5.9.

#### **Step IV: Getting All Possible Four-Unit Models from Two-Unit Models**

Next sets of four-unit models are obtained by adding two-unit models to two-unit models shown in Fig. 5.5 in all possible ways i.e. in series or in parallel, as in Step I. For example, to the two-unit model in Fig. 5.5(i), adding two-unit block in Fig. 5.5(i), as third and fourth unit, gives three four-unit models as shown in Fig. 5.10(i), (ii) and (iii).

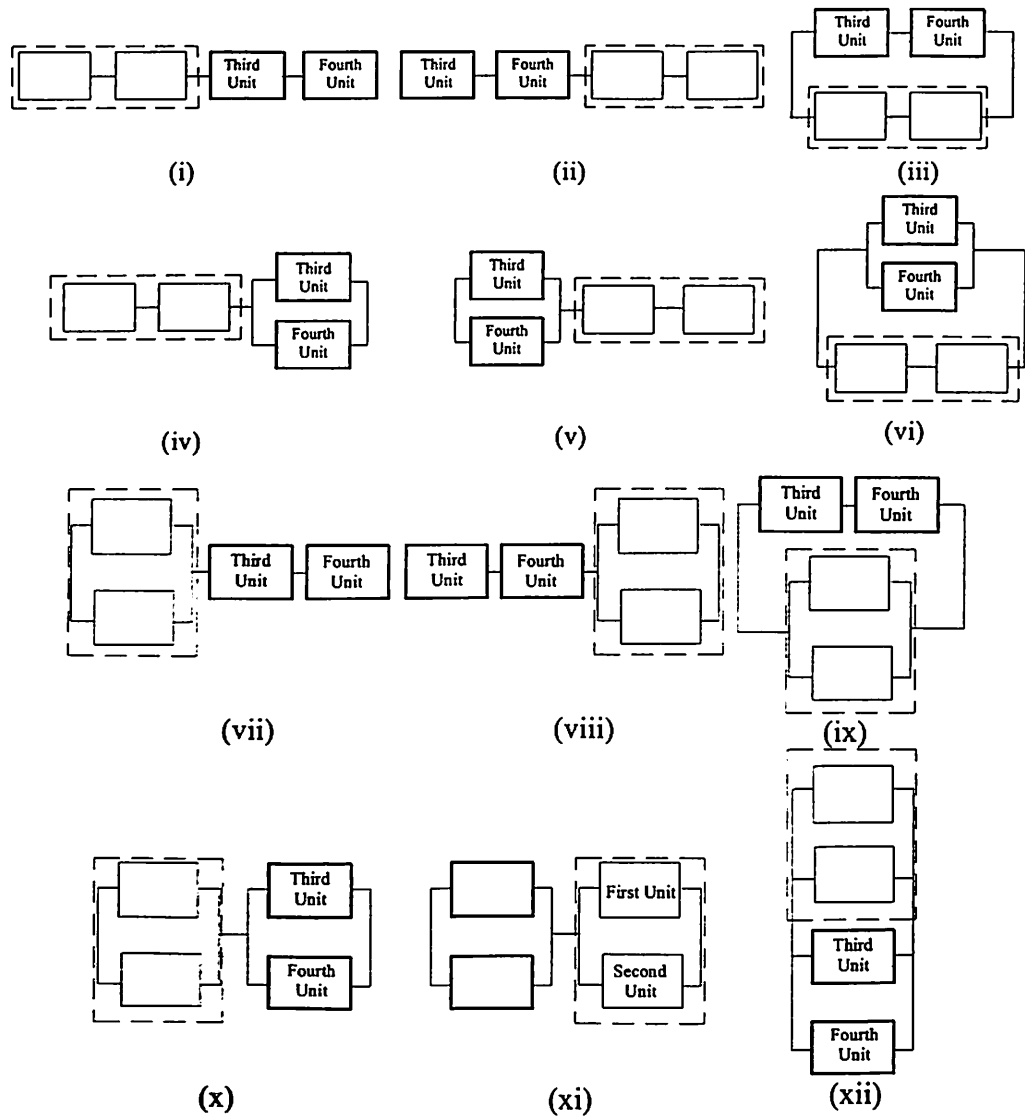




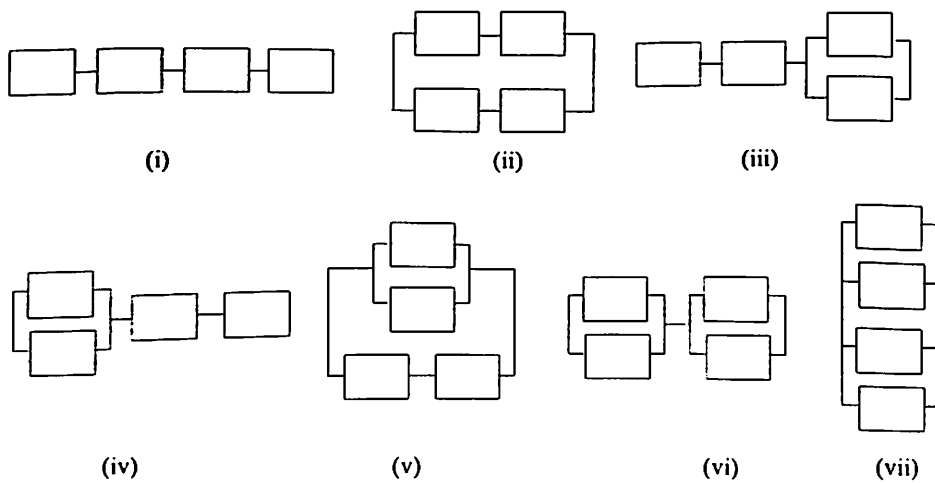
**Fig. 5.9** Thirteen Distinct Four-Unit Models Obtained from Three-Unit Models

Similarly, to the two-unit model shown in Fig. 5.5(i), adding two-unit block in Fig. 5.5(ii), as third and fourth unit, gives three more four-unit models as shown in Fig. 5.10(iv) through (vi). Repeating the procedure with two-unit model shown in Fig. 5.5(ii), six more four-unit models are obtained, which are shown in Fig. 5.10(vii) through (xii). In all, twelve possible four-unit models are obtained from two distinct two-unit models.

As in Step I, all boxes are equivalent and labeling of the box as third and fourth unit is removed. From the label removal, Fig. 5.10(i) and (ii) becomes identical. Similarly Fig. 5.10(iv) and (viii), Fig. 5.10(v) and (vii), Fig. 5.10(vi) and (ix), Fig. 5.10(x) and (xi) are also identical respectively. Thus, distinct possible four-unit models obtained from two-unit models are only seven as shown in Fig. 5.11.



**Fig. 5.10** Twelve Possible Four-Unit Models Obtained from Two-Unit Models



**Fig. 5.11** Seven Distinct Four-Unit Models Obtained from Two-Unit Models

### Step V: Getting Distinct Four-Unit Models

Thirteen distinct Four-unit models have been obtained from three-unit models (Fig. 5.9) and eight distinct Four-unit models are obtained from two-unit models (Fig. 5.11). From Fig. 5.9 and Fig. 5.11, it is observed that Fig. 5.9(i) and Fig. 5.11(i) are identical. Similarly, the models shown in Fig. 5.9(v), (vi), (ix), (xiv) and Fig. 5.11(v), (iv), (iii), (vi), (viii) are correspondingly identical. From the twenty four-unit models in Fig. 5.9 and 5.11, fifteen four-unit models are found to be distinct representing fifteen unique series-parallel combination of four-units. These fifteen models are shown in Fig. 5.12.

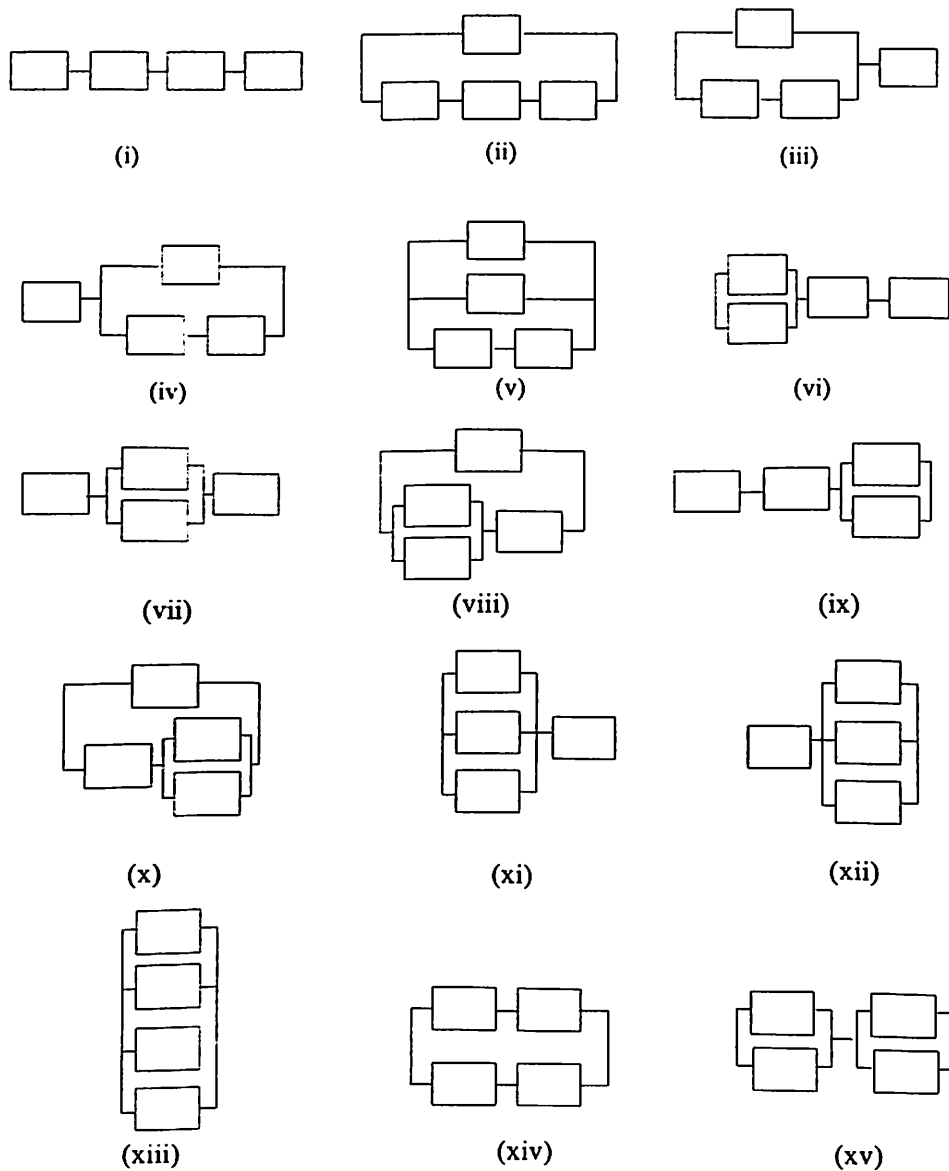


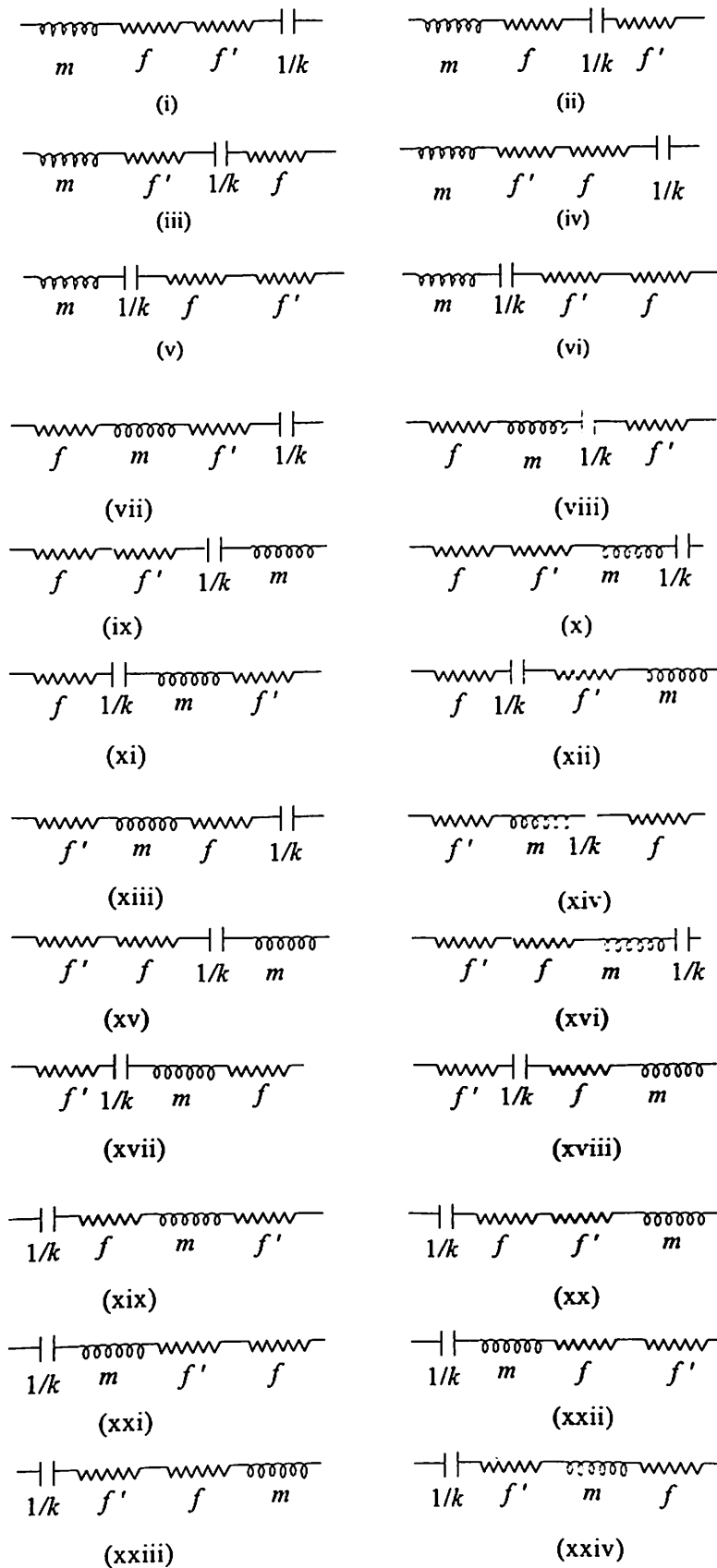
Fig. 5.12 Fifteen Distinct Four-Unit Models

## Step VI: Getting All possible Interactions of Four Analogous Mechanical Elements from Distinct Four-Unit Models

In the process to develop all possible system models, as equivalent electric circuits, the next step is assigning of different mechanical analogous elements  $(m, f, f', 1/k)$  representing corresponding electrical elements  $(L, R, R', \bar{c})$  in the different boxes of fifteen four-unit models. As there are no preferences either among the units or elements for assignment, the first box of a four-unit model has four choices among four equally likely elements to be filled with. Since the assignment of one element excludes it from further consideration as assignment events being mutually exclusive, the next box is left with the choice of assignment from remaining three elements. After filling of second box, only two elements are left for the third box and finally only one element is left for the last box. Each unique assignment represents a possible interaction among elements of the system and, hence, a possible model of the system.

Thus, factorial-four interactions of four elements are possible for each of the fifteen distinct four unit models shown in Fig. 5.12. For example, factorial four or twenty-four possible assignments of four elements to the first four-unit model in Fig. 5.12(i) give twenty-four models. These twenty-four models are shown in Fig. 5.13 as electrical circuits with analogous mechanical parameters and are referred as Combination-1. The mechanical analogous parameters are used for representing electrical circuit elements throughout the present work.

Repeating the above procedure for remaining fourteen four-unit models in Fig. 5.12, in all fifteen combinations are obtained with  $15 \times 4! = 360$  possible four parameter models named as Combination-1 through Combination-15. The fifteen combinations each with twenty-four possible electrical analogous models are given in Appendix II in Fig. II.1 to Fig. II.15.



**Fig 5.13** Combination-1: Four-Parameter System Models Corresponding to Model in Fig. 5.12(i)

## 5.5 SELECTION OF KINEMATICALLY VALID-SYSTEMS

In the previous section, all possible models of four-parameter systems, which may model Brownian motion of non-rigid nanoparticle, were developed. Some of the models may not be valid, as they may not satisfy certain kinematical and other constraints. These constraints are defined and are applied as selection criterion to the 360 possible combinations (see Appendix II). Selection of possible candidates for modeling Brownian motion of nanoparticle is carried in this section.

The process of selection is step-by-step applied as follows. First, a kinematic feature of the system of nanoparticle performing Brownian motion is identified and defined as a constraint of the system. The constraint is applied to all possible models in each of the fifteen combinations and the models, which satisfy the identified feature, are selected and others filtered out.

### 5.5.1 Selection Criterion 1

The first filtering of 360 electrical analog models is done based on electrical equivalence of two models. The electrical equivalence is defined as follows

#### **Definition 5.1**

Two electrical systems are considered to be electrically identical, if and only if, the over all impedances of the two systems is same, and the current flow through each element is not altered because of change of location of electrical elements in the systems. Two systems that are not electrically identical are called as electrically distinct.

The electrical equivalence as defined above is considered as Selection Criterion 1 and is applied as first filter. Among 360 possible electrical analog models in Appendix II, some models are electrically identical. For example, in Fig. 5.13, model (ii) is electrically identical to model (i) and hence model (ii) is filtered out. In fact, the remaining twenty-two models in Fig. 5.13 are also electrically identical to model (i) and get filtered out. Only one model (any of the twenty four arrangements) is selected from combination-1 after applying Selection Criterion 1. This model is shown in Fig. II.16 in Appendix II.

Similarly, for Combination-2 (Fig. II.2): models (i)-(vi), models (vii)-(xii), models (xiii)-(xviii), and models (xix)-(xxiv) are correspondingly identical, hence only four distinct models are selected from Combination-2. These four models are shown in Fig. II.17 in Appendix II.

For Combination-3 (Fig. II.3): models (i)-(ii), models (iii)-(iv), models (v)-(vi), models (vii)-(viii), models (ix)-(x), models (xi)-(xii), models (xiii)-(xiv), models (xv)-(xvi), models (xvii)-(xviii), models (xix)-(xx), models (xxi)-(xxii), and models (xxiii)-(xxiv) are correspondingly identical, hence in all twelve distinct models are selected from Combination-3. These twelve models are shown in Fig. II.18 in Appendix II.

For Combination-4 (Fig. II.4): models (i)-(ii), models (iii)-(iv), models (v)-(vi), models (vii)-(viii), models (ix)-(x), models (xi)-(xii), models (xiii)-(xiv), models (xv)-(xvi), models (xvii)-(xviii), models (xix)-(xx), models (xxi)-(xxii), and models (xxiii)-(xxiv) are correspondingly identical, hence in all twelve distinct models are selected from Combination-4. These twelve models are shown in Fig. II.19 in Appendix II.

For Combination-5 (Fig. II.5): models (i), (ii), (xv) and (xvi), models (iii), (iv), (ix) and (x), models (v), (vi), (xxiii) and (xxiv), models (vii), (viii), (xiii) and (xiv), models (xi), (xii), (xix) and (xx), models (xvii), (xviii), (xxi) and (xxii), are correspondingly identical, hence in all six distinct models are selected from Combination-5. These six models are shown in Fig. II.20 in Appendix II.

For Combination-6 (Fig. II.6): models (i), (ii), (vii), and (viii), models (iii), (iv), (xiii), (xiv), models (v), (vi) (xix), (xx), models (ix), (x), (xv), (xvi), models (xi)-(xii), (xxi) and (xxii), models (xvii)-(xviii), (xxiii) and (xxiv) are correspondingly identical, hence in all six distinct models are selected from Combination-6. These six models are shown in Fig. II.21 in Appendix II.

For Combination-7 (Fig. II.7): models (i), (ii), (vii), and (viii), models (iii), (iv), (xiii), (xiv), models (v), (vi) (xix), (xx), models (ix), (x), (xv), (xvi), models (xi), (xii), (xxi) and (xxii), models (xvii), (xviii), (xxiii) and (xxiv) are

correspondingly identical, hence in all six distinct models are selected from Combination-7. These six models are shown in Fig. II.22 in Appendix II.

For Combination-8 (Fig. II.8): models (i)-(ii), models (iii)-(iv), models (v)-(vi), models (vii)-(viii), models (ix)-(x), models (xi)-(xii), models (xiii)-(xiv), models (xv)-(xvi), models (xvii)-(xviii), models (xix)-(xx), models (xxi)-(xxii), and models (xxiii)-(xxiv) are correspondingly identical, hence in all twelve distinct models are selected from Combination-8. These twelve models are shown in Fig. II.23 in Appendix II.

For twenty-four models in Combination-9 (Fig. II.9), models (i), (ii), (vii) and (viii) are found to be electrically identical and give only one selected model. Also, models (iii), (iv), (xiii) and (xiv), models (v), (vi), (xix) and (xx), models (ix), (x), (xv) and (xvi), models (xi), (xii), (xxi) and (xxii), models (xvii), (xviii), (xxiii) and (xxiv) are correspondingly electrically identical. Thus in all from combination-9, only six models are distinct. These six models are shown in Fig. II.24 in Appendix II.

For Combination-10 (Fig. II.10): models (i)-(ii), models (iii)-(iv), models (v)-(vi), models (vii)-(viii), models (ix)-(x), models (xi)-(xii), models (xiii)-(xiv), models (xv)-(xvi), models (xvii)-(xviii), models (xix)-(xx), models (xxi)-(xxii), and models (xxiii)-(xxiv) are correspondingly identical, hence in all twelve distinct models are selected from Combination-10. These twelve models are shown in Fig. II.25 in Appendix II.

For Combination-11 (Fig. II.11): models (i)-(vi), models (vii)-(xii), models (xiii)-(xviii), and models (xix)-(xxiv) are correspondingly identical, hence only four distinct models are selected from Combination-11. These four models are shown in Fig. II.26 in Appendix II.

For Combination-12 (Fig. II.12): models (i)-(vi), models (vii)-(xii), models (xiii)-(xviii), and models (xix)-(xxiv) are correspondingly identical, hence only four distinct models are selected from Combination-12. These four models are shown in Fig. II.27 in Appendix II.



For Combination-13 (Fig. II.13): all twenty-four models identical, hence in all only one distinct model is selected from Combination-13 and is shown in Fig. II.28 in Appendix II.

For Combination-14 (Fig. II.14): models (i), (ii), (vii), (viii), (xvii), (xviii), (xxiii) and (xxiv), models (iii), (iv), (xi), (xii), (xiii), (xiv), (xxi) and (xxii), models (v), (vi), (ix), (x), (xv), (xvi), (xix) and (xx), are correspondingly identical, hence in all three distinct models are selected from Combination-14. These three models are shown in Fig. II.29 in Appendix II.

For Combination-15 (Fig. II.15): models (i), (vi), (viii), (x), (xv), (xvii), (xx) and (xxiii), models (ii), (iv), (vii), (xii), (xiii), (xviii), (xxii) and (xxiv), models (iii), (v), (ix), (xi), (xiv), (xvi), (xix) and (xxi), are correspondingly identical, hence in all three distinct models are selected from Combination-15. These three models are shown in Fig. II.30 in Appendix II.

Hence, the total number of electrically distinct models after applying Selection Criterion 1 is ninety-two. These electrically distinct models are further subjected to other criterions in next section.

### 5.5.2 Selection Criterion 2

In a mechanical system, if mass is moving with a velocity  $\dot{x}$  then resistive force due to damping is proportional to  $\dot{x}$ , that is, for  $m$  and  $f$  elements both should have same velocity. Hence, in the electrical analog of mechanical system, the model should have  $R$  and  $L$  ( $f$  and  $m$ ) elements so arranged that they should have same current (velocity). The models, which do not satisfy this condition, are rejected. This is considered as Selection Criterion 2

For combination-1, after applying Selection Criterion 1, only one electrically distinct model was selected having all four elements in series (see Fig. II.16). In this series model same current flows through all elements. This satisfies the Selection Criterion-2 and, therefore, may be a possible system model. Thus, criterion-2 does not reject the model.

For Combination-2, four models satisfy Selection Criterion 1 (see Fig. II.17). Except for the model in Fig. II.17(iii) and (iv), none other model have  $f$  and  $m$

element in series. These two models in Fig. II.17(iii) and (iv), therefore, satisfy Selection Criterion 2 and are carried for further investigation.

For Combination-3, out of twelve models satisfying Selection criterion 1 (see Fig. II.18), only two models in Fig. II.18(viii) and (xi) satisfy Selection Criterion 2 and are carried further for investigation.

For Combination-4, there are twelve electrically distinct models satisfying Selection Criterion 1 (see Fig. II.19). Except for two models in Fig. II.19(viii) and (xi), none other model satisfy Selection Criterion-2. Thus out of twelve models, ten are rejected and two in Fig. II.19(viii) and (xi) are carried for further investigation.

For Combination-5, there are six models satisfying Selection Criterion-1 (see Fig. II.20). Except for model in Fig. II.20(vi), other five models do not satisfy the Selection Criterion-2. The model in Fig. II.20(vi) is carried for further investigation.

For combination-6 (see Fig. II.21), one out of six model, namely model in Fig. II.21(i), satisfy Selection Criterion 2 and is carried for further investigation.

For combination-7 (see Fig. II.22), one out of six models namely model in Fig. II.22(i), satisfy Selection Criterion 2 and is carried for further investigation.

For combination-8 (see Fig. II.23), none among twelve electrically distinct models, satisfy the Selection Criterion 2 and hence all twelve models gets rejected.

For Combination-9, there are six possible electrically distinct models of elements (See Fig. II.24). Except for the model corresponding to Fig. II.24 (i), none other model satisfy Selection Criterion 2. The model in Fig. II.24(i) satisfies the Selection Criterion 2 and is carried further for investigation.

For Combination-10, there are twelve models satisfying Selection Criterion 1 (see Fig. II.25). Among the twelve models, none of the model satisfy Selection Criterion 2. So all are rejected and filtered out of further investigation.

For combination-11, none among four electrically distinct models (see Fig. II.26), satisfy Selection Criterion 2 and hence all four models get rejected.

For Combination-12, among four models satisfying Selection Criterion 1 (see Fig. II.27), none satisfy Selection Criterion 2, therefore, all are rejected.

For Combination-13, the only model satisfying Selection Criterion 1 (see Fig. II.28) does not satisfy Selection Criterion 2 and hence, is rejected for further investigation.

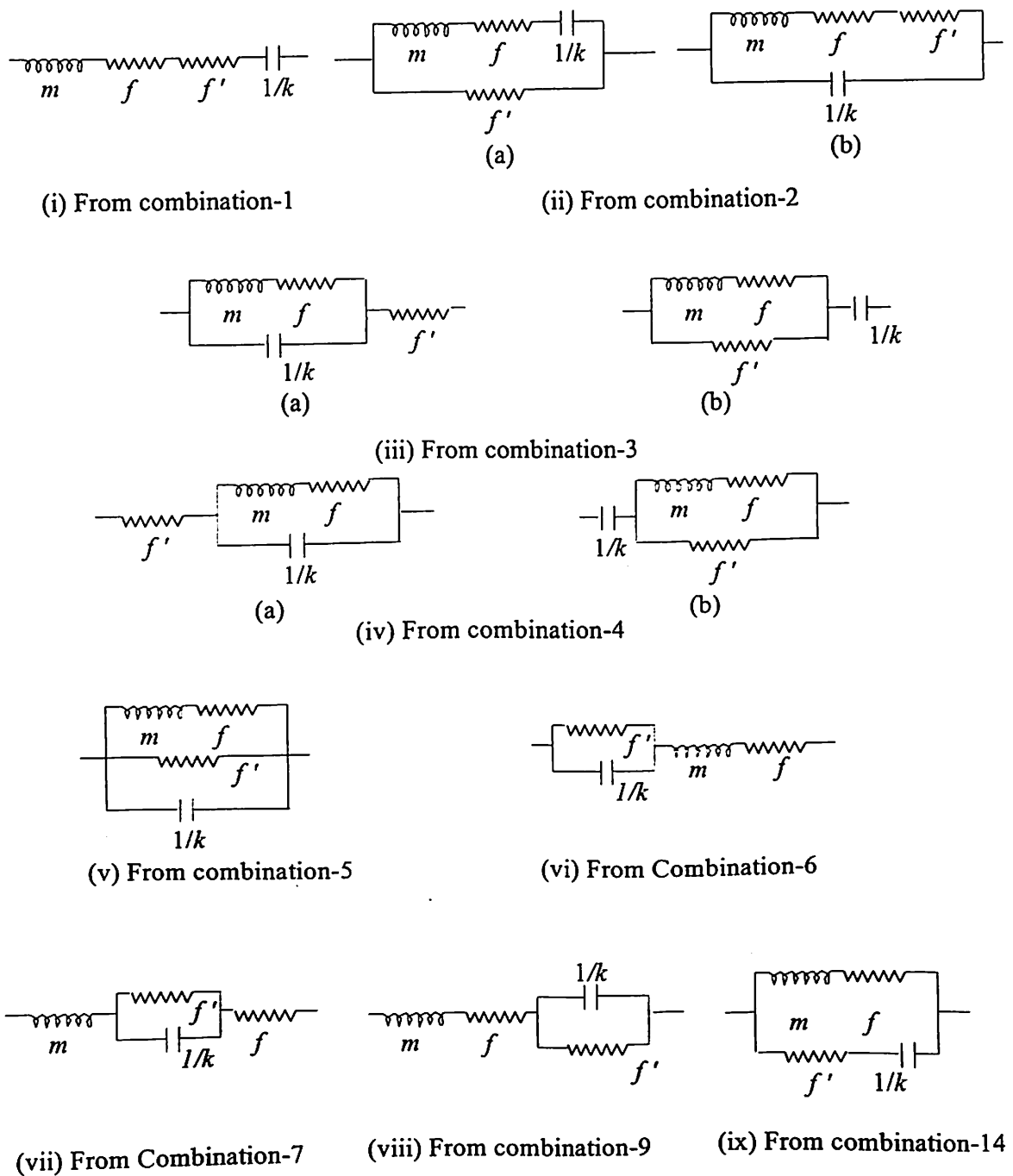
For Combination-14, there are three models satisfying Selection Criterion 1 (see Fig. II.23). Except for model in Fig. II.29(ii), other two models do not satisfy Selection Criterion 2 and hence, are rejected. The model in Fig. II.29(ii) satisfying Selection Criterion 2 is carried further for investigation.

For combination-15 (see Fig. II.30), among three models, none satisfies selection criterion-2 and hence are rejected.

The number of rejected model based on their inability to satisfy Selection Criterion 2 totals to 80. Thus, from ninety-two models satisfying Section criterion 1, eighty models get rejected according to Selection Criterion 2. The remaining twelve models are shown in Fig. 5.14 and are subjected to last selection criterion.

### **5.5.3 Selection Criterion-3**

The twelve models shown in Fig. 5.14 are tested for their possibility to represent Brownian motion of a free nanoparticle. A free particle cannot be harmonically bound about a global equilibrium position, because by definition, such particles are not free to move in space whereas the nanoparticle under consideration is a free particle. Thus models, which give a harmonic term in the mathematical model, are rejected. The mathematical model representing the electrical analog model is derived for each of the remaining twelve possible models using Kirchoff's law and the third criterion is applied to check the suitability of the models to represent Brownian motion.



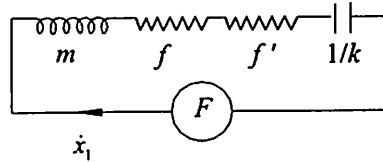
**Fig. 5.14** Possible System Models Satisfying Selection Criterion-1 and 2

To obtain the mathematical model, a free noise generator with force  $F(t)$  is applied to each of the model to complete the electrical analog circuit. The mathematical model in the form of a second order differential equation for the position variable  $x_1$  representing mechanical analog of charge flowing through the mass  $m$  representing mechanical analog of inductance is obtained. The velocity  $\dot{x}_1 = dx_1/dt$  is mechanical analog of current flowing through inductance. The

second order differential equation in  $x_1$  is equivalent to Langevin equation model of free nanoparticle.

**(a) Mathematical Model for Model in Fig. 5.14(i)**

The electrical analog circuit corresponding to model in Fig. 5.14(i) is shown with voltage source in Fig. 5.15 as possible Model I.



**Fig. 5.15** Possible Model I

Applying Kirchoff's law to the circuit gives the following equation

$$F = m \frac{d\dot{x}_1}{dt} + \dot{x}_1(f + f') + k \int_{-\infty}^t \dot{x}_1 dt \quad (5.1)$$

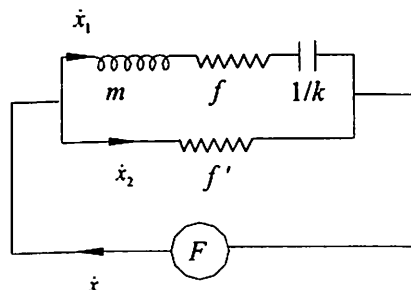
Equation (5.1) on simplification gives

$$F = m \frac{d^2 x_1}{dt^2} + (f + f') \frac{dx_1}{dt} + kx_1 + C \quad (5.2)$$

where  $C$  is constant of integration. Equation (5.2) is a second order differential equation for a harmonically bound system as it contains a term  $kx_1$  corresponding to a harmonic force. The Langevin model of Brownian motion of free particle does not contain this spring force. Therefore, equation (5.2) does not model a free particle performing Brownian motion and does not satisfy Selection Criterion 3. Hence, model in Fig. 5.14(i) is rejected as a possible system model.

**(b) Mathematical Model for Model in Fig. 5.14(ii)(a)**

In Fig. 5.14(ii)(a) a free noise generator with voltage  $F(t)$  is added as shown in Fig. 5.16. Keeping the notation of current  $\dot{x}_1$  through inductance, the current in the main branch as  $\dot{x}$ , and considering current  $\dot{x}_2$  through  $f'$ , the model obtained is shown in Fig. 5.16 as possible Model II



**Fig. 5.16** Possible Model II

Applying Kirchoff's law to the circuit gives the following equation

$$F = m \frac{d\dot{x}_1}{dt} + \dot{x}_1 f + k \int_{-\infty}^t \dot{x}_1 dt \quad (5.3)$$

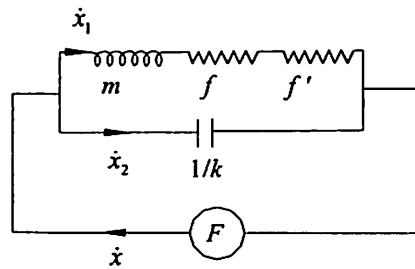
which on simplification gives

$$F = m \frac{d^2 x_1}{dt^2} + f \frac{dx_1}{dt} + kx_1 + C \quad (5.4)$$

where  $C$  is constant of integration. Equation (5.4) contains term of harmonic force and therefore this model also does not satisfy Selection Criterion 3 and hence rejected.

**(c) Mathematical Model for Model in Fig. 5.14(ii)(b)**

In Fig. 5.14(ii)(b) a free noise generator with voltage  $F(t)$  is added as shown in Fig. 5.17. Keeping the notation of current  $\dot{x}_1$  through inductance, the current in the main branch as  $\dot{x}$ , and considering current  $\dot{x}_2$  through capacitance  $1/k$ , the model obtained is shown in Fig. 5.7 as possible Model III.



**Fig. 5.17** Possible Model III

Applying Kirchoff's Voltage law to the circuit gives the following equation

$$F = m \frac{d^2 x_1}{dt^2} + (f + f') \frac{dx_1}{dt} \quad (5.5)$$

Equation (5.5) is the required mathematical model, which does not contain any term proportional to displacement  $x_1$  and therefore models a free particle and is further selected as a possible model according to Selection Criterion 3.

**(d) Mathematical Model for Model in Fig. 5.14(iii)(a)**

In Fig. 5.14(iii)(a) and a free noise generator with voltage  $F(t)$  is added as shown in Fig. 5.18. Keeping the notation of current  $\dot{x}_1$  through inductance, the current in the main branch  $\dot{x}$ , and considering current  $\dot{x}_2$  through capacitance  $1/k$ , the model obtained is shown in Fig. 5.18 as possible Model IV.

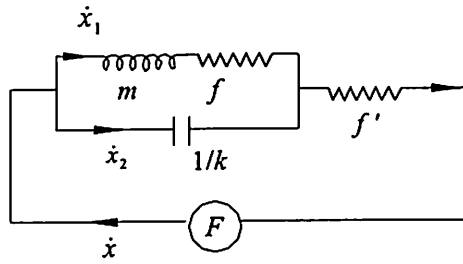


Fig. 5.18 Possible Model IV

Applying Kirchoff's law to the circuit gives the following equation

$$F = m \frac{d\dot{x}_1}{dt} + \dot{x}_1 f + \left( \dot{x}_1 + \frac{1}{k} \frac{d\left(m \frac{d\dot{x}_1}{dt} + \dot{x}_1 f\right)}{dt} \right) f' \quad (5.6)$$

Equation (5.6) on simplification gives

$$F = m \frac{d^2 x_1}{dt^2} + (f + f') \frac{dx_1}{dt} + \frac{mf'}{k} \frac{d^3 x_1}{dt^3} + \frac{ff'}{k} \frac{d^2 x_1}{dt^2} \quad (5.7)$$

From equation (5.7), a mathematical model in the form of second order differential equation can be obtained, which will be equivalent to Langevin equation. In order to get the second order differential equation as mathematical model, equation (5.7) on integration gives

$$\int F dt = m \frac{dx_1}{dt} + (f + f')x_1 + \frac{mf'}{k} \frac{d^2 x_1}{dt^2} + \frac{ff'}{k} \frac{dx_1}{dt} + C \quad (5.8)$$

where  $C$  is constant of integration. Equation (5.8) contains harmonic term and therefore the model does not satisfy Selection Criterion-3 and hence is rejected.

**(e) Mathematical Model for Model in Fig. 5.14(iii)(b)**

In Fig. 5.14(iii)(b) a free noise generator with voltage  $F(t)$  is added as shown in Fig. 5.19. Keeping the notation of current  $\dot{x}_1$  through inductance, the current in the main branch  $\dot{x}$ , and considering current  $\dot{x}_2$  through resistance  $f'$ , the model obtained is shown in Fig. 5.19 as possible Model V.

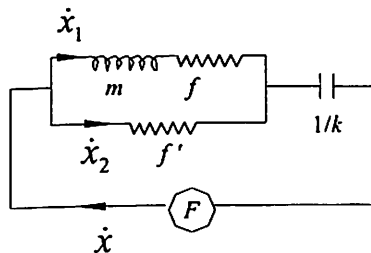


Fig. 5.19 Possible Model V

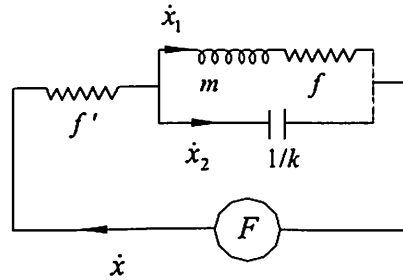
Applying Kirchoff's law to the circuit gives the following equation

$$F = m \frac{d^2 x_1}{dt^2} + \left( f + \frac{mkf}{f'} \right) \frac{dx_1}{dt} + k \left( 1 + \frac{f}{f'} \right) x_1 \quad (5.9)$$

Equation (5.9) contains a harmonic force terms proportional to displacements and so does not satisfy Selection Criterion 3 and therefore this model is also rejected.

**(f) Mathematical Model for Model in Fig. 5.14(iv)(a)**

In Fig. 5.14(iv)(a) a free noise generator with voltage  $F(t)$  is added as shown in Fig. 5.20. Keeping the notation of current through inductance as  $\dot{x}_1$  and considering the current in the main branch  $\dot{x}$ , current  $\dot{x}_2$  through  $f'$ , the model obtained is shown in Fig. 5.20 as possible Model VI.



**Fig. 5.20** Possible Model VI

Applying Kirchoff's law to the circuit gives the following equation

$$F = \frac{1}{k} \left( m \frac{d^3 x_1}{dt^3} + f' \frac{d^2 x_1}{dt^2} + \frac{dx_1}{dt} \right) f' + m \frac{d^2 x_1}{dt^2} + f \frac{dx_1}{dt} \quad (5.10)$$

From equation (5.10), a mathematical model in the form of second order differential equation can be obtained, which will be equivalent to Langevin equation. In order to get the second order differential equation as mathematical model, equation (5.10) on integration gives

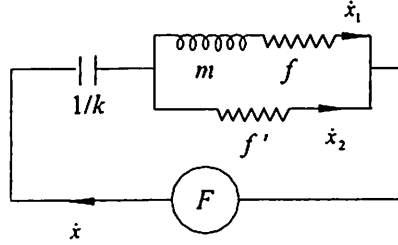
$$\int F dt = \frac{f'}{k} \left( m \frac{d^2 x_1}{dt^2} + f' \frac{dx_1}{dt} + x_1 \right) + m \frac{dx_1}{dt} + f x_1 + C \quad (5.11)$$

where  $C$  is constant of integration. Equation (5.11) contains harmonic term in  $x_1$  and therefore the model does not satisfy selection criterion-3 and hence, Model VI is rejected.



**(g) Mathematical Model for Model in Fig. 5.14(iv) (b)**

In Fig. 5.14(iv)(b) a free noise generator with voltage  $F(t)$  is added as shown in Fig. 5.21. Keeping the notation of current  $\dot{x}_1$  through inductance, the current in the main branch as  $\dot{x}$ , and considering current  $\dot{x}_2$  through  $f'$ , the model obtained is shown in Fig. 5.21 as possible Model VII.



**Fig. 5.21** Possible Model VII

Applying Kirchoff's law to the circuit gives the following equation

$$\frac{1}{k} \frac{dF}{dt} = \frac{m}{k} \frac{d^3 x_1}{dt^3} + \left( \frac{m}{f'} - \frac{f}{k} \right) \frac{d^2 x_1}{dt^2} + \left( 1 + \frac{f}{f'} \right) \frac{dx_1}{dt} \quad (5.12)$$

From equation (5.12), a mathematical model in the form of second order differential equation can be obtained, which will be equivalent to Langevin equation. In order to get the second order differential equation as mathematical model, equation (5.12) on integration gives

$$\frac{F}{k} = \frac{m}{k} \frac{d^2 x_1}{dt^2} + \left( \frac{m}{f'} - \frac{f}{k} \right) \frac{dx_1}{dt} + \left( 1 + \frac{f}{f'} \right) x_1 + C \quad (5.13)$$

where  $C$  is constant of integration. Equation (5.13) contains harmonic term in  $x_1$  and therefore the model does not satisfy selection criterion-3 and hence, Model VII is rejected.

**(h) Mathematical Model for Model in Fig. 5.14(v)**

In Fig. 5.14(v) and a free noise generator with voltage  $F(t)$  is added as shown in Fig. 5.22. Keeping the notation of current  $\dot{x}_1$  through inductance, the current in the main branch  $\dot{x}$ , and considering current  $\dot{x}_2$  and  $\dot{x}_3$  through resistance  $f'$ , and capacitance  $1/k$  respectively, the model obtained is shown in Fig. 5.22 as Model possible VIII.

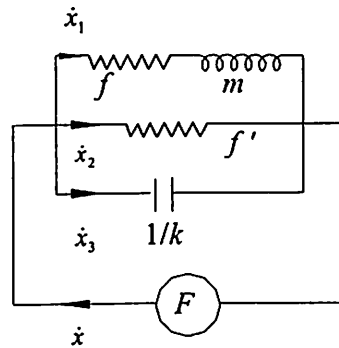


Fig 5.22 Possible Model VIII

Applying Kirchoff's law to the circuit gives the following equation

$$F = m \frac{d^2 x_1}{dt^2} + f \frac{dx_1}{dt} \quad (5.14)$$

Equation (5.14) is the required mathematical model, which does not contain any term proportional to displacement  $x_1$  and therefore models a free particle and is further selected as a possible model according to Selection Criterion 3.

**(j) Mathematical Model for Model in Fig. 5.14(vi)**

In Fig. 5.14(vi) a free noise generator with voltage  $F(t)$  is added as shown in Fig. 5.23. Keeping the notation of current  $\dot{x}_1$  through inductance, and considering the current in the branches as  $\dot{x}_2$  and  $\dot{x}_3$ , the model obtained is shown in Fig. 5.23 as possible Model IX.

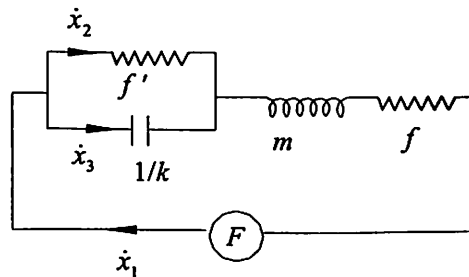


Fig. 5.23 Possible Model IX

Applying Kirchoff's law to the circuit gives the following five equations

$$\frac{mf'}{k} \frac{d^3 x_1}{dt^3} + \left( \frac{ff'}{k} - m \right) \frac{d^2 x_1}{dt^2} - (f + f') \frac{dx_1}{dt} = \frac{f'}{k} \frac{dF}{dt} - F \quad (5.15)$$

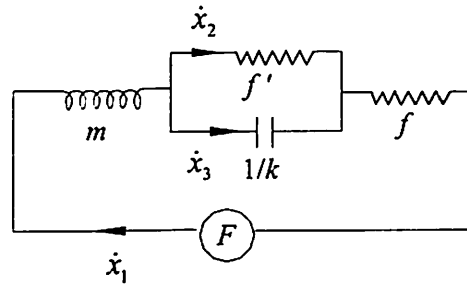
Equation (5.15) on integration yields second order differential equation given as

$$\frac{mf'}{k} \frac{d^2 x_1}{dt^2} + \left( \frac{ff'}{k} - m \right) \frac{dx_1}{dt} - (f + f')x_1 + C = \frac{f'}{k} F - \int F dt \quad (5.16)$$

where  $C$  is constant of integration. Equation (5.16) contains terms representing harmonic force, which bounds the particle and does not satisfies the Selection Criterion 3. Hence, Model IX also gets rejected.

**(k) Mathematical Model for Model in Fig. 5.14(vii)**

In Fig. 5.14(vii) a free noise generator with voltage  $F(t)$  is added as shown in Fig. 5.24. Keeping the notation of current  $\dot{x}_1$  through inductance, and considering the current in the branches as  $\dot{x}_2$  and  $\dot{x}_3$ , the new possible model obtained is shown in Fig. 5.24 as Model X.



**Fig. 5.24** Possible Model X

Applying Kirchoff's law to the circuit gives the following equation

$$F + \frac{f'}{k} \frac{dF}{dt} = \frac{mf'}{k} \frac{d^3 x_1}{dt^3} + \left( \frac{f'}{k} + m \right) \frac{d^2 x_1}{dt^2} + (f + f') \frac{dx_1}{dt} \quad (5.17)$$

From equation (5.17), a mathematical model in the form of second order differential equation can be obtained, which will be equivalent to Langevin equation. In order to get the second order differential equation as mathematical model, equation (5.17) on integration gives

$$\int F dt + \frac{f'}{k} F = \frac{mf'}{k} \frac{d^2 x_1}{dt^2} + \left( \frac{f'}{k} + m \right) \frac{dx_1}{dt} + (f + f')x_1 + C \quad (5.18)$$

where  $C$  is constant of integration. Equation (5.18) contains terms representing forces proportional to displacement. But the presence of terms representing forces proportional to  $x$  harmonically bounds the particle and does not satisfies the Selection Criterion 3. Hence, Model X also gets rejected.

**(l) Mathematical Model for Model in Fig. 5.14(viii)**

As for previous case, the electrical analog circuit with voltage  $F(t)$  put across the system model, shown in Fig. 5.14(viii), is shown in Fig. 5.25. Considering

current in different branches as  $\dot{x}_2$  and  $\dot{x}_3$ , the model is shown in Fig. 5.25 as possible Model XI.

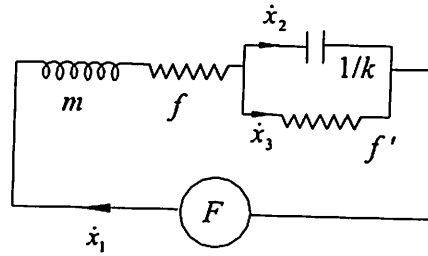


Fig. 5.25 Possible Model XI

Applying Kirchoff's law to the circuit gives the equation

$$\dot{x}_1 = \frac{1}{f'} \left( F - \dot{x}_1 f - m \frac{d\dot{x}_1}{dt} \right) + \frac{1}{k} \frac{d \left( F - \dot{x}_1 f - m \frac{d\dot{x}_1}{dt} \right)}{dt} \quad (5.19)$$

Equation (5.19) on simplification gives

$$\frac{dx_1}{dt} = \frac{1}{f'} \left( F - f \frac{dx_1}{dt} - m \frac{d^2 x_1}{dt^2} \right) + \frac{1}{k} \left( \frac{dF}{dt} - f \frac{d^2 x_1}{dt^2} - m \frac{d^3 x_1}{dt^3} \right) \quad (5.20)$$

From equation (5.20), a mathematical model in the form of second order differential equation can be obtained, which will be equivalent to Langevin equation. In order to get the second order differential equation as mathematical model, equation (5.20) on integration gives

$$x_1 = \frac{1}{f'} \left( Ft - fx_1 - m \frac{dx_1}{dt} \right) + \frac{1}{k} \left( F - f \frac{dx_1}{dt} - m \frac{d^2 x_1}{dt^2} \right) + C \quad (5.21)$$

where  $C$  is constant of integration. Equation (5.21) contains terms representing harmonic force and, therefore, does not satisfy the Selection Criterion-3. Hence, Model XI also gets rejected.

#### (m) Mathematical Model for Model in Fig. 5.14(ix)

In Fig. 5.14(ix) a free noise generator with voltage  $F(t)$  is added as shown in Fig. 5.26. Keeping the notation of current  $\dot{x}_1$  through inductance, the current in the main branch  $\dot{x}$ , and considering current  $\dot{x}_2$  through resistance  $f'$  and capacitance  $1/k$ , the model obtained is shown in Fig. 5.26 as possible Model XII.

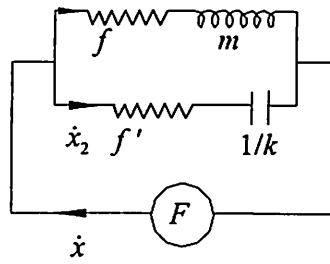


Fig. 5.26 Possible Model XII

Applying Kirchoff's law to the circuit gives the following equation

$$F = m \frac{d^2 x_1}{dt^2} + f \frac{dx_1}{dt} \quad (5.22)$$

Equation (5.22) does not contain any term proportional to displacement  $x_1$  and therefore models a free particle and is further selected as a possible model according to Selection Criterion 3.

The number of rejected models on the basis of their inability to satisfy criterion-3 is nine and only three models remain for further analysis. The summary of selection of three models from all possible 360 models is given in Table 5.2. The three models satisfying Selection Criterion 1, Criterion 2 and Criterion 3 are mentioned as valid models in column 7 of Table 5.2.

## 5.6 SELECTED SYSTEM MODELS

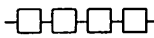
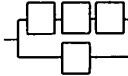
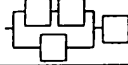
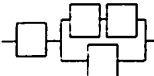
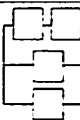
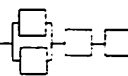
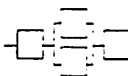

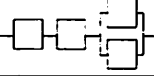
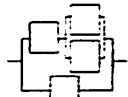
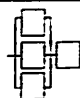
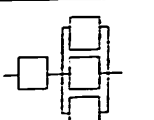
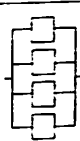
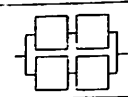
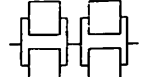
The three models surviving three selection criteria are shown in Fig. 5.27 and are denoted as Model 8, Model 9 and Model 10, respectively for further analysis (Model 1 through Model 7 were analyzed in Chapter 3 and Chapter 4). The numbering of valid models is in continuity to seven models developed in previous chapter.

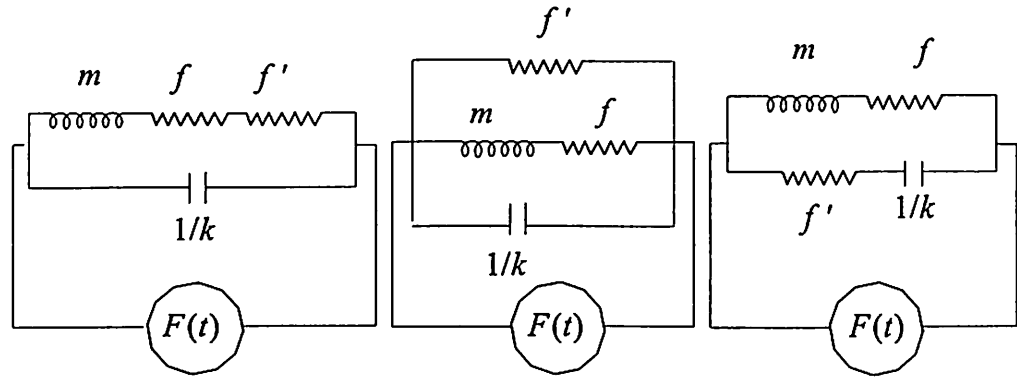
The mathematical models for the three models developed in the previous section in equations (5.5), (5.14), and (5.22) and are written again for convenience

Model 8

$$F(t) = m \frac{d^2 x_1}{dt^2} + (f + f') \frac{dx_1}{dt} \quad (5.23)$$

**Table 5.2** Possible Models of Four Parameter System

S.No.	Possible Distinct Arrangement of Four-Units	Possible Models	No. of Distinct Models Criterion 1	No. of Models Rejected based on		No. of Valid Models
				Criterion 2	Criterion 3	
(1)	(2)	(3)	(4)	(5)	(6)	(7)
1.		24	1	-	1	-
2.		24	4	2	1	1
3.		24	12	10	2	-
4.		24	12	10	2	-
5.		24	6	5	-	1
6.		24	6	5	1	-
7.		24	6	5	1	-
8.		24	12	12	-	-
9.		24	6	5	1	-
10.		24	12	12	-	-
11.		24	4	4	-	-
12.		24	4	4	-	-
13.		24	1	1	-	-
14.		24	3	2	-	1
15.		24	3	3	-	-
<b>Total</b>		<b>360</b>	<b>92</b>	<b>80</b>	<b>9</b>	<b>3</b>



(i) Model 8

(ii) Model 9

(iii) Model 10

**Fig. 5.27** Equivalent Electric Analog Circuits for Three Valid Models

Model 9

$$F(t) = m \frac{d^2 x_1}{dt^2} + f \frac{dx_1}{dt} \quad (5.24)$$

Model 10

$$F(t) = m \frac{d^2 x_1}{dt^2} + f \frac{dx_1}{dt} \quad (5.25)$$

Equations (5.23)-(5.25) can be written as a single equation in a general form as

$$\frac{d^2 x}{dt^2} + \beta \frac{dx}{dt} = n(t) \quad (5.26)$$

where  $x_1$  are replaced by  $x$ ,  $n(t) = F(t)/m$  is the scaled thermal noise impulse input, and  $\beta$  for the three models are, respectively

Model 8

$$\beta = \frac{(f + f')}{m} \quad (5.27)$$

Model 9

$$\beta = \frac{f}{m} \quad (5.28)$$

Model 10

$$\beta = \frac{f}{m} \quad (5.29)$$

The expected value of variance in output  $x(t)$  for scaled thermal noise impulse input  $n(t)$  in Equation (5.26) with autocorrelation  $\alpha \delta(\tau)$  has been derived for a rigid particle Model 1 (Ref. Equation 3.7) and reproduced below for convenience as

$$E\{x^2(t)\} = \frac{\alpha}{2\beta^3} (1 - e^{-\beta t}) (2\beta t - 1 + e^{-\beta t}) \quad (5.30)$$

where 
$$\alpha = \frac{2\kappa T f}{m^2} \quad (5.31)$$

In rigid nano-particle model, the damping from nano-particle is assumed insignificant and its contribution from medium alone. In contrast, non-rigid model of nano-particle considers damping from medium as well as from nano-particle to contribute to total damping. The total damping from medium and nano-particle is denoted by  $f_{eq}$  and replaces  $f$  in equation (5.31) for non-rigid model. For the three valid models (Refer Fig.5.27) of possible models, the values of  $f_{eq}$  have been obtained from electric circuits shown in Fig. (5.27) as

Model 8

$$f_{eq} = \frac{(f + f') \left( \frac{k}{\omega} \right)^2}{(f + f')^2 + \left( \omega m - \frac{k}{\omega} \right)^2} \quad (5.32)$$

Model 9

$$f_{eq} = \frac{(mk + ff')mf'k - \left( mkff'^2 + \frac{k^2 ff'(f + f')}{\omega^2} \right)}{(mk + ff')^2 + \left( \omega mf' - \frac{k(f + f')}{\omega} \right)^2} \quad (5.33)$$

Model 10

$$f_{eq} = \frac{(ff' + mk)(f + f') + \left( \omega mf' - \frac{fk}{\omega} \right) \left( \omega m - \frac{k}{\omega} \right)}{(f + f')^2 + \left( \omega m - \frac{k}{\omega} \right)^2} \quad (5.34)$$

where  $\omega$  is the frequency in radians per second. Substitution of  $f_{eq}$  from equations (5.32) to (5.34) in equation (5.31) gives three values of  $\alpha$  for the three models respectively, which along with the value of  $\beta$  are used to obtain variance expressions for the three models.

## 5.7 FORMULATION OF VARIANCE EXPRESSION

A typical type of fundamental time domain noise source is a Gaussian white noise with zero mean and variance  $E\{F^2(t)\}$ . The thermal noise is one type of white noise, which has been considered in derivation of equation (5.30). The variance for



rigid nano-particle is given by equation (5.30). In order to obtain variance for the three selected non-rigid models, the expression for  $\beta$  is substituted in equation (5.30) from equations (5.27) to (5.29) and  $\alpha$  for the three non-rigid models from equation (5.31) with substitution of  $f_{eq}$  from equations. (5.32) to (5.34). The expressions for variance for the three non-rigid models obtained are

Model 8

$$E\{x^2(t)\} = \frac{\kappa T m}{(f + f')^2} \left\{ 1 - e^{-\frac{(f+f')t}{m}} \right\} \left\{ \frac{\left(\frac{k}{\omega}\right)^2}{(f + f')^2 + \left(\omega m - \frac{k}{\omega}\right)^2} \right\} \left\{ \frac{2(f + f')t}{m} - 1 + e^{-\frac{(f+f')t}{m}} \right\} \quad (5.35)$$

Model 9

$$E\{x^2(t)\} = \frac{\kappa T m}{f^3} \left\{ \frac{(mk + ff')m f' k - \left( mkf f'^2 + \frac{k^2 ff'(f + f')}{\omega^2} \right)}{(mk + ff')^2 + \left( \omega m f' - \frac{k(f + f')}{\omega} \right)^2} \right\} PQ \quad (5.36)$$

Model 10

$$E\{x^2(t)\} = \frac{\kappa T m}{f^3} \left\{ \frac{(f f' + m k)(f + f') + \left( \omega m f' - \frac{fk}{\omega} \right) \left( \omega m - \frac{k}{\omega} \right)}{(f + f')^2 + \left( \omega m - \frac{k}{\omega} \right)^2} \right\} PQ \quad (5.37)$$

where  $P = \{1 - e^{-f'/m}\}$  and  $Q = \left\{ \frac{2ft}{m} - 1 + e^{-f'/m} \right\}$

The variance models given by equations (5.35) to (5.37) are simulated to validate the three models in next section.

## 5.8 SIMULATION OF THREE NON-RIGID MODELS

The three models are subjected to two validity criterions of non-negativity and finiteness of variance defined in Chapter 4 in sections 4.2.1 and 4.2.2. In order to validate the models, the simulation over a large parametric range is carried out for two nanoparticles namely, silicon and polystyrene. The two nanoparticles are chosen because the variance plots for the two are available as published experimental results in the work of Sasaki [2000] and Nakroshis [2003], respectively. The parametric

values for the two nanoparticles are given in section 4.4.1 and 4.4.2 and are written for convenience in table 5.3.

**Table 5.3** Parametric Values for Silicon and Polystyrene Nanoparticle Given in Published Experimental Results

Parameter	Silicon [Sasaki 2000]	Polystyrene [Nakroshis 2003]
Density ( $\rho$ )	2300 kg/m <sup>3</sup>	1060 kg/m <sup>3</sup>
Temperature of Surrounding	273 K	296.01±0.3 K
Radius of Nanoparticle ( $r$ )	40 nm	0.51 ± 0.01 $\mu$ m
Viscosity of surrounding medium water ( $\eta$ )	1.8×10 <sup>-3</sup> N s/m <sup>2</sup>	(936 ± 15)×10 <sup>-6</sup> N s/m <sup>2</sup>

From these parameters mass  $m$  and  $f'$  of nanoparticle and damping coefficient  $f$  of medium are computed and are tabulated in Table 5.4 for the two nanoparticles.

**Table 5.4** Parametric Values Deduced for Brownian motion of Non-Rigid Nanoparticle

Parameter	Silicon	Polystyrene
$m$	6.16×10 <sup>-19</sup> kg	(5.88 ± 0.35)×10 <sup>-16</sup> kg
$f'$	6.51×10 <sup>-17</sup> k/c' N s/m	(6.65 ± 0.75)×10 <sup>-14</sup> k/c' N s/m
$f$	1.356×10 <sup>-9</sup> N s/m	(9.00 ± 0.32)×10 <sup>-9</sup> N s/m

The value of spring constant is assumed as  $k = 2.3$  N/m, time is varied from  $1/\beta$  to  $10/\beta$  in steps of  $1/\beta$  s and  $c'$  is varied from  $1 \times 10^{-10}$  to 100 m in various step size in different range. The three models of non-rigid nanoparticles are simulated for  $\psi$  values with respect to time for the three models as was done for impact transfer models in Chapter 4. The function  $\psi$  is obtained in next section for the three models.

### 5.8.1 Time Dependent Functions Corresponding to Variance of Three Models

In order to test the validity of the three models, two validity criteria are defined in section 4.2.1 and 4.2.2 and are applied to the three models, Model 8

through Model 10. According to the two criteria, the variance values of the models should be positive and finite. With the aim to test the positivity and finiteness of the variances of the three models, a function  $\psi$  is defined in Chapter 4 in section 4.3 as the time dependent part of the variance value devoid of positive scale multiplier. The function  $\psi$  is simulated in place of variance value because this reduces the computations giving the trend sought for validation. The function  $\psi$  is obtained for the three models next.

**(a) Function  $\psi$  for Model 8**

For Model 8, the function  $\psi$  is obtained from equation (5.35) as the time dependent part devoid of positive scale multiplier and is given as

$$\psi = \left\{ 1 - e^{-(f+f')t/m} \right\} \left\{ \frac{2(f+f')t}{m} - 1 + e^{-(f+f')t/m} \right\} \quad (5.38)$$

**(b) Function  $\psi$  for Model 9**

For Model 9, the function  $\psi$  is obtained from equation (5.36) as the time dependent part devoid of positive scale multiplier and is given as

$$\psi = \left\{ 1 - e^{-ft/m} \right\} \left\{ \frac{2ft}{m} - 1 + e^{-ft/m} \right\} \quad (5.39)$$

**(c) Function  $\psi$  for Model 10**

For Model 10, the function  $\psi$  is obtained from equation (5.37) as the time dependent part devoid of positive scale multiplier and is given as

$$\psi = \left\{ 1 - e^{-ft/m} \right\} \left\{ \frac{2ft}{m} - 1 + e^{-ft/m} \right\} \quad (5.40)$$

It is observed from equation (5.39) and equation (5.40) that the function  $\psi$  for the Model 9 and Model 10 are identical. The functions given by equation (5.38) to equation (5.39) are simulated for the two nanoparticles with  $\psi$  plotted on y-axis and time on x-axis. The simulation for silicon nanoparticle is done first in next section.

**5.8.2 Simulation of Function  $\psi$  for Silicon Nanoparticle**

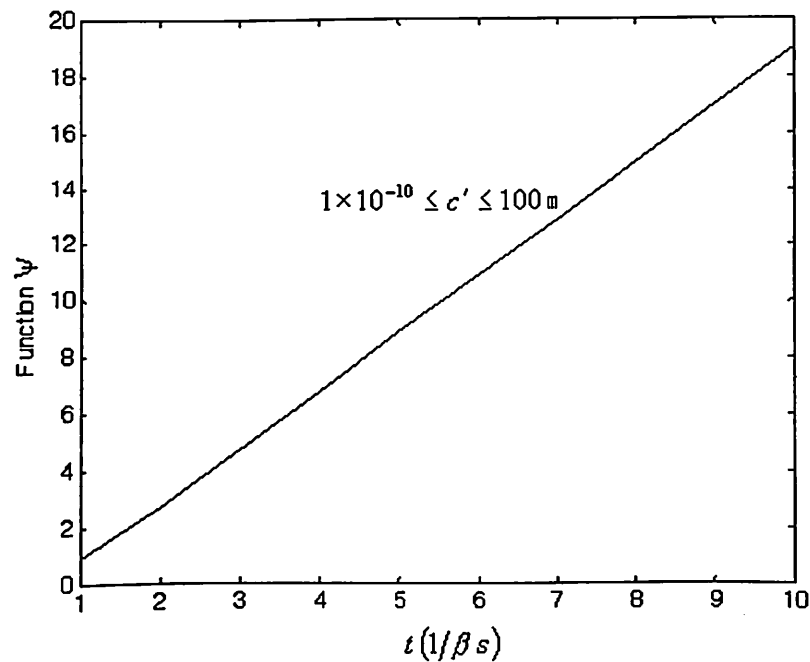
For simulation of  $\psi$  considering silicon nanoparticle, the parametric values are taken from Table 5.3 and Table 5.4. The simulation results for the three models are given in the following section.

**(a) Simulation of Function  $\psi$  for Model 8**

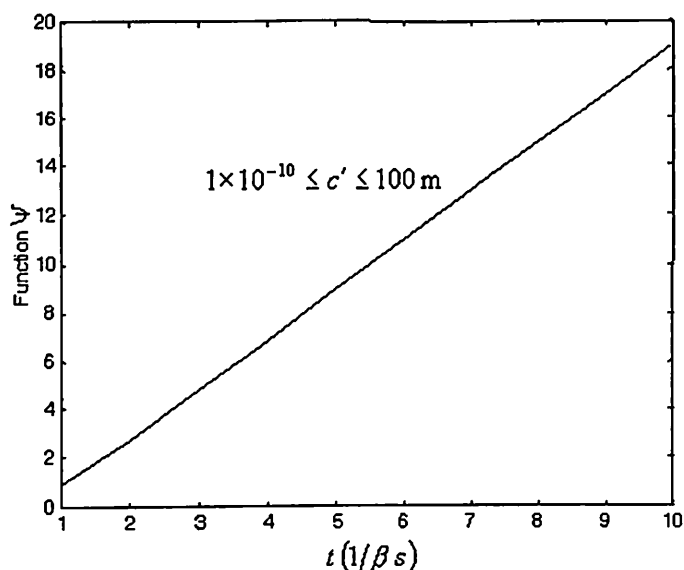
The values of  $\psi$  are obtained using equation (5.38) for specified range of  $c'$  and are shown in Fig. 5.28. It is observed from simulation results that Model 8 predicts positive and finite values of function  $\psi$  in the entire range of parametric variation and is invariant to  $c'$ . The positivity and fineness is in accordance to validity Criterion 1 and Criterion 2 given in Chapter 4, Section 4.2.

**(b) Simulation of Function  $\psi$  for Model 9 and Model 10**

The values of  $\psi$  are obtained using equation (5.39) for specified range of  $c'$  and are shown in corresponding plots in Fig. 5.29. It is observed from simulation results that Model 9 and Model 10 predicts positive and finite values of function in the entire range of parametric variation and is invariant to  $c'$ . The positivity and finiteness is in accordance to validity Criterion 1 and Criterion 2 given in Chapter 4.



**Fig. 5.28** Simulation of  $\psi$  v/s Time for Silicon Nanoparticle using Model 8



**Fig. 5.29** Simulation of  $\psi$  v/s Time for Silicon Nanoparticle using Model 9 and Model 10

### 5.8.3 Simulation of Function $\psi$ for Polystyrene Nanoparticle

For simulation of  $\psi$  considering polystyrene nanoparticle, the parametric values are taken from Table 5.3 and Table 5.4. For the three models, the simulation results are given in the following section.

#### (a) Simulation of Function $\psi$ for Model 8

The values of  $\psi$  are obtained using equation (5.38) for different range of  $c'$  and are shown in corresponding plots in Fig. 5.30. It is observed from simulation results that Model 8 predicts positive and finite values of function value in the entire range of parametric variation.

Comparing the simulation results for polystyrene nanoparticle with that of silicon nanoparticle (Refer Fig. 5.28), it is observed that for polystyrene nanoparticle, the function  $\psi$  varies in certain range of  $c'$ . The variation in  $\psi$  for polystyrene is because the  $f'$  values for polystyrene are one thousand times greater than that for silicon nanoparticle. Thus, a change in  $f'$  corresponding to a change in  $c'$  causes a significant change in the value of  $\psi$  in case of polystyrene nanoparticle.

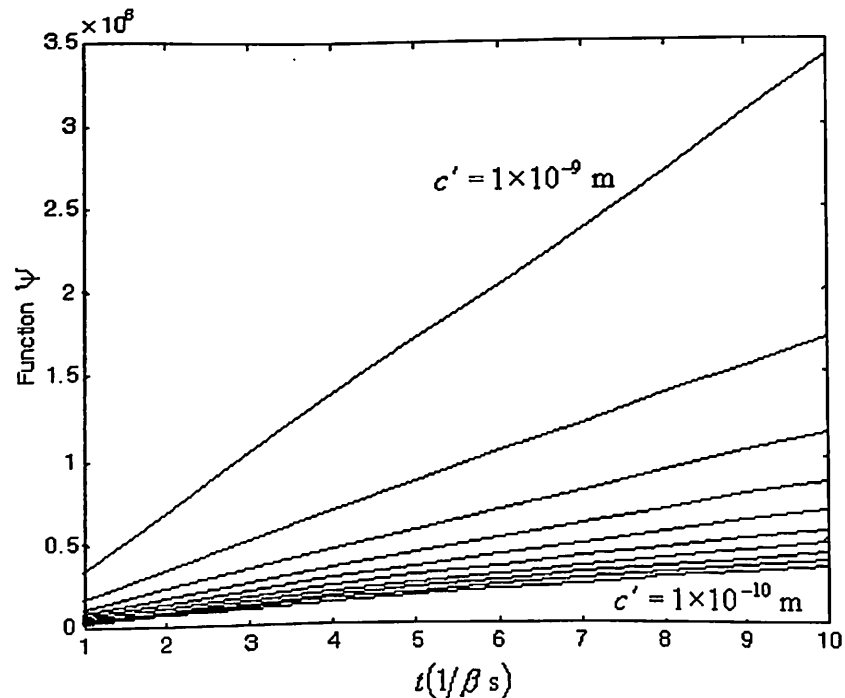
Moreover, the initial increase in  $\psi$  with increasing  $c'$  is because of larger increase in linear term  $2(f + f')t/m$  in comparison to exponential term in equation (5.95). This happens for values of  $c'$  for which  $f' > f$ , after which the

trend turns around. At very large values of  $c'$ , the parameter  $f'$  becomes insignificant in comparison to  $f$  and therefore a change in  $f'$  hardly contributes to a change of  $\psi$  showing invariance with  $c'$ . Thus, the linear term with time in equation (5.95) increases with  $c'$ .

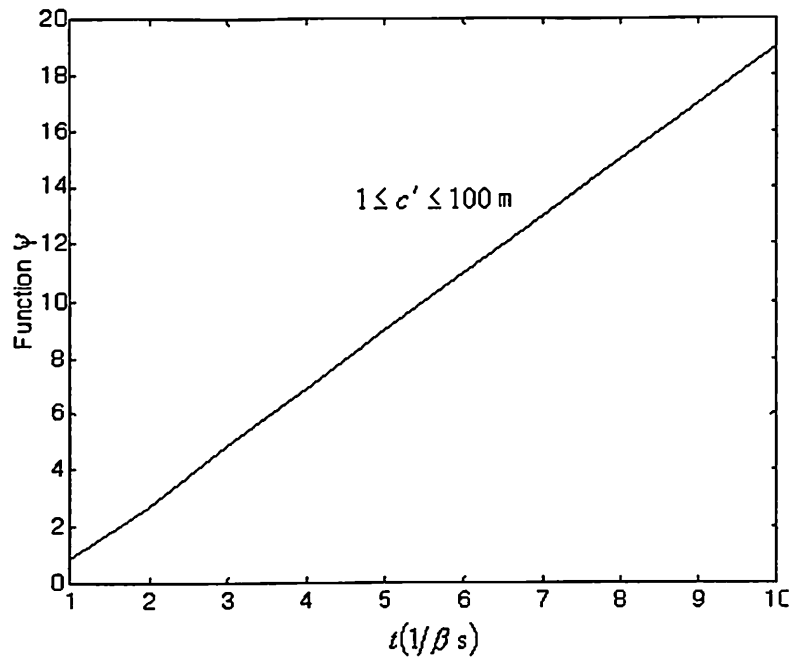
A few plots depicting increase in  $\psi$  value are shown in Fig. 5.26(i) and the invariance of  $\psi$  with  $c'$  is shown in Fig. 5.26(ii). The simulated results predicting positive and finite function values are in accordance to validity Criterion 1 and Criterion 2. The model represents a valid Brownian motion model of non-rigid nanoparticle.

**(b) Simulation of Function  $\psi$  for Model 9 and Model 10**

The values of  $\psi$  are obtained using equation (5.39) for different range of  $c'$  and are shown in in Fig. 5.31. It is observed from simulation results that Model 9 and Model 10 predicts positive and finite values of function value in the entire range of parametric variation and is invariant to  $c'$ . The absence of  $c'$  dependent terms in equation (5.39) gives the invariant values of  $\psi$ . The positive and finite  $\psi$  is in accordance to validity Criterion 1 and Criterion 2. The models represent a valid Brownian motion model of non-rigid nanoparticle



(i) Simulation in Parameter Range:  $1 \times 10^{-10} \leq c' \leq 1 \times 10^{-9}$  m in Steps of  $1 \times 10^{-9}$  m



(ii) Simulation in Parameter Range:  $1 \leq c' \leq 100 \text{ m}$  in Steps of 10 m

Fig. 5.30 Function  $\psi$  v/s Time for Polystyrene Nanoparticle using Model 8

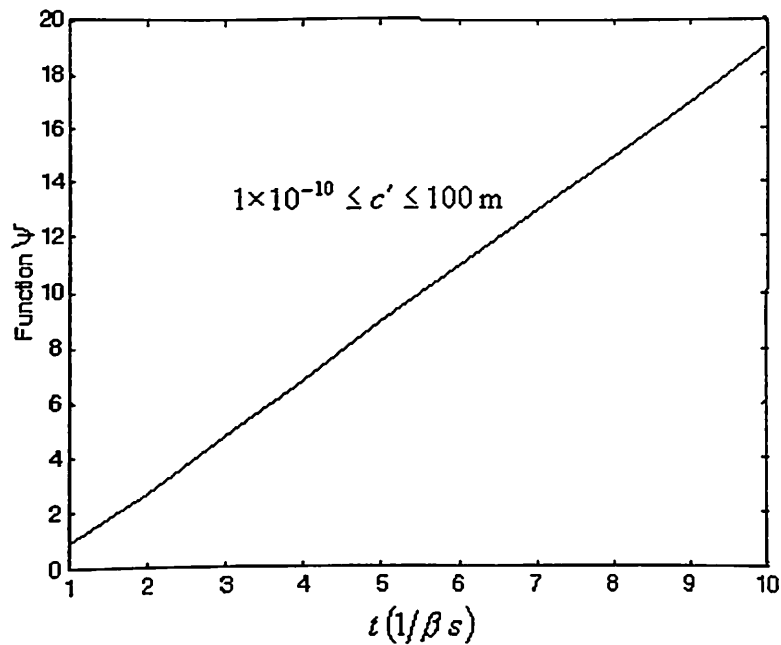


Fig. 5.31 Simulation of  $\psi$  v/s Time for Polystyrene Nanoparticle using Model 9 and Model 10

## 5.9 VERIFICATION OF MODELS WITH EXPERIMENTAL RESULTS

The three models have been simulated for two nanoparticles to establish their validity according to Criterion 1 and Criterion 2 in the previous section. All the three

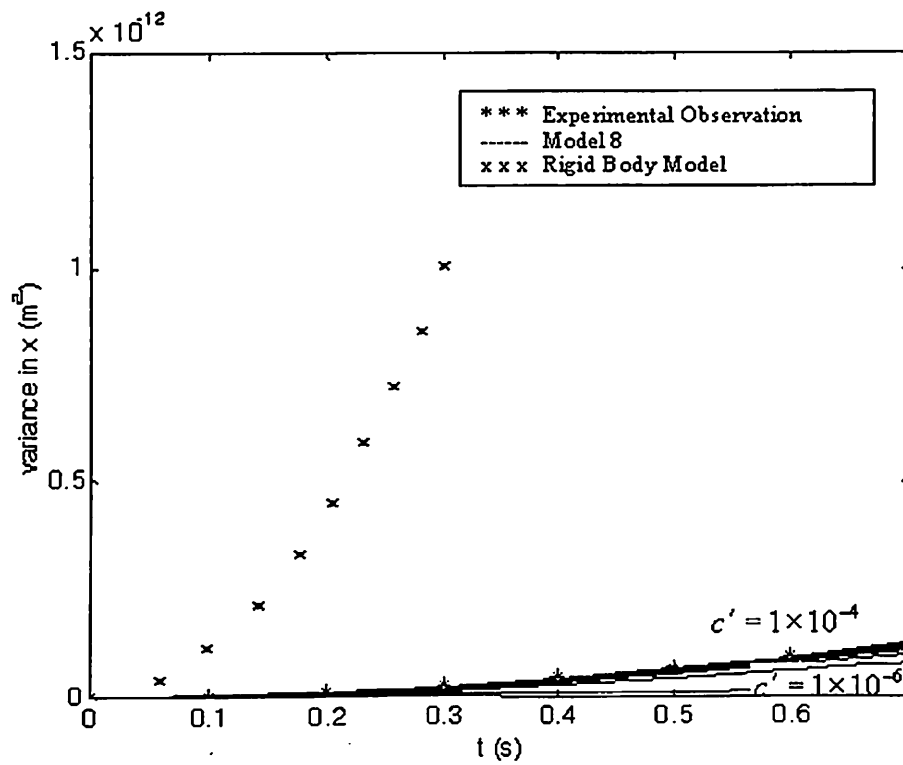
models were found to satisfy the two criteria. These three models are now simulated for Brownian motion to test them against the two published experimental results in the field of engineering sciences, corresponding to Brownian motion of nanoparticle at the extremities of nano-domains. In order to test the three models with published results, the three models are simulated to obtain variance in position in next section. The variance in position  $x$  ( $m^2$ ) is plotted on  $y$ -axis and time in seconds on  $x$ -axis with  $c'$  as a parameter.

### 5.9.1 Brownian Motion of Silicon Nanoparticle

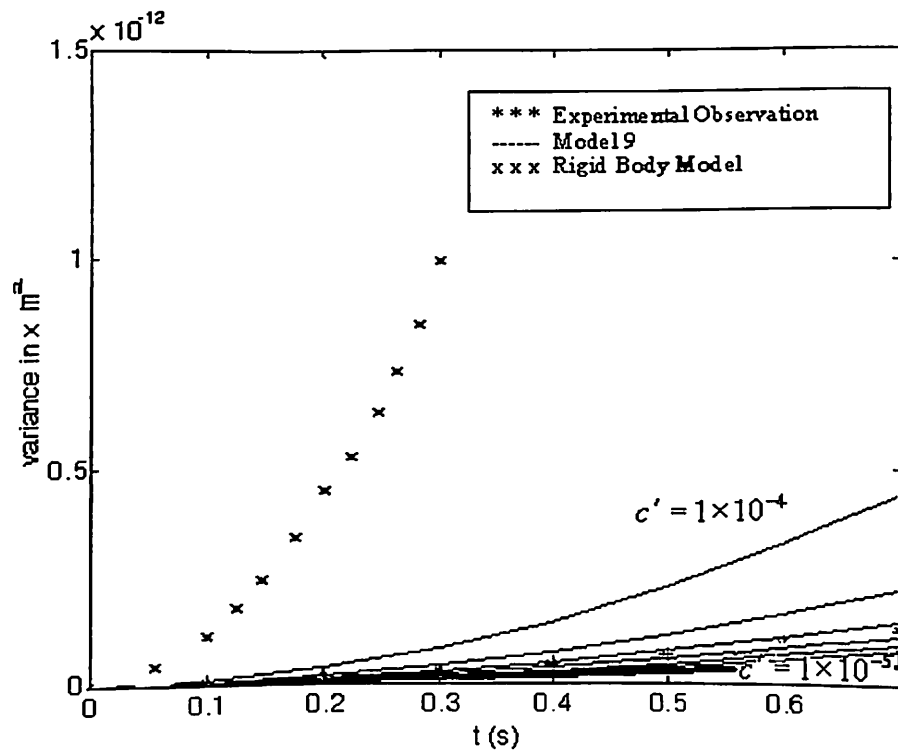
The variance in angular position with respect to time  $E\{\theta^2(t)\}$  of Silicon nanoparticle has been used to obtain the viscosity of super cooled water [Sasaki 2000]. The variance in angular position is related to variance in position  $E\{x^2(t)\}$  as:  $E\{x^2(t)\} = l^2 E\{\theta^2(t)\}$ , where  $l$  is the distance of nanoparticle from the substrate used for observation and is given as  $l = 30 \mu m$  in Sasaki [2000]. The various parametric values in the experiment by Sasaki are given in Table 5.3. Using the parameters from Table 5.3 and Table 5.4, the variances in position  $E\{x^2(t)\}$  with respect to time are calculated from the three models (equations (5.35) to (5.37)) for  $\omega = 60 \text{ GHz}$ ,  $1 \times 10^{-4} \leq c' \leq 1 \times 10^2 \text{ m}$ ,  $k = 300 \text{ N/m}$  and results are shown in Fig. 5.32. The value of  $\omega$  is chosen as 60 GHz, which is one-tenth of the frequency at which quantum effects cannot be neglected [Engberg 1995].

The published experimental results from Sasaki and predicted variance by rigid body model are also superimposed in Fig. 5.28. It is observed from Fig. 5.28(i) to Fig. 5.28(iii) that the results obtained from rigid body model are substantially different from experimental observation. The rigid body model predicts variance values, which are substantially larger than observed values given by Sasaki. The results predicted by the three non-rigid nanoparticle models matches quite precisely with experimental observations. It is observed that the published experimental results match for  $c' = 5 \times 10^{-5} \text{ m}$ ,  $c' = 7.5 \times 10^{-5} \text{ m}$ ,  $1 \leq c' \leq 1 \times 10^2$  for the three models, Model 8, Model 9 and Model 10, respectively.

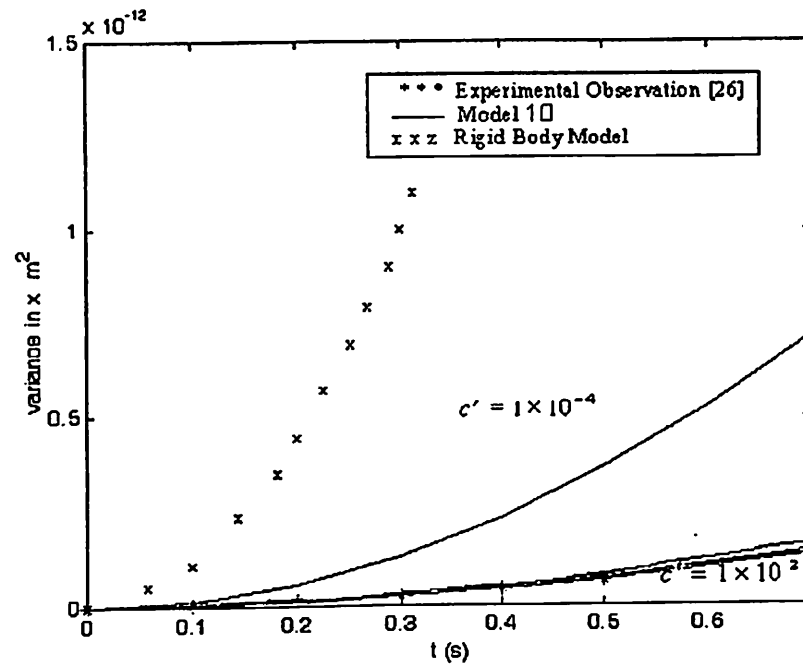




(i) Model 8:  $1 \times 10^{-6} \leq c' \leq 1 \times 10^{-4}$  m in Steps of  $c' = 1 \times 10^{-5}$  m



(ii) Model 9:  $1 \times 10^{-5} \leq c' \leq 1 \times 10^{-4}$  m in Steps of  $c' = 1 \times 10^{-5}$  m



(iii) Model 10:  $1 \times 10^{-4} \leq c' \leq 1 \times 10^2$  m in Steps of  $c' = 1 \times 10^{-2}$  m

**Fig. 5.32** Comparison of Variance in Position of Silicon Nanoparticle for Experimental observation [Sasaki 2000], Rigid Body Model and Developed Models

### 5.9.2 Brownian Motion of Polystyrene Nanoparticle

The variance in position with respect to time for polystyrene nanoparticle is available as published experimental results with the values of various parameters for the nanoparticle and its environment as given in Table 5.3. From these parameters, the mass and damping coefficient of nanoparticle and damping coefficient of medium is obtained and is given in Table 5.4. In order to get variance of polystyrene nanoparticle analytically from the three models, the simulation of variance with respect to time for the three models has been done by varying  $c'$  and  $t$ . The additional parameters required for non-rigid considerations of nanoparticle are  $\omega$ ,  $k$  and  $f'$ . Considering the value of  $\omega = 60$  GHz,  $k = 2.3$  N/m, the simulation is done by varying constant  $c'$  from  $1 \times 10^{-10}$  to 100 m in various steps size, and incrementing  $t$  in steps of 1 s from 0 to 10 s.

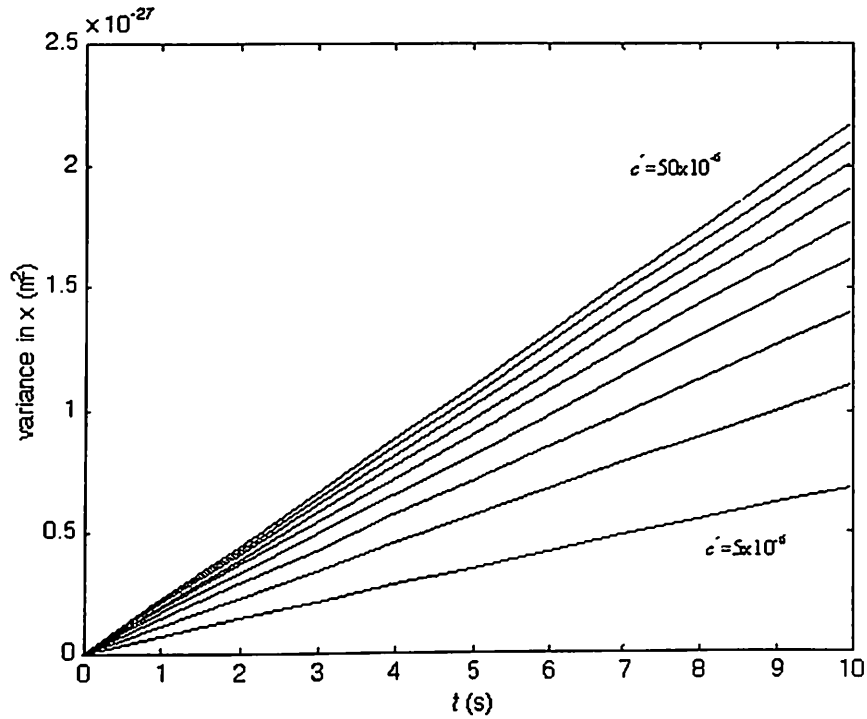
The variances obtained using the equations (5.35) to (5.37) corresponding to the three models are shown for a range of  $c'$  values in Fig. 5.33. It is observed from the results obtained that the variance for all the three models varies linearly with time, as was expected, because the results are obtained for  $t \gg 1/\beta$ . At larger

times, the time dependent part in the three models becomes linear as the exponential terms becomes negligible. This implies that for the chosen parameters diffusion constant, characterized by the slope of variance, is constant for any given value of  $c'$ .

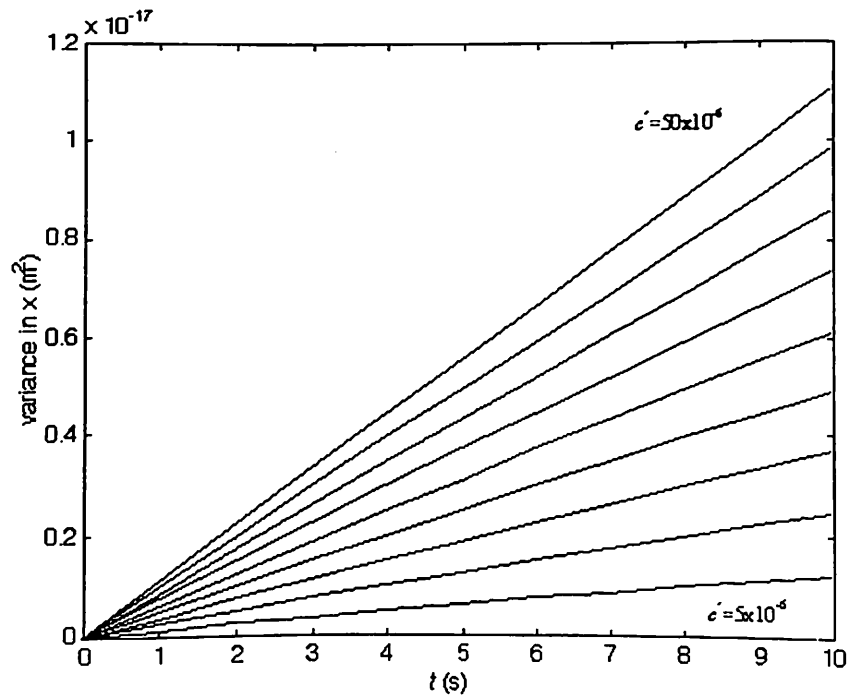
It is also observed from Fig. 5.33(i) and (ii) that for Model 8 and Model 9, diffusion constant value increases with increasing  $c'$  while a turn around of trend is shown by Model 10, Fig. 5.33 (iii). Also, the diffusion constant value obtained from Model 10 is more sensitive to parameter  $c'$  at its lower values. The reported experimental value of diffusion constant for polystyrene nanoparticle [Nakroshis 2003] is of the order of  $10^{-12}$  m<sup>2</sup>/s. The diffusion constants obtained from Model 8 and Model 9 are of the order of  $10^{-26}$  m<sup>2</sup>/s and  $10^{-16}$  m<sup>2</sup>/s, respectively while diffusion constant from Model 10 is of the order of  $10^{-12}$  m<sup>2</sup>/s. The magnitude of diffusion constant values predicted by Model 8 and Model 9 are substantially lower than the reported values, indicating that Model 8 and Model 9 are not able to accurately predict Brownian motion for non-rigid polystyrene nanoparticle. In order to confirm further, the simulation was done over an extended range of  $c'$  from  $1 \times 10^{-14}$  to 100 m in steps of  $1 \times 10^{-14}$  m for Model 8 and Model 9 and by varying of  $\omega$  from 50 MHz to 500 GHz in the steps of 10 MHz. It was found that diffusion constant obtained from Model 8 and Model 9 remained much lesser than observed values for any value of  $c'$  or  $\omega$ . Since the diffusion constant obtained from Model 8 and Model 9 are found to be far from reported experimental results, these two models do not verify with the experimental results.

The published experimental results [Nakroshis 2003], diffusion constant predicted by rigid body model, and results obtained from Model 10 are together plotted in Fig. 5.34, for comparison. It is seen from Fig. 5.34 that the diffusion constant obtained from rigid body model of nanoparticle is lower than the reported experimental values. It is also observed that diffusion constant obtained from Model 10 has large variations depending on the values of the parameter  $c'$  and lies on either side of reported experimental results. It is observed that diffusion constant obtained from Model 10 matches the reported experimental values for

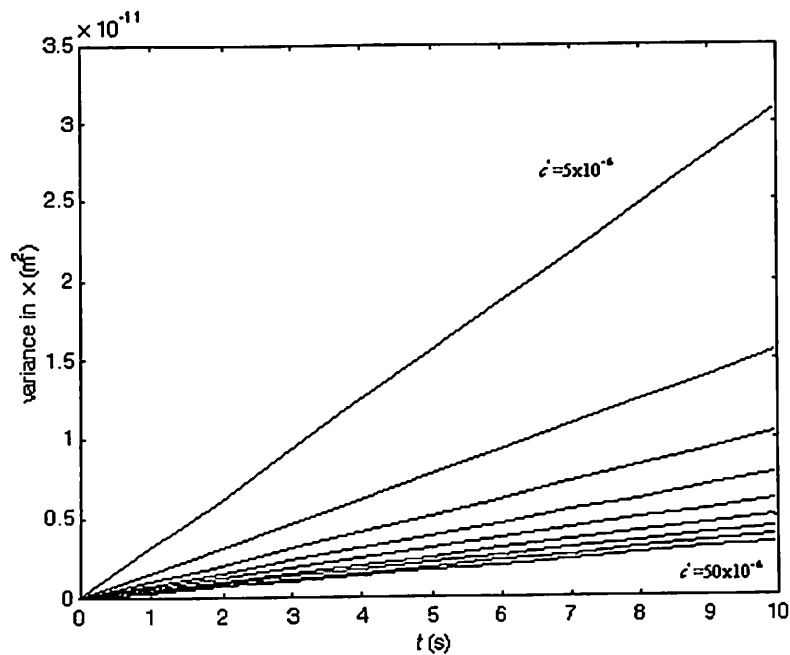
$8.33 \times 10^{-6} \geq c' \geq 8.51 \times 10^{-6}$  m, which gives the corresponding range of  $f'$  values as  $1.84 \times 10^{-8} \geq f' \geq 1.80 \times 10^{-8}$  N s/m.



(i) Model 8:  $5 \times 10^{-6} \leq c' \leq 50 \times 10^{-6}$  m in Steps of  $5 \times 10^{-6}$  m



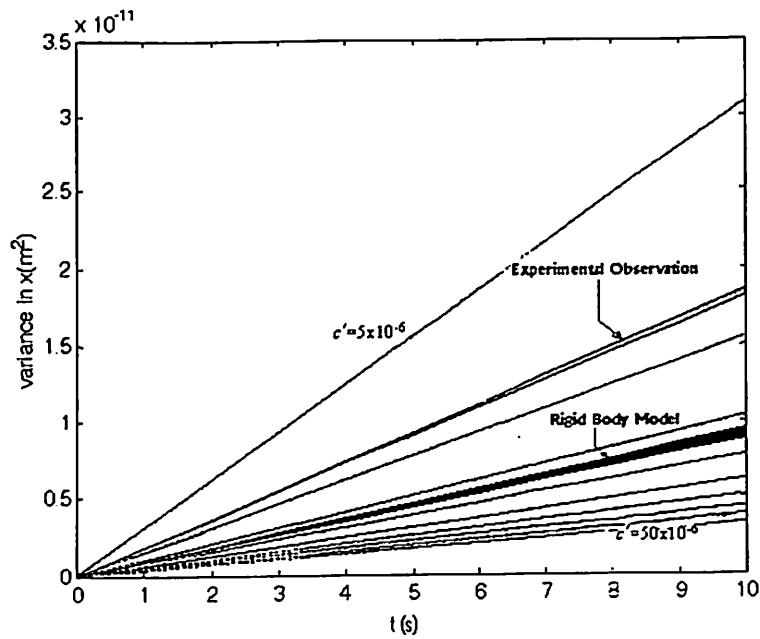
(ii) Model 9:  $5 \times 10^{-6} \leq c' \leq 50 \times 10^{-6}$  m in Steps of  $5 \times 10^{-6}$  m



(iii) Model 10:  $5 \times 10^{-6} \leq c' \leq 50 \times 10^{-6}$  m in Steps of  $5 \times 10^{-6}$  m

**Fig. 5.33** Variance in Position of Polystyrene Nanoparticle for Developed Models

In the above exercise of verification, it is observed that variance predicted by rigid body model never matches with published results. For silicon nanoparticle, rigid body model predicts variance lower than observed values and in case of polystyrene nanoparticle; the predictions from rigid body model are substantially larger than observed values. On the other hand, the simulated results from Brownian motion models considering non-rigidity of nanoparticle verify with published experimental results. Among the three valid models, Model 8 and Model 9 matched with published results for silicon only. The silicon nanoparticle is of 40 nm radius and lies at the lower domains of nano-regimes. The Model 8 and Model 9 are unable to predict the observed values for a wide simulated range of parameters. It is observed that Model 10 verifies with both the published results at the two extremities of nano-domains. Therefore, Model 10 is a better model with wider range of application in comparison to Model 8 and Model 9. The verification shows that inclusions of additional properties in rigid body model do not contradict the observed motion but affirm it more precisely.

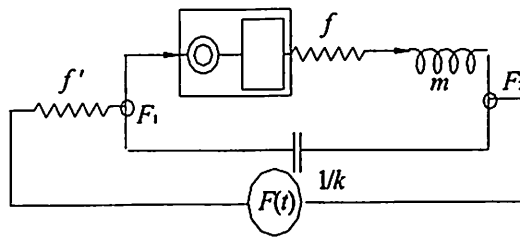


**Fig. 5.34** Comparison of Variance in Position of Polystyrene Nanoparticle for Experimental observation [Nakroshis 2003], Rigid Body Model and Model 10

## 5.10 COMPARISON OF SYSTEMS MODEL WITH IMPACT TRANSFER MODEL

In the last section, it is convincingly shown by simulation that the developed Brownian motion models of non-rigid nanoparticles match the experimental observations. It is also observed that Model 10 is valid for a wider range of sizes and at this stage is a better model. The development of Model 10 is done in the present chapter in order to explore the possibility of sub-systems in impact transfer Model 7 developed in Chapter 4. Whereas Model 7 was developed hypothesizing sub-systems of unmodeled features of the Brownian motion and fixed property interaction in the model, the Model 10 is developed removing both the limitations of Model 7.

In order to compare impact transfer Model 7 (Refer Fig. 4.11) with system Model 10 (refer Fig. 5.27(iii)), Model 7 is represented as a system model in Fig. 5.35 by adding the nodes with potentials  $F_1$  and  $F_2$  and a free noise generator with voltage  $F(t)$  in Fig. 4.11 as shown in Fig. 5.35.



**Fig. 5.35** Equivalent Electric Analog Circuit for Impact Transfer Model 7

Comparing electric analog circuit of Model 7 in Fig. 5.35 with that of Model 8, Model 9 and Model 10 in Fig. 5.27, it is observed that capacitance is in parallel with resistance  $f$  and inductance  $m$  in all four models. Another feature, which is consistent in all four models, Model 7 through Model 10, is that resistance  $f$  and inductance  $m$  are in series.

In Model 7, sub-system  $\text{⊗-□}$  was used as a feature to alter the nature of input to resistance  $f$  (Refer Fig. 5.35). The alternate input to resistance  $f$  keeping inductance  $m$  in series can also be obtained by changing the potential across the two nodes  $F_1$  and  $F_2$ , which has been achieved in Model 8, Model 9 and Model 10 by changing the interaction of resistance  $f'$  with other parameters. For example in Model 10, resistance  $f'$  is in series with capacitance and this interaction models Brownian motion in wider range in nano-domains. The work done in this chapter is summarized in next section.

## 5.11 EPILOGUE

In the present chapter, a search for possible Brownian motion model of non-rigid nanoparticle is carried out using systems modeling approach. In order to do the search, first, a four-parameter systems model is introduced for Brownian motion of non-rigid nanoparticle. In the next step, all possible interaction models of four-parameter are developed using a systematic procedure described in the form of an algorithm. It was found that there are 360 interactions possible. This is followed by identifying a few features of the Brownian motion and defining the identified features as selection criterion. In all three selection criterion are defined and all 360 possible models are subjected to testify the selection criterion. The possible models not satisfying the selection criterion are filtered out. It is found that only three models survive the systematic filtering, which is summarized in Table 5.2. The

variance models are formulated for the three surviving system models and are given in equations (5.35) to (5.37). The three systems models are shown in Fig. 5.27 and are called as Model 8, Model 9 and Model 10 for further investigation.

The three models are subjected to validity test against the criterion of positive and finite variance defined in Chapter 4. The selected three models are found to testify against the two validity criteria. The three models are further verified with published experimental results. The two published results are considered at the two extremes of size in nano-domains. The first belongs to Brownian motion of Silicon nanoparticle at the lower end of nano-domains and the second result belongs to polystyrene nanoparticle of size at the upper boundary of nano-domains. Among the three models, two models namely, Model 8 and Model 9 are found to verify with only one published result whereas Model 10 verifies with both observations. This suggests that Model 10 is a better model of Brownian motion of non-rigid nanoparticle. It is also observed that rigid body model do not match with observations and predicts lower variance in case of silicon nanoparticle and a higher variance in case of polystyrene nanoparticle in comparison to observed values. The rigid body model, therefore, does not model Brownian motion in nano-domains. A better choice, therefore, is Model 10 for predicting Brownian motion of nano-sized bodies. The verification of the Brownian motion models of non-rigid nanoparticle with published results is noteworthy, as the same results cannot be explained using a rigid body model. The verification justifies the idea mooted and explored in the present thesis.

It is further observed that three Models predict a linear variation of variance at  $t \gg 1/\beta$ . The linear variation in variance models normal diffusion mode of Brownian motion of nanoparticle. The modes like directed diffusion showing non-linear variation of variance are generic to many physical phenomenon. In order to model the directed diffusion mode, the three models are simulated for an altered input closely related to white noise input in next chapter.



One must have faith that the incomprehensible can be  
cleared up otherwise he will not ponder over it

*Johann Wolfgang Von Goethe*

## CHAPTER 6

# APPLICATION OF NON-RIGID NANOPARTICLE TO MODEL DIRECTED-DIFFUSION MODE

## 6.1 INTRODUCTION

In the previous chapter, the three non-rigid nanoparticle models have been developed and verified with published experimental results. The three models predict linear variation of variance at large times corresponding to normal diffusion mode. For the non-linear variation of variance at large times, directed diffusion models are used, which are developed using Diffusion equation approach. As a first application of the three Brownian motion models of non-rigid nanoparticle developed using Langevin approach in previous chapter, the three models for Brownian motion of non-rigid nanoparticle directed-diffusion are developed and simulated in this chapter. To model directed-diffusion mode, an alteration of input is proposed and explored in the present chapter. The altered input model is presented in next section.

## 6.2 INPUT MODELING

The input used in correlation technique is thermal noise  $n(t)$ . A typical type of fundamental time domain noise source is a Gaussian white noise with zero mean. The thermal noise is a special case of white noise with instantaneous correlation. Transient thermal impulse is proposed as input to develop models for directed diffusion mode having non-linear variance at large times. This is a variation of thermal impulse and is applied as input to models developed namely Model 8, Model 9 and Model 10. The behavior of the three models with transient thermal noise as input is studied.

The thermal impulse assumes an instantaneous correlation with no time dependence between the expected value of the impulse force at two instances. The two consecutive impacts in thermal impulse take place instantaneously with impact energy

transfer to nanoparticle in zero time in thermal impulse. The consideration of the two consecutive impacts in time continuum with no correlation models an idealized situation. A more realistic situation is a thermal impulse with an exponential model of correlation of input. This is the transient thermal noise, which models a non-instantaneous correlation exponential in nature. The exponent is assumed to depend on the elastic and dissipative properties of the matter.

The proposition of time dependent correlation counters the argument that there is no correlation between two consecutive events in time continuum. The autocorrelations for thermal impulse is given by equation (3.7) as

$$R_{nn}(t_1, t_2) = \alpha \delta(\tau) \quad (6.1)$$

For Transient Thermal Noise, the autocorrelation is modeled as

$$R_{nn}(t_1, t_2) = \begin{cases} \alpha(1 - e^{-2\xi t_2}) & \text{for } t_1 > t_2 \\ \alpha(1 - e^{-2\xi t_1}) & \text{for } t_1 < t_2 \end{cases} \quad (6.2)$$

where  $\xi$  is the parameter modeled as equal to  $\frac{k}{f'}$  taking into account the non-rigid parameters influencing the input.

The variance for rigid body model, Model 1, and three non-rigid nanoparticle models, Model 8, Model 9 and Model 10, have been obtained for thermal impulse as input and are given by equations (4.1), (5.35), (5.36) and (5.37). The variance expressions for the three non-rigid models for transient thermal noise input are formulated in next section.

### 6.3 VARIANCE FOR TRANSIENT THERMAL NOISE INPUT

Using Algorithm 1 for computing variance (Refer Chapter 3, Section 3.9), according to Step I, the autocorrelation of input is required and is modeled as given by equation (6.2). In the next step, the impulse response of the mathematical model of the Brownian motion is obtained. The mathematical model in the case of thermal impulse input is given by equation (3.15), which is obtained by the integration of Langevin equation (3.5) (Refer Chapter 3, Section 3.5). In order to obtain equation (3.15) from

equation (3.5), the velocity is considered stationary [Papoulis 1991]. In the present case, since the input is transient thermal noise, the velocity cannot be considered stationary. The non-stationary aspect of velocity can be accounted by considering mathematical model given by equation (3.5) directly instead of equation (3.15). The impulse response of the system given by equation (3.5) is given as [Nagrath 1993]

$$h(\tau) = \frac{(1 - e^{-\beta\tau})}{\beta} \quad (6.3)$$

According to Step III of the Algorithm 1, the cross correlation of position of nanoparticle  $x(t)$  and input  $n(t)$  is obtained as

$$R_{xn}(t_1, t_2) = \int_{-\infty}^{\infty} R_{nn}(t_1 - \tau, t_2) h(\tau) d\tau \quad (6.4)$$

Substituting  $R_{nn}(t_1, t_2)$  from equation (6.2) and replacing  $t_1$  with  $t_1 - \tau$  and inserting impulse response in equation (6.4), gives

$$R_{xn}(t_1, t_2) = \int_{-\infty}^{\infty} \alpha (1 - e^{-2\xi(t_1 - \tau)}) \left( \frac{1 - e^{-\beta\tau}}{\beta} \right) d\tau \quad (6.5)$$

Integration of equation (6.5), gives

$$R_{xn}(t_1, t_2) = \frac{\alpha}{\beta^2} \left\{ \beta t_1 - 1 + e^{-\beta t_1} - \frac{\beta}{2\xi} (1 - e^{-2\xi t_1}) + \left\{ \frac{\beta}{(2\xi - \beta)} \right\} \{ e^{-\beta t_1} - e^{-2\xi t_1} \} \right\} \quad (6.6)$$

The autocorrelation in position of the nanoparticle for transient thermal noise as with thermal impulse input is obtained considering Step IV of the Algorithm 1 as

$$R_{xx}(t_1, t_2) = \int_{-\infty}^{\infty} R_{xn}(t_1, t_2 - \tau) h(\tau) d\tau \quad (6.7)$$

Substituting  $R_{xn}(t_1, t_2)$  from equation (6.5), impulse response from equation (6.3) and replacing  $t_2$  with  $t_2 - \tau$  and inserting impulse response in equation (6.7) and gives

$$R_{xx}(t_1, t_2) = \frac{\alpha}{\beta^4} \left\{ \beta t_2 - 1 + e^{-\beta t_2} \right\} \left\{ \beta t_1 - 1 + e^{-\beta t_1} - \frac{\beta}{2\xi} (1 - e^{-2\xi t_1}) + \left\{ \frac{\beta}{(2\xi - \beta)} \right\} \{ e^{-\beta t_1} - e^{-2\xi t_1} \} \right\} \quad (6.8)$$

The variance in position  $E\{x^2(t)\}$  is obtained using Step V of the Algorithm 1 and equation (6.8) as

$$E\{x^2(t)\} = \frac{\alpha}{\beta^4} \left\{ \beta t - 1 + e^{-\beta t} \right\} \left\{ \beta t - 1 + e^{-\beta t} - \frac{\beta}{2\xi} (1 - e^{-2\xi t}) + \left\{ \frac{\beta}{(2\xi - \beta)} \right\} \left\{ e^{-\beta t} - e^{-2\xi t} \right\} \right\} \quad (6.9)$$

Substitution of  $f_{eq}$  from equations (5.32) to (5.34) in equation (5.31) gives three values of  $\alpha$  for the three non-rigid nanoparticle models, respectively, which along with the values of  $\beta$  from equations (5.27) to (5.29) and equation (6.8) are used to obtain variance expressions for the three models.

### 6.3.1 Variance from Model 8 with Transient Thermal Noise Input

The  $f_{eq}$  from equation (5.32) for Model 8 is given as

$$f_{eq} = \frac{(f + f') \left( \frac{k}{\omega} \right)^2}{(f + f')^2 + \left( \omega m - \frac{k}{\omega} \right)^2} \quad (6.10)$$

Equation (6.10) on substitution in equation (5.31) replacing  $f$  gives  $\alpha$  for Model 8 as

$$\alpha = \frac{2\kappa T}{m^2} \frac{(f + f') \left( \frac{k}{\omega} \right)^2}{(f + f')^2 + \left( \omega m - \frac{k}{\omega} \right)^2} \quad (6.11)$$

Substitution of  $\alpha$  from equation (6.11) and  $\beta$  from equation (5.27) in equation (6.9) gives the variance for Model 8 with transient thermal noise as input

$$E\{x^2(t)\} = \frac{2\kappa T m^2}{(f + f')^4} \left\{ \frac{(f + f') (k/\omega)^2}{(f + f')^2 + (\omega M - K/\omega)^2} \right\} \left\{ \frac{(f + f') t}{m} - 1 + e^{-(f + f') t/m} \right\} \left\{ \frac{(f + f') t}{m} - 1 + e^{-(f + f') t/m} - \frac{(f + f')}{2\xi m} (1 - e^{-2\xi t}) + \left\{ \frac{(f + f')}{(2\xi - (f + f')/m)m} \right\} \left\{ e^{-\beta t} - e^{-2\xi t} \right\} \right\} \quad (6.12)$$

### 6.3.2 Variance from Model 9 with Transient Thermal Noise Input

The  $f_{eq}$  from equation (5.33) for Model 9 is given as

$$f_{eq} = \frac{(mk + ff')mf'k - \left( mkff'^2 + \frac{k^2 ff'(f + f')}{\omega^2} \right)}{(mk + ff')^2 + \left( \omega mf' - \frac{k(f + f')}{\omega} \right)^2} \quad (6.13)$$

Equation (6.13) on substitution in equation (5.31) replacing  $f$  gives  $\alpha$  for Model 9 as

$$\alpha = \frac{2\kappa T}{m^2} \frac{(mk + ff')mf'k - \left( mkff'^2 + \frac{k^2 ff'(f + f')}{\omega^2} \right)}{(mk + ff')^2 + \left( \omega mf' - \frac{k(f + f')}{\omega} \right)^2} \quad (6.14)$$

Substitution of  $\alpha$  from equation (6.14) and  $\beta$  from equation (5.28) in equation (6.9) gives the variance for Model 9 with transient thermal noise as input

$$E\{x^2(t)\} = \frac{2\kappa T m^2}{f^4} \left\{ \frac{(mk + ff')(mf'k) - \left( mkff'^2 - kff'(f + f')/\omega^2 \right)}{(mk + ff')^2 + \left( \omega mf' - k(f + f')/\omega \right)^2} \right\} P^n Q^n \quad (6.15)$$

$$\text{where } P^n = \left( \frac{f t}{m} - 1 + e^{-f t/m} - \frac{f}{2\xi m} (1 - e^{-2\xi t}) + \left( \frac{f}{(2\xi - f/m)m} \right) (e^{-\beta t} - e^{-2\xi t}) \right)$$

$$\text{and } Q^n = \left( \frac{f t}{m} - 1 + e^{-f t/m} \right)$$

### 6.3.3 Variance from Model 10 with Transient Thermal Noise Input

The  $f_{eq}$  from equation (5.34) for Model 10 is given as

$$f_{eq} = \frac{(ff' + mk)(f + f') + \left( \omega mf' - \frac{fk}{\omega} \right) \left( \omega m - \frac{k}{\omega} \right)}{(f + f')^2 + \left( \omega m - \frac{k}{\omega} \right)^2} \quad (6.16)$$

Equation (6.16) on substitution in equation (5.31) replacing  $f$  gives  $\alpha$  for Model 10 as

$$\alpha = \frac{2\kappa T}{m^2} \frac{(ff' + mk)(f + f') + \left( \omega mf' - \frac{fk}{\omega} \right) \left( \omega m - \frac{k}{\omega} \right)}{(f + f')^2 + \left( \omega m - \frac{k}{\omega} \right)^2} \quad (6.17)$$

Substitution of  $\alpha$  from equation (6.17) and  $\beta$  from equation (5.29) in equation (6.9) gives the variance for Model 10 with transient thermal noise as input

$$E\{x^2(t)\} = \frac{2\kappa T m^2}{f^4} \left\{ \frac{(ff' + mk)(f + f') + (\omega mf' - fk/\omega)(\omega m - k/\omega)}{(f + f')^2 + (\omega m - k/\omega)^2} \right\} P^n Q^n \quad (6.18)$$

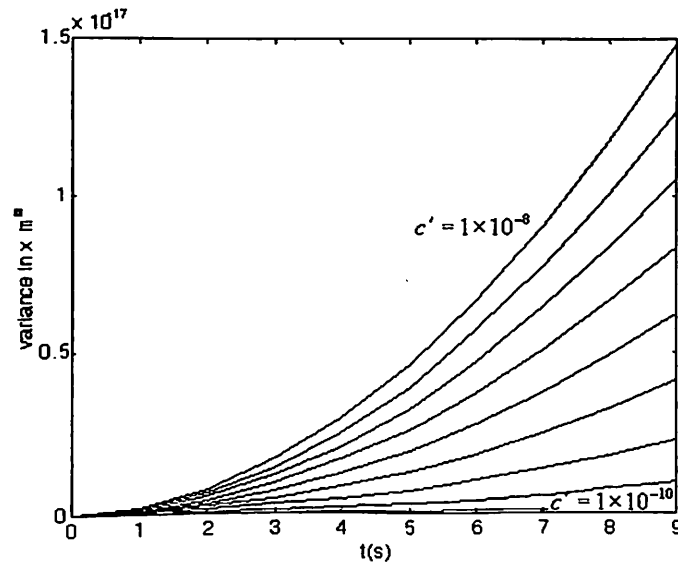
Equations (6.12), (6.15) and (6.18) are the variance expressions for transient thermal noise as input corresponding to three models, respectively. These variances  $t$  are simulated to explore the response in next section.

## 6.4 SIMULATION OF VARIANCE FOR TRANSIENT THERMAL NOISE INPUT

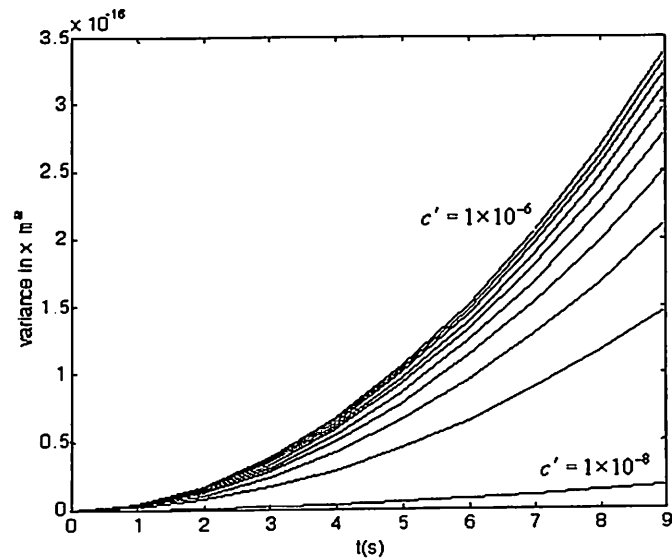
The simulation for three variance models developed in previous section is done for  $t \gg 1/\beta$  assuming the material of nano-particle as silicon with parameters given in Table 5.3 and 5.4. The value of  $k$  is assumed as 2.3 N/m,  $c'$  is varied from  $1 \times 10^{-10}$  – 100m. The frequency  $\omega$  is taken as 60 GHz, which is one-tenth of the frequency where quantum effects cannot be neglected. The simulation results of variance values are plotted on  $y$ -axis with time on  $x$ -axis.

### (a) Simulation of Variance from Model 8 for Transient Thermal Noise Input

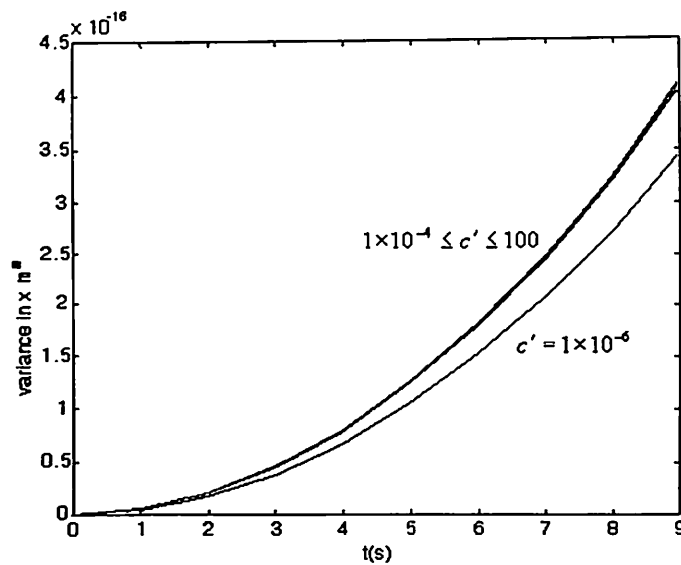
The variance in position of nanoparticle is obtained using equation (6.12) and is shown in Fig. 6.1. It is observed from simulation results that variance increases non-linearly with time. The non-linear variance has been referred as Non-Brownian motion by [Sasaki 2001] and models directed-diffusion mode of Brownian motion.



(i) Variance for the Range  $1 \times 10^{-10} \leq c' \leq 1 \times 10^{-8}$  m in Steps of  $1 \times 10^{-9}$  m



(ii) Variance for the Range  $1 \times 10^{-8} \leq c' \leq 1 \times 10^{-6}$  m in Steps of  $1 \times 10^{-7}$  m



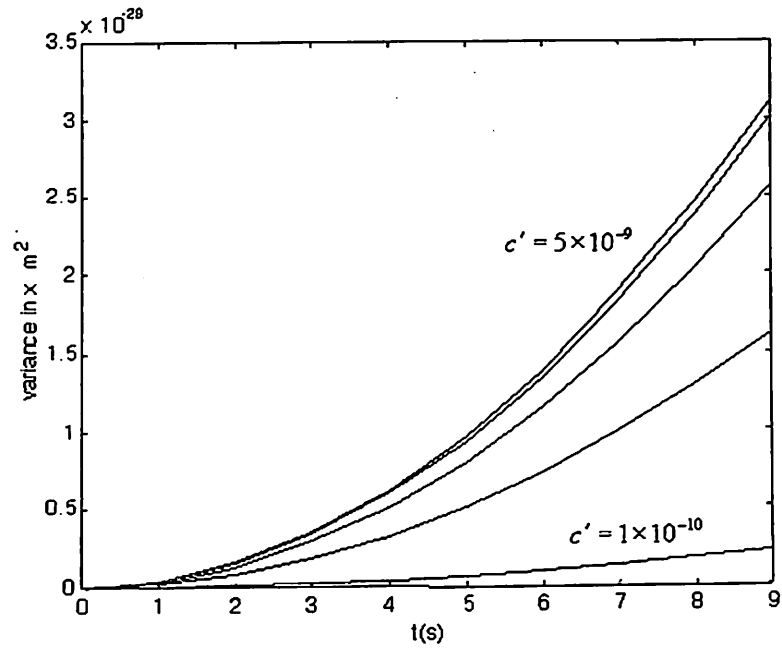
(iii) Variance for the Range  $1 \times 10^{-6} \leq c' \leq 1 \times 10^{-4}$  m in Steps of  $1 \times 10^{-4}$  m

**Fig. 6.1** Variance of Silicon Nanoparticle for Model 8 with Transient Thermal Noise Input

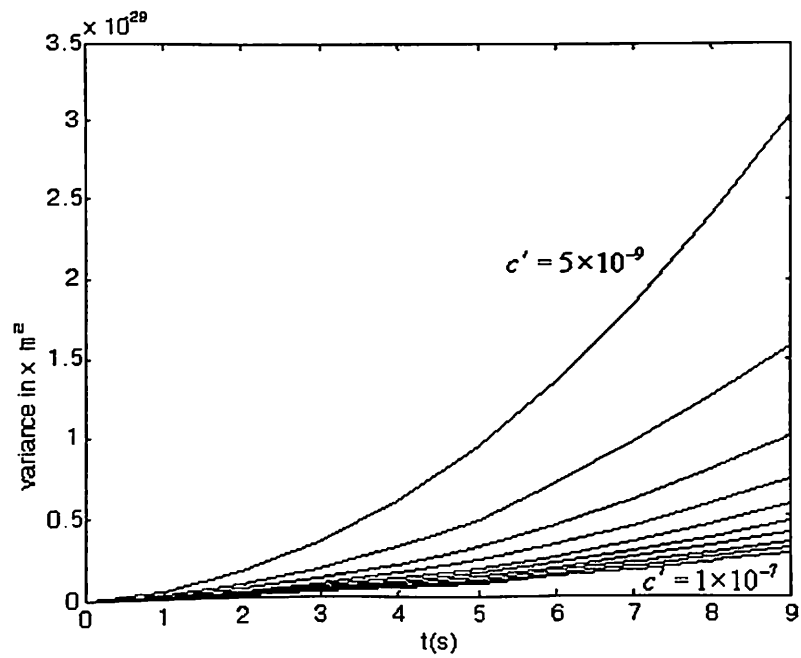
**(b) Simulation of variance from Model 9 for Transient Thermal Noise Input**

The variance in position of nanoparticle obtained using equation (6.15) is shown in Fig. 6.2. It is observed from simulation results that variance increases non-linearly

with time. The non-linear variation of variance models directed diffusion mode of Brownian motion.

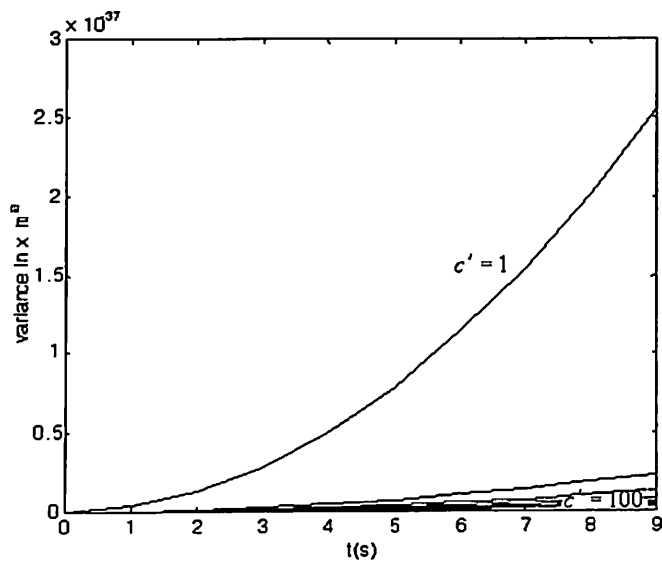


(i) Variance for the Range  $1 \times 10^{-10} \leq c' \leq 5 \times 10^{-9}$  m in steps of  $1 \times 10^{-9}$  m



(ii) Variance for the Range  $5 \times 10^{-9} \leq c' \leq 1 \times 10^{-7}$  m in steps of  $1 \times 10^{-8}$  m



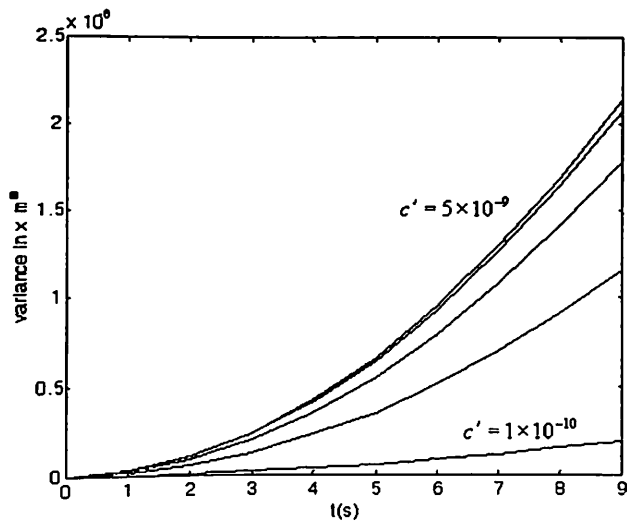


(iii) Variance for the Range  $1 \leq c' \leq 100$  m in steps of 10 m

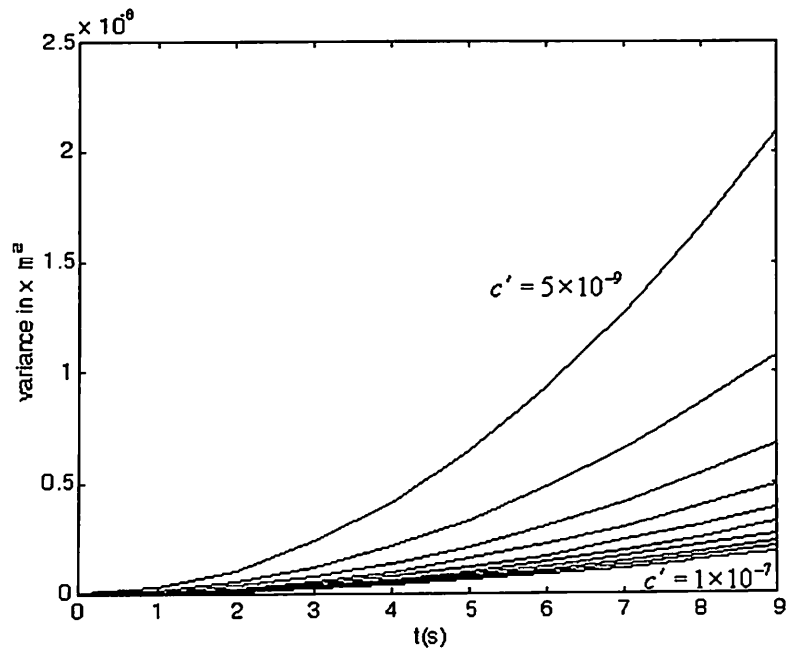
**Fig. 6.2** Variance of Silicon Nanoparticle for Model 9 with Transient Thermal Noise Input

**(c) Simulation of Variance from Model 10 for Transient Thermal Noise Input**

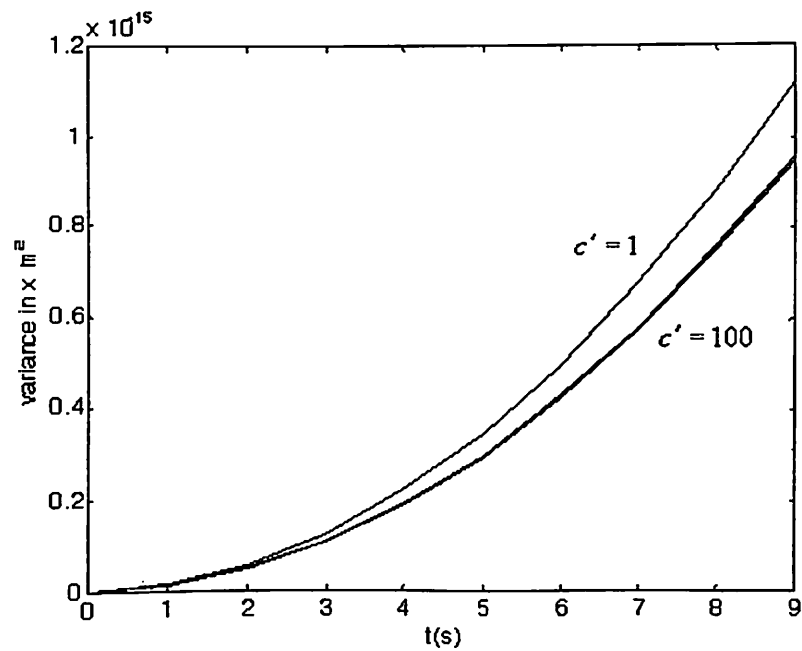
The variance in position of nanoparticle is obtained using equation (6.18) and is shown in Fig. 6.3. It is observed from simulation results that variance increase non-linearly with time. The non-linear variation of variance models directed diffusion mode of Brownian motion.



(i) Variance for the Range  $1 \times 10^{-10} \leq c' \leq 5 \times 10^{-9}$  m in steps of  $1 \times 10^{-9}$  m



(ii) Variance for the Range  $5 \times 10^{-9} \leq c' \leq 1 \times 10^{-7}$  m in steps of  $1 \times 10^{-8}$  m



(iii) Variance for the Range  $1 \leq c' \leq 100$  in steps of 10

**Fig. 6.3** Variance of Silicon Nanoparticle for Model 10 with Transient Thermal Noise

A comparison of the simulation results in Fig. 6.1 to Fig. 6.3 shows that Model 9 and Model 10 behaves in a similar manner in the range of parametric variations but the

magnitude of variance in case of Model 10 is substantially larger than that in case of Model 9. Model 8 shows a turn around behaviour in the parametric range of  $5 \times 10^{-9} \leq c' \leq 100$ . The magnitude of variance as predicted by Model 8 is larger than Model 9 but is substantially lower than Model 10. The important observation is that variance variation is non-linear with respect to time in all the three models with transient thermal noise input. This suggests that input with non-instantaneous correlation models directed diffusion mode of Brownian motion [Sharma 2003 (ii)]. The response of the four models with the two inputs is summarized in Table 6.1.

## 6.5 EPILOGUE

The present chapter starts with observation that the three Brownian motion models of non-rigid nanoparticle model the normal mode of diffusion characterized by linear variation of variance at large times. It is observed that input considered in the three models is having instantaneous autocorrelation, which is an idealizing assumption. In order to model another mode of diffusion namely, directed diffusion characterized by non-linear variation of variance at large times, an alteration of input is proposed. The altered model of input has non-instantaneous autocorrelation characterized by an exponential function in time. The exponential function also contains non-rigid nanoparticle parameters  $k$  and  $f'$ . The Chapter further contains the development of variance models using transient thermal noise input. The simulation of variance of the three models with transient thermal noise input predicts a non-linear variation of variance with time. The non-linear variation models the directed diffusion mode of Brownian motion. The consideration of transient thermal noise inputs with inclusion of non-rigid parameters therefore suggests an extended application of the present thesis to model different types of diffusion modes and can be further explored.

In another application, the three models are used to predict the Brownian motion of a single degree of freedom nanorobot. The nanorobotic manipulator will perform the Brownian motion, which needs to be analyzed for control and manipulation in nano-domains. The three verified models are considered along with the rigid body model to predict the Brownian motion of a single degree of freedom nanorobotic link in the next Chapter.

## CHAPTER 7

# **BROWNIAN MOTION APPLICATION FOR NANO-ROBOT DYNAMICS**

### 7.1 INTRODUCTION

The three non-rigid nanoparticle Brownian motion models, Model 8, Model 9 and Model 10 applied to predict the dynamics of a single degree of freedom nanorobotic manipulator in this Chapter. The Chapter starts with a brief introduction to micro and nanorobots and a classification of robotic manipulators followed by review on state of art in nanomanipulation. The model predicting dynamics of nanomanipulator is developed next and the developed models are used to predict the response of a single degree of freedom nanorobotic manipulator due to thermal agitation resulting in Brownian motion. The classification of robots based on size is given in next section.

### 7.2 ROBOTIC MANIPULATORS-OVING DOWN THE SIZE

Word “robot” comes from robota meaning forced labor or worker. A robot according to Robot Industries Association, USA is a reprogrammable, multifunctional manipulator designed to move material, parts, tools, or specialized devices through various programmed motions for the performance of a variety of tasks [Mittal 2003]. Nano-robots extend robot capabilities to the nanoscale. One or more of the features desired in a nano-robot are reprogrammable behavior, adaptability to environment and remote controllability. According to Fatikow [1997], the robots can be classified according to size as miniature, micro and nano-robots.

The size of a miniature robot is few cubic centimeters and it is fabricated by assembling conventional miniature components. The size of a microrobot is few hundred cubic micrometers and is fabricated using microfabrication technologies like bulk machining or surface micromachining. The nano-robots have the sizes of few

hundred cubic nanometers and the advancing nanotechnology is used for fabrication of nano-robots.

The small sized robots are also classified based on the size of different components of the robots. Based on the sizes of components, the robots are categorized in three categories. In first category, only the actuators for operation of the robot are miniaturized. For example, the nanoscale motion for gripping is given by a miniaturized piezoelectric component, whereas the positioning of the piezoelectric component is done using macro-actuators. In second category, the positioning actuators are also miniaturized. The third category has the miniaturization of power supply as well.

Another classification of small sized robots is based on the functionality like performing task in biotechnology area, microsurgery, and process industry or in microassembly. Small sized manipulators falling under either of these categories encounters difficulties such as handling of micro components as bulk material, damages during transportation, sensitivity to dust particles, humidity, temperature, and vibration.

The smallest among the various categories namely nanorobot is in research stage and is pursued by many researchers. Robots do the nanomanipulations at present with macro-sized mechanism attached to miniaturized actuator for manipulation. The state of art of nanomanipulation and status of research on nanorobots is presented in next section.

### 7.3 STATE OF ART IN NANOMANIPULATION

The possibility of nanorobots was first proposed by Richard Feynman in his talk "There's Plenty of Room at the Bottom," in 1959, who stated that machines could make smaller machines, and those smaller machines could make smaller machines up to a point where the machines would be in the molecular scale [Feynman 1992]. Feynman's nanorobots became a hot topic two decades ago when dramatic development in technology made the ideas of nanorobots feasible. Bining [Bining1985] invented Scanning Tunneling Microscopy (STM) as a new technique to study the surface structure with atomic scale resolution.

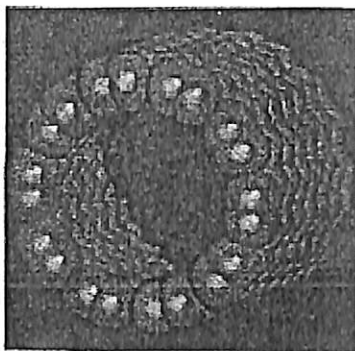
This invention was quickly followed by the development of a whole family of related techniques, which, together with STM, may be classified in the general category of Scanning Probe Microscopy (SPM) techniques. Of these later techniques, the most important is Atomic Force Microscopy (AFM) [Ferrari 2001]. All types of SPM instruments are based on the idea that if one rubs a finger along a surface, it is easy to distinguish velvet from steel or wood from tar. The different surfaces exert different forces on the finger, as one drags it on the different surfaces and finger acts as a force-sensor. This idea is implemented in scanning force microscopy where a probe also called as tip scans the surface. For example, in AFM, the force exerted on the probe tip is measured using optical feedback lever and electronics. SPM instruments have been used successfully to manipulate the individual molecule beads on the molecular abacus [Ratner 2003]. The AFM tip has been used as a robotic hand to precisely position nano objects and assemble them under computer control.

Scanning probe nanomanipulation are inherently very elegant but suffer from two limitations- these are expensive and are significantly slow. According to Ratner, although great advances have been made in building machines that use hundreds or even thousands of probe tips at the same time, but making nanostructures by manipulating atoms with SPM instruments is still very much like making automobiles by hand.

In order to overcome the difficulties with macro-sized nanomanipulators, Drexler [Drexler1992] proposed nanorobot as a molecular machine performing self-assembly and hypothesized bottom-up technique for microfabrication. Freitas [Freitas1998] discussed the communication methodology between nanorobots and macro-world. In another work, Freitas discussed the working of nanorobot in blood streams as a medical application [Freitas2000]. The potential use of biological nanomotors is pursued in contemporary research to be used in nanorobots. Lyshevski has discussed various key problems in modeling, analysis, simulation and controls of biological nanomotors [Lyshevski 2001]. Recent demonstration of working nanomotors that can be used as nanoactuators in nanomachines, has brought possibility of making nanorobots a step closer to its realization. Fennimore [Fennimore 2003] had reported

fabrication and successful operation of a fully synthetic nanometer scale electromechanical actuator.

Apart from nanoactuators, the nanorobot construction requires nanolinks and assembly techniques. Fukuda [Fukuda 2003] has demonstrated the technology for separating and assembling of Carbon Nanotubes (CNT). The CNTs are cylindrical graphene sheets of  $sp^2$ -bonded carbon atoms and were discovered by Richard Smalley in 1985. The CNT shape themselves into chemically stable tubes with one atom thick walls [Weber 1999]. These miniscule vessels are 100 times stronger than steel and can form hollow beam (Refer Fig. 7.1) that could potentially encapsulate power sources and drive mechanisms at molecular level making a link of nanorobot [Qian 2002].



**Fig. 7.1** Single Walled Carbon Nanotube (Reprint from [Qian 2002])

Requicha [Requicha 2003] in his survey on nanorobots has observed that the technology for realization of nanorobots and the related problems in utilization of nanorobots is advancing at very fast pace in last decade. Among other observations of Requicha, it has been pointed that the motion due to thermal agitation of the nano-robot is significant and will be a vital issue in the control of nano-robot. The motion due to thermal agitation is negligible if the nano-robot is operated at very low temperatures but this involves complex technology, high cost and is clearly impractical. For room temperature nanomanipulation using nano-robots, CNT acting as nano-links of a nano-robot will be affected by thermal agitation and will perform Brownian motion. The investigation of Brownian motion of nanolink is vital for understanding the dynamics of nano-robot and its control. The Brownian motion models developed in the previous

Chapter are used to predict the motion attributable to thermal agitation. This is done in the next section.

## 7.4 DYNAMIC MODELING OF BROWNIAN MOTION IN NANO-ROBOTS

The nano-link will be experiencing a continuous motion due to thermal impacts from surrounding medium. These are pronounced in nano-domains as discussed in earlier part of the thesis. The Brownian motion caused by thermal agitation may make the process of control of motion of nano-robot impossible. This difficulty does not arise in control of macro manipulators, as thermal agitation forces are negligible in comparison to inertial forces. It is imperative to study the motion due to thermal agitation for controlling the motion of nano-robot. As in case of nanoparticle, the nano-robot's dynamics is modeled using classical Newtonian equations and including the stochastic force of thermal agitation. This formulation is identical to Langevin model and, therefore, the models of Brownian motion obtained in previous chapters can be applied to predict the dynamics of nanorobot.

The non-rigid nanoparticle Brownian motion models developed are utilized to develop the dynamic model of a single degree of freedom (1-DOF) nano-robot. The classical model of the robot is presented first followed by formulation of Langevin model for 1-DOF nano-robot using the non-rigid nanoparticle Brownian motion models.

### 7.4.1 Classical dynamic Model of a 1-DOF Manipulator

The classical dynamic model has been developed in various texts on Robotics using either Newtonian or Lagrangian approach [Mittal 2004]. The lagrangian function is defined as

$$\Delta = KE - PE \quad (7.1)$$

where KE is kinetic energy of the manipulator and PE is potential energy of the system. The equation of motion according to Lagrange-Euler model is given as

$$\frac{d}{dt} \frac{\partial \Delta}{\partial \dot{q}_i} - \frac{\partial \Delta}{\partial q_i} = \tau_i \quad (7.2)$$



where  $q_i, \dot{q}_i$  and  $\tau_i$  are generalized position, velocity and force for  $i^{\text{th}}$  degree of freedom. Using equation (7.2), the scalar dynamic model of 1-DOF manipulator is obtained as

$$D\ddot{\theta} + V(\theta, \dot{\theta}) + G(\theta) + h = \tau \quad (7.3)$$

where  $D$  is manipulator inertia tensor;  $V(\theta, \dot{\theta})$  are terms related to Centrifugal and Coriolis forces; gravity force is  $G(\theta)$  and  $h$  denotes the friction term. The joint position is denoted by  $\theta$  and joint velocity is denoted by  $\dot{\theta}$ . The generalized force at the joint is  $\tau$ .

#### 7.4.2 Langevin Equation for 1-DOF Nano-Robot

The gravity force is negligible in nano-domains and is dropped from equation (7.3). The dynamic model of the 1-DOF manipulator is obtained from equation (7.3) and is given as [Mittal 2004]

$$\frac{m_{nl}l^2}{3}\ddot{\theta} + h = \tau \quad (7.4)$$

where  $m_{nl}$  is the mass and  $l$  is the length of nanolink, respectively. In order to explore the motion due to thermal agitation, the generalized force is modeled as stochastic torque  $\tau_i$  due to thermal agitation in equation (7.4). Considering the friction term as the resistive force from surrounding medium characterized by the friction coefficient  $6\pi l\eta$  to be acting at center of gravity of the nano-link, the resistive force due to medium is given by the Stokes law as  $6\pi l\eta\dot{x}_{cg}$ , where  $\dot{x}_{cg}$  is the velocity of the center of gravity of the link. Considering link to be uniform, the  $\dot{x}_{cg}$  is related to joint variable  $\dot{\theta}$  as  $\dot{x}_{cg} = \frac{l}{2}\dot{\theta}$  and, therefore, using the resistive torque is obtained as  $3\pi l^2\eta\dot{\theta}$ . Substituting the resistive torque in equation (7.4) gives

$$\frac{m_{nl}l^2}{3}\ddot{\theta} + 3\pi l^2\eta\dot{\theta} = \tau_i \quad (7.5)$$

In order to get the format similar to Langevin model, equation (7.5) on substitution of

$\ddot{\theta} = \frac{d^2\theta}{dt^2}$  and  $\dot{\theta} = \frac{d\theta}{dt}$  and rearrangement is written as

$$\frac{d^2\theta}{dt^2} + \frac{F'}{M} \frac{d\theta}{dt} = \frac{\tau_t}{M} \tau_t \quad (7.6)$$

where  $M = m_n l^2 / 3$  and  $F' = 3\pi l^2 \eta$ . Equation (7.6) is identical to Langevin equation (3.4) for a free nanoparticle given below for comparison with equation (7.6).

$$\frac{d^2x}{dt^2} + \frac{f}{m} \frac{dx}{dt} = \frac{F(t)}{m} \quad (7.7)$$

Comparing the two equations, velocity of equivalent nanoparticle  $\dot{\theta}$  is  $v$ , mass of equivalent nanoparticle  $M$  is  $m_n l^2 / 3$  and damping coefficient  $F'$  is  $3\pi l^2 \eta$ . Since equation (7.6) is analogous to equation (7.7), the variance in position obtained from equation (7.7) and given in equation (3.9) can be used to obtain the variance model for the equation (7.6) modeling 1-DOF nano-robot. The variance for the non-rigid nanoparticles given by equation (5.35) through (5.37) are used similarly to obtain non-rigid Brownian motion models of 1-DOF nano-robot in next section.

## 7.5 VARIANCE FOR 1-DOF NANO-ROBOT

The variance models for rigid nanoparticle (Model 1) and non-rigid nanoparticles (Model 8 through Model 10) has been obtained and given by equation (3.9), equations (5.35) through (5.37), respectively. Since the 1-DOF nano-robot model of Brownian motion is equivalent to the Langevin model of free nanoparticle as shown in previous section, the variance for 1-DOF is obtained by substituting analogous parameters of 1-DOF nano-robot model in respective variance models of rigid and non-rigid nanoparticle. The variance expressions are obtained in next section.

### 7.5.1 Rigid Body Model of Nano-Robot

The variance model for the rigid nanoparticle, which is Model 1 is given by equation (3.9). written for convenience as

$$E\{x^2(t)\} = \frac{\alpha}{2\beta^3} (2\beta t - 1 + e^{-\beta t}) (1 - e^{-\beta t}) \quad (7.8)$$

In order to get parameter analogous to  $\alpha$  in equation (7.8) denoted by  $\alpha''$ , the autocorrelation of generalized torque is required. The autocorrelation of thermal noise considering impulse force is  $\frac{2\kappa T f}{m^2}$  (Refer equation (3.6)). For the worst case, the effect of thermal impacts is modeled to act at the distal end of the link so that corresponding generalized torque is the distance  $l$  multiplied by the stochastic input  $n(t)$ . The autocorrelation of torque is obtained by multiplying the autocorrelation of force by  $l^2$  [Papoulis 1991] and is given as

$$R_{\tau,\tau} = \frac{2\kappa T f l^2}{m^2} \quad (7.9)$$

Substituting  $F'$  in place of  $f$  and  $M$  in place of  $m$  in equation (7.9) the parameter  $\alpha''$  is given as

$$\alpha'' = \frac{2\kappa T F' l^2}{M^2} \quad (7.10)$$

The parameter  $\beta$  in equation (7.8) is replaced by analogous parameter  $\beta'$  for 1-DOF nano-robot as

$$\beta' = F'/M \quad (7.11)$$

The variance in angular position of the 1-DOF nanorobot according to rigid body model, therefore, is given as

$$E\{\theta^2(t)\} = \frac{\alpha''}{2\beta'^3} (2\beta't - 1 + e^{-\beta't}) (1 - e^{-\beta't}) \quad (7.12)$$

Equation (7.12) gives the rigid body dynamic model of Brownian motion of 1-DOF nano-robot nanolink.

The three non-rigid models developed in Chapter 5 are used to model the dynamics of the 1-DOF nanorobot Brownian motion equivalent to non-rigid nanoparticle in the next sub-section.

### 7.5.2 Non-Rigid Model of Nano-Robot

The Brownian motion models of non-rigid nanoparticle developed in previous chapters suggests that in nano-domains, non-rigid models will predict the dynamics more

precisely. Accordingly, the three non-rigid nanoparticle models namely, Model 8, Model 9 and model 10 are used to model the dynamics of 1-DOF nano-robot. The variance in angular position of the 1-DOF is obtained for the three models next.

**(a) Variance in  $\theta$  from Model 8**

The variance of non-rigid nanoparticle from Model 8 is given by equation (5.35) written for clarity and convenience sake as

$$E\{x^2(t)\} = \frac{\kappa T m}{(f + f')^2} \left\{ 1 - e^{-\frac{(f+f')t}{m}} \right\} \left\{ \frac{\left(\frac{k}{\omega}\right)^2}{(f + f')^2 + \left(\omega m - \frac{k}{\omega}\right)^2} \right\} \left\{ \frac{2(f + f')t}{m} - 1 + e^{-\frac{(f+f')t}{m}} \right\} \quad (7.13)$$

The variance for 1-DOF nano-robot from equation (7.13) is obtained by replacing analogous parameters  $M$  and  $F'$  in place of  $m$  and  $f$  and multiplying by  $l^2$  to account for generalized torque autocorrelation as explained in previous section. The variance is given as

$$E\{\theta^2(t)\} = \frac{\kappa T M l^2}{(F' + f')^2} \left\{ 1 - e^{-\frac{(F'+f')t}{M}} \right\} \left\{ \frac{\left(\frac{k}{\omega}\right)^2}{(F' + f')^2 + \left(\omega M - \frac{k}{\omega}\right)^2} \right\} \left\{ \frac{2(F' + f')t}{M} - 1 + e^{-\frac{(F'+f')t}{M}} \right\} \quad (7.14)$$

**(b) Variance in  $\theta$  from Model 9**

The variance of non-rigid nanoparticle from Model 9 is given by equation (5.36) written for clarity and convenience sake as

$$E\{x^2(t)\} = \frac{\kappa T m}{f^3} \left\{ \frac{(mk + ff')m f' k - \left( mkf f'^2 + \frac{k^2 ff'(f + f')}{\omega^2} \right)}{(mk + ff')^2 + \left( \omega mf' - \frac{k(f + f')}{\omega} \right)^2} \right\} PQ \quad (7.15)$$

where  $P = \{1 - e^{-f t/m}\}$  and  $Q = \left\{ \frac{2ft}{m} - 1 + e^{-f t/m} \right\}$

The variance for 1-DOF nano-robot from equation (7.15) is obtained by replacing analogous parameters  $M$  and  $F'$  in place of  $m$  and  $f$  and multiplying by  $l^2$  to account for generalized torque autocorrelation as explained in previous section. The variance is given as

$$E\{\theta^2(t)\} = \frac{\kappa T M l^2}{F'^3} \left\{ \frac{(Mk + F'f')M f' k - \left( MkF' f'^2 - \frac{kF'f'(F' + f')}{\omega^2} \right)}{(Mk + F'f')^2 + \left( \omega Mf' - \frac{k(F' + f')}{\omega} \right)^2} \right\} \quad (7.16)$$

$$\left\{ 1 - e^{-\frac{F't}{M}} \right\} \left\{ \frac{2F't}{M} - 1 + e^{-\frac{F't}{M}} \right\}$$

### (c) Variance in $\theta$ from Model 10

The variance of non-rigid nanoparticle from Model 10 is given by equation (5.37) written for clarity and convenience sake as

$$E\{x^2(t)\} = \frac{\kappa T m}{f^3} \left\{ \frac{(ff' + mk)(f + f') + \left( \omega mf' - \frac{fk}{\omega} \right) \left( \omega m - \frac{k}{\omega} \right)}{(f + f')^2 + \left( \omega m - \frac{k}{\omega} \right)^2} \right\} PQ \quad (7.17)$$

The variance for 1-DOF nano-robot from equation (7.17) is obtained by replacing analogous parameters  $M$  and  $F'$  in place of  $m$  and  $f$  and multiplying by  $l^2$  to account for generalized torque autocorrelation as explained in previous section. The variance is given as

$$E\{x^2(t)\} = \frac{\kappa T m}{f^3} \left\{ \frac{(mk + ff')m f' k - \left( mkf f'^2 + \frac{k^2 ff'(f + f')}{\omega^2} \right)}{(mk + ff')^2 + \left( \omega mf' - \frac{k(f + f')}{\omega} \right)^2} \right\} PQ \quad (7.15)$$

where  $P = \{1 - e^{-f t/m}\}$  and  $Q = \left\{ \frac{2ft}{m} - 1 + e^{-f t/m} \right\}$

The variance for 1-DOF nano-robot from equation (7.15) is obtained by replacing analogous parameters  $M$  and  $F'$  in place of  $m$  and  $f$  and multiplying by  $l^2$  to account for generalized torque autocorrelation as explained in previous section. The variance is given as

$$E\{\theta^2(t)\} = \frac{\kappa T M l^2}{F'^3} \left\{ \frac{(Mk + F'f')M f' k - \left( MkF' f'^2 - \frac{kF'f'(F' + f')}{\omega^2} \right)}{(Mk + F'f')^2 + \left( \omega Mf' - \frac{k(F' + f')}{\omega} \right)^2} \right\} \quad (7.16)$$

$$\left\{ 1 - e^{-\frac{F't}{M}} \right\} \left\{ \frac{2F't}{M} - 1 + e^{-\frac{F't}{M}} \right\}$$

### (c) Variance in $\theta$ from Model 10

The variance of non-rigid nanoparticle from Model 10 is given by equation (5.37) written for clarity and convenience sake as

$$E\{x^2(t)\} = \frac{\kappa T m}{f^3} \left\{ \frac{(ff' + mk)(f + f') + \left( \omega mf' - \frac{fk}{\omega} \right) \left( \omega m - \frac{k}{\omega} \right)}{(f + f')^2 + \left( \omega m - \frac{k}{\omega} \right)^2} \right\} PQ \quad (7.17)$$

The variance for 1-DOF nano-robot from equation (7.17) is obtained by replacing analogous parameters  $M$  and  $F'$  in place of  $m$  and  $f$  and multiplying by  $l^2$  to account for generalized torque autocorrelation as explained in previous section. The variance is given as

$$E\{\theta^2(t)\} = \frac{\kappa T M l^2}{F'^3} \left\{ \frac{(F' f' + M k)(F' + f') + \left( \omega M f' - \frac{F' k}{\omega} \right) \left( \omega M - \frac{k}{\omega} \right)}{(F' + f')^2 + \left( \omega M - \frac{k}{\omega} \right)^2} \right\} \left\{ 1 - e^{-\frac{F' t}{M}} \right\} \left\{ \frac{2F' t}{M} - 1 + e^{-\frac{F' t}{M}} \right\} \quad (7.18)$$

The variance in angular position for three non-rigid nanoparticle models and rigid body model are simulated considering the material of nano-link as Carbon in next section.

## 7.6 SIMULATION OF BROWNIAN MOTION OF NANOROBOT

The rigid and non-rigid models of 1-DOF nano-robot developed in previous section are used to simulate the response of the nano-robot made of CNT. The various parameters related to CNT nanolink are taken from Wong [1997] and are

$$\text{Density } (\rho) = 1800 \text{ kg/m}^3$$

$$\text{Temperature of surrounding } (T) = 296.01 \text{ K}$$

$$\text{Length of nano-tube } (l) = 500 \text{ nm}$$

$$\text{Inner Diameter of nanotube } (d_i) = 35.3 \text{ nm}$$

$$\text{Outer Diameter of nanotube } (d_o) = 45.3 \text{ nm}$$

$$\text{Viscosity of surrounding medium water } (\eta) = 1.003 \times 10^{-3} \text{ Ns/m}^2$$

The non-rigid parameter  $k$  is assumed equal to 2.3 N/m as in simulation of Silicon nanoparticle (Refer Chapter 5, Section 5.8). The parameter  $c'$  is varied from  $1 \times 10^{-10}$  to 100 m in various step size in different range. These parameters give the values of mass  $m_{nl}$  of nano-link, mass of equivalent nanoparticle  $M$ , damping coefficient of medium  $f$  damping coefficient of equivalent medium  $F'$  and damping coefficient of equivalent nanoparticle  $f'$  as:

$$m_{nl} = \frac{\pi(d_o - d_i)^2 l \rho}{4} = 5.69 \times 10^{-19} \text{ kg}$$

$$M = \frac{m_{nl} l^2}{3} = 4.74 \times 10^{-32} \text{ kg m}^2$$

$$F' = \frac{3\pi d^2}{\eta} 2.36 \times 10^{-15} \text{ m}^3 / \text{N s}$$

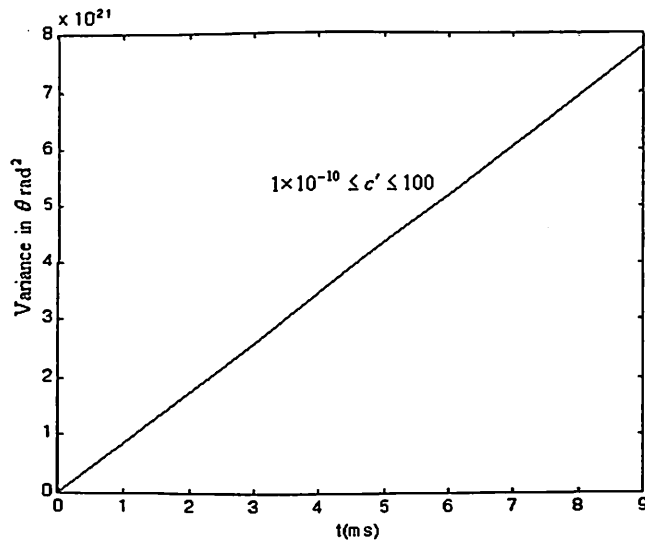
$$\varphi = \frac{4c'}{3l} 2 \times 10^{-4} - 2 \times 10^8$$

$$f' = \frac{Mk}{\varphi F'} 3.46 \times 10^{-13} - 3.46 \times 10^{-25}$$

The simulation of variance attributable to thermal agitation from the rigid body model is done next.

### 7.6.1 Simulation for Rigid Body Model

The variance obtained using equation (7.12) for above parameters is shown in Fig. 7.2. It is observed from Fig. 7.2 that rigid body model predicts positive and finite values of variance in angular position of the 1-DOF nano-robot. The rigid body model does not depend on the parametric variation and is invariant to  $c'$ .



**Fig. 7.2** Variance in Angular Position of 1-DOF Nano-robot using Rigid Body Model

The simulation of variance attributable to thermal agitation from the three non-rigid models is done next.

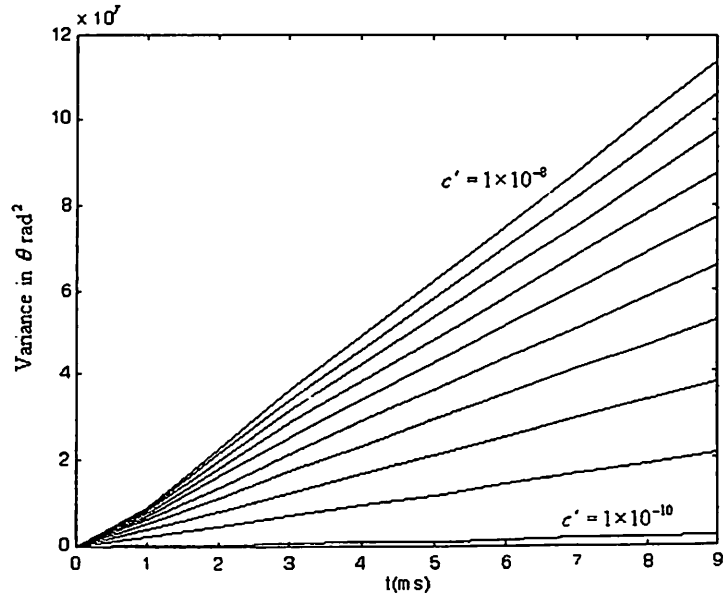
### 7.6.2 Simulation of Non-Rigid Model

For simulation of variance using three non-rigid models, the parametric values are given at the beginning of the section. The simulation results for the three models are given in the following section.

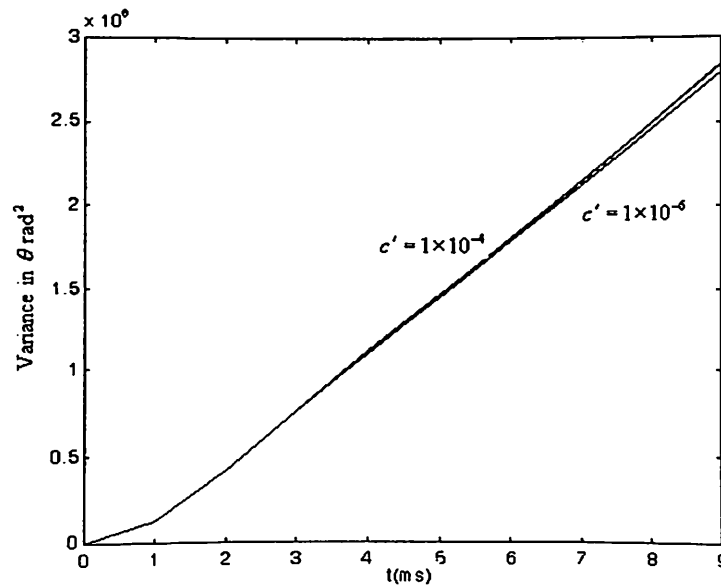


**(a) Variance using Model 8**

The variance obtained using equation (7.14) for is shown in Fig. 7.3. It is observed from Fig. 7.3 that variance increases with increasing  $c'$  upto a value of  $c' = 1 \times 10^{-4}$  m after which there is no significant change in variance for a change of  $c'$ .



(i) Variance for:  $1 \times 10^{-10} \leq c' \leq 1 \times 10^{-9}$  m in Steps of  $1 \times 10^{-9}$  m



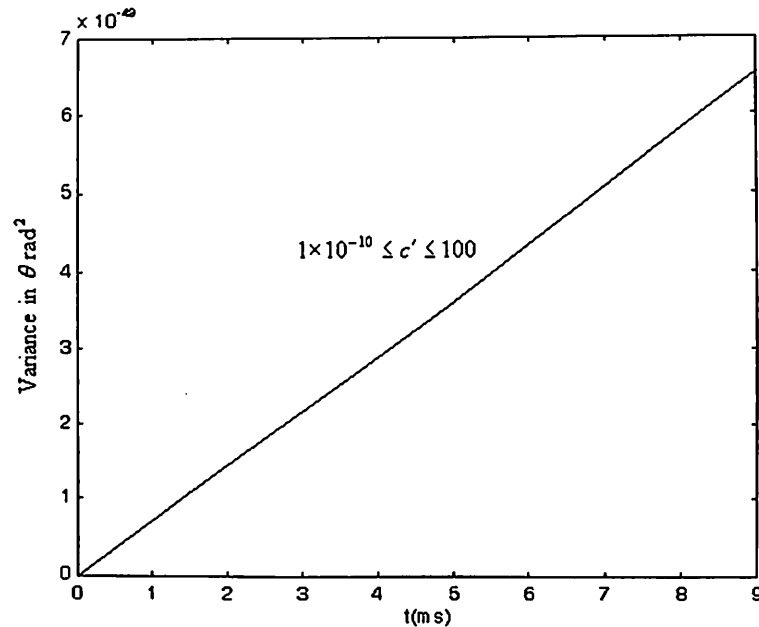
(ii) Variance for:  $1 \times 10^{-6} \leq c' \leq 1 \times 10^{-4}$  m in steps of  $1 \times 10^{-5}$  m

**Fig. 7.3** Variance in Angular Position of 1-DOF Nano-Robot v/s Time using Model 8

Moreover, comparing Fig. 7.2 and Fig. 7.3, it is observed that variance predicted by Model 8 is substantially greater than that predicted by the rigid body model.

**(b) Variance using Model 9**

The variance obtained using equation (7.15) is shown in Fig. 7.4. It is observed from simulation that variance is invariant to a change in  $c'$ . This is because there is no significant change in  $f_{eq}$  for any change of  $c'$ . Comparing Fig. 7.2 and Fig. 7.4, it is observed that variance predicted by Model 9 is substantially lower than that predicted by the rigid body model.



**Fig. 7.4** Variance in Angular Position of 1-DOF Nano-Robot v/s Time using Model 9

**(c) Variance using Model 10**

The variance obtained using equation (7.18) is shown in Fig. 7.5. It is observed from simulation that variance is invariant to a change in  $c'$ . This is because there is no significant change in  $f_{eq}$  for a change of  $c'$ . Thus, for the trend of invariant variance, Model 10 behaves similar to Model 9 but the absolute value of variance at different times predicted by Model 10 is substantially greater than Mode 9. Further comparing Fig. 7.2 and Fig. 7.5, it is observed that variance predicted by Model 10 is same as that predicted by the rigid body model.

From the results predicted by different models, it is observed that for the specified range of parametric values, the variance in angular position varies in the range of  $10^{-49} - 10^6 \text{ m}^2$ . Model 9 and Model 10 predicts that variance is insensitive to variation of  $c'$ . Model 8 shows some increase in variance for increase in  $c'$  upto a value of  $c' = 1 \times 10^{-4} \text{ m}$ . Moreover, the variation in variance from Model 8 is greater than other two Models. Model 9 predicts the least variance whereas Model 10 compares with rigid Body Model.

At this stage, it is noted that in order to verify the predictions from Model 8, Model 9 and Model 10, experimental observation are required.

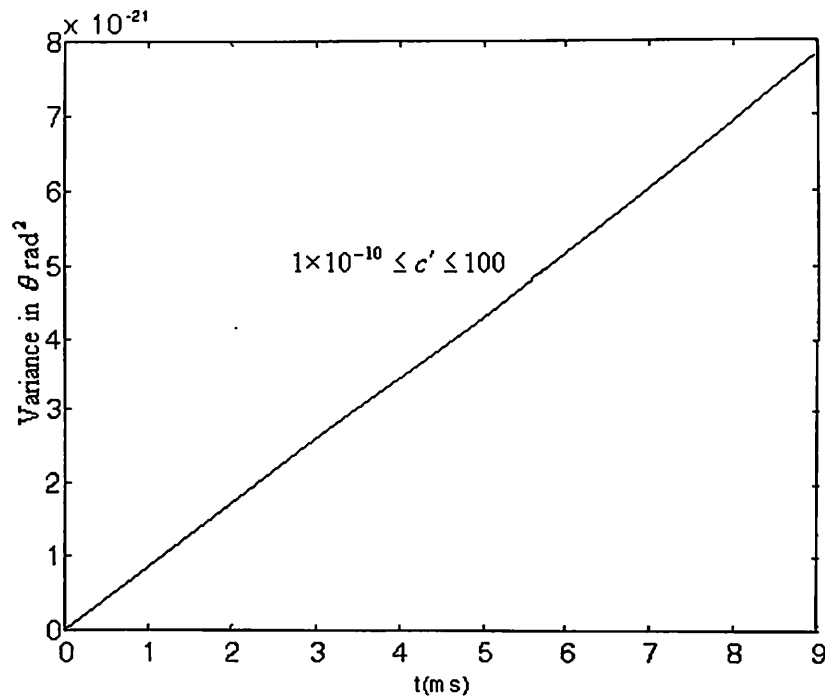


Fig. 7.5 Variance in Angular Position of Nanolink v/s Time using Model 10

## 7.7 EPILOGUE

In the present Chapter, an attempt is made to apply the developed models of Brownian motion of non-rigid nanoparticle to predict the Brownian motion of a single degree of freedom nanorobotic manipulator. The Brownian motion will be vital issue in controls of nanorobotic manipulator. In order to understand the nanomanipulation, a

review of state of art on nanomanipulation is presented. This is followed by the presentation of dynamic model of macro robotic manipulator using Lagrange-Euler model. The thermal agitation force are included in the macro model of robotic manipulator and an assumption of movement neglecting gravity led to the formulation of dynamic model of single degree of freedom nanomanipulator as equivalent to the model of a free floating nanoparticle. The work on Brownian motion in the present thesis therefore becomes relevant not only for free floating nanoparticles, which models autonomous nanorobotic manipulators working in a fluid like bloodstream, but also models individual links of nanorobotic manipulators as equivalent free floating nanoparticles. Correspondingly, the three verified non-rigid models with the two types of inputs discussed in previous chapters along with the rigid body model are used to predict the dynamics of nano-link attributable to the thermal agitation. It is found that Model 10 predicts the dynamic behavior of nanolink comparable to that predicted by rigid body model. The experiments should be carried out in order to verify the predictions from the three models developed in the present chapter. The next Chapter gives the conclusion and further work to the thesis.

Our language is wise; there is a difference between  
"I am convinced" and "I have been convinced".

*Karel Capek*

## CHAPTER 8

# CONCLUSIONS

### 8.1 INTRODUCTION

In the thesis, the problem of dynamics in nano-size regimes has been investigated. It was identified that when we go below the micro size and try to analyze or model the dynamic behavior of mechanical systems at the nanometer level, we must account for the motion due to thermal molecular agitation from the surrounding medium, which are quite pronounced in sub-micrometer domains.

Literature review pointed that in dynamics attributable to thermal agitation, non-rigidity will have significant influence on the dynamics in nano-domains. The literature was found to be devoid of any non-rigid Brownian motion model. The Brownian motion models for non-rigid nanoparticle have been developed in this thesis using impact transfer methodology and systems approach. The models were simulated for a wide range of parameters and valid models for non-rigid nanoparticle performing Brownian motion have been found. These models have been verified with published experimental results. The developed models of Brownian motion of non-rigid nanoparticle have been applied to the problems of directed-diffusion and also to predict the dynamics of a single degree of freedom nano-robot.

The work done is summarized and the investigation in the thesis led to some inferences, which are elaborated in the next section and the scope of further work at the end brings a finale to the present work with compelling conviction that every end is the commencement of a new beginning.

## 8.2 INFERENCES

For nanomachines embedded in a fluid, the thermal agitation due to the medium influences the machine's movement substantially. The nanomachine itself can be regarded as a free-floating nanoparticle in a fluid. The work in this dissertation involved development of different models for Brownian motion of non-rigid nanoparticle, their validation through simulations and verification with published experimental results.

### 8.2.1 Non-Rigidity of Nanoparticle Influences Brownian Motion

The entire available literature on Brownian motion was based on the assumption that the nanoparticle is rigid. The rigid body assumption implies that the motion of the particle is not influenced by the deformations of the nanoparticle caused by the applied impacts from the medium.

It was also noted that in nano-domains, the bodies have low value of spring constant  $k$  as observed by Wong [Wong 1997] and Roukes [Roukes 2000], while the rigid body has a value of  $k$  as infinity. This implied that rigid body assumption in nano-domains is incorrect and therefore the influence of local deformations on dynamics needs to be investigated. Another observation from literature review is Deng's [Deng 2003] suggestion of storing metabolic energy by nanoparticle, which supports the view of introducing non-rigidity in nano-domains because non-rigid elements only can store energy. It is concluded that for Brownian motion, therefore, additional properties like non-rigidity characterized by spring element and dissipation characterized by a damping element must be included to get a clear and precise picture of dynamics in nano-domains.

### 8.2.2 An Impact Transfer Model for Non-rigid Nanoparticle

To develop Brownian motion model of non-rigid nanoparticle, the impact transfer in Brownian motion was explored first and different possibilities of impact transfer were modeled. The non-rigid nanoparticle is characterized by its elastic and dissipative properties. The damping from the medium and from the non-rigid nanoparticle was considered as equivalent damping coefficient-representing resistance to global and local motion of non-rigid nanoparticle. Using the Ornstein-Uhlenbeck model of Brownian

motion of rigid nanoparticle as impact transfer model, the interaction of elastic and dissipative properties of nanoparticle ( $f'$  and  $k$ ) is introduced as a sub-system. The sub-system was included in the Ornstein-Uhlenbeck model in six possible ways. These six models were named as Model 2 through Model 7, with Model 1 used for the rigid body model. Extensive simulation of variance in position from six models carried out over a wide range of parametric values were subjected to two identified validity criterions of non-negativity and finiteness of variance. It was found that the five of the six impact transfer models did not satisfy the two criterions. The rejection of the five models led to following assertions

- Rejection of single integration models namely, Model 2 and Model 3 suggested the need of exploration of alternate possible model for elastic and dissipative properties.
- Failure of Model 4 with no integration implies that input and output represents two different physical quantities and, therefore, input has to be a higher order derivative of output, which is position of the nanoparticle.
- Rejection of double integration models, Model 5 and Model 6 implied that thermal noise could not result in jerks on the nanoparticle.

Model 7 was found to be valid and affirmed the proposition of introduction of additional elastic parameters of nanoparticle in rigid body Brownian motion model. These results for impact transfer in non-rigid nanoparticle have been published [Sharma 2004(i)].

### 8.2.3 Relation Between Rigid and Non-Rigid Parameters

It was seen in the six mathematical models of variances of impact transfer in non-rigid nanoparticle that denominator at contained a term  $(2\alpha' - \beta)$ . It means that if  $2\alpha'$  is equal to  $\beta$ , then denominator is zero and the variance will becomes infinite. Since, the infinite variance for a real physical process is not possible, it implies that  $2\alpha'$  should never be equal to  $\beta$ . Therefore, it was assumed that  $2\alpha' = \varphi\beta$ , where  $\varphi$  is a constant that cannot be unity. The assumption on substitution of  $\alpha'$  and  $\beta$  in parametric form results

into relation  $k = \phi f f' / 2m$ . This assumed relation was simulated for parametric values of two materials namely, silicon Carbide and Carbon, for which the published experimental results for non-rigid parameter  $k$  as a function of size are available. It was found that simulation results match with published experimental results. These results have been published [Sharma 2003(i)].

#### **8.2.4 Brownian Motion Model of Non-Rigid Nanoparticle using Systems Approach**

The Model 7, which was obtained by hypothesizing a particular interaction of properties of nanoparticle in impact transfer, has the major drawback that a physical explanation of the model cannot be found. Another limitation is that a fixed interaction of non-rigid properties has been assumed while there can be a number of other possible and contending interactions possible to model the impact transfer process. To overcome this, it was decided to adapt a systems-modeling approach to get a model for Brownian motion of non-rigid nanoparticle.

The non-rigid nanoparticle Brownian motion was represented as a four-parameter system model  $(m, f, f', k)$  and all possible models of interactions of these four parameters were found. An algorithm was developed to systematically develop all possible interactions. It was found that a total of three hundred and sixty possible interaction models are possible. The characteristic features for the Brownian motion were identified and were used as the three selection criterions for these models. The interaction possibilities that were unable to meet the three selection criterions were rejected. Only three models satisfied the selection criterions. The three selected Brownian motion models of the non-rigid nanoparticle were simulated for two different materials namely, Silicon and Polystyrene. The silicon and polystyrene nanoparticles were used as the sizes of these two nanoparticles in the published results were at the lower and upper boundaries of nano-domains.

The simulation results of the three models, named as Model 8, Model 9, and Model 10, were subjected to verification with published experimental results for these



two materials. It is found that results obtained from Model 10 confirmed with both the published results, while the results from Model 8 and Model 9 matched for Silicon nanoparticle and did not match the polystyrene nanoparticle. It may be possible to draw an inference at this stage that Model 10 is better than Model 8 and Model 9 as it is valid for a wider range in nano-domains whereas Models 8 and Model 9 have limitations and are valid in the lower end of nano-domains. This work has been accepted for publication [Sharma 2004(ii)].

### **8.2.5 Application to Model Directed Diffusion Mode of Brownian Motion**

It was observed that variation of variance for the three models, Model 8, Model 9 and Model 10, is linear for large times indicating their applicability to normal diffusion mode of Brownian motion of nanoparticle. As an extended application of the models, the three non-rigid models were applied to model the directed-diffusion mode of Brownian motion of nanoparticle. The directed-diffusion mode is characterized by a non-linear variation of variance. In order to model the directed-diffusion mode using the three models, an input was modeled as transient thermal noise instead of white noise. The transient thermal noise autocorrelation model considered non-rigid parameters apart from rigid nanoparticle parameters.

The three-variance models were developed using system model, Model 8, Model 9 and Model 10, for the transient thermal noise and were simulated over wide parametric range. It was found that all three models show non-linear variation of variance even at large times for the transient thermal noise input. Since in case of the rigid nanoparticle, the transient thermal noise with non-rigid parameters cannot be considered, the Model 1 can be applied for normal diffusion mode only. It was, therefore, noted that non-rigid nanoparticle Brownian motion model can be used to model Directed diffusion mode and all three models predicts identically on the aspect. This work has been published [Sharma 2003(ii)]

### **8.2.6 Prediction of Dynamics a 1-DOF Nano-Robot**

The three Brownian motion models of non-rigid nanoparticle have been applied to predict the dynamics of a 1-DOF nano-robot, attributable to thermal agitation from

surrounding medium. The Brownian motion models for the one-degree of freedom nano-robot have been developed using the three developed models for Brownian motion of non-rigid nanoparticle and Lagrange-Euler approach. The three dynamic models for the single degree of freedom nano-robot were simulated over a wide range of parameters for Carbon nanotubes to obtain the variance. The variance obtained from the three models was compared with the variance obtained using the rigid body model as benchmark. It has been found that Model 8 and Model 9 predict variance in angular position of nano-robot away from the rigid body model while the predictions of variance in angular position of the nanrobot from Model 10 were identical to the rigid body model predictions. In the absence of any published theoretical or experimental observations for motion of nano-robots, no conclusions can be drawn.

### 8.3 FUTURE PERSPECTIVES

The thesis explored the dynamics of non-rigid nanoparticles and developed some models for Brownian motion of non-rigid nanoparticle and applied these models to directed diffusion and nano-robots. It was not possible to consider and include all aspects of the problem as well as the findings of this thesis, which have opened up several new horizons in the understanding of nanotechnology. These need to be explored further and could be independent thesis topics. Some of the possible areas where explorations are required are elaborated below.

The dynamic response to thermal agitation has been investigated in present thesis. The dynamics in nano-domains for the contribution from other forces viz. Vander-Waal's forces, Electrostatic forces and Adhesive forces, which become significant in nano-domains needs to be explored. The investigation of each of these forces is a comprehensive exercise and will help in understanding and applying nanotechnology.

In the present work, it was assumed that the damping coefficient is characterized by the Stokes law and the elasticity of surrounding medium was not considered because the point of investigation was nanoparticle and not the medium. The surrounding medium

may not be always viscous and other types of medium including elasticity of medium can be further explored.

In the present work, a lumped-parameter model of non-rigid nanoparticle has been assumed. The models of non-rigid nanoparticle Brownian motion need to be extended to distributed parameters. The Brownian motion models of distributed parameter non-rigid nanoparticles may be able to give better results. The distributed parameter analysis is involved and complex and is a complete investigation in itself.

For simulation of variance, variation of non-rigid parameters  $c'$  was carried over a large range while  $k$  was assumed constant. The work can be further extended for investigating the effect of variation of other non-rigid parameters like  $\omega$  and  $k$  on variance values. This will be a complementary work to the present thesis.

The two additional parameters representing non-rigid behavior of nanoparticle introduced in the present thesis were shown to be related and the relation was verified by simulation. An experimental confirmation of the relation between the parameters  $(m, f, f', k)$  would be step forward in understanding dynamics of nanoparticle. This would require adequate facility and an experimental setup for observation of variance in position of a nanoparticle. Once the experimental setup is available, variations like effect of variation in size, material etc. of nanoparticle on variance can be explored. For example, using the observed variance of two nanoparticles of same size and same material, an inverse problem can be formulated to obtain the parameters from the non-rigid models.

In case of dynamic modeling of nano-robot, the exploration can be further pursued with a multi-degree of freedom nano-robot. The exploration of multi-degree of freedom nanorobotic manipulator will introduce non-linear coupled terms in the mathematical model of variance. The extraction of extra joints torques attributable to these additional terms will be an involved and comprehensive exercise in solving non-linear stochastic models.

The application of Brownian motion models to nano-robots can be also investigated from the control point of view. The positioning inaccuracies that can result due to Brownian motion of nano-robot need special control measures. From the models developed, the variance in position is available. To control such nano-robots, a stochastic or neuro-fuzzy control scheme can be developed and used.

To summarize, it has been convincingly established using the modeling and simulation tools that the non-rigidity of a nanoparticle is relevant both in terms of explaining a few hitherto unresolved issues in nano-domain and from future application point of view of nanotechnology. The new vistas opened up will lead to betterment of human life using the nanoscience and nanotechnology.

## CORRELATION TECHNIQUE AND ITS APPLICATION TO RIGID NANOPARTICLE

This appendix contains correlation techniques details, which has been used in the thesis as the prime tool to develop variance models of Brownian motion considering non-rigidity of nanoparticles. The six impact transfer models in Chapter 3 and Chapter 4 and the three systems model in Chapter 5 have been expressed in terms of variances. The variance for all models are obtained using time domain analysis called as correlation technique and is detailed next section. The technique is further applied to obtain variance for a rigid nanoparticle.

### I.1 CORRELATION TECHNIQUE

In order to analyze a linear system with real impulse response function  $h(\tau)$ , a real process  $y(t)$  as input and  $x(t)$  as real output, the functional relation between  $y(t)$ ,  $h(\tau)$  and  $x(t)$  is given by convolution integral as [Papoulis 1991]

$$x(t) = \int_{-\infty}^{\infty} y(t - \tau)h(\tau)d\tau \quad (I.1)$$

The input-output relation can be considered as signal processing by the system. A signal whose value cannot be predicted precisely but is known in terms of probabilistic description, such as mean value, mean squared value and so on, is a random signal. Stochastic signal is a dynamic random signal. In case of stochastic signals we use autocorrelation as a measure of input and output signals [Lathi 2000]. Autocorrelations are nothing but the expected value of a physical variable at two different times. Taking expected values on both sides of equation (I.1), the convolution integral for stochastic signals, gives

$$E\{x(t)\} = \int_{-\infty}^{\infty} E\{y(t - \tau)\}h(\tau)d\tau \quad (I.2)$$

where  $E\{x(t)\}$  is the response of the system to stochastic input and is known as expected value of the output  $x(t)$ . The convolution integral in equation (I.2) is conventionally represented as

$$E\{x(t)\} = E\{y(t)\} * h(t) \quad (I.3)$$

The relation between the expected values of input and output can be represented by a block diagram as shown in Figure I.1.

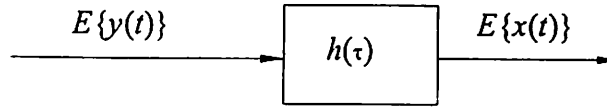


Fig. I.1 Expected Value of Response  $E\{x(t)\}$  for a System with Impulse Response  $h(\tau)$  and Input with expected value  $E\{y(t)\}$

For deterministic signals, the product of output and input signals at time instances  $t_1$  and  $t_2$  ( $t_1 > t_2$ ) respectively is given by the convolution integral of input with impulse response as

$$x(t_1)y(t_2) = \int_{-\infty}^{\infty} y(t_1 - \tau)y(t_2)h(\tau)d\tau \quad (I.4)$$

where  $y(t_1 - \tau)$  is the value of input at time  $t_1 - \tau$  and  $y(t_2)$  is the value of input at time  $t_2$ . For stochastic signals, taking expected values on both sides in equation (I.4) gives

$$E\{x(t_1)y(t_2)\} = \int_{-\infty}^{\infty} E\{y(t_1 - \tau)y(t_2)\}h(\tau)d\tau \quad (I.5)$$

or

$$R_{xy}(t_1, t_2) = \int_{-\infty}^{\infty} R_{yy}(t_1 - \tau, t_2)h(\tau)d\tau \quad (I.6)$$

where  $R_{xy}(t_1, t_2)$  is the cross-correlation between  $x$  and  $y$  and  $R_{yy}(t_1 - \tau, t_2)$  is the autocorrelation of input. Using the convolution integral notation, the equation (I.6) is written as

$$R_{xy}(t_1, t_2) = R_{yy}(t_1 - \tau, t_2) * h(t_1) \quad (I.7)$$

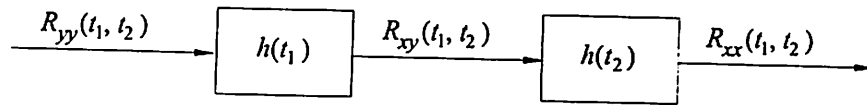
From the cross correlation  $R_{xy}(t_1, t_2)$ , the autocorrelation  $R_{xx}(t_1, t_2)$  of output  $x(t)$  using convolution integral can be obtained as

$$R_{xx}(t_1, t_2) = \int_{-\infty}^{\infty} R_{yy}(t_1, t_2 - \tau) h(\tau) d\tau \quad (I.8)$$

or

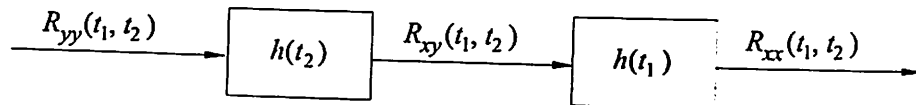
$$R_{xx}(t_1, t_2) = R_{yy}(t_1, t_2 - \tau) * h(t_2) \quad (I.9)$$

Equation (I.7) and (I.9) are combined to obtain autocorrelation of output  $R_{xx}(t_1, t_2)$  and the overall block diagram is shown in Figure I.2.



**Fig. I.2** Autocorrelation of Response  $R_{xx}(t_1, t_2)$  of System with Impulse Response  $h(\tau)$  and Input with autocorrelation  $R_{yy}(t_1, t_2)$  for  $(t_1 > t_2)$

It has been shown that precedence of  $t_1$  or  $t_2$  does not affect the final result and a similar response is obtained for  $(t_1 < t_2)$ , which is diagrammatically shown in Figure I.3 [Papoulis 1991].



**Fig. I.3** Autocorrelation of Response  $R_{xx}(t_1, t_2)$  of System with Impulse Response  $h(\tau)$  and Input with autocorrelation  $R_{yy}(t_1, t_2)$  for  $(t_1 < t_2)$

The variance of the output of the model  $E\{x^2(t)\}$  is obtained using equation (I.9) by substituting  $t_1 = t_2 = t$  as

$$E\{x^2(t)\} = R_{xx}(t, t) \quad (I.10)$$

The correlation technique is applied to a free particle in order to get the variance of output for given autocorrelation of input and known impulse response of the system in next section.

## I.2 MOTION OF FREE PARTICLE

The basic model of variance of small sized particle given by Einstein for Brownian motion of a free particle is derived using correlation technique. In order to

obtain the variance in position of the small sized particle, the stochastic differential equation defining the dynamics of small sized particle, also called as Langevin equation, is considered. The Langevin equation for no external force is given as

$$\frac{dv}{dt} + \beta v = n(t) \quad (\text{I.11})$$

where  $v$  is the velocity of small sized particle,  $\beta$  is system parameter and is defined as the ratio of damping coefficient  $f$  from surrounding medium and mass  $m$  of the small sized particle ( $\beta = f/m$ ) and  $n(t)$  is white noise input. The substitution of velocity  $v = dx/dt$  in equation (I.11) gives

$$\frac{d^2x}{dt^2} + \beta \frac{dx}{dt} = n(t) \quad (\text{I.12})$$

Integrating equation (I.12) gives

$$\frac{dx}{dt} - \frac{dx_0}{dt} + \beta(x - x_0) = \int n(t) dt \quad (\text{I.13})$$

where  $x_0$  is the position of particle at  $t = 0$ ,  $dx_0/dt$  is velocity of nanoparticle at  $t = 0$ . Assuming conditions at  $t = 0$  as  $v_0 = dx_0/dt$  and  $x_0 = 0$ , equation (I.13) gives

$$\frac{dx}{dt} + \beta x = w(t) + v_0 \quad (\text{I.14})$$

where  $w(t)$  is the integrated white noise  $\int n(t) dt$ . In order to obtain the autocorrelation of input  $w(t) + v_0$  in equation (I.13), the autocorrelation of  $v_0$  is obtained first. The autocorrelation of  $v_0$  denoted as  $R_{vv}(t = 0)$  is inverse Fourier transform of the spectrum of  $v_0$  and is given as [Papoulis 1991]

$$R_{vv}(t = 0) = \frac{1}{2\pi} \int_{-\infty}^{\infty} S_{vv}(\omega) e^{j\omega t} d\omega \quad (\text{I.15})$$

where  $S_{vv}(\omega)$  is the spectrum of  $v_0$  and is obtained by dividing spectrum of  $n(t)$  by transfer function of the Langevin equation (I.11) as

$$S_{vv}(\omega) = \frac{S_n(\omega)}{|j\omega + \beta|^2} = \frac{\alpha}{\omega^2 + \beta^2} \quad (\text{I.16})$$



where the spectrum  $S_n = 2\kappa Tf/m^2 = \alpha$ ;  $\kappa$  is Boltzman constant,  $T$  is absolute temperature of system,  $f$  is damping coefficient of surrounding medium and  $m$  is the mass of small sized particle. Substituting  $S_w(\omega)$  from equation (I.16) in equation (I.15) and integrating gives

$$R_{vv}(t=0) = \frac{\alpha}{2\beta} \quad (I.17)$$

or

$$E\{v_0^2\} = \frac{\alpha}{2\beta} \quad (I.18)$$

where  $E\{v_0^2\} = R_{vv}(t=0)$  is the variance of  $v_0$ . Furthermore, the random variable  $v_0$  is independent of the process  $w(t)$  for  $t > 0$ . Considering  $y(t) = w + v_0$  in equation (I.14), the autocorrelation of  $y(t)$  denoted as  $R_{yy}(t_1, t_2)$  is obtained as

$$R_{yy}(t_1, t_2) = E\{y(t_1)y(t_2)\} = E\{w(t_1)w(t_2)\} + E\{v_0^2\} \quad (I.19)$$

where  $E\{w(t_1)w(t_2)\}$  is the autocorrelation of  $w(t)$  and is obtained by integrating autocorrelation of  $n(t)$  as  $w(t)$  is integration of  $n(t)$ . The autocorrelation of  $n(t)$  is given as

$$R_{nn}(t_1, t_2) = \alpha \delta(\tau) \quad (I.20)$$

The autocorrelation of  $w(t)$  denoted by  $R_{ww}(t_1, t_2)$  is obtained by integrating equation (I.20) as

$$R_{ww}(t_1, t_2) = \begin{cases} \alpha t_2; & t_1 > t_2 \\ \alpha t_1; & t_1 < t_2 \end{cases} \quad (I.21)$$

Substituting values from equation (I.18) and equation (I.21) in equation (I.19) gives the autocorrelation of  $y(t)$  as

$$R_{yy}(t_1, t_2) = \begin{cases} \alpha t_2 + \frac{\alpha}{2\beta}; & t_1 > t_2 \\ \alpha t_1 + \frac{\alpha}{2\beta}; & t_1 < t_2 \end{cases} \quad (I.22)$$

Using the correlation technique described in Section I.1, the cross correlation between input and output of system defined by equation (I.14) is obtained using convolution integral given by equation (I.6). Substituting for  $R_{yy}(t_1, t_2)$  from equation

(I.22) for  $t_1 < t_2$  and the impulse response  $h(\tau)$  from equation (I.14) as  $e^{-\beta\tau}$  in equation (I.6), the cross correlation  $x(t)$  and  $y(t)$  is obtained as

$$R_{xy}(t_1, t_2) = \iint_{-\infty}^{\infty} \left( \alpha(t_1 - \tau) + \frac{\alpha}{2\beta} \right) e^{-\beta\tau} d\tau \quad (\text{I.23})$$

For finite time and since the Brownian motion system under consideration is casual, the limits of integration get changed to 0 to  $t_1$ . Equation (I.23) on integration with changed limits gives

$$R_{xy}(t_1, t_2) = \frac{\alpha}{2\beta^2} (2\beta t_1 - 1 + e^{-\beta t_1}) \quad (\text{I.24})$$

The autocorrelation of output  $x(t)$  for  $t_1 < t_2$  is obtained using equation (I.8), (I.24) and impulse response  $e^{-\beta\tau}$  as

$$R_{xx}(t_1, t_2) = \frac{\alpha}{2\beta^2} (2\beta t_1 - 1 + e^{-\beta t_1}) \int_{-\infty}^{\infty} e^{-\beta\tau} d\tau \quad (\text{I.25})$$

Integrating for finite time and casual system, the integration limits get changed to 0 to  $t_2$ . Equation (I.24) on integration with changed limits gives

$$R_{xx}(t_1, t_2) = \frac{\alpha}{2\beta^3} (2\beta t_1 - 1 + e^{-\beta t_1}) (1 - e^{-\beta t_2}) \quad (\text{I.26})$$

So variance of  $x(t)$  is obtained using equation (I.10) by substituting  $t_1 = t_2 = t$  in equation (I.26) as

$$E\{x^2(t)\} = \frac{\alpha}{2\beta^3} \left\{ (2\beta t - 1 + e^{-\beta t}) (1 - e^{-\beta t}) \right\} \quad (\text{I.27})$$

Equation (I.27) is the Ornstein-Uhlenbeck Brownian motion model of a rigid particle. For  $t \gg 1/\beta$ , the exponential terms in equation (I.26) becomes negligible and the equation reduces to

$$E\{x^2(t)\} = \frac{\alpha t}{\beta^2} = 2\lambda t \quad (\text{I.28})$$

where diffusion coefficient  $\lambda = \alpha/2\beta^2$ . Equation (I.27) is the Einstein's model for Brownian motion of rigid particle.

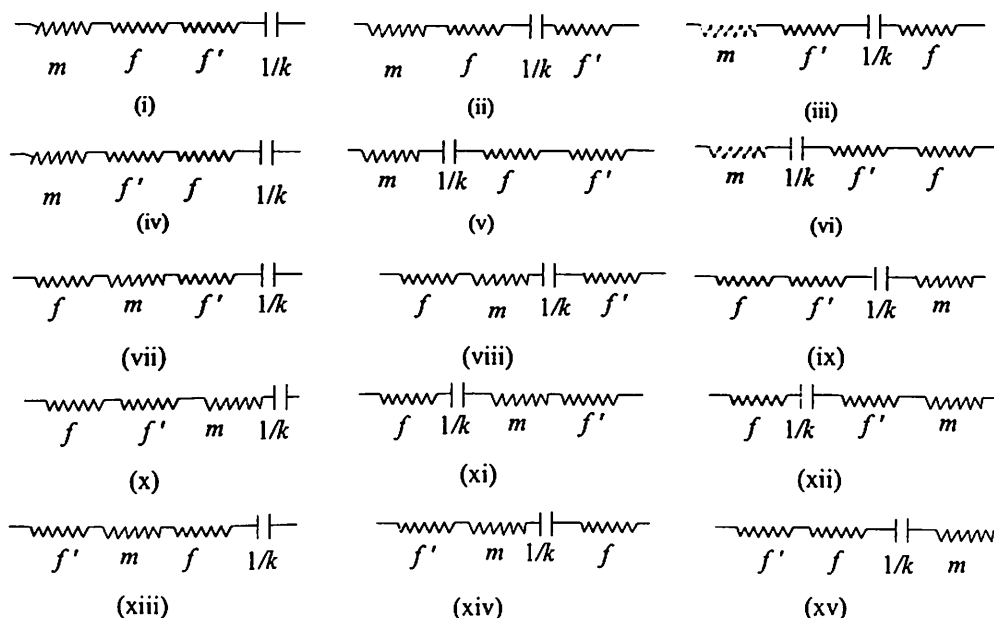
The correlation technique detailed in this appendix and applied to rigid particle to obtain the variance model is used in the thesis for obtaining variance models for non-rigid nanoparticle.

## POSSIBLE INTERACTION MODELS IN NON-RIGID BROWNIAN MOTION SYSTEM

This appendix contains different possible interaction models of four-parameters (4-P) developed in Chapter 5 to model the Brownian motion system of non-rigid nanoparticle. The four parameters  $(m, f, f', 1/k) \equiv (L, R, R', \bar{c})$  as defined in Chapter 5 represent lumped properties of non-rigid nanoparticle and surrounding medium. The 360 possible interaction models are obtained as described in the algorithm to obtain possible models in Section 5.4.

### II.1 ALL POSSIBLE ELECTRICAL ANALOG MODELS

This section gives all 360 possible models of interaction among four-parameters. These electrical analog models are grouped in fifteen categories denoted as Combination-1 to Combination-15 corresponding to fifteen unique four-parameter models in Fig. 5.8 with twenty-four models in each combination. These fifteen combinations are shown in Fig. II.1 to Fig. II.15.



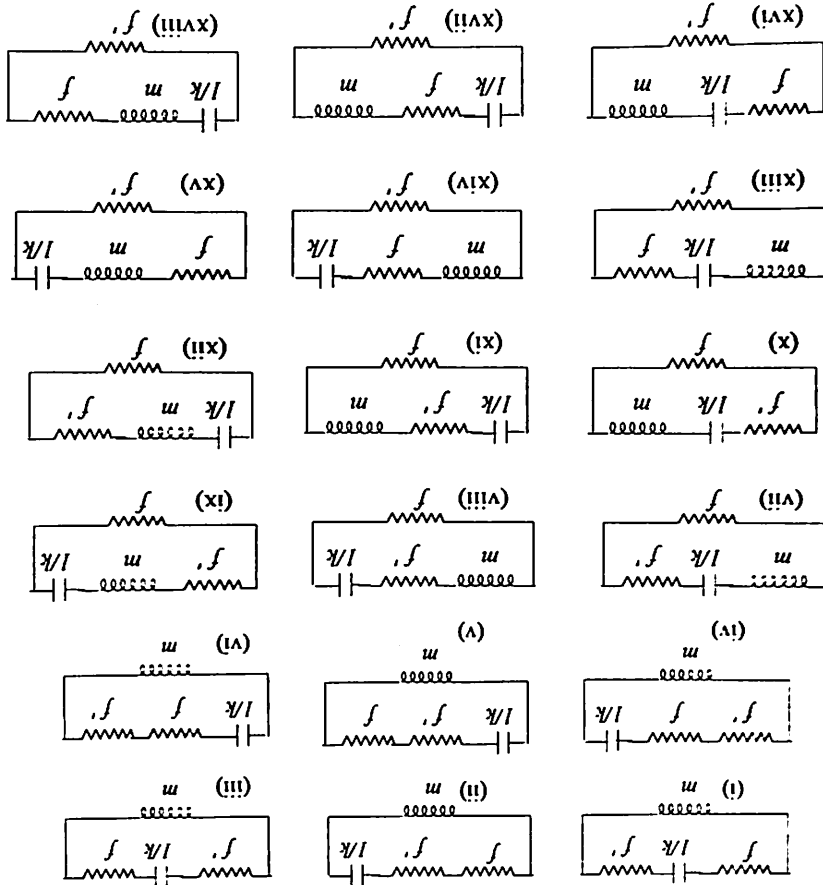
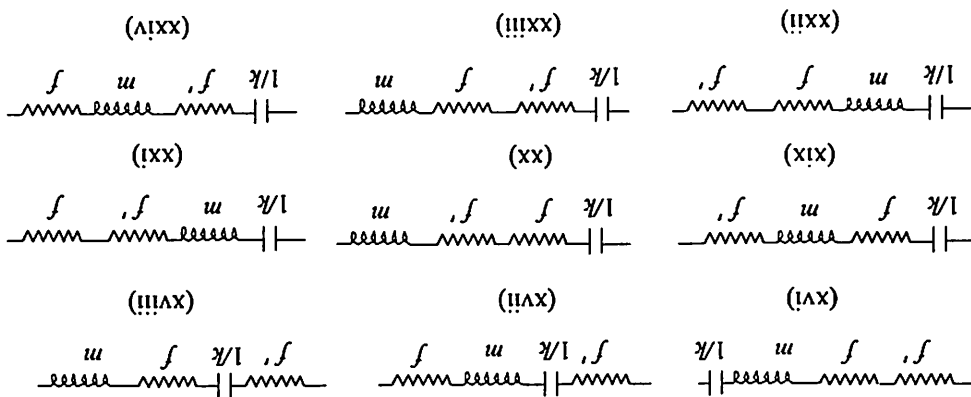


Fig. II.1 Combination 1: Twenty-Four 4-P Models corresponding to Model given in Fig. 5.12(i)



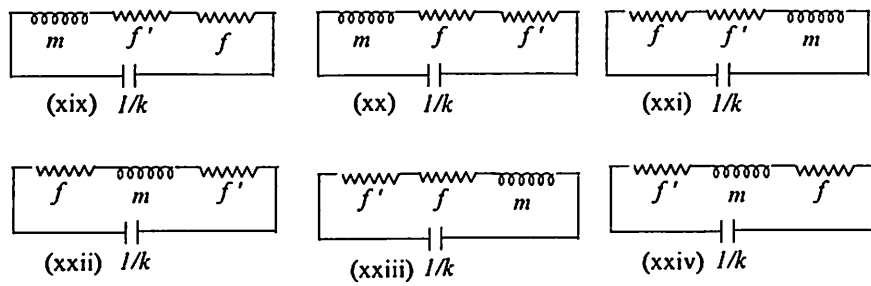


Fig. II.2 Combination 2: Twenty-Four 4-P Models Corresponding to Model given in Fig.5.12(ii)

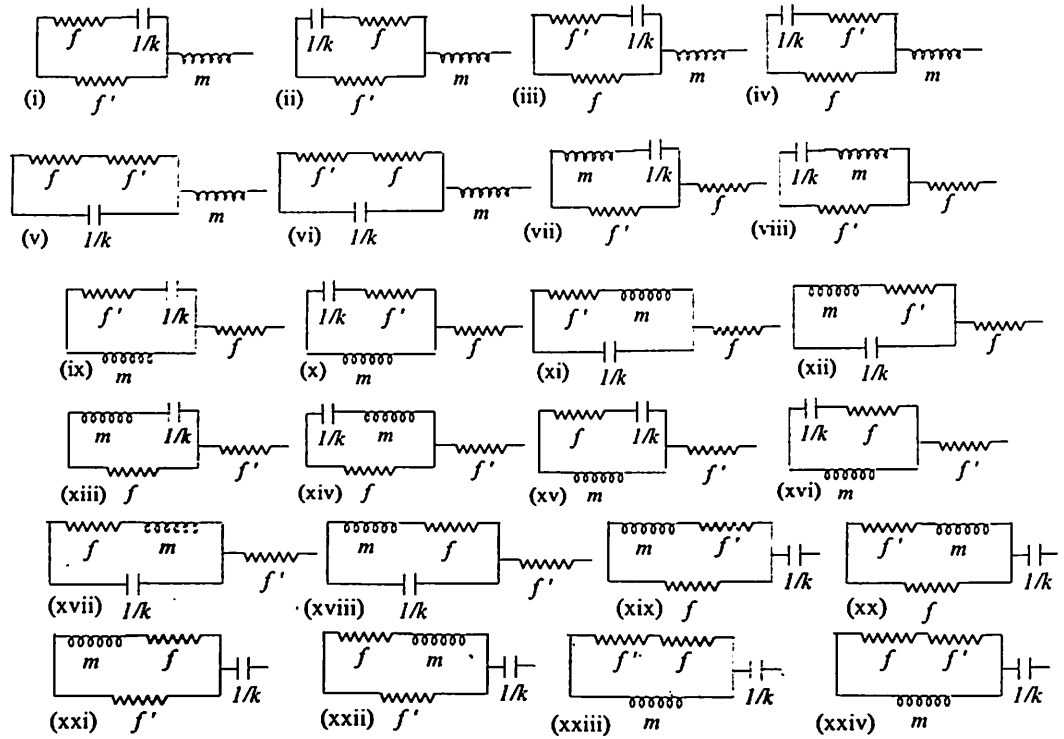
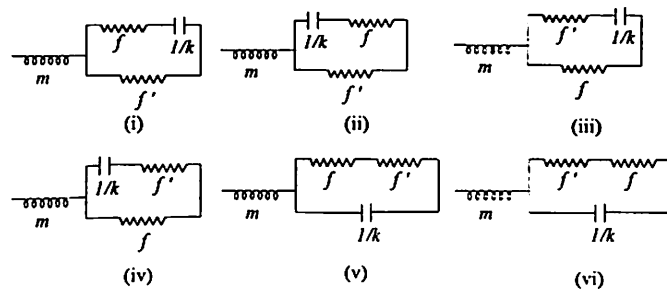


Fig. II.3 Combination 3: Twenty-Four 4-P Models Corresponding to Model given in Fig.5.12 (iii)



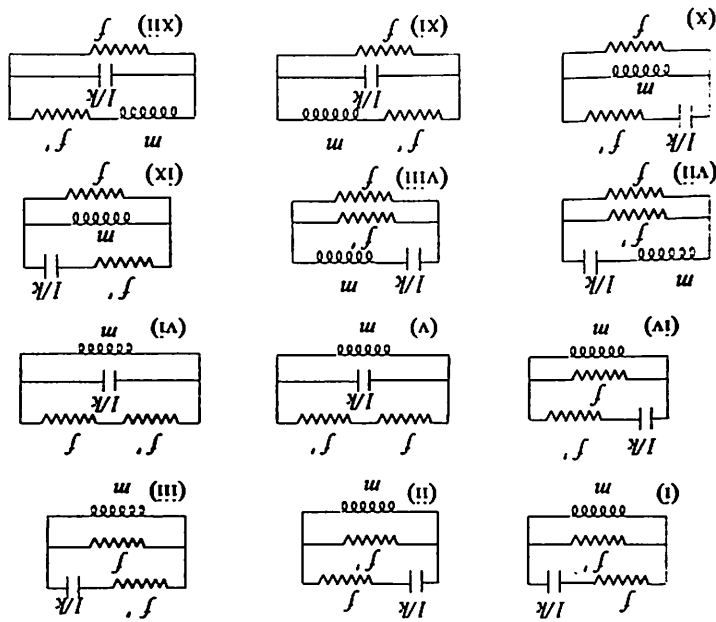
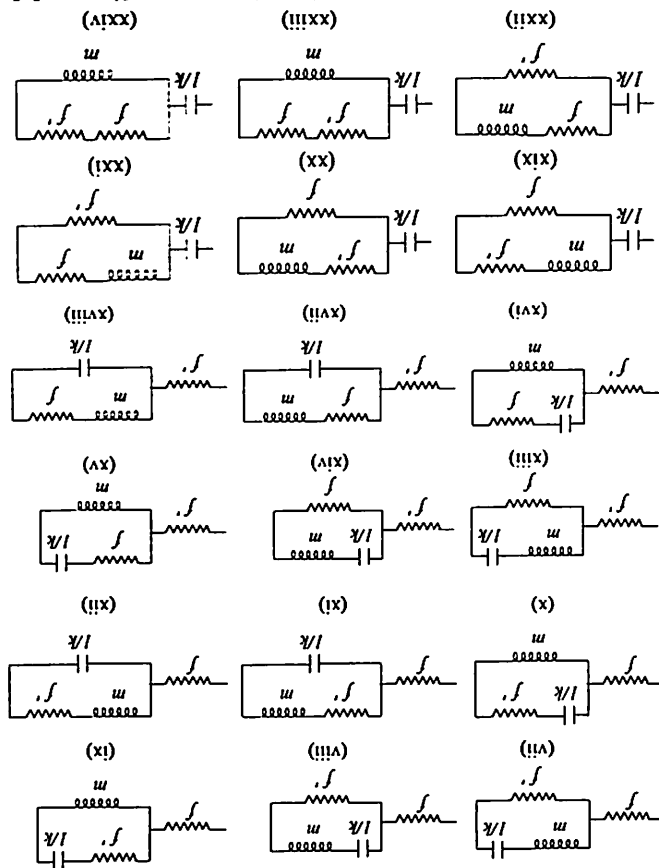


Fig. II.4 Combination 4: Twenty-Four 4-P Models Corresponding to Model given in Fig. 5.12(iv)



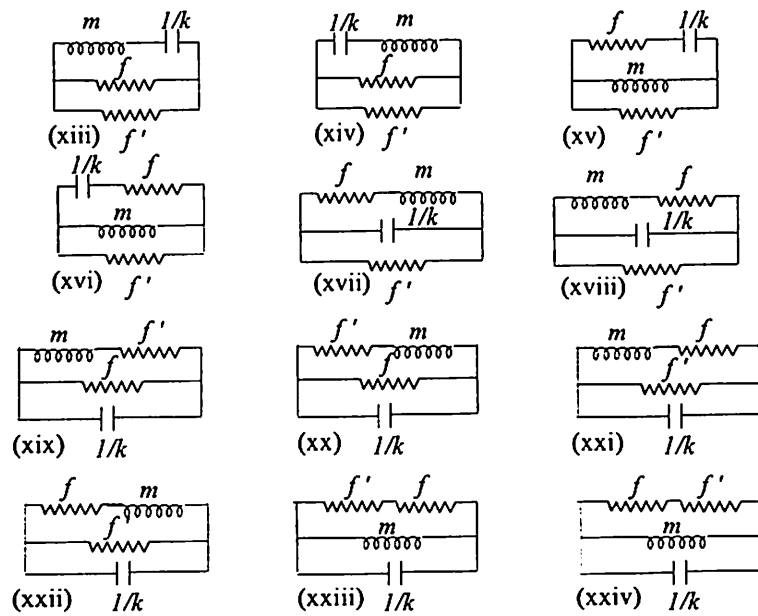


Fig. II.5 Combination 5: Twenty-Four 4-P Models Corresponding to Model given in Fig. 5.12 (v)

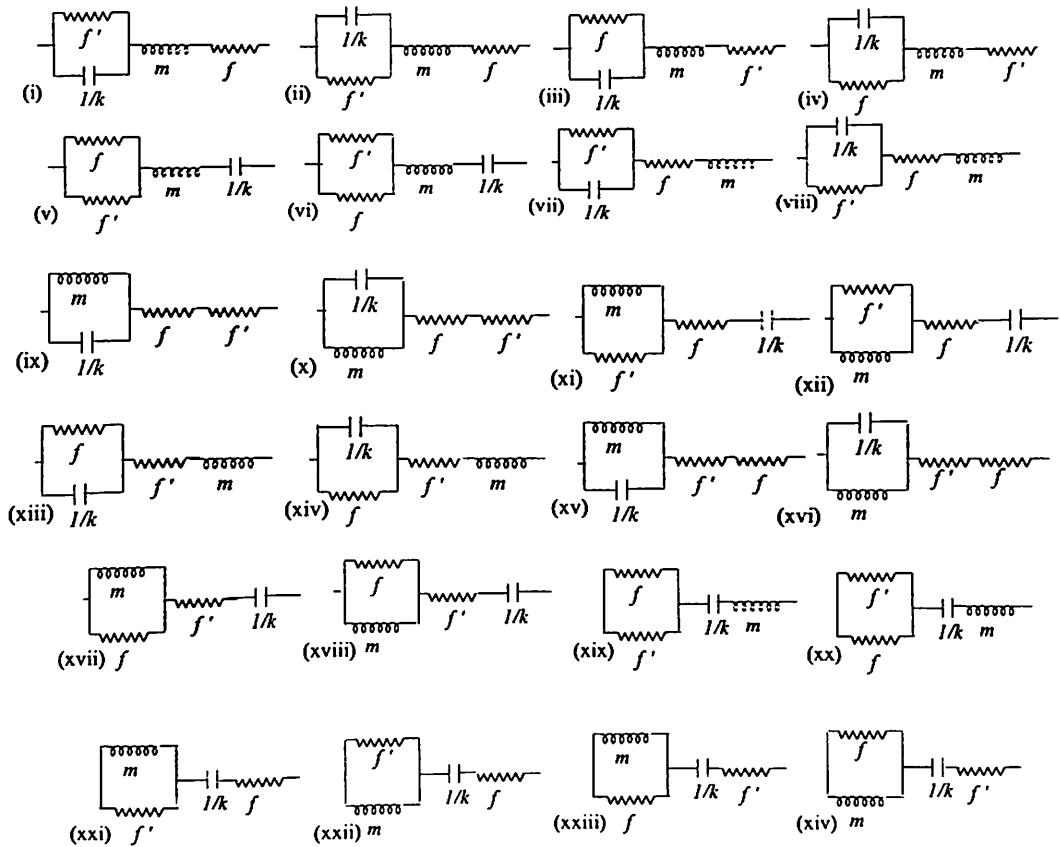


Fig. II.6 Combination 6: Twenty-Four 4-P Models Corresponding to Model given in Fig. 5.12 (vi)

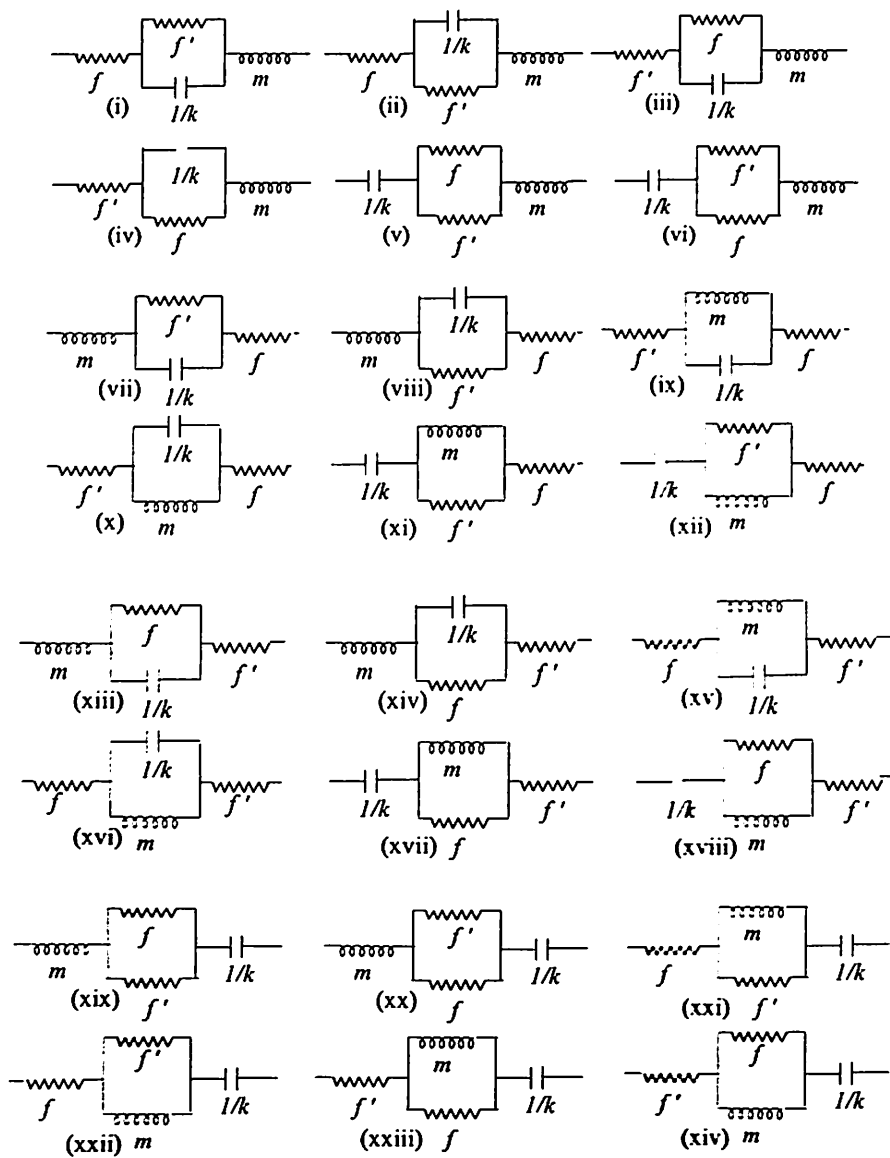
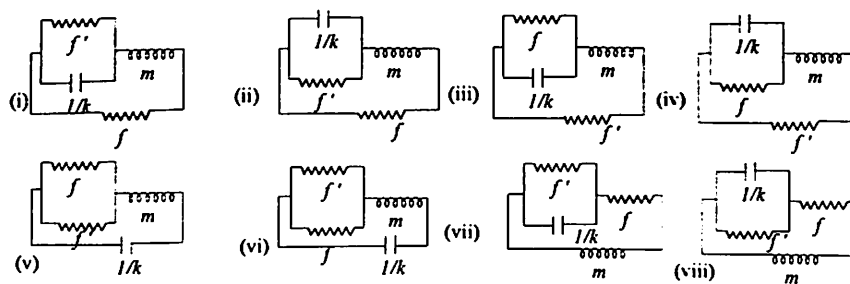


Fig. II.7 Combination 7: Twenty-Four 4-P Models Corresponding to Model given in Fig.5.12 (vii)





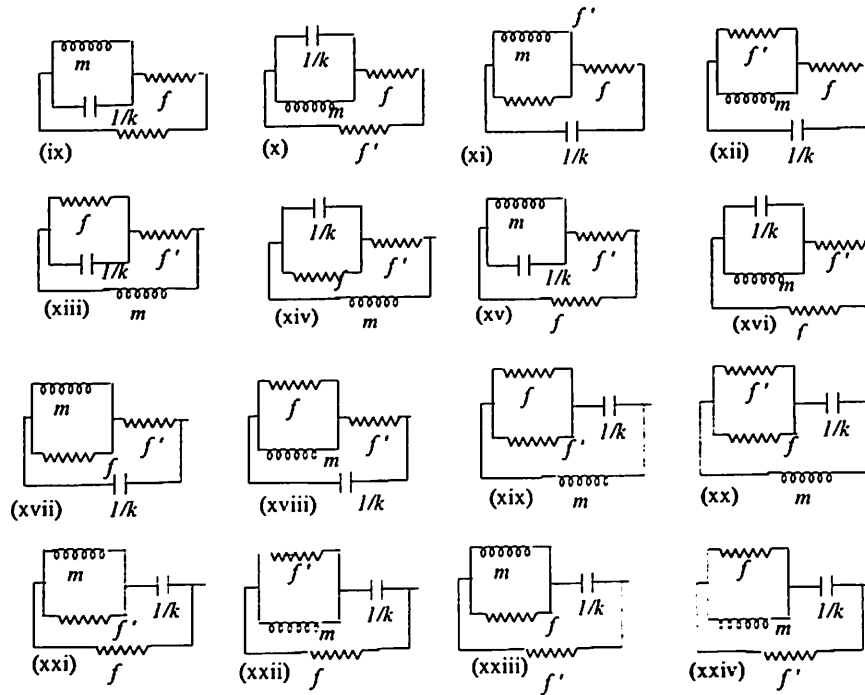
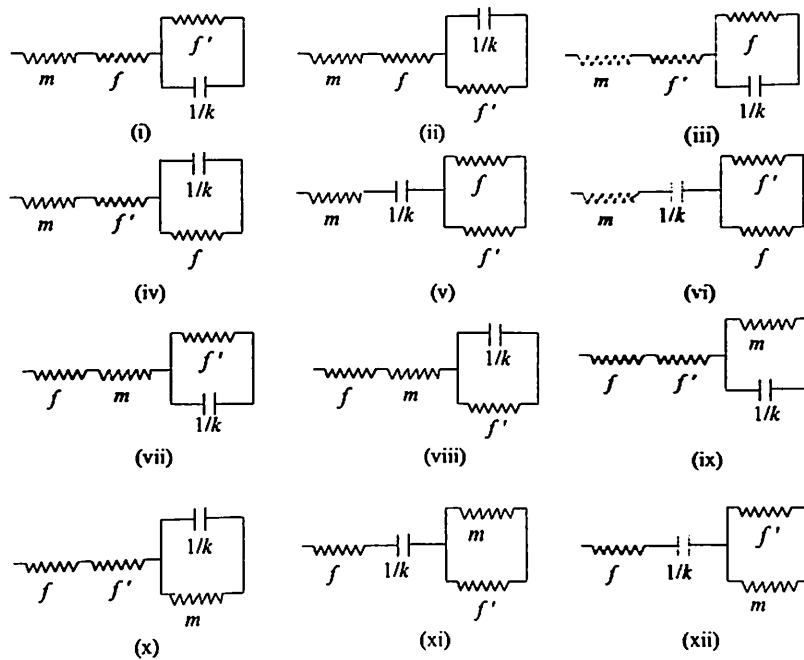


Fig. II.8 Combination 8: Twenty-Four 4-P Models Corresponding to Model given in Fig.5.12 (viii)



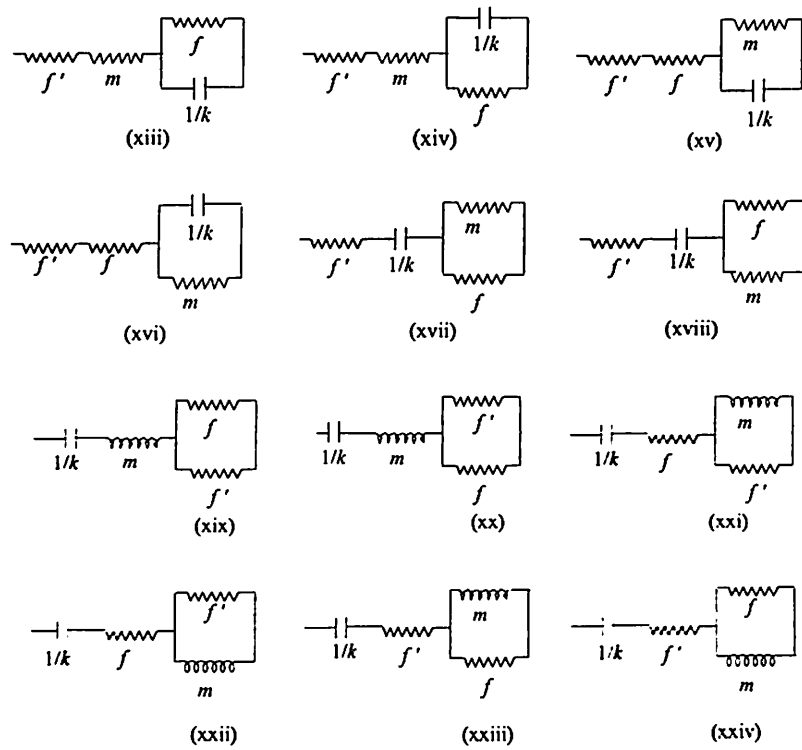
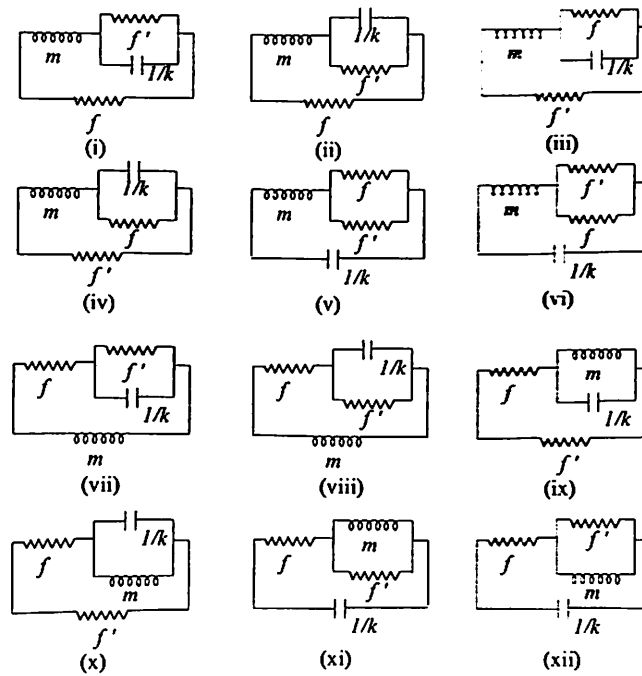


Fig. II.9 Combination 9: Twenty-Four 4-P Models Corresponding to Model given in

Fig.5.12 (ix)



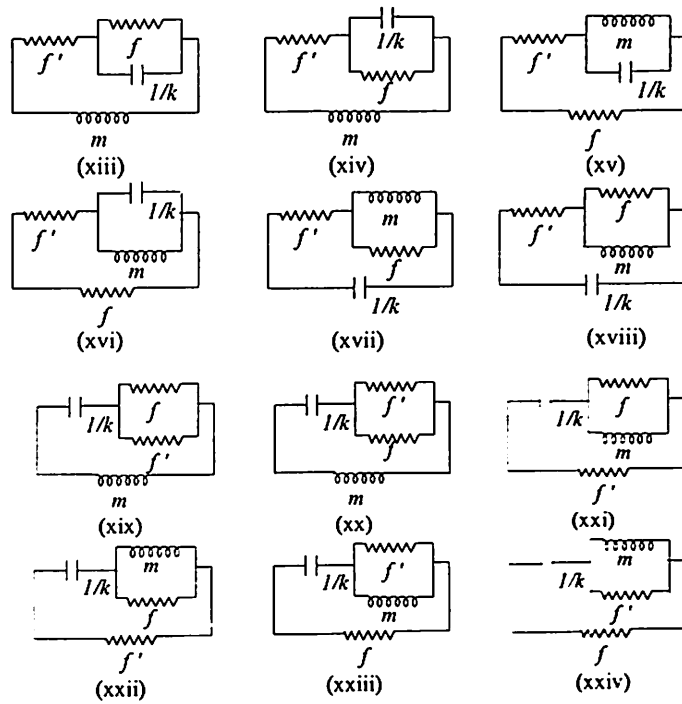
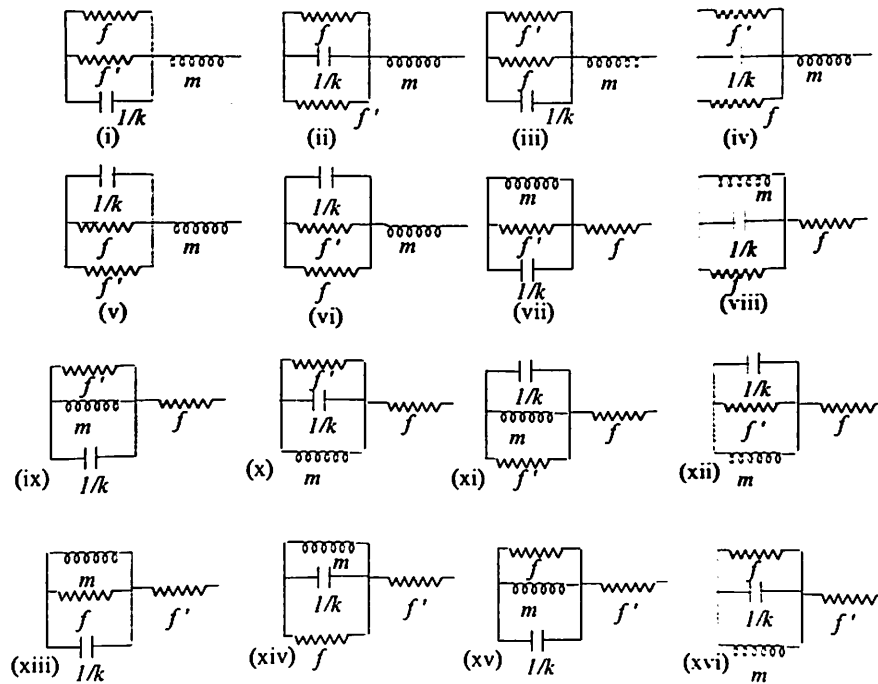


Fig. II.10 Combination 10: Twenty-Four 4-P Models Corresponding to Model given in Fig.5.12(x)



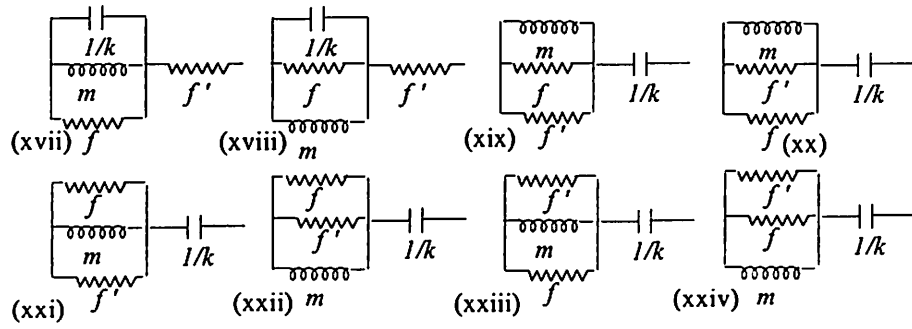
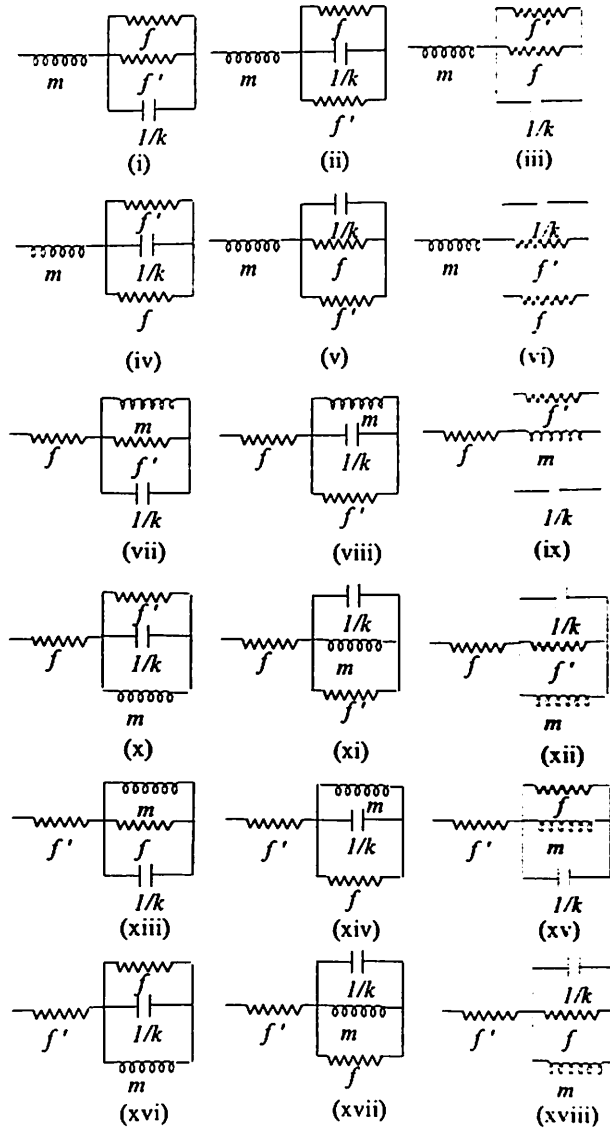


Fig. II.11 Combination 11: Twenty-Four 4-P Models Corresponding to Model given in Fig.5.12(xi)



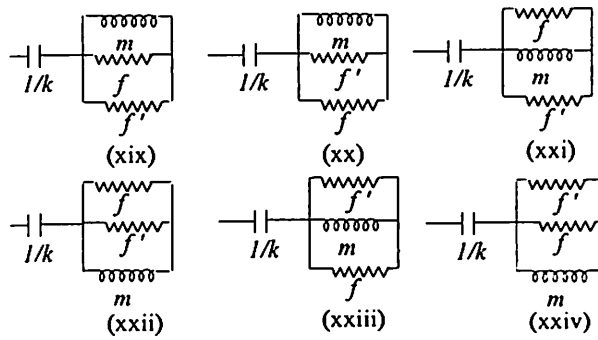


Fig. II.12 Combination 12: Twenty-Four 4-P Models Corresponding to Model given in Fig.5.12(xii)

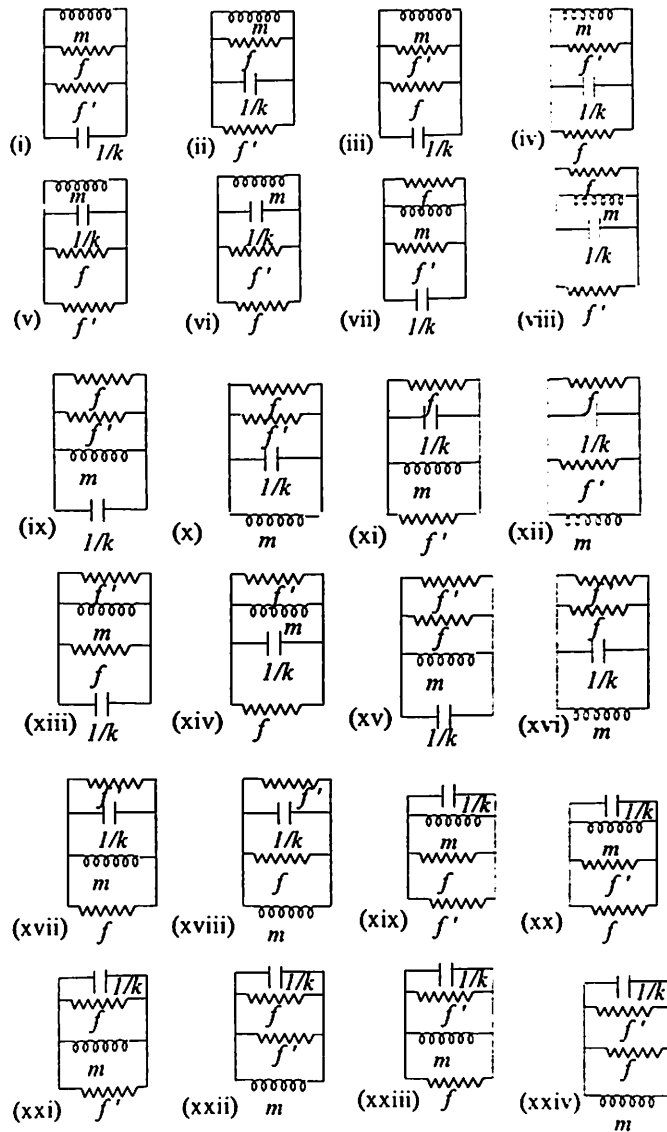


Fig. II.13 Combination 13: Twenty-Four 4-P Models Corresponding to Model given in Fig.5.12 (xiii)

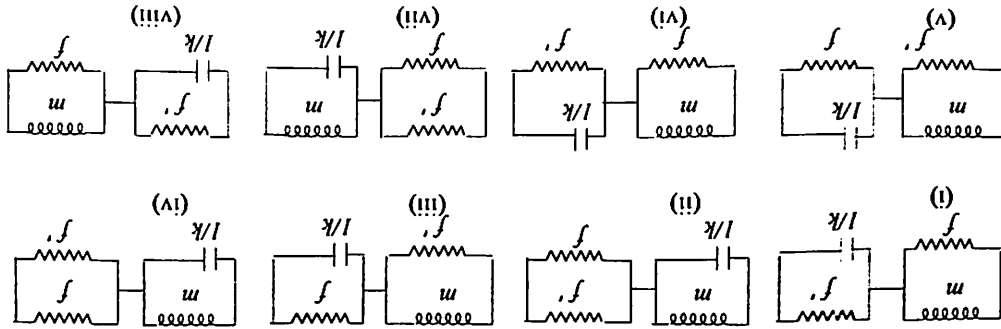
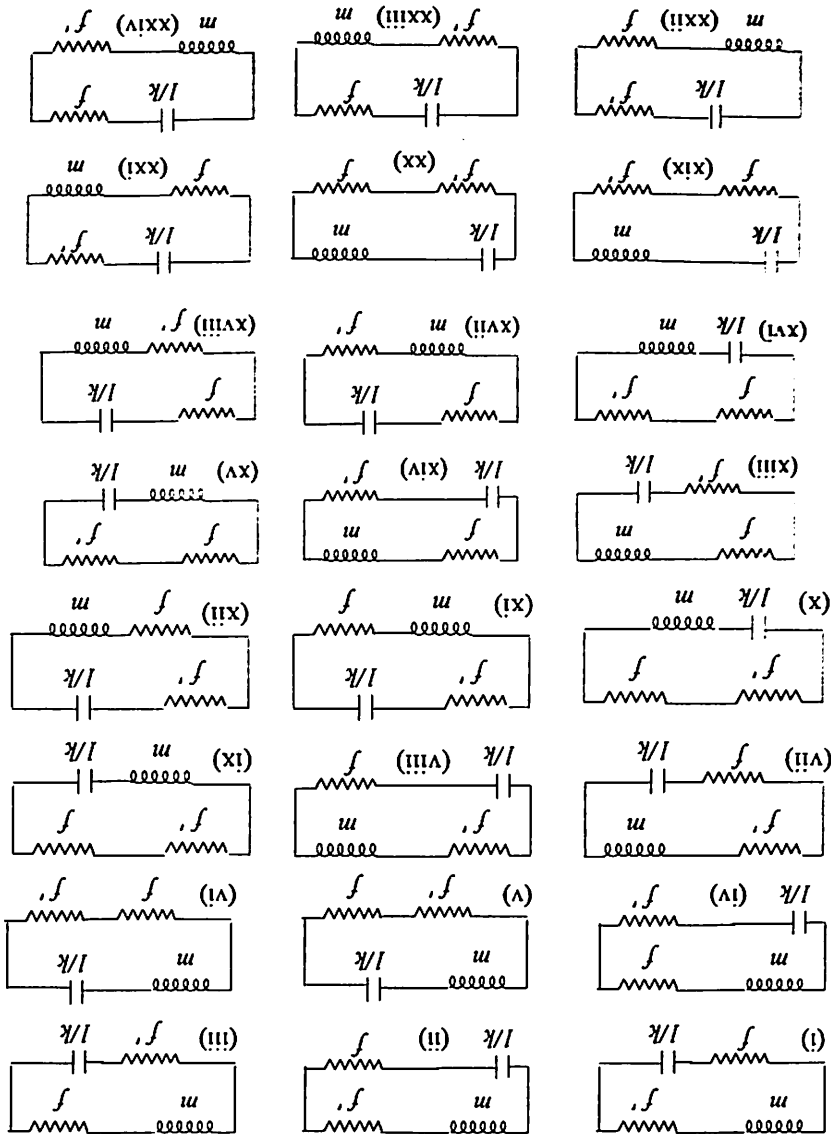
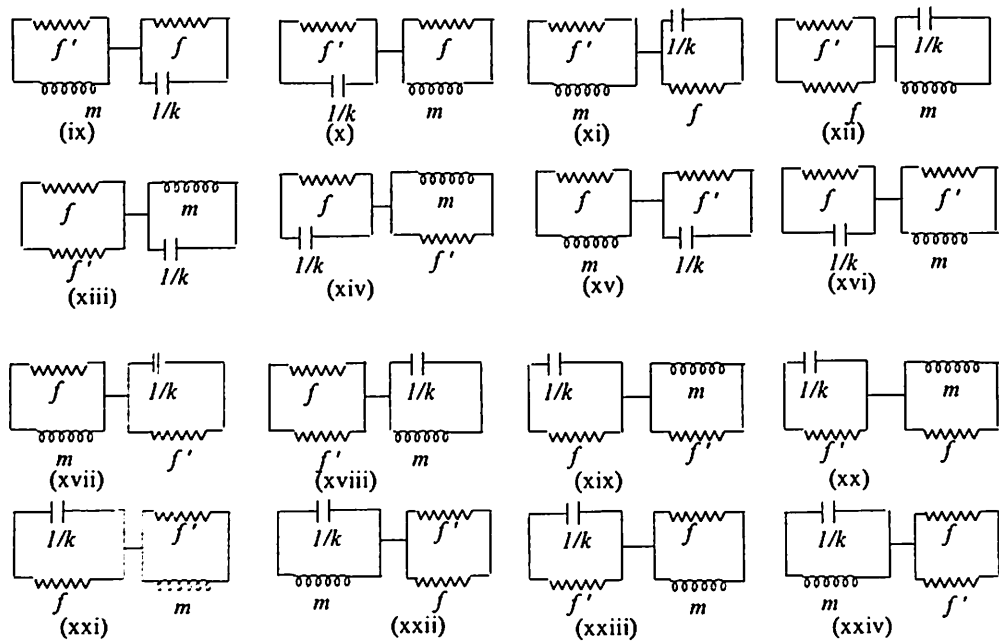


Fig. II.14 Combination 14: Twenty-Four 4-P Models Corresponding to Model given in Fig.5.12 (xiv)

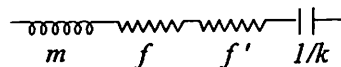




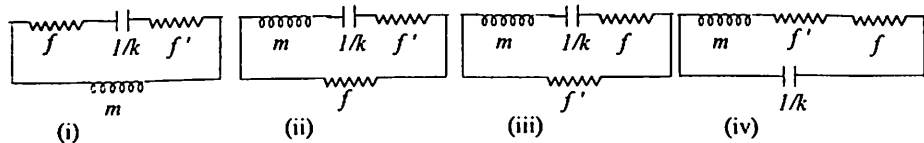
**Fig. II.15** Combination 15: Twenty-Four 4-P Models Corresponding to Model given in Fig.5.8 (xv)

## II.2 Possible Electrical Analog Models After Applying Selection Criterion 1

The reduced set of ninety-two electrical analog models which satisfy the Selection Criterion 1 of being electrically distinct from total of 360 models are given in this section. These electrical analog models are again grouped in fifteen categories corresponding to Combination-1 to Combination-15 and are shown in Fig. II.16 to II.30.



**Fig. II.16** Single 4-P Model Corresponding to Combination 1 Satisfying Selection Criterion 1



**Fig. II.17** Four 4-P Model Corresponding to Combination 2 Satisfying Selection Criterion 1

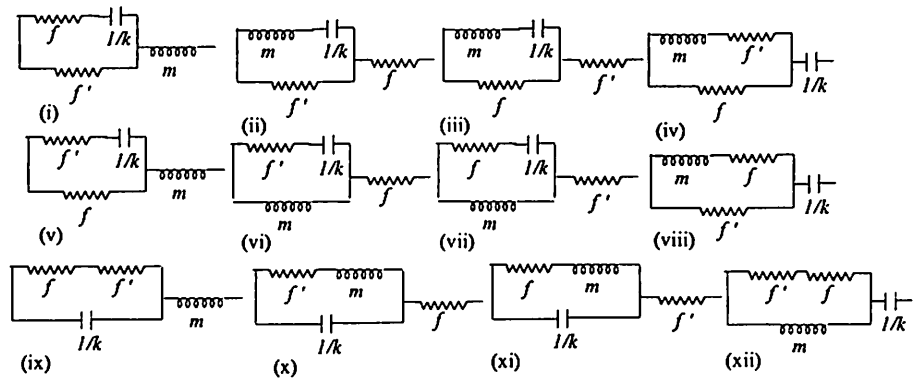


Fig. II.18 Twelve 4-P Model Corresponding to Combination 3 Satisfying Selection Criterion 1

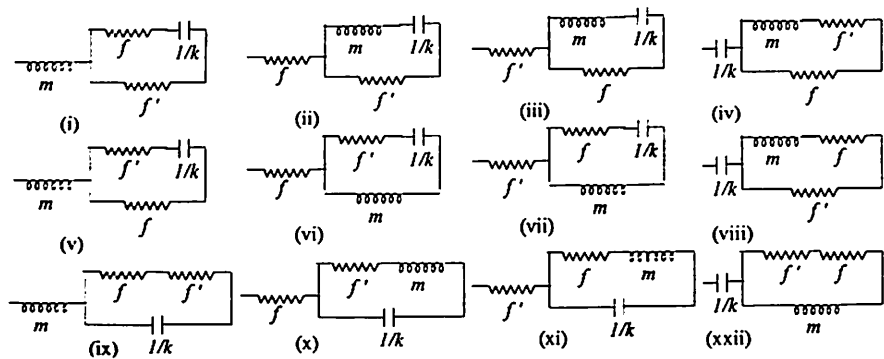


Fig. II.19 Twelve 4-P Model Corresponding to Combination 4 Satisfying Selection Criterion 1

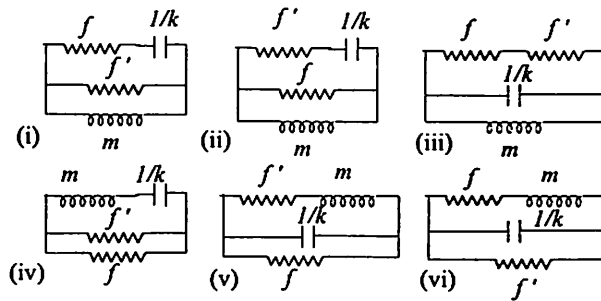


Fig. II.20 Six 4-P Model Corresponding to Combination 5 Satisfying Selection Criterion 1

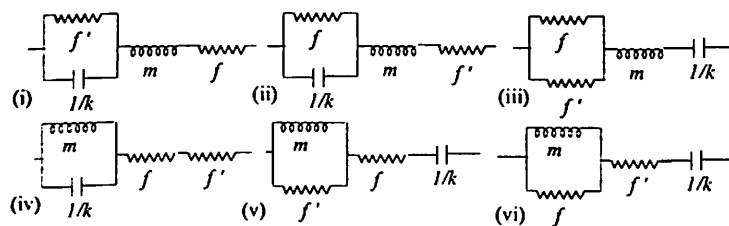


Fig. II.21 Six 4-P Model Corresponding to Combination 6 Satisfying Selection Criterion 1





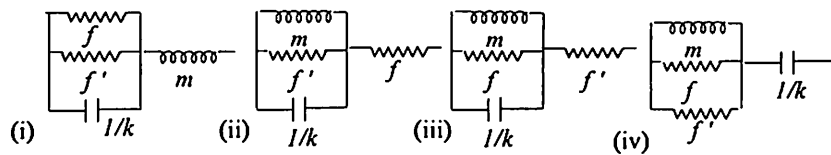


Fig. II.26 Four 4-P Model Corresponding to Combination 11 Satisfying Selection Criterion 1

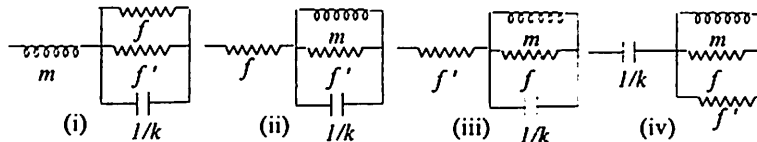


Fig. II.27 Four 4-P Model Corresponding to Combination 12 Satisfying Selection Criterion 1

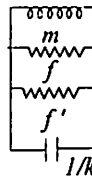


Fig. II.28 Single 4-P Model Corresponding to Combination 13 Satisfying Selection Criterion 1

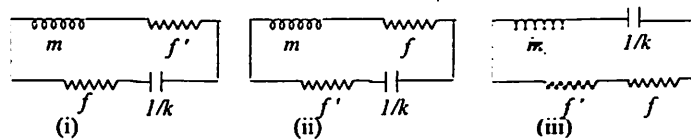


Fig. II.29 Three 4-P Model Corresponding to Combination 14 Satisfying Selection Criterion 1

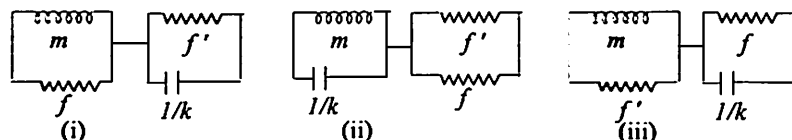


Fig. II.30 Three 4-P Model Corresponding to Combination 15 Satisfying Selection Criterion 1

## REFERENCES

- [Arakawa 1994] Arakawa K., Krotkov E., "Modeling of Natural Terrain Based on Fractal Geometry", *Systems and Computers in Japan*, Vol. 25, No. 11, pp 99-113, 1994.
- [Arnold 1974] Arnold L., *Stochastic differential equations: Theory and application*, John Wiley & Sons, NY, 1974.
- [Austumian 1994] Austumian R.D., Bier M., "Fluctuation Driven Ratchets: Molecular Motor", *Phy. Rev. Lett.*, Vol. 72, No. 11, pp 1766-1769, 1994.
- [Barnsley 1993] Barnsley M.F., *Fractals Everywhere*, Academic Press, NY, 1993.
- [Barraquand 1990] Barraquand J., Latombe J.C., "A Monte-Carlo Algorithm for Path Planning with Many Degrees of Freedom", in *Proc. 1990 IEEE Int. Conf. Rob. & Autom.*, Vol. 3, pp 1712-1725, 1990.
- [Beiser 1987] Beiser A., *Concepts of Modern Physics*, McGraw Hill, NY, 1987.
- [Benesch 2003] Benesch T. Yiaccoumi S. Tsouris C., "Brownian Motion in Confinement", *Phy. Rev. E.*, Vol. 68, No. 2, pp 021401-(1-5), 2003.
- [Berne 1966] Berne B.J., Boon J.P., Rice S.A., "On the Calculation of Autocorrelation Functions of Dynamical Variables", *J. Chem. Phys.*, Vol. 45, No. 4, pp 1086-1096, 1966.
- [Bining 1985] Bining G., Rohrer H., "The Scanning Tunneling Microscope", *Scientific American*, Vol. 253, pp 50-56, 1985.
- [Birdsall 1991] Birdsall C.K., "Particle-in-Cell Charged-Particle Simulation Plus Monte Carlo Collision with Neutral Atoms PIC-MCC", *IEEE Tr. Plasma Sci.*, Vol. 19, No. 1, pp 65-85, 1991.
- [Blinder 1974] Blinder S. M., *Foundations of Quantum Dynamics*, Academic Press, NY, 1974.

- [Bouchard 1990] Bouchard J. P., Georges A., "Anomalous Diffusion in Disordered Media, Statistical Mechanisms, Models and Physical Application", *Phy. Rep.*, Vol. 195, pp 127-293, 1990.
- [Brekke 1994] Brekke K.A., Oksendal B., "Optimal Switching in an Economic Activity Under Uncertainty", *Siam J. Control and Optimization*, Vol. 32, No. 4, pp 1021-1036, 1994.
- [Broeck 1982] Broeck Van Den C, "A Stochastic Description of Longitudinal Dispersion in Uniaxial Flows", *Physica A*, Vol. 112, No.1-2, pp 343-352, 1982.
- [Brown 1966] Brown R., *The World of Atom*, in *Basic Books*, Vol. 1, H. Brooseand and L. Motz (Ed.), NY, pp 206-212, 1966.
- [Callen 1951] Callen H.B., Welton T.A., "Irreversible Generalized Noise", *Phy. Rev.*, Vol. 83, pp 34-40, 1951.
- [Cao 2001] Cao J., "Single Molecular Tracking of Heterogeneous Diffusion", *Phy. Rev. E*, Vol. 63, pp 041101 (1-7), 2001.
- [Case 1971] Case K.M., "Velocity Fluctuations of a Body in Fluid", *Phy. Fluids*, Vol.14, No.10, pp 2091-2095, 1971.
- [Chandrasekhar 1943] Chandrasekhar S., "Stochastic problems in Physics and Astronomy", *Rev. Mod. Phy.*, Vol. 15, pp 1-89, 1943.
- [Chandrasekhar 1949] Chandrasekhar S., "Brownian Motion, Dynamical Friction and Stellar Dynamics", *Rev. Mod. Phys.*, Vol.21, No. 1, pp 383-388, 1949.
- [Chauwin 1995] Chauwin J.F., Ajdari A., Prost J., "Motor Protein Models", *Eur. Phys. Lett.*, Vol. 32, pp 373-380, 1995.
- [Chen 1989] Chen C.C., Daponte J., Fox M., "Fractal Feature Analysis and Classification in Medical Imaging", *IEEE Tr. Medical Imaging*, Vol. 8, pp 133-142, 1989.
- [Chen 1999] Chen Y., Yan B., Miura R., "Asymmetry and Directional Reversal in Fluctuation-Induced Biased Brownian Motion", *Phy. Rev. E*, Vol. 60, No. 4, pp 3771-3775, 1999.

- [Chow 1972] Chow T.S., Hermans J.J., "Effect of Inertia on the Brownian Motion of Rigid Particles in a Viscous Fluid", *J. Chem. Phys.*, Vol. 56, No. 6, pp 3150-3154, 1972.
- [Chow 1997] Chow T.S., "Noise and Fluctuation of Rough Surfaces", *Phys. Rev. Lett.*, Vol. 79, No. 6, pp 1086-1089, 1997.
- [Clerc 1992] Clerc H.J.H., Schram P.P.J.M., "Brownian Particles in Shear Flow and Harmonic Potentials: A Study of Long-Time Tails", *Phys. Rev. A*, Vol. 46, No. 4, pp 1942-1950, 1992.
- [Cox 1952] Cox R.T., "Brownian Motion in the Theory of Irreversible Processes", *Rev. Mod. Phys.*, Vol. 24, No. 4, pp 312-320, 1952.
- [Cukier 1969] Cukier R.I., Deutsch J.M., "Microscopic Theory of Brownian Motion: The Multiple-Time Scale Point of View", *Phys. Rev.*, Vol. 177, No. 1, pp 240-244, 1969.
- [Czopnik 2001] Czopnik R., Garbaczewski P., "Brownian Motion in a Magnetic Field", *Phys. Rev. E*, Vol. 63, No. 2, pp 021105-(1-9), 2001.
- [Deng 2004] Deng M.L., Zhu W.Q., "Stationary Motion of Active Brownian Particles", *Phys. Rev. E*, vol. 69, No. 4, pp 046105-(1-9), 2004.
- [Dorofeyev 1999] Dorofeyev I, Fuschs H, Gotsman B., "Brownian Motion of Microscopic Solids under the Action of Fluctuating Electromagnetic Fields", *Phys. Rev. Lett.*, Vol. 83, No. 12, pp 2402-2405, 1999.
- [Drexler 1992] Drexler K. E., *Nanosystems: Molecular Machinery, Manufacturing and Computation*, Wiley, NY, 1992.
- [Dufty 1974] Dufty J.W., "Gaussian Model for Fluctuation of a Brownian Particle", *Phys. Fluids*, Vol.17, No. 2, pp 328-333, 1974.
- [Einstein 1905] Einstein A., "On the Movement of Small Particles Suspended in Stationary Liquids Required by the Molecular-Kinetic Theory of Heat", *Ann. Phys.*, Vol. 17, pp 549-560,

translation by Anna Beck in "The Collected Papers of Albert Einstein", Princeton Univ. Press, Princeton, NJ, Vol. 2, pp 123-134, 1905.

- [Engberg 1995] Engberg J., Larsen T., *Noise Theory of Linear and Non Linear Circuits*, John Wiley & Sons, NY, 1995, Ch 2.
- [Fedder 1996] Fedder T.J., Brust-Mascher I, Slattery J.P., Baird B., Webb W.W., "Constrained Diffusion or Immobile Fraction on Cell Surface: A New Interpretation" *J. Biophys.*, Vol. 70, pp 2767-2773, 1996.
- [Fennimore 2003] Fennimore A.M., Yuzvinsky T.D., Han W.Q., Fuhrer M.S., Cumings J., Zetti A., "Rotational Actuators Based on Carbon Nanotubes", *Nature*, Vol. 424, pp 408-410, 2003.
- [Fernandez 1982] Fernandez de la Mora J., Mercer J.M., "Modified Fokker-Planck Equation for the Motion of Brownian Particles in a Non-Uniform Gas", *Phy. Rev. A*, Vol. 26, No. 4, pp 2178-2186, 1982.
- [Ferrari 2001] Ferrari M., *Biomedical Microdevices*, Kluwer Academic Publishers, Boston, 2001.
- [Feynman 1963] Feynman R., Leighton R.B., Sands M., *The Feynman Lectures on Physics, Vol. 1*, Addison-Wesley, Reading, MA, 1963.
- [Foister 1980] Foister R.T., Van Den Ven T.G.M., "Diffusion of Brownian Particles in Shear Flows", *J. Fluid Mech.*, Vol. 96, pp 105-132, 1980.
- [Fox 1970] Fox R.F., Uhlenbeck G., "Contribution to Non-Equilibrium Thermodynamics I: Theory of Hydrodynamics Fluctuation", *Phys. Fluids*, Vol. 13, No. 8, pp 1893-2204, 1970.
- [Fox 2001] Fox R.F., Choi M.H., "Rectified Brownian Motion and Kinesin Motion along Microtubules", *Phy. Rev. E*, Vol. 63, No. 5, pp 051901-(1-9), 2001.

- [Freitas 1998] Freitas, R., 1998, "Exploratory Design in Medical Nanotechnology: A Mechanical Artificial Red Blood Cell." *Artificial Cells, Blood Substitutes, and Immobile Biotech*, Vol. 26, pp 411-430.
- [Freitas 2000] Freitas, R., "Say Ah", *Science*, Vol. 40, pp 26-31, 2000.
- [Frisch 1979] Frisch H.L., Forgacs G., "Inverse Dynamics Problem for the Liouville Equation", *Phy. Rev. A*, Vol. 20, No. 2, pp , 1979.
- [Fujimasa 1996] Fujimasa I., *Micromachines: A New Era in Mechanical Engineering*, Oxford Science Publication, UK, 1996.
- [Fukuda 2003] Fukuda T., Arai F., Dong L., "Assembly of Nanodevices with Carbon Nanotubes through Nanorobotic Manipulations", *Proc. IEEE*, Vol. 91, No. 11, pp 1803-1818, 2003.
- [Gillespie 1993] Gillespie D.T., "Fluctuation and Dissipation in Brownian Motion", *Am. J. Phys.*, Vol. 61, pp 1077-1083, 1993.
- [Gillespie 1996(i)] Gillespie D.T., "Exact Numerical Solution of the Ornstein-Uhlenbeck Process and its Integral", *Phy. Rev. E*, Vol. 54, pp 2084-2091, 1996.
- [Gillespie 1996(ii)] Gillespie D.T., "The Mathematics of Brownian Motion and Johnson Noise", *Am. J. Phy.*, Vol. 64, pp 225-240, 1996.
- [Girish 2004] Girish R., Sharma N.N., Mittal R.K., "Study on Motor Protein Models and Related Problems", in *Proc. of National Conf. Nanotechnology*, NANOSPHERE-2004, 11-12 June, Chennai, India, 2004.
- [Goldstein 2002] Goldstein H., Poole C. and Safko J., *Classical Mechanics*, Pearson Education Inc., Singapore, 2002.
- [Gordon 1989] Gordon L., Yu C.P., "Diffusional Particle Deposition in the Human Nose and Mouth", *Aerosol Science and Technology*, Vol. 11, No. 3, pp 213-220, 1989.
- [Grimmett 2000] Grimmett G.R., Stirzaker D.R., *Probability and Random Process*, Clarendon Press, Oxford, 2000.

- [Grosberg 1968] Grosberg S. W., *Advanced Mechanics*, John Wiley & Sons, NY, 1968.
- [Gross 1955] Gross E.P., "Shape of Collision Broadened Spectra", *Phy. Rev.*, Vol. 97, pp 395-403, 1955.
- [Grossman 1992] Grossman S.J., Vila J.L., "Optimal Dynamic Trading with Leverage Constraints", *J. Financial and Quantitative Analysis*, Vol. 27, pp 151-169, 1992.
- [Harris 1976] Harris S., "Diffusion Coefficient for a Brownian Particle", *Am. J. Phys.*, Vol. 44, pp 291-294, 1976.
- [Haugh 1973] Haugh E.H., Martin Lof A, "Fluctuation Hydrodynamics and Brownian Motion", *J. Stat. Phy.*, Vol. 7, 259-281, 1973.
- [Haw 2002] Haw M.D., "Colloidal Suspensions, Brownian Motion, Molecular reality: A Short Story", *J. Phys: Condens. Matter*, Vol. 14, pp 7769-7779, 2002.
- [Hernandez 1996] Hernandez-Contreras M. Medina-Noyola M., "Rotational Diffusion of Nonspherical Brownian Particles in a Suspension of Spheres", *Phy. Rev. E*, Vol. 54, No. 6, pp 6586-6595, 1996.
- [Housner 1961] Housner G. W. and Hudson D. E., *Applied Mechanics: Vol. II*, Van Nostrand, East-West Press, 1961.
- [Ito 1964] Ito K., McKean H.P. Jr., *Diffusion Processes and Their Sample Paths*, Academic Press, NY, 1964.
- [Jasnow 1975] Jasnow D., Gerjuoy E., "Langevin Equation with Stochastic Damping: Possible Application to Critical Binary Fluids", *Phy. Rev. A*, Vol. 11, No. 1, pp 340-349, 1975.
- [Julicher 1997] Julicher F., Ajdari A., Prost J., "Modeling Molecular Motors", *Rev. Mod. Phys.*, Vol. 69, No. 4, pp 1269-1281, 1997.
- [Karlin 1966] Karlin S., *A first course in Stochastic Processes*, Academic Press, NY, 1966.



- [Katayama 1966] Katayama T., Terauti R., "Brownian Motion of a Single Particle Under Shear Flow", *Eur. J. Phys.*, Vol. 17, pp 136-140, 1996.
- [Kato 1972] Kato H., Tachibana M., Oikawa K., "On the Drag of a Sphere in Polymer Solutions", *Bull. JSME*, Vol. 15, No. 90, pp 1556-1567, 1972.
- [Kittel 1981] Kittel C., Knight W. D., Ruderman M.A., *Mechanics*, Vol. 1, Berkeley Physics Course, Kui Keong Print. Co. Pte. Ltd., Singapore, 1981.
- [Knobloch 1992] Knobloch E., Merryfield W.J., "Enhancement of Diffusive Transport in Oscillatory flows", *Astroph. J.*, Vol. 401, pp 196-205, 1992.
- [Koyama 1992] Koyama J., Hara H., "Scaled Langevin Equation to Describe the 1/f Spectrum", *Phy. Rev. A*, Vol. 46, No. 4, pp 1844-1850, 1992.
- [Kruglak 1988] Kruglak H., "Brownian Motion: A Laboratory Experiment", *Phy. Educ.*, Vol. 23, pp 306-309, 1988.
- [Kubo 1986] Kubo R., "Brownian Motion and Nonequilibrium Statistical Mechanics", *Science*, Vol. 233, pp 330-334, 1986.
- [Kursnoglu 1963] Kursnoglu B., "Brownian Motion in a Magnetic Field", *Phy. Rev.*, Vol. 132, No.1, pp 21-26, 1963.
- [Kusumi 1996] Kusumi A., Sako Y., "Cell Surface Organization by the Membrane Skeleton", *Curr. Opin. Cell. Biol.*, Vol. 8, pp 566-574, 1996.
- [Landau 1960] Landau L.D., Lifschitz E.M., *Fluid Mechanics*, Addison-Wesley, Reading, MA, 1960.
- [Langevin 1908] Langevin P., "On the Theory of Brownian Motion", *C.R. Acad. Sci., Paris*, Vol. 146, pp 530-533, 1908, English translation by D.S. Lemons and A. Gythial in Paul Langevin's 1908 Paper "On the Theory of Brownian Motion", *Am. J. Phys.*, Vol. 65, pp 1079-1081, 1997.

- [Lathi 2000] Lathi B.P., *Signal Processing and Linear Systems*, Oxford Univ. Press, 2000.
- [Lebowitz 1963] Lebowitz J.L., Rubin E., "Dynamic Study of Brownian Motion", *Phy. Rev.*, Vol. 131, pp 2381-2396, 1963.
- [Lee 2003] Lee Y., Allson A., Abbott D., Stanley H.E., "Minimal Brownian Ratchet: An Exact Solvable Model", *Phy. Rev. Lett.*, Vol. 91, No. 22, pp 220601-(1-4), 2003.
- [Leggas 1999] Leggas M., Eckstein E.C., "Characterizing Cell Motion in Flowing Blood", in *Proc. First Joint BMES/EMBS Conf. Serving Humanity, Advanced Technology*, Oct. 13-16, Atlanta, GA, USA , pp 43-45, 1999.
- [Lemons 1999] Lemons D.S., Kaufman D.L., "Brownian Motion of a Charged Particle in a Magnetic Field", *IEEE Trans. Plasma Sci.*, Vol. 27, No. 5, pp 1288-1296, 1999.
- [Lim 2002] Lim S.C., Muniandy S.V., "Self-Diffusion Gaussian Processes for Modeling Anomalous Diffusion", *Phy. Rev. E*, Vol. 66, pp 021114-(1-14), 2002.
- [Lyshevski 2001] Lyshevski M.A., "Motion of Brownian Molecular Motor: Nanoscale-Based Modeling, Analysis and Control", *Proc. Am. Controls Conf.*, Arlington, VA, June 25-27, pp 4574-4578, 2001.
- [Lyshevski 2002] Lyshevski M.A., "Brownian Motion Analysis and its Application to Nanosystems", *Proc. IEEE Int. Conf. Nanotechnology IEEE-NANO 2002*, pp 151-155, 2002.
- [Magnasco 1993] Magnasco M.O., "Forced Thermal Ratchets", *Phy. Rev. Lett.*, Vol. 71, No. 10, pp 1977-1981, 1993.
- [Mandelbrot 1982] Mandelbrot B.B., *The Fractal Geometry of Nature*, Freeman, San Francisco, CA, 1982.
- [Marshall 1982] Marshall W.T., "Brownian Motion, the Second Law and Boltzman", *Eur. J. Phy.*, Vol. 3, pp 215-222, 1982.

- [McCarty 1973] McCarty P., Horsethemke W, "Effective Diffusion Coefficient for Steady Two-Dimensional Convection Flow", *Phy. Rev. A*, Vol. 37, pp 2112-2117, 1973.
- [Mehaffey 1977] Mehaffey J.R., Cukier R.L., "Kinetic-Theory Derivation of the Stokes-Einstein Law", *Phy. Rev. Lett.*, Vol. 38, No. 19, pp 1039-1042, 1977.
- [Mittal 2004] Mittal R.K., Nagrath I.J., *Robotics and Controls*, Tata McGraw Hill, New Delhi, 2004.
- [Mizoguchi 1992] Mizoguchi H., Mizumo I., Tagaki S., "Design and Fabrication of Light Driven Pump", *IEEE J. of MEMS*, Vol. 7, pp 373-379, 1992.
- [Modak 1984] Modak R.S., "A Simple Model for the Study of Free Brownian Motion", *Am. J. Phys.*, Vol. 52, pp 43-45, 1984.
- [Montgomery 1971] Montgomery D., "Brownian Motion from Boltzman's Equation", Vol. 14, No. 10, *Phys. Fluids*, pp 2088-2090, 1971.
- [Mori 2001] Mori H., Fujisaka H., "Transport and Entropy Production Due to Chaos or Turbulence", *Phy. Rev. E*, Vol. 63, No. 2, pp 026302-(1-11), 2001.
- [Nagrath 1982] Nagrath I.J., Gopal M., *Systems Modeling and Analysis*, Tata McGraw Hill, New Delhi, 1982.
- [Nagrath 1993] Nagrath I.J., Gopal M., *Control Systems Engineering*, Wiley Eastern Ltd., New Delhi, 1993.
- [Nakroshis 2003] Nakroshis P., Amoroso M., Legere J., Smith C., "Measuring Boltzman's Constant using Video Microscopy of Brownian Motion", *Am. J. Phys.*, Vol. 71, No. 6, pp 568-573, 2003.
- [Nemoto 2000] Nemoto I., "A Viscoelastic Model of Phagosome Motion within Cells Based on Cytomagnetometric Measurements", *IEEE Tr. Biomedical Engg.*, Vol. 47, No. 2, pp 170-182, 2000.
- [Nye 1973] Nye M.J., *Molecular Reality*, MacDonald, London, 1973.

- [Nyquist 1929] Nyquist H., "Thermal Agitation of Electric Charge in Conductors", *Phy. Rev.*, Vol. 32, pp 110-113, 1929.
- [Ochi 1990] Ochi M. K., *Applied Probability and Stochastic in Engineering and Physical Sciences*, John Wiley & Sons, NY, 1990.
- [Onsager 1931] Onsager L., "Reciprocal Relation in Irreversible Processes I", *Phy. Rev.*, Vol. 37, pp 405-426, 1931.
- [Ouyang 1994] Ouyang H.F., Huang Z.Q., Ding E.J., "1/f Noise and One-Dimensional Brownian Motion in a Singular Potential", *Phy. Rev. E*, Vol. 50, No. 4, pp 2491-2495, 1994.
- [Papoulis 1991] Papoulis A., *Probability, Random Variables and Stochastic Process*, McGraw Hill, NY, 1991.
- [Piasceck 2002] Piasceck J., "A Model of Brownian Motion in an Inhomogenous Environment", *J. Phys.: Condens. Matter*, Vol. 14, pp 9265-9273, 2002.
- [Powles 1978] Powles J.G., "Brownian Motion-June 1827", *Phys. Educ.*, Vol. 13, 310-312, 1978.
- [Qian 2002] Qian D., Wagner G.J., Liu W.K., Yu M. and Rouff S.R., "Mechanics of Carbon Nanotubes", *Appl Mech Rev*, Vol 55, No 6, pp 495-533, 2002.
- [Raikher 1996] Raikher Y.L., Rusakov V., "Dynamic Response of a Magnetic Suspension in a Viscoelastic Fluid", *Phy. Rev. E*, Vol. 54, pp 3846-3852, 1996.
- [Ratner 2003] Ratner M., Ratner D., *Nanotechnology*, Pearson Education Inc., New Delhi, 2003.
- [Requicha 2003] Requicha A.A.G., "Nanorobots, NEMS and Nanoassembly", *Proc. IEEE*, Vol. 91, No. 11, pp 1922-1933, 2003.
- [Resibois 1964] Resibois P., Davis H.T., "Transport Equation of a Brownian Particle in a External Field", *Physica*, Vol. 30, pp 1077-1091, 1964.

- [Rodriguez 1988] Rodriguez R.F., "Brownian Motion and Correlation Function in a Viscoelastic Fluid", *J. Phys. A: Math. Gen.*, Vol.21, pp 2121-2130, 1988.
- [Ross 1983] Ross S.M., *Stochastic Processes*, John Wiley & Sons, NY, 1983.
- [Roukes 2000] Roukes M.L., "Nano Electromechanical Systems" in *Tech. Digest of 2000 Solid-State Sensor and Actuator Workshop*, Hilton Isl., SC, 6/4-8/2000, pp 1-10, 2000.
- [Rousselet 1994] Rousselet J., Salome L., Ajdari A., Prost J., "Directional Motion of Brownian Ratchets Induced by Asymmetric Potentials", *Nature*, Vol. 370, pp 446-447, 1994.
- [Rull 1989] Rull L.F., Miguel E-De, Morales J.J., Maria J.N., "Brownian Motion in an Isothermal-Isobaric Bath: Mass and Size Dependence", *Phy. Rev. A*, Vol. 40, No. 10, pp 5856-5859, 1989.
- [Ryskin 1988] Ryskin G., "Brownian Motion in a Rotating Fluid: Diffusivity is a Function of Rotating Rate", *Phy. Rev. Lett.*, Vol. 61, No. 13, pp 1442-1445, 1988.
- [Sack 1956] Sack R.A., "A Modification of Smoluchowski's Diffusion Equation", *Physica*, Vol. 22, pp 917-918, 1956.
- [Sagues 1986] Sagues F., Horsethemke W., "Diffusive Transport in Spatially Periodic Hydrodynamic Flows", *Phy. Rev. A*, Vol. 34, pp 4136-4143, 1986.
- [Sasaki 2000] Sasaki Y.C., Suzuki Y., Yagi N., Adachi S., Ishibashi M., Suda M., Toyota K., Yanagihara M., "Tracking of Individual Crystal using Diffracted X-Ray", *Phy. Rev. E*, Vol. 62, No. 3, pp 3843-3847, 2000.
- [Sasaki 2001] Sasaki Y.C., Okimura Y., Adachi S., Suda H., Taniguchi Y., Yagi N., "Picometer-Scale Dynamical X-Ray Imaging of Single DNA Molecule", *Phys. Rev. Lett.*, Vol. 87, No. 24, pp 248102 (1-4), 2001.

- [Saxton 1990] Saxton M.J., "Lateral Diffusion in an Archipelago: Single Particle Diffusion", *Biophys. J.*, Vol. 64, pp 1053-1062, 1990.
- [Saxton 1997] Saxton M.J., Jacobson K., "Single-Particle Tracking: Application to Membrane Dynamics", *Annu Rev. Biophys. Biomol. Struct.*, Vol. 26, pp 373-399, 1997.
- [Schweitzer 1998] Schweitzer, F., Ebeling W. Tilsch B., "Complex Motion of Brownian Particles with Energy Depots", *Phy. Rev. Lett.*, Vol. 80, No. 23, pp 5044-5047, 1998.
- [Shariman 1987] Shariman B I, "Diffusive Transport in a Rayleigh-Benard Convection Cell", *Phy. Rev. A*, Vol. 36, pp 261-267, 1987.
- [Sharma 2003(i)] Sharma N.N., Ganesh M, Mittal R.K., "Nano-Electromechanical System Impact Spectrum Modeling and clubbing of Structural Properties", (accepted to be published), *Instt. Engineers, India*, 2003.
- [Sharma 2003(ii)] Sharma N.N., Mittal R.K., "On the theory of Non-Brownian Motion", in *Proc. of INAE Conf. on Nanotechnology ICON-2003*, Chandigarh, India, 21-22 Dec., pp 586-596, 2003.
- [Sharma 2004(i)] Sharma N.N., Ganesh M., Mittal R.K., "Non-Brownian Motion of Nanoparticle: An Impact Process Model", *IEEE Tr. Nanotechnology*, Vol. 3, No.1, pp 180-186, 2004.
- [Sharma 2004(ii)] Sharma N.N., Mittal R.K., 2004(ii) "Brownian Motion of Nanoparticle Considering Non-Rigidity of Matter", (in print) *IEEE Tr. Nanotechnology*, 2004.
- [Singh 2003] Singh R.P., Pandey A.K., "Energy Dissipation, Squeeze Film Damping and Quality Factor in Microstructure", in *Proc. INAE Conf. on Nanotechnology, ICON-2003*, Chandigarh, India, pp 160-171, 2003.
- [Smith 1994] Smith W.T., "Investment, Uncertainty and Price Stabilization Schemes", *J. Economics Dynamics and Controls*, Vol. 18, pp 561-579, 1994.

- [Smoluchowski 1907] Smoluchowski M. von, "Essai d'une théorie cinétique du mouvement Brownien et des milieux troubles", Bull. Int. Acad. Sci., Cracovie, pp 577-602, 1907.
- [Sparling 1984] Sparling L.C., Reihl L.E., "Translational and Rotational Brownian Motion in Water", Phy. Rev. A., Vol. 29, No. 4, pp 2194-2203, 1984.
- [Srokowski 1998] Srokowski T., "Solving the Generalized Langevin Equation with Algebraically Correlated Noise", Phy. Rev. E, Vol. 57, No. 4, pp 3839-3838, 1998.
- [Srokowski 2001] Srokowski T., "Stochastic Processes with Finite Correlation Time: Modeling and Application to the Generalized Langevin Equation", Phy. Rev. E, Vol. 64, No. 3, pp 031102-(1-9), 2001.
- [Szu 1975] Szu H.H., "Brownian Motion of Elastically Deformable Bodies", Phy. Rev. A, Vol. 11, No. 1, pp 350-359, 1975.
- [Takahashi 1952] Takahashi H., "Brownian Motion of Irregular Shaped Bodies" J. Phys. Soc. Japan, Vol. 7, pp 439-433, 1952.
- [Taylor 1953] Taylor G.I., "Dispersion of Soluble Matter in Solvent Flowing Slowly Through a Tube", Proc. R. Soc. A, Vol. 219, pp 186-203, 1953.
- [Taylor 1976] Taylor T. T., *Mechanics: Classical and Quantum*, Pergamon Press, NY, 1976.
- [Trefan 1992] Trefan G. Grigolim P., West B.J., "Deterministic Brownian Motion", Phy. Rev. A, Vol. 45, No. 2, pp 1249-1252, 1992.
- [Uhlenbeck 1930] Uhlenbeck G. E., Ornstein L. S., "On the Theory of Brownian Motion", Phys. Rev., Vol. 36, pp 823-841, 1930.
- [Vale 1993] Vale R.D., "Measuring Single Protein Motor at Work", Science, Vol. 260, pp 169-170, 1993.
- [Verga 1991] Verga A.D., "Brownian Motion Constrained to Enclose a Given Area", J. Phy. A: Math Gen., Vol. 24, pp L561-L564, 1991.

- [Volkov 2001] Volkov V.S., Leonov A.I., "Rotational Brownian Motion of Axisymmetric Particles in a Maxwell Fluid", *Phy. Rev. E*, Vol. 64, No. 5, pp 051113-(1-9), 2001.
- [Wang 1945] Wang M. C., Uhlenbeck G. E., "On the Theory of the Brownian Motion II", *Rev. Mod. Phys.*, Vol. 17, pp 323-342, 1945.
- [Wang 1992] Wang K.C., "Long-Time Correlation and Biased Anomalous Diffusion", *Phy. Rev. A*, Vol. 45, No. 2, pp 833-837, 1992.
- [Wang 2003] Wang H., "Mathematical Theory of Molecular Motors and a New Approach for Uncovering Motor Mechanism", in *Proc. IEEE Nanobiotechnology*, Vol. 150, No. 3, pp 127-133, 2003.
- [Wax 1954] Wax N. (ed.), *Selected papers on noise and stochastic process*, Dover NY, 1954.
- [Weber 1999] Weber D., "Nanomedicine" *J. Health Forum*, Vol. 42, pp 32-36, 1999.
- [Welty 1984] Welty J. R., Wicks C. E., Wilson R. E., *Fundamentals of Momentum, Heat and Mass Transfer*, NY, John Wiley & Sons, Ch. 23, pp 460, 1984.
- [Wien 1990] Wein L.M., "Brownian Networks with Discretionary Routings", *Operation Research*, Vol. 39, no. 2, pp 322-340, 1990.
- [Wiener 1923] Wiener N., "Differential Space", *J. Math and Phy.*, Vol. 2, pp 132-174, 1923.
- [Wiener 1938] Wiener N., "The Homogenous Chaos", *Am. J. Math.*, Vol. 60, pp 897-936, 1938.
- [Wiener 1949] Wiener N., *Extrapolation, Interpolation and Smoothing of Stationary Time series with Engineering Applications*, MIT Press, Cambridge, MA, 1949.
- [Williamson 1968] Williamson J.H., "Brownian Motion of Electron", *J. Phys. A (Proc. Phys. Soc.)*, Vol. 1, No. 2, pp 629-644, 1968.



- [Wong 1997] Wong E., Sheehan P.E., Lieber C.M., "Nanobeam Mechanics: Elasticity, Strength and Toughness of Nanorods and Nanotubes", Science, Vol. 277, pp 1971-1975, 1997.
- [Xiang 1993] Xiang N., "Stochastic Motion of Charged Particle in a Magnetic Field", Phy. Rev. E, Vol. 48, No. 2, pp 1590-1592, 1993.
- [Yanagida 1989] Yanagida T., "Observation of Molecular Motion for Gliding Muscle", in Frontiers in Biophysics: Protein, Muscle Contraction and Brain and Neurons, Japanese Society of Biophysics, Baifukann, Tokyo, Japan, pp 121-33, 1989.
- [Zhang 1990] Zhang P., Barad H., Martinez A., "Fractal Dimension Estimation of Fractional Brownian Motion", IEEE Proc.-1990, Southeastcon, pp 934-938, 1990.
- [Zwanzig 1970] Zwanzig R., Bixon M., "Hydrodynamic Theory of the Velocity Correlation Field", Phy. Rev. A, Vol. 2, No. 5, pp 2005-2012, 1970.
- [Zwanzig 1975] Zwanzig R., Bixon M., 'Compressibility Effects in the Hydrodynamic Theory of Brownian Motion" J. Fluid Mech., Vol. 69, No. 1, pp 21-25, 1975.

## LIST OF PUBLICATIONS

### JOURNAL PAPERS

1. Sharma N.N., Mittal R.K., "Brownian Motion of Nanoparticle Considering Non-Rigidity of Matter: A System Modeling Approach" (in print), *IEEE Tr. Nanotechnology*, Manuscript No. 0089-2003.R1, Oct. 2004.
2. Sharma N.N., Ganesh M., Mittal R.K., "Non-Brownian Motion of Nanoparticles: An Impact Process Model", *IEEE Trans. on Nanotechnology*, Vol. 3, No.1, pp 180-186, Mar. 2004.
3. Sharma N.N., Ganesh M., Mittal R.K., "Nano-Electromechanical System Impact Spectrum Modeling and Clubbing of Structural Properties", (in print) *IE (J)*, April 2003.

### CONFERENCE/WORKSHOP PAPERS

1. Girish R., Sharma N.N., Mittal R.K., "Study on Motor Protein Models and Related Problems", in *Proc. of National Conference on Nanotechnology NANOSHERE-2004*, Chennai, India, pp 42-49, 11-12 June, 2004.
2. Sharma N.N., Mittal R.K., "On the Theory of Non-Brownian Motion in Nano-Regimes", in *Proc. of Int. INAE Conference on Nanotechnology ICON-2003*, Chandigarh, India, pp 586-596, 21-22 Dec. 2003.
2. Sharma N.N., Mittal R.K., "Natural selection of Quantized levels in GA Optimized Fuzzy Logic Controller", in *Proc. of II International Conference on Computational Intelligence, Robotics and Autonomous Systems (CIRAS-2003)*, NUS, Singapore, PS05-5, 31-36, 15-18 Dec.2003.
3. Sharma N.N., "Introduction to MEMS & Nanotechnology" in *Proc. UGC Refresher Course on World Class Manufacturing Systems*, BITS, Pilani, India, ed. R.B. Kodali, MECH 23-MECH 26, 8-28 Dec. 2003.
4. Sharma N.N., "Microsensors & Microactuators" in *Proc. UGC Refresher Course on World Class Manufacturing Systems*, BITS, Pilani, India, ed. R.B. Kodali, MECH 34-MECH 39, 8-28 Dec. 2003.
5. Sharma N.N., Mittal R.K., "Performance analysis of rule based fuzzy controlled robotic manipulator using ANOVA", in *Proc. of National Seminar on Current Applications of Computers in Design Engineering*, Jodhpur, India, pp 23-30, March 3-4, 2001.
6. Sharma N.N., Mittal R.K., "Examination of Design model's influence on control performance of Robotic manipulator", in *Proc. of IX IASTED International Conference on Artificial Informatics (AI-2001)*, Innsbruck, Austria, 131-136, Feb. 19-23, 2001.
7. Sharma N.N., "Advanced Dynamics for Engineers", EDD Notes (Used as text for Post Graduate M.E. (Design) course-Dynamics & Vibrations), BITS, Pilani, India, 2000.

## **BIOGRAPHIES**

### **Biography of Candidate**

N N Sharma has done his B.E. in Mechanical Engineering from Regional College of Engineering, Srinagar, India in 1990. After working for seven years in industries, he joined academics and completed his M.E. in Mechanical Engineering in 1998 from Birla Institute of Technology & Science (BITS), Pilani, India. Since then he joined as a faculty in Mechanical Engineering Group, BITS, Pilani.

His research interests apart from MEMS and Nanotechnology includes design and control of Robotic manipulators. He is an active member of the working group at Center for Robotics and Intelligent Systems (CRIS) at BITS. He has published two papers in International journal of IEEE Transaction on Nanotechnology, one in national journal of Institution of Engineers and seven International and national conference papers. Among his academic achievements are successful completion of a short term course on “Computational Methods for Engineers” organized at IIT, Kanpur. N.N. Sharma has participated in Internal Workshop on “Computation and Optimization” at IIT, Kharagpur. He has visited Austria in the International Conference on Artificial Informatics AI-2001 with the financial support from CSIR, INDIA and Singapore in the International Conference on Computational Intelligence, Robotics and Automation with the financial support of AICTE, INDIA to present technical papers.

### **Biography of Guide**

Dr. R. K. Mittal is Professor of Mechanical Engineering and Computer Science at Birla Institute of Technology and Science (BITS), Pilani, India. He received his B.E.(Hons.) (1973) and M.E. (1975) in Mechanical Engineering from BITS, Pilani. Subsequently, he joined as faculty and has been with BITS since 1975. He diversified in areas of systems, control systems, computer science and did Ph.D. in Software Engineering from BITS.

He became Associate Professor in 1990 and Professor in 1995. He is the founder member of the Center for Robotics and Intelligent Systems (CRIS), established in 1992 and was its coordinator till 2000. He is currently Dean of Academic Registration &

Counselling Division at BITS. He is member of IEEE, Branch Counsellor for IEEE Students Branch at BITS and President of BITS Alumni Association.

His fields of research include robust robotic designs, 2D/3D robot path planning, MEMS, micro and nano robots, NEMS, Software Engineering, and Software Testing and Databases. He has published and presented several papers in international and national journal and conferences. Dr. Mittal in the authors of two textbooks: Robotics & Control (coauthor Prof. I.J. Nagrath), Tata McGraw Hill, New Delhi, India and Elements of Manufacturing Processes (coauthored with Dr. B.S.N. Parashar), Prentice Hall of India, New Delhi, India.